

Dissertation

submitted to the
Combined Faculties for the Natural Sciences and for Mathematics
of the Ruperto-Carola University of Heidelberg, Germany
for the degree of
Doctor of Natural Sciences



Structural Characterisation of the Mammalian SRP Receptor

Oliver Schlenker

2006

Dissertation

submitted to the
Combined Faculties for the Natural Sciences and for Mathematics
of the Ruperto-Carola University of Heidelberg, Germany
for the degree of
Doctor of Natural Sciences

presented by

Diplom-Biochemiker Oliver Schlenker
born in Lübeck, Germany
Oral examination.....

Structural Characterisation of the Mammalian SRP Receptor

Referees: Prof. Dr. Irmgard Sinning
Prof. Dr. Bernhard Dobberstein

TABLE OF CONTENTS

ACKNOWLEDGEMENTS	I
ABSTRACT	II
ZUSAMMENFASSUNG	III
PUBLICATIONS	IV
ABBREVIATIONS	V
1 INTRODUCTION	1
1.1 PROTEIN TARGETING IN THE EUKARYOTIC CELL	1
1.2 THE SRP CYCLE	2
1.3 THE SIGNAL RECOGNITION PARTICLE (SRP)	4
1.4 THE TRANSLOCON	6
1.5 SMALL GTPASES: STRUCTURAL AND FUNCTIONAL CHARACTERISTICS	8
1.6 GTPASES IN THE SRP CYCLE	12
1.6.1 <i>SRP54</i>	12
1.6.2 <i>The Signal Recognition Particle Receptor</i>	14
1.7 GTPASES REGULATE THE SRP CYCLE	16
1.8 AIM OF THIS WORK	19
2 RESULTS	20
2.1 EXPRESSION AND PURIFICATION OF SR AND SRP PROTEINS	20
2.1.1 <i>SR$\alpha^{His}:\beta\Delta TM$</i>	21
2.1.2 <i>SRX2$^{His}:\beta\Delta TM$</i>	22
2.1.3 <i>Seleno-L-Methionine Substituted SRX2$^{His}:\beta\Delta TM$</i>	23
2.1.4 <i>SRαNG^{His} (SR$\alpha N\Delta 314-NHis$)</i>	24
2.1.5 <i>SR$\beta\Delta TM^{His}$</i>	26
2.1.6 <i>SRP54DHis (SRP54C$^{term}\Delta 68-His$)</i>	27
2.1.7 <i>SRP54NGHis (SRP54C$^{term}\Delta 208$)</i>	29
2.2 RECONSTITUTION OF DIFFERENT SR:SRP COMPLEXES	32
2.2.1 <i>Reconstitution of Trimeric SR:SRP Complexes</i>	32
2.2.2 <i>Pentameric Complex Reconstitution: SR$\alpha^{His}:\beta\Delta TM$:SRP54DHis:SRP19His:RNA¹⁰⁴</i>	39
2.2.3 <i>Analysis of SR:SRP Complex Reconstitution</i>	40
2.3 STRUCTURE DETERMINATION OF SRX $^{His}:\beta\Delta TM$	44
2.3.1 <i>Crystallisation</i>	44
2.3.2 <i>Data Collection and Processing</i>	45
2.3.3 <i>Structure Determination by Molecular Replacement</i>	49
2.3.4 <i>Refinement</i>	50
2.4 THE STRUCTURE OF SRX $^{His}:\beta\Delta TM$ -GTP	55
2.4.1 <i>Overall Structure</i>	55
2.4.2 <i>The SRX$^{His}:\beta\Delta TM$-GTP Homodimer</i>	56
2.4.3 <i>The GTP-binding pocket</i>	59
2.4.4 <i>The SRX$^{His}:\beta\Delta TM$-GTP interface</i>	61
2.5 CHARACTERISATION OF INTERACTIONS WITH SR AND COMPONENTS OF THE SRP CYCLE	64
2.5.1 <i>SR$\beta\Delta TM$ Translocon Interaction</i>	64
2.5.2 <i>SR-SRP:RNC Interaction</i>	68
3 DISCUSSION	70
3.1 THE STRUCTURE OF THE MAMMALIAN SRP RECEPTOR: SRX $^{His}:\beta\Delta TM$	71
3.1.1 <i>The SRX$^{His}:\beta\Delta TM$-GTP ‘Dimer’</i>	71

3.1.2	Comparison with SRX:SR β Δ TM-GTP from Yeast	72
3.1.3	SRX as Effector for SR β	75
3.1.4	Longin Domains	77
3.1.5	GTPase: Longin Domain Complexes at Endomembranes	79
3.1.6	A molecular Explanation for a Genetic Disease	82
3.2	ANALYSIS OF INTERACTIONS WITH SR AND COMPONENTS OF THE SRP CYCLE	83
3.2.1	SR β Δ TM Binds in its Nucleotide-free Form to the Translocon	83
3.2.2	Analysis of the SR Interacting with the SRP:RNC Complex	87
4	OUTLOOK	89
5	MATERIALS AND METHODS	90
5.1	CHEMICALS, ENZYMES AND CLONING KITS	90
5.2	CLONING, EXPRESSION AND PURIFICATION OF SR- AND SRP PROTEINS	91
5.2.1	SR α ^{His} : β Δ TM	91
5.2.2	Cloning of SR α : β Δ TM	92
5.2.3	SRX2 ^{His} : β Δ TM	92
5.2.4	Seleno-L-Methionine Substituted Expression and Purification of SRX2 ^{His} : β Δ TM _{SeMet}	93
5.2.5	SRX2 ^{His} : β Δ TM / SR α ^{His} : β Δ TM mutants	93
5.2.6	SR α NG ^{His} (SR α N Δ 314-N ^{term} His)	94
5.2.7	SR β Δ TM	96
5.2.8	SRP54D (SRP54C ^{term} Δ 68)	96
5.2.9	SRP54NG (SRP54C ^{term} Δ 208)	99
5.3	COMPLEX FORMATION STUDIES	101
5.3.1	Trimeric Complex: SR α ^{His} : β Δ TM:SRP54D ^{His}	101
5.3.2	Pentameric Complex Formation: SR α ^{His} : β Δ TM:SRP54D ^{His} :SRP19:RNA ¹⁰⁴	102
5.3.3	Trimeric Complex Formation Pull-Down: SR α : β Δ TM:SRP54NG ^{CHis}	103
5.3.4	Analysis of SR:SRP Complex Formation	104
5.4	CRYSTALLISATION AND STRUCTURE DETERMINATION OF SR α X2 ^{His} : β Δ TM	104
5.4.1	Crystallisation of SR α X2 ^{His} : β Δ TM	104
5.4.2	Freezing and Mounting	105
5.4.3	Data Collection	105
5.4.4	Structure Determination and Model Refinement	105
5.4.5	Determination of the Selenium K-shell absorbance peak	106
5.5	IMMOBILISED PEPTIDE LIBRARY SCAN	107
5.5.1	Probing the SR β :Sec61p interaction by an immobilised peptide library	107
5.5.2	Probing the SR β ribosome interaction by an immobilised peptide library	108
5.6	HPLC ANALYSIS	108
5.7	PROGRAMS USED FOR FIGURES IN THE TEXT	109
5.8	CRYSTALLOGRAPHIC BACKGROUND	109
5.8.1	Crystal Systems and Bravais Lattices	109
5.8.2	Bragg's Law	111
5.8.3	Data Collection and Reciprocal Lattice	112
5.8.4	The Phase Problem and Electron Density Calculation	114
5.8.5	Molecular Replacement	116
5.8.6	Anomalous Dispersion	117
5.8.7	Isomorphous Replacement	120
5.8.8	Data Processing	121
5.8.9	Refinement and Evaluation of the Model	121
5.9	LIST OF BUFFERS	125
5.9.1	SR α ^{His} : β Δ TM	125
5.9.2	SRX2 ^{His} : β Δ TM	125
5.9.3	SRX2 ^{His} : β Δ TM _{SeMet}	126
5.9.4	SR α NG ^{His}	127
5.9.5	SRP54D ^{His}	127
5.9.6	SRP54NG ^{His}	127
5.9.7	Trimeric Complex: SR α ^{His} : β Δ TM:SRP54D ^{His}	128
5.9.8	Pentameric Complex Formation: SR α ^{His} : β Δ TM:SRP54D ^{His} :SRP19:RNA ¹⁰⁴	128
5.9.9	Trimeric Complex Formation Pull-Down: SR α : β Δ TM:SRP54NG ^{CHis}	128

5.9.10 Analysis of SR:SRP Complex Formation	129
5.9.11 Immobilised Peptide Library Scan	129
5.9.12 Buffer for HPLC analysis	129
5.9.13 Crystallisation and Structure Determination of $SR\alpha X2^{His}:\beta\Delta TM$	129
5.10 LIST OF PRIMERS	130
5.10.1 $SRX2^{His}:\beta\Delta TM$ / $SR\alpha^{His}:\beta\Delta TM$ mutants	130
5.10.2 $SR\alpha NG^{His}$	130
5.10.3 $SRP54D^{His}$	130
5.10.4 $SRP54NG^{His}$	131
BIBLIOGRAPHY	132

Acknowledgement

First I would like to thank Prof. Irmi Sinning for giving me the opportunity to work on this project and for supportive supervision and inspiring discussions.

My special thanks go to Klemens Wild for advice in crystallography and encouraging discussions.

I also want to kindly thank Prof. Bernhard Dobberstein for being my second supervisor.

Many thanks also go to also Prof. Roland Beckmann and Dr. Mario Halic for fruitful collaboration and interesting discussions.

The cooperation with Dr. Ben Abell is highly appreciated and led to very productive results.

Matthew Groves was a helping hand in the beginning of my PhD studies showing me the purification procedure and I am very grateful for his support.

I am grateful to Dr. Milan Spasic for many inspiring discussions and for the time spent together.

Many thanks go to Astrid Hendricks for excellent technical support and for the nice working atmosphere.

It was a pleasure working with Dr. Felix Findeisen, Felix Heise, Dr. Ulrike Dürrwang, Dr. Badri Konkimalla and Sami Caner. I have enjoyed working with you and would like to send my special gratitude for accompanying me during my dissertation. I wish you all the best in the future.

Special thanks also go to Andi, Ingo, Niels, Valo, Michael, Linus and Alex for their encouraging spirit and companionship outside the lab.

Last but not least I would especially like to thank my mother, Fritz and Christina for their enduring support, patience and understanding throughout my postgraduate education.

Abstract

In eukaryotes, secretory and membrane proteins are targeted to the endoplasmic reticulum (ER) membrane for cotranslational translocation. This requires the specific interaction of the signal recognition particle (SRP), a ribonucleoprotein, with its receptor (SR). The eukaryotic SR is a heterodimeric protein consisting of $SR\alpha$ and $SR\beta$ which is anchored to the ER membrane. In all three kingdoms of life the conserved GTPases in SRP and SR (in eukaryotes SRP54 and $SR\alpha$, respectively) enable the formation of the docking complex in a GTP dependent manner.

$SR\beta$ is the third and least understood GTPase participating in cotranslational targeting in eukaryotes. Therefore a more detailed view on the GTPase cycle of $SR\beta$ and functionally relevant $SR\beta$ effector interactions should be obtained. X-ray structure analysis was used to determine the structure of a soluble form of $SR\beta$ ($SR\beta\Delta TM$) in its GTP bound state in complex with a fragment of $SR\alpha$. The structure allows to precisely define the minimal $SR\beta$ binding domain of $SR\alpha$ (SRX). The homology to other small GTPases and the underlying principles of regulation together with previous biochemical data allow to attribute a functional role to SRX in the activation of the $SR\beta$ GTPase.

An immobilised peptide library was used in order to examine the interaction of SR with the translocon. Evidence is presented that the apo- and likely the GDP bound form of $SR\beta\Delta TM$ ($SR\beta\Delta TM$ -apo/GDP) bind to cytosolic loops of the translocon in contrast to $SR\beta\Delta TM$ -GTP in complex with SRX^{His} or $SR\alpha^{His}$. These experiments suggest that the SRX binding surface of $SR\beta$ -GTP, as observed in the $SRX^{His}:\beta\Delta TM$ -GTP X-ray structure, is the same as engaged in $SR\beta\Delta TM$ -apo/GDP binding to the translocon. $SR\beta\Delta TM$ -apo binds to peptides of several cytosolic loop regions of the translocon. Mapping of these regions on the available structure of the homologous translocon from *Methanococcus jannaschii* suggests that $SR\beta\Delta TM$ -apo/GDP blocks the translocation pore.

Based on the molecular structure of the $SRX^{His}:\beta\Delta TM$ -GTP SRX belongs to the SNARE-like superfamily with the common fold of the longin domains (LDs). The common principles of the LD family are analysed by a comparison of surface hydrophobicity and structure based sequence alignment with structurally known LDs. Putative LDs are considered according to secondary structure prediction and primary sequence alignment. The interaction of small GTPases with LDs is suggested to be important for the assembly of large complexes at or targeting of vesicles to the endomembrane system.

Important structural information on the mammalian SRP:SR complex are still missing, including the arrangement of the individual protein subunits and the positioning of the SRP RNA. Extensive purification and assembly of a pentameric SRP:SR complex, consisting of $SR\alpha:\beta\Delta TM$, SRP54, SRP19 and a 104 base pair long SRP RNA, was set up in order to establish the basis for further structural studies on this macromolecular complex.

Zusammenfassung

In eukaryotischen Zellen werden sekretorische und Membranproteine cotranslational zum Endoplasmatischen Retikulum (ER) transportiert. Dies erfordert die Interaktion des Signalerkennungspartikels (Signal Recognition Particle, SRP), einem Ribonukleoprotein, mit seinem Rezeptor (SR). Der eukaryotische SR ist ein Heterodimer, der aus $SR\alpha$ und dem membranverankerten $SR\beta$ aufgebaut ist. In allen drei Königreichen des Lebens vermittelt die GTP-abhängige Wechselwirkung zwischen den in SR und SRP konservierten GTPasen die Bildung des Docking-Komplexes. $SR\beta$ ist die dritte, am wenigsten verstandene GTPase, die an der co-translationalen Translokation beteiligt ist.

Der GTPase-Zyklus von $SR\beta$ wurde weiter aufgeklärt und funktionell relevante Schnittstellen zwischen $SR\beta$ und seinen Effektoren untersucht. Mit Hilfe von Röntgenstrukturanalyse wurde die Struktur einer löslichen Form von $SR\beta$ ($SR\beta\Delta TM$) im GTP-Zustand mit einem Fragment von $SR\alpha$ bestimmt. Mit Hilfe dieser Struktur wurde die minimale $SR\beta$ -Bindungsdomäne von $SR\alpha$ präzise definiert. Durch einen detaillierten Vergleich mit den Strukturen von anderen kleinen GTPasen und deren Effortorkomplexen, sowie bekannten biochemischen Daten, konnte der SRX-Domäne eine funktionelle Rolle bei der Aktivierung der GTPase $SR\beta$ abgeleitet werden.

Eine immobilisierte Peptidbibliothek wurde benutzt, um die Interaktion des Translokons mit dem SR zu untersuchen. Es wird gezeigt, dass $SR\beta\Delta TM$ in der Apo- und wahrscheinlich auch in der GDP-gebundenen Form ($SR\beta\Delta TM$ -apo/GDP) an zytosolische Loopregionen des Translokons bindet, aber nicht in der GTP-Form im Komplex mit SRX^{His} oder $SR\alpha^{His}$. Für die Bindung des Translokons wird von $SR\beta$ offenbar die selbe Oberfläche benutzt wie zur Bindung der SRX-Domäne. $SR\beta\Delta TM$ -apo bindet an zahlreiche zytosolische Loopregionen des Translokons. Durch Veranschaulichung dieser Regionen anhand der Struktur des homologen Translokons von *Methanococcus jannaschii* kann vorgeschlagen werden, dass $SR\beta\Delta TM$ -apo/GDP die Translokationspore blockiert.

Basierend auf der Röntgenstruktur des $SRX^{His}:\beta\Delta TM$ -GTP-Komplexes kann gezeigt werden, dass SRX zur Familie der SNARE-ähnlichen Proteine gehört mit dem allgemeinen Faltungsmuster der Longin-Domänen (LDs). Die grundsätzlichen Prinzipien der LD-Familie werden anhand von LDs mit bekannter Struktur analysiert, durch Vergleich der Oberflächenhydropathizität und der Primärsequenz. Die Interaktion von kleinen GTPasen mit LDs ist daher wichtig für den Aufbau von grossen Komplexen oder Vesikeln an und den Transport von Vesikeln in Endomembran-Systeme.

Wichtige molekulare Informationen über den Säugetier-SRP:SR-Komplex fehlen immer noch. Die aufwendige Aufreinigungsmethode und Rekonstitution eines pentameren SRP:SR-Komplexes bestehend aus $SR\alpha:\beta\Delta TM$, SRP54, SRP19 und einer 104 Basenpaare langen SRP-RNA wurde etabliert, als Basis für weitere strukturelle Studien an diesem makromolekularen Komplex.

Publications

Parts of this thesis are included in the following publications:

Oliver Schlenker, Astrid Hendricks, Irmgard Sinning, Klemens Wild: The structure of the mammalian SRP receptor as prototype for the interaction of small GTPases with longin domains. *J. Biol. Chem.* 2006, **281**: 8898–8906

Mario Halic, Marco Gartmann, **Oliver Schlenker**, Thorsten Mielke, Martin R. Pool, Irmgard Sinning, Roland Beckmann: Signal Recognition Particle Receptor Exposes the Ribosomal Translocon Binding Site. *Science* 2006, **312**:745-747

Benjamin M. Abell, Martin R. Pool, **Oliver Schlenker**, Irmgard Sinning, Stephen High: Signal recognition particle mediates post-translational targeting in eukaryotes. *Embo J.* 2004, **23**:2755-2764

Abbreviations

Å	Ångström, 1 Å = 1 x 10 ⁻¹⁰ m
AP	adaptor protein
Arf	adenosine diphosphate ribosylation factor
AU	absorption unit
B	β-subunit of the signal recognition particle
βΔTM	β-subunit of the signal recognition particle receptor lacking the N-terminal transmembrane region
BisTris	2-[bis(2-hydroxyethyl)amino]-2-(hydroxymethyl)propane-1,3-diol
bp	base pair
C-terminal	carboxy-terminal
COP	coat protomer
cp	chloroplast
DNA	deoxyribonucleic acid
DTT	1,4-dithiothreitol
<i>E. coli</i>	<i>Escherichia coli</i>
ER	endoplasmic reticulum
EDTA	ethylenediaminetetraacetic acid
EM	electron microscopy
eV	electron Volt
F	structure factor
Ffh	SRP fifty-four homologue
Fo	experimentally observed structure factor
Fc	calculated structure factor (determined from a model)
FT	flow-through
FtsY	filamentous sensitive protein Y
G protein	GTPase
G domain	GTPase domain
GAP	GTPase activating protein
GDP	guanosine diphosphate
GEF	guanyl nucleotide exchange factor
GF	gel filtration chromatography, size exclusion chromatography
GMPPCP	guanylyl 5'-(β, γ-methylenediphosphonate)
GMPPNP	phosphoaminophosphonic acid-guanylate ester
GTP	guanosine triphosphate
GTPase	guanosine triphosphate hydrolase catalysing the reaction GTP → GDP + P _i
IPTG	isopropyl-thio-β-D-galactopyranoside
I	intensity
HEPES	4-(2-Hydroxyethyl)-1-piperazineethanesulfonic acid
K _D	dissociation constant
kD	kilodalton
λ	wavelength
L	lysis buffer
LD	longin domain
M	methionine-rich, C-terminal domain of SRP54
<i>M. jannaschii</i>	<i>Methanococcus jannaschii</i>
MAD	multi-wavelength anomalous dispersion
MIR	multiple isomorphous replacement
MIRAS	multiple isomorphous replacement with anomalous scattering

MP	membrane protein
mRNA	messenger RNA (ribonucleic acid)
MTG	2-monothioglycerol
MW	molecular weight
N-terminal	amino-terminal
NEB	New England Biolabs, Ipswich, USA
NG	catalytic core of SRP GTPases
ON	over night
PBS	phosphate buffered saline
P _i	inorganic phosphate
PCC	protein conducting channel
PMT	phosphate buffered saline supplemented with 0.5 % milkpowder and 0.05 % of the detergent Tween-20
Q	quaternary ammonium (functional group used on anion exchange chromatography matrix)
R-factor	reliability factor
rmsd	root mean square deviation
RNA	ribonucleic acid
RNA ¹⁰⁴	104 base pair RNA sequence of the signal recognition particle RNA
RNC	ribosome nascent chain complex
RT	room temperature
σ	signal background
SAD	single wavelength dispersion
Sar	secretion-associated and Ras-related
SED1	spondyloepiphyseal dysplasia tarda
SED2	protein causing the disease spondyloepiphyseal dysplasia tarda
SIR	single isomorphous replacement
SIRAS	single isomorphous replacement with anomalous scattering
SDS-PAGE	sodium dodecyl sulfate polyacrylamide gel electrophoresis
SeMet	L-selenomethionine
SNARE	soluble NSF attachment protein receptor(s) (where NSF indicates <i>N</i> -ethylmaleimide-sensitive factor)
SP	Sulphopropyl (functional group used on cation exchange chromatography matrix)
SR	signal recognition particle receptor
SR α	α -subunit of the signal recognition particle receptor
SR α^{His}	α -subunit of the signal recognition particle receptor with an amino-terminal hexa-histidine tag
SR α NG	NG domain of SR α , amino-terminal deletion mutant of SR α (SR $\alpha\Delta$ 314)
SR α NG ^{His}	NG domain of SR α with an amino-terminal hexa-histidine tag
SR β	β -subunit of the signal recognition particle receptor
SR $\beta\Delta$ TM	β -subunit of the signal recognition particle receptor lacking the N-terminal transmembrane region
SRP	signal recognition particle
SRP19	19 kD protein of the signal recognition particle
SRP54	54 kD protein of the signal recognition particle
SRP54D	carboxy-terminal deletion mutant of SRP54 (SRP54 Δ 68)
SRP54D ^{His}	SRP54D with an hexa-histidine tag
SRP54D ^{NHis}	SRP54D with an amino-terminal hexa-histidine tag

SRP54D ^{CHis}	SRP54D with an carboxy-terminal hexa-histidine tag
SRP54NG	carboxy-terminal deletion mutant of SRP54 (SRP54 Δ 208)
SRP54NG ^{His}	NG domain of SRP54 with an hexa-histidine tag
SRP54NG ^{NHis}	NG domain of SRP54 with an amino-terminal hexa-histidine tag
SRP54NG ^{CHis}	NG domain of SRP54 with an carboxy-terminal hexa-histidine tag
SRX	minimal SR β binding domain of SR α , located at the N-terminus of SR α (130 residues for human SR α)
SRX2	N-terminal domain of SR α including the SRX domain (176 amino acids for human SR α)
SRX2 ^{His}	N-terminal domain of SR α including the SRX domain (176 amino acids for human SR α) with an amino-terminal hexa-histidine tag
T. aq.	<i>Thermus aquaticus</i>
TAE	diethylcarbamoymethyl-2-methylbenzoate
TBAB	<i>tert</i> -butyl ammonium bromide
<i>T. aquaticus</i>	<i>Thermus aquaticus</i>
TM	transmembrane region
TRAPP	transport protein particle
Tris	2-amino-2-(hydroxymethyl)propane-1,3-diol
tRNA	transfer RNA (ribonucleic acid)
V _e	elution volume
X	SRX (Minimal SR β binding domain of SR α)
y	yeast (<i>Saccharomyces cerevisiae</i>)

Abbreviations for Amino Acids

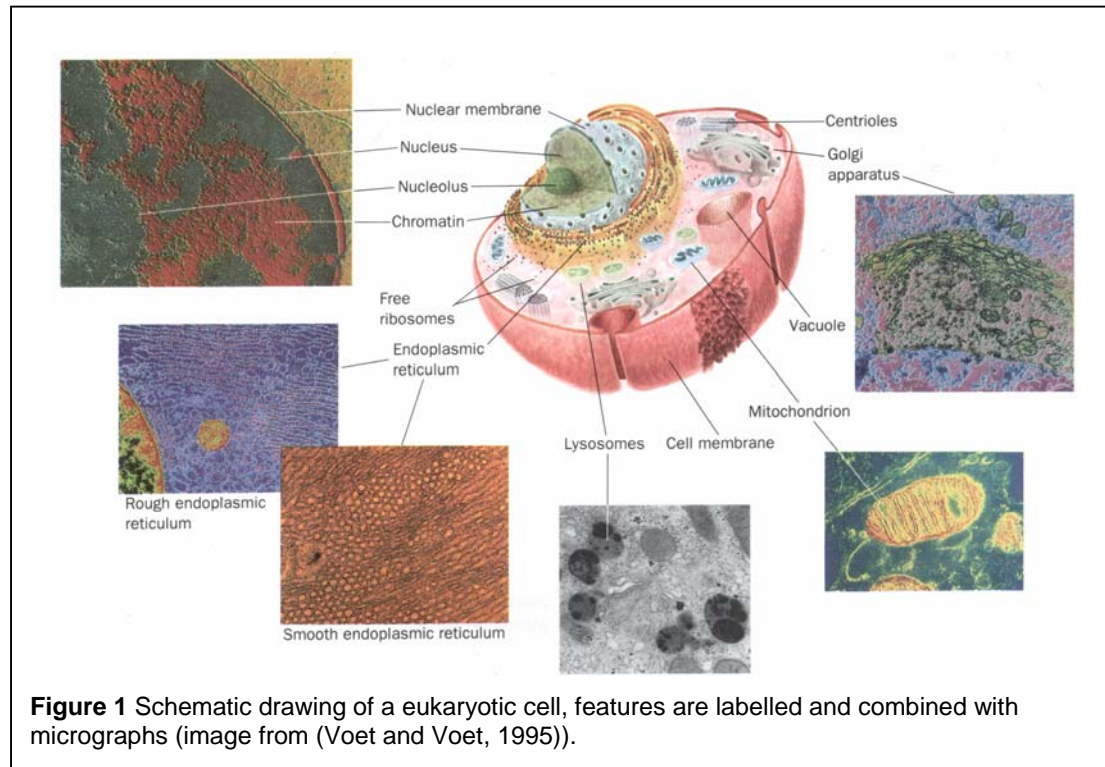
A	Ala	Alanine
C	Cys	Cysteine
D	Asp	Aspartic acid
E	Glu	Glutamic acid
F	Phe	Phenylalanine
G	Gly	Glycine
H	His	Histidine
I	Ile	Isoleucine
K	Lys	Lysine
L	Leu	Leucine
M	Met	Methionine
N	Asn	Asparagines
P	Pro	Proline
Q	Gln	Glutamine
R	Arg	Arginine
S	Ser	Serine
T	Thr	Threonine
V	Val	Valine
W	Trp	Tryptophane
Y	Tyr	Tyrosine
X		any residue

For my mother and Christina.

1 Introduction

1.1 Protein Targeting in the Eukaryotic Cell

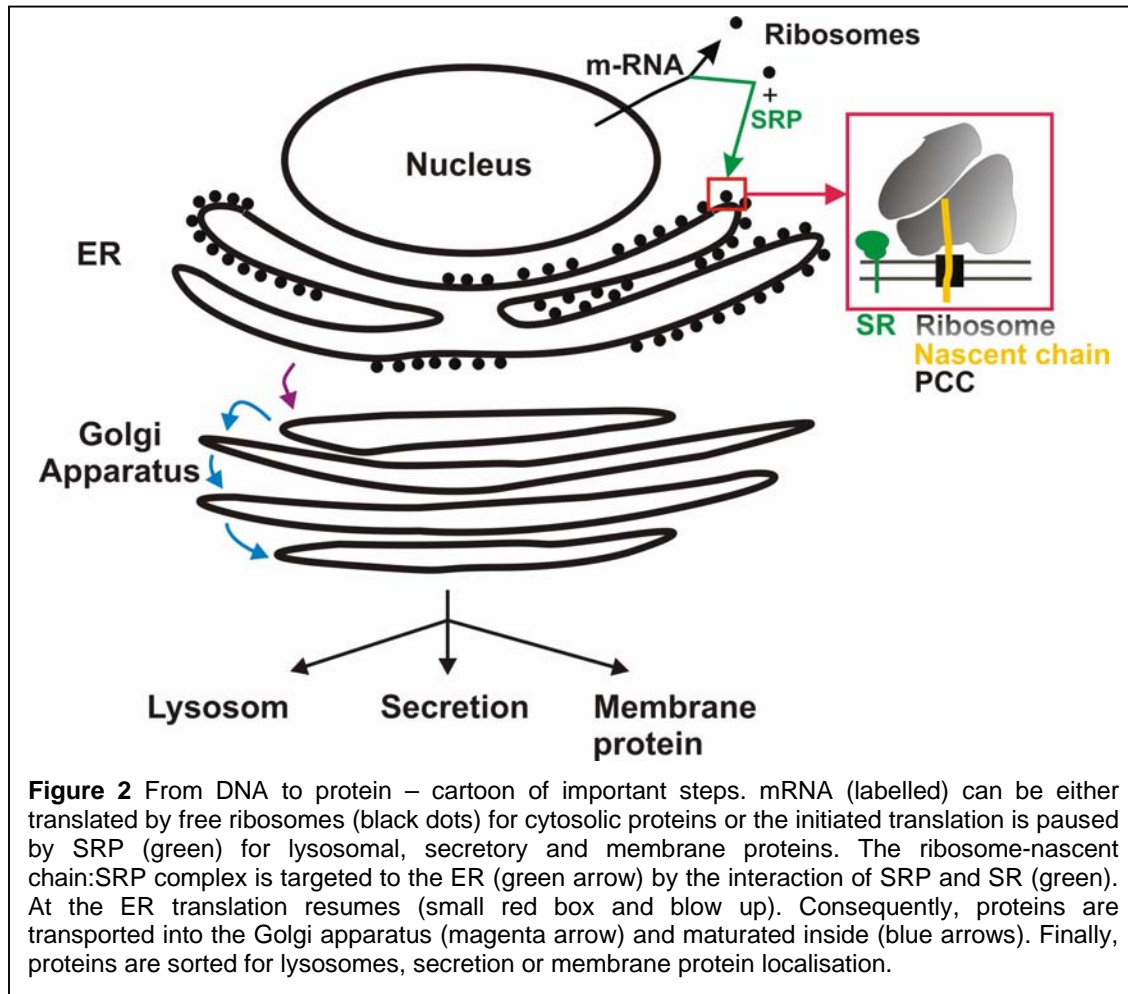
In eukaryotic cells different membrane enclosed compartments form an elaborate endomembrane system (Figs. 1, 2). Therefore, proteins must be sorted according to their site of action which in general is directed by a signal sequence. Proteins without a special targeting signal remain in the cytosol.



Newly synthesised secretory and membrane proteins (MPs) are transported to the endoplasmic reticulum (ER) which is very important for protein folding and modification as well as lipid synthesis. The membranous network of the Golgi apparatus is responsible for further maturation and sorting of secretory and membrane proteins.

The main mode for proteins to enter the ER is cotranslational translocation where the translating ribosome is targeted to the ER membrane and the nascent chain is inserted into the protein conducting channel (PCC, translocon). The signal recognition particle (SRP) and its receptor (SR) at the ER membrane are key players in this targeting step (Fig. 2). Alternatively, proteins can be translated completely in the cytosol, stabilised by the interaction with chaperones and then access the ER

lumen through the translocon (post-translational translocation). The ER is a check point for correct protein folding and also the compartment in which proteins can be modified by N-linked glycans.



1.2 The SRP Cycle

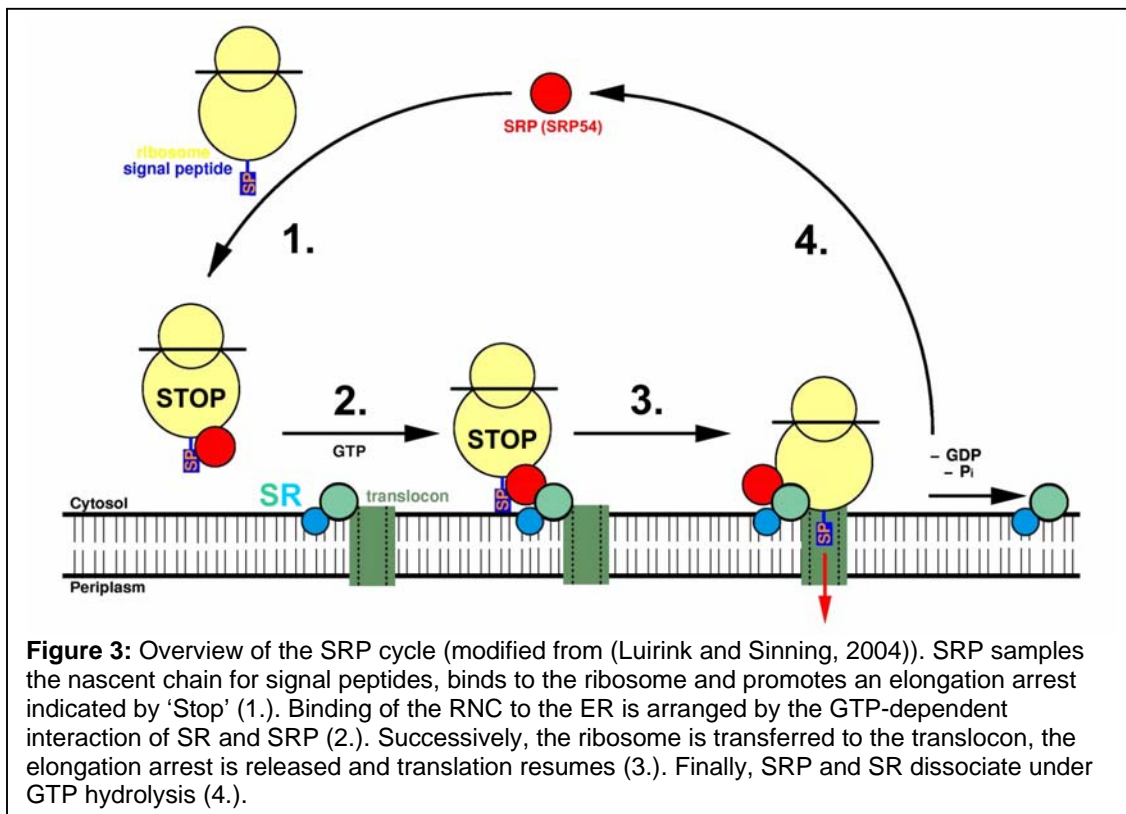
In eukaryotes, the 80S ribosome and the newly synthesised protein assemble to the so called ribosome nascent chain complex (RNC). RNCs of translated secretory and membrane proteins are targeted in a GTP dependent process to the ER termed cotranslational translocation. Cotranslational translocation requires recognition of a hydrophobic N-terminal signal peptide by the ribonucleoprotein SRP and targeting of the RNC to the ER membrane.

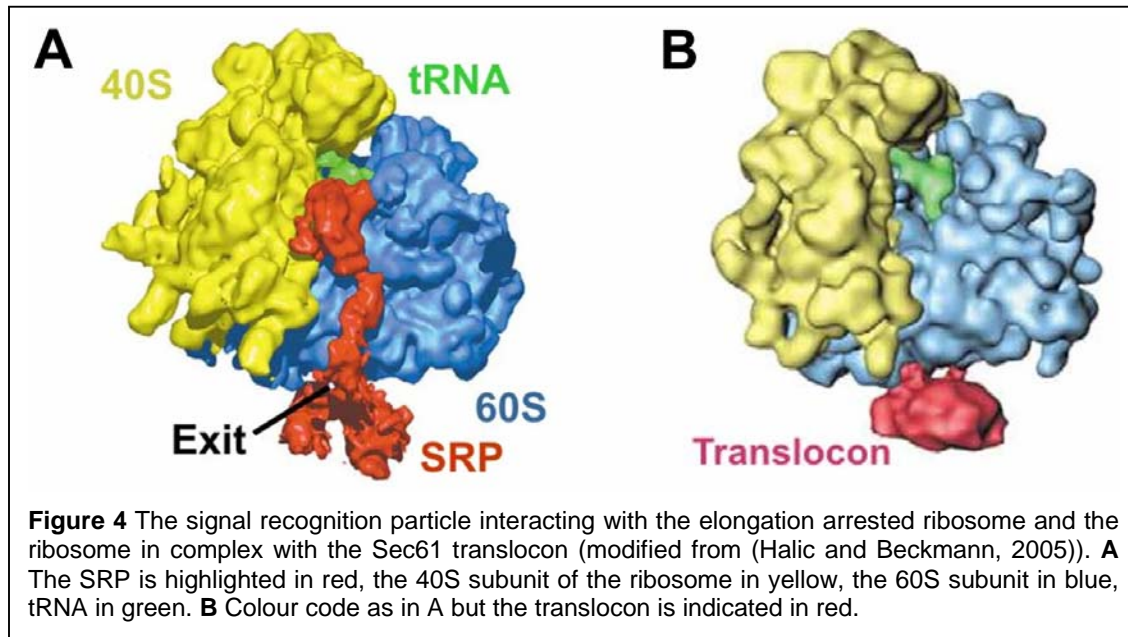
The SRP cycle (Fig. 3) is initiated when SRP recognises the hydrophobic signal sequence at the ribosomal polypeptide exit site. Signal sequence binding pauses translation (elongation arrest (Walter and Blobel, 1981)) by SRP interacting

with the site of protein synthesis between the ribosomal subunits. The matching size (250 Å (Halic et al., 2004)) and elongated shape of SRP (Halic et al., 2004) allows communicating between the site of protein synthesis and the ribosomal polypeptide exit site (Fig. 4A) which are located 100 Å apart (Beckmann et al., 2001).

The RNC is targeted in eukaryotes to the ER (in prokaryotes to the plasma membrane) by a GTP-dependent process, in which SRP interacts with its cognate receptor (SR) enabling the formation of the docking complex (Fig. 3, see below) (for review, see (Halic and Beckmann, 2005; Keenan et al., 2001; Lührink and Sinning, 2004)). In eukaryotes, the SR is a hetero-dimer consisting of SR α and SR β (Tajima et al., 1986)). The nascent chain is transferred to the Sec61 translocon, the elongation arrest is released and SR and SRP dissociate (Fig. 3). In Fig. 4B a cryo electron microscopy (cryo-EM) structure is shown of the ribosome in complex with the translocon. After dissociation from SR, SRP is available for a new round of targeting. The exact sequence of events during nascent chain transfer is poorly understood.

In principle, SRP cycles in eukaryotic and prokaryotic cells share the conserved four steps of the SRP cycle as shown in Fig. 3.





1.3 The Signal Recognition Particle (SRP)

Eukaryotic SRP is a ribonucleoprotein consisting of six proteins (SRP9, 14, 19, 54, 68, 72, called according to their molecular weight) and a scaffolding 7SL RNA (Fig. 5) consisting of 300 nucleotides. The RNA is organised in two domains: The *Alu* domain is named according to the homologous *Alu* domains of small repetitive sequences and the small cytoplasmic *Alu* RNAs (Chang et al., 1996; Weiner, 1980) with a conserved three way junction of stems (Andersen et al., 2006; Strub et al., 1991). The 150 bp S domain appears as an insertion in the *Alu* domain sequence (Gundelfinger et al., 1983).

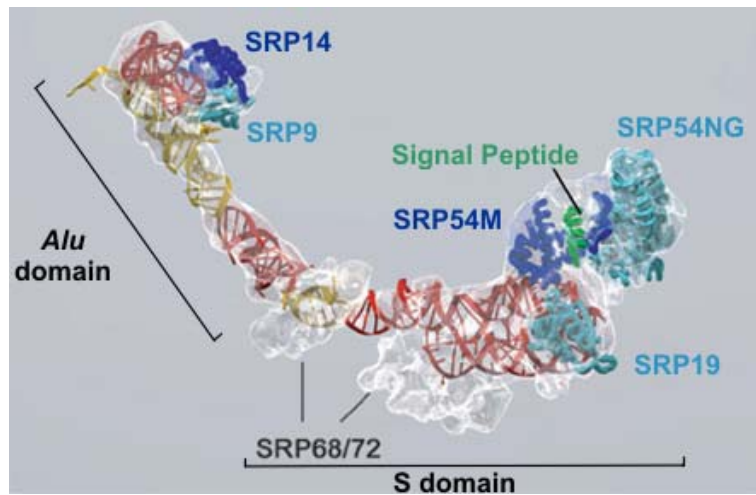


Figure 5 SRP electron density determined from the ribosome:SRP complex. Proteins and RNA models are fitted (if available) according to density (modified from (Halic et al., 2004)). SRP68/72 positions are considered to fill unexplained electron density. RNA is highlighted in red and yellow with *Alu* and S domain labelled. All SRP proteins are indicated as well as the position of the signal peptide (green). SRP54 consists of three domains (N, G and M domains). NG and M domains are differentiated.

The *Alu* domain is complexed to SRP9 and 14 and initiates the elongation arrest by binding in between the ribosomal subunits (Fig. 4A) (Halic et al., 2004). The elongation arrest is not required for cotranslational translocation (Siegel and Walter, 1985). The S domain binds to the remaining four SRP proteins (SRP19, 54, 68, 72; reviewed in (Halic and Beckmann, 2005; Keenan et al., 2001; Lührink and Sinning, 2004; Wild et al., 2004)) (Fig. 5) including the conserved SRP54 which is important for signal peptide and SR binding (see below).

In archaea, chloroplasts and bacteria, SRP is less complex (Table 1). SRP54 and its homologues (fifty four homologue, Ffh) represent the conserved core of the SRP and fulfil all functions required for cotranslational targeting (RNA-, signal sequence- and SR binding). Archeal SRP comprises homologues of SRP54 and SRP19, and 7S RNA. Bacterial SRP consists of a 48 kD Ffh (P48) and the 4.5 S RNA (reviewed in (Keenan et al., 2001; Lührink and Sinning, 2004)).

Eukaryotes			Archea	Eubacteria	Chloroplast
	Mammals	Yeast			
Proteins belonging to S Domain	SRP54	SRP54p	SRP54	Ffh (48 kD)	cpSRP54
	SRP19	Sec65p	SRP19	-	-
	SRP72	SRP72p	-	-	-
	SRP68	SRP68p	-	-	-
Proteins belonging to <i>Alu</i> Domain	SRP14	SRP14p	-	-	-
		SRP21p			
	SRP9	(SRP9 related)	-	-	-
-	-	-	-	-	cpSRP43
RNA	7 SL SRP RNA	7 SL SRP RNA (ScR1)	7 SL SRP RNA	4.5 S RNA	-

Table 1 Table of SRP proteins and their homologues in the three domains of life and chloroplasts. Table adapted from (Schunemann, 2004), archeal SRP reviewed in (Zwieb and Eichler, 2002), for yeast SRP see (Brown et al., 1994; Van Nues and Brown, 2004), cpSRP is reviewed in (Schunemann, 2004).

1.4 The Translocon

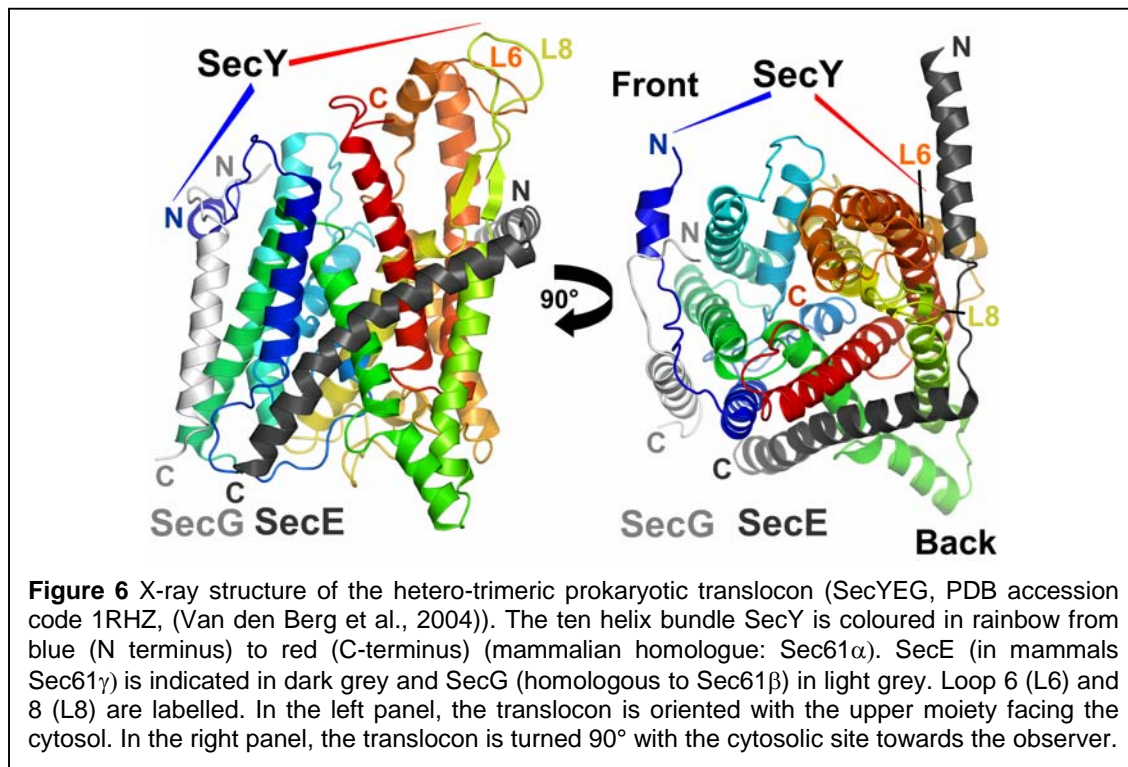
The translocon is an essential component in cotranslational translocation because it binds the RNC and allows the translocation of the nascent chain into the ER and coordinates the insertion of membrane proteins into the ER membrane (for review see (Matlack et al., 1998)).

The translocon in eukaryotes has been named protein conducting channel (PCC), Sec61 complex, Sec61p complex and Sec61 $\alpha\beta\gamma$ complex, according to its subunits. The prokaryotic homologue of the Sec61 complex was termed SecY complex or SecYEG, according to its subunits (for more information, see (Corsi and Schekman, 1996; Rapoport et al., 1996; Wickner and Leonard, 1996)). SecY forms the channel pore (Fig. 6) and is homologous to Sec61 α in mammals (termed Sec61p and Ssh1p in yeast). One of the two smaller subunits associating to the central pore is in prokaryotes SecE which is homologous to Sec61 γ in mammals and Sss1p in yeast. The third subunit in the translocon is in prokaryotes SecG with homology to Sec61 β in mammals (termed Sbh1p and Sbh2p in yeast). The degree of

conservation can be demonstrated by the high degree of sequence identity between the *Homo sapiens* Sec61 α and the *Methanococcus jannaschii* SecY which is 33.8 %.

Recently, the X-ray structure of the translocation pore from *Methanococcus jannaschii* has been determined (Van den Berg et al., 2004) (Fig. 6). SecY appears as a bundle of ten transmembrane helices (TMs) with a cytoplasmic funnel-like cavity formed by the loops between the TMs. A front and a back side have been proposed for the translocation pore with the two smaller subunits SecE and SecG forming the 'back'. SecG contains only one TM and the N-terminus is exposed to the cytosol. The third subunit, SecE shows two helices which bind to SecY like a clamp. The N-terminal helix of SecE anchors to the cytosolic side of the ER membrane, while the C-terminal helix is inserted into the membrane.

The three translocon subunits are involved in co- and posttranslational translocation (see below). Recently complementation assays performed with a yeast strain deficient in the Sec61 α homologue Sec61p have shown that the cytosolic loops L6 and L8 of Sec61p play an important role in protein translocation (Cheng et al., 2005). Mutations within loop L8 but not L6 influence the Sec61p-ribosome interaction. Loop L6 has been found to affect a different step in co-translational translocation, possibly the interaction with the SR.

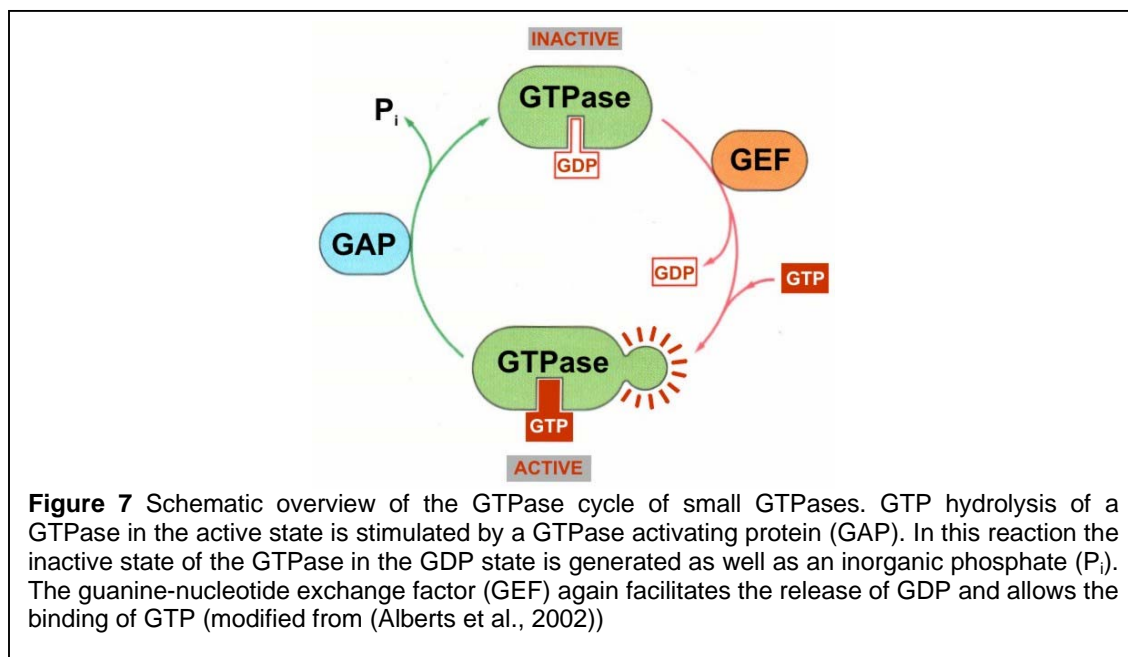


1.5 Small GTPases: Structural and Functional Characteristics

GTPases represent molecular switches featuring two functional states. In the active state, they bind guanosin-*tri*-phosphate (GTP) as substrate and catalyse its hydrolysis. Consequently, they reach the inactive, guanosin-*di*-phosphate (GDP) bound state (Fig. 7, (Bourne et al., 1990; Vetter and Wittinghofer, 2001)).

Small GTPases feature a common structural core characterised by the Rossmann fold (Rossmann et al., 1974) also known as nucleotide-binding fold with a three layer architecture ($\alpha/\beta/\alpha$). The central β -sheet spans six anti-parallel β -strands. Characteristically, small GTPases contain five conserved consensus elements, termed G-elements (G1-G5), which are important for nucleotide binding (Bourne et al., 1991; Sprang, 1997; Vetter and Wittinghofer, 2001) (Tables 2, 3; Fig. 8A). The loops including the G-elements G2 and G3 change their conformation upon GTP hydrolysis, these flexible regions are therefore called switch I and switch II, respectively.

Small Ras-like GTPases are a large group of small GTPases sharing structural and functional characteristics with Ras. Small Ras-like GTPases comprise a conserved structural fold, a characteristically ~30 % sequence identity (Corbett and Alber, 2001), a slow intrinsic hydrolysis rate and a relatively high affinity for nucleotide (Luirink and Sinning, 2004; Sprang, 1997). The low hydrolysis rate of small Ras-like GTPases is increased by GTPase activating proteins (GAPs).



Guanyl nucleotide exchange factors (GEFs) facilitate the release of GDP and stabilise the nucleotide-free state (Vetter and Wittinghofer, 2001). Binding of GTP is favoured by the excess of GTP versus GDP inside the cell. In the SRP system, SR β is the only Ras-like GTPase.

In contrast to classical small Ras-like GTPases, SRP54, SR α and their respective homologues in different species form a special class of small GTPases called SRP GTPases (Bourne et al., 1990). The flagellum protein FlhF shares the common fold of SRP GTPase but is dispensable for protein secretion (Zanen et al., 2004).

SRP GTPases are characterised by a much lower affinity for nucleotides compared to regular Ras-like GTPases ($K_D = 2 - 80$ pM for Ras and Ran, and $2 - 10$ μ M for SRP GTPases) (Jagath et al., 1998; Moser et al., 1997) and are stable even in the empty form (Rapiejko and Gilmore, 1997). The SR/FtsY and SRP54/Ffh form this special subclass of SRP GTPases (see below).

SRP GTPases differ structurally from classical small Ras-like GTPases by an $\alpha/\beta/\alpha$ insertion (Montoya et al., 1997; Moser et al., 1997) named I box, which is located between G2 (Switch I) and G3 (switch II) (Fig. 8B). The I box is proposed to function as a build-in GEF (Montoya et al., 1997; Moser et al., 1997). It is suggested that SRP GTPases are relatively stable in the empty form (Rapiejko and Gilmore, 1997). This is also supported by X-ray structures of SRP GTPases and their conserved NG domain core in the nucleotide-free state (Freymann et al., 1997; Montoya et al., 1997; Montoya et al., 2000; Ramirez et al., 2002; Rosendal et al., 2003).

For general reviews on GTPase protein folds and their mechanism, see (Sprang, 1997; Vetter and Wittinghofer, 2001).

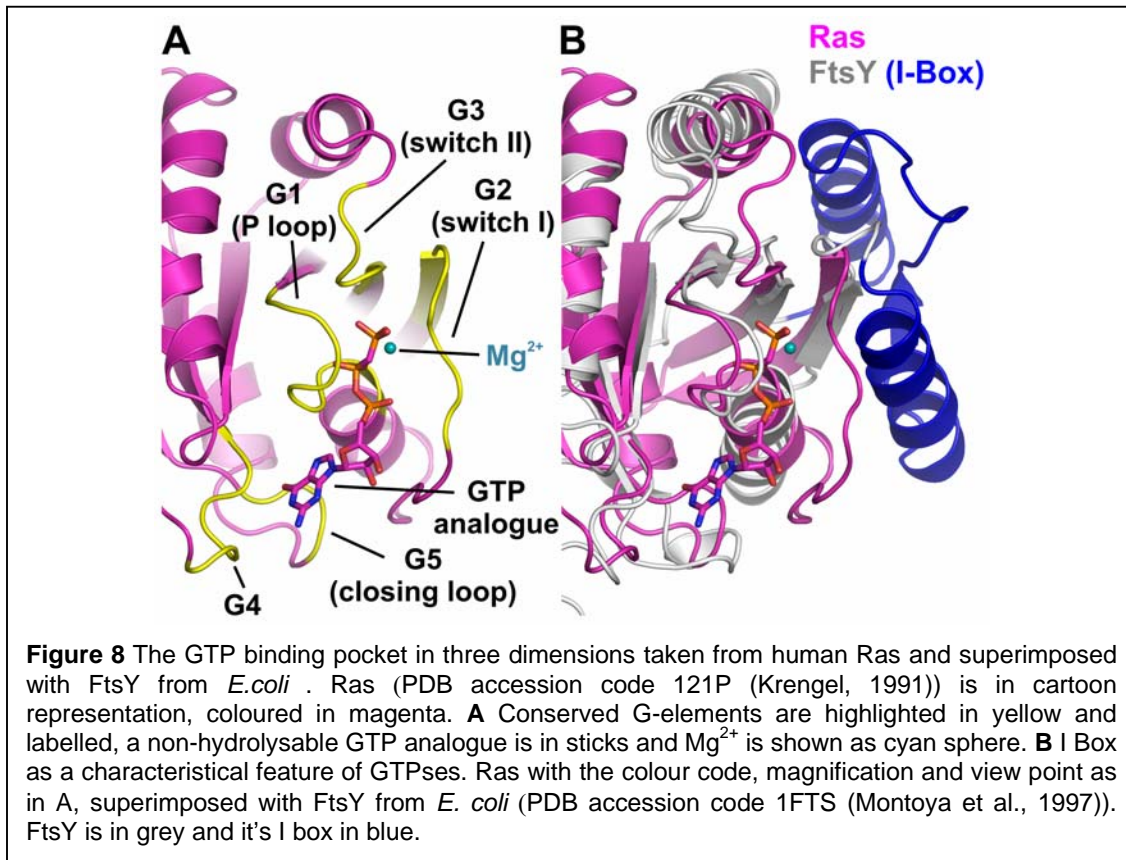
	Consensus sequence	Function
G1 (P Loop)	GxxxxGK(S/T)	Contacts α - and β -phosphate, Mg^{2+} is bound via serine/threonine
G2 (in switch I)	Includes one conserved T, that can be replaced by S	Mg^{2+} coordination in the GTP bound form; topology in SRP GTPases is here different due to the insertion of the I box featuring a $\alpha\beta\alpha$ -fold.
G3 (in switch II)	DxxG	Mg^{2+} coordination (for the conserved aspartate via an water molecule) and γ -phosphate binding; includes the catalytic residue which is important for positioning the nucleophile water for hydrolysis (His119 in SR β);
G4	(N/T)(K/Q)xD	Nucleotide specificity; the conserved aspartate recognises N1 and N2 of the guanosin base, altering this aspartate to an asparagine changes substrate specificity to XTP (Xanthosin- <i>triphosphate</i>) (for SR β this was shown by (Legate et al., 2000)).
G5 (closing loop)	-	Nucleotide coordination (via backbone contact of Ala246 for SR β)

Table 2: Consensus elements of GTP binding proteins. The five G elements are shown with their consensus sequence (there is no for G5) and the respective sequence in SR β as well as their function.

	G1	G2	G3
Consensus	GxxxxGK (S / T)	S / T	DxxG
SRβ (mouse)	⁶⁹ GLCDS ⁷⁶ G K T	⁹⁰ TQTSITDSS ⁹⁸	¹¹⁵ DLPG ¹²⁰ H E
SRβ (human)	⁶⁹ GLCDS ⁷⁶ G K T	⁹⁰ TQTSITDSC ⁹⁸	¹¹⁵ DLPG ¹²⁰ H E
SRβ _y (SRP102p)	⁴⁵ GPQNS ⁵² G K T	⁶⁶ TVVSQEPLS ⁷⁴	⁸⁷ DFFG ⁹² H V
Sar1 (human)	³² GLDNAG ³⁹ K T	⁵³ HVPTLHPTS ⁶¹	⁷⁵ DLGG ⁸⁰ H E
Arf1 (human)	²⁴ GLDAAG ³¹ K T	⁴⁵ TIPTIGFNV ⁵³	⁶⁷ DVG ⁷² G Q D
Ras (human)	¹⁰ GAGGV ¹⁷ G K S	³² YDPTIEDSY ⁴⁰	⁵⁷ DTAG ⁶² Q E

	G4	G5
Consensus	(N / T) (K / Q) xD	-
SRβ (mouse)	¹⁷⁸ NKQ ¹⁸³ D I A	²⁴⁵ SAK ²⁴⁷
SRβ (human)	¹⁷⁸ NKQ ¹⁸³ D I A	²⁴⁵ SAK ²⁴⁷
SRβ _y (SRP102p)	¹⁵⁴ NK ¹⁵⁹ S E L F	²²⁷ SIN ²²⁹
Sar1 (human)	¹³⁴ NK ¹³⁹ I D R T	¹⁷⁹ SVL ¹⁸¹
Arf1 (human)	¹²⁶ NKQ ¹³¹ D L P	¹⁵⁹ CAT ¹⁶¹
Ras (human)	¹¹⁶ NK ¹²¹ C D L A	¹⁴⁵ SAK ¹⁴⁷

Table 3 Conservation of GTP binding elements of SRβ and its homologues. Residues conserved all through the proteins used here for comparisons are in red, strongly similar residues are in green. The residue following the conserved G in G3 represents the residue crucial for positioning the catalytic water molecule. Numbers of the first and last residue of each G-element sequence are given. Primary sequence alignment was done with ClustalW (Thompson et al., 1994) and corrected according to determined structures for G2 and G5 (accession codes: mouse SRβ: 2FH5, yeast SRβ: 1NRJ, yeast Sar1: 1M2O chain B (not included in this figure), human Arf1: 1J2J chain A, human Ras: 1CLU).



1.6 GTPases in the SRP cycle

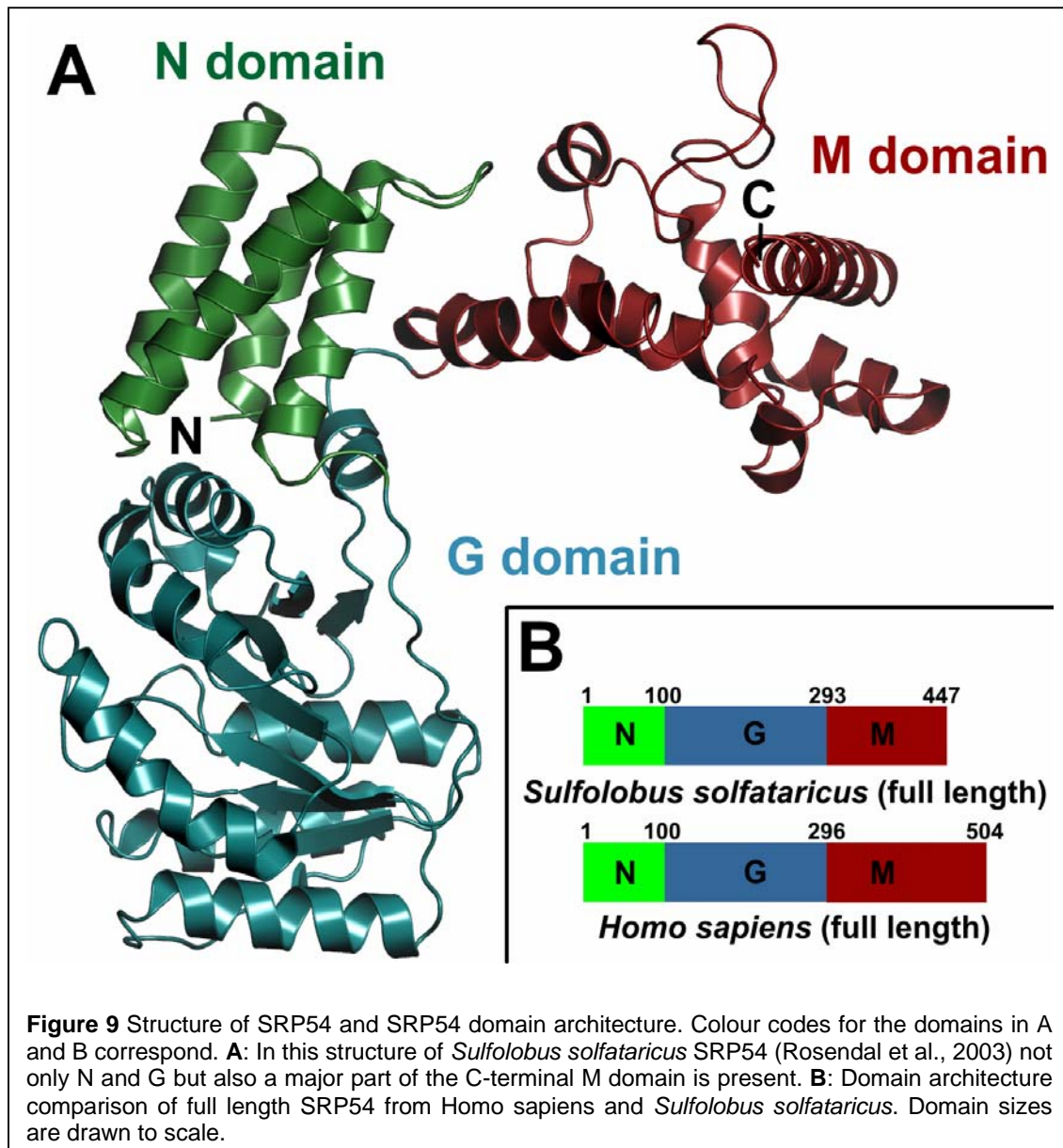
1.6.1 SRP54

SRP54 is a multi-domain protein comprising an N-terminal (N), a central GTPase (G) and a C-terminal methionine-rich (M) domain (Fig. 9). SRP54 covers all features of SRP required to function in cotranslational translocation and is the only SRP subunit which is conserved in all three kingdoms of life (Table 1). Essential SRP features are RNA and signal peptide binding (with the SRP54M domain) and GTP dependent binding to the SR (with the SRP54G domain). Unusually, the chloroplast SRP system possesses no RNA. Accordingly, chloroplast SRP54 does not contact RNA but it binds with its C-terminus the unique SRP43 protein (Groves et al., 2001). In general, the SRP54M domain (22 kD) samples and binds nascent chains emerging from the ribosome for signal peptides in order to select proteins for cotranslational translocation (Lutcke et al., 1992; Romisch et al., 1990; Zopf et al., 1990).

The NG domains (35 kD) represent the catalytic core of SRP54 (and SR α , see below) and are therefore often noted together as NG domain. The N-terminal N domain forms a four-helix bundle and packs tightly against the G domain which is the

GTPase domain of the SRP. The C-terminal M domain has been structurally determined and includes a hydrophobic groove responsible for signal peptide binding (Clemons et al., 1999; Keenan et al., 1998).

The M domain of SRP54 has also been determined in atomic detail either in complex with RNA (Batey et al., 2000), bound to the S domain and SRP19 (Kuglstatter et al., 2002), and in context with the NG domain with and without RNA (Rosendal et al., 2003).



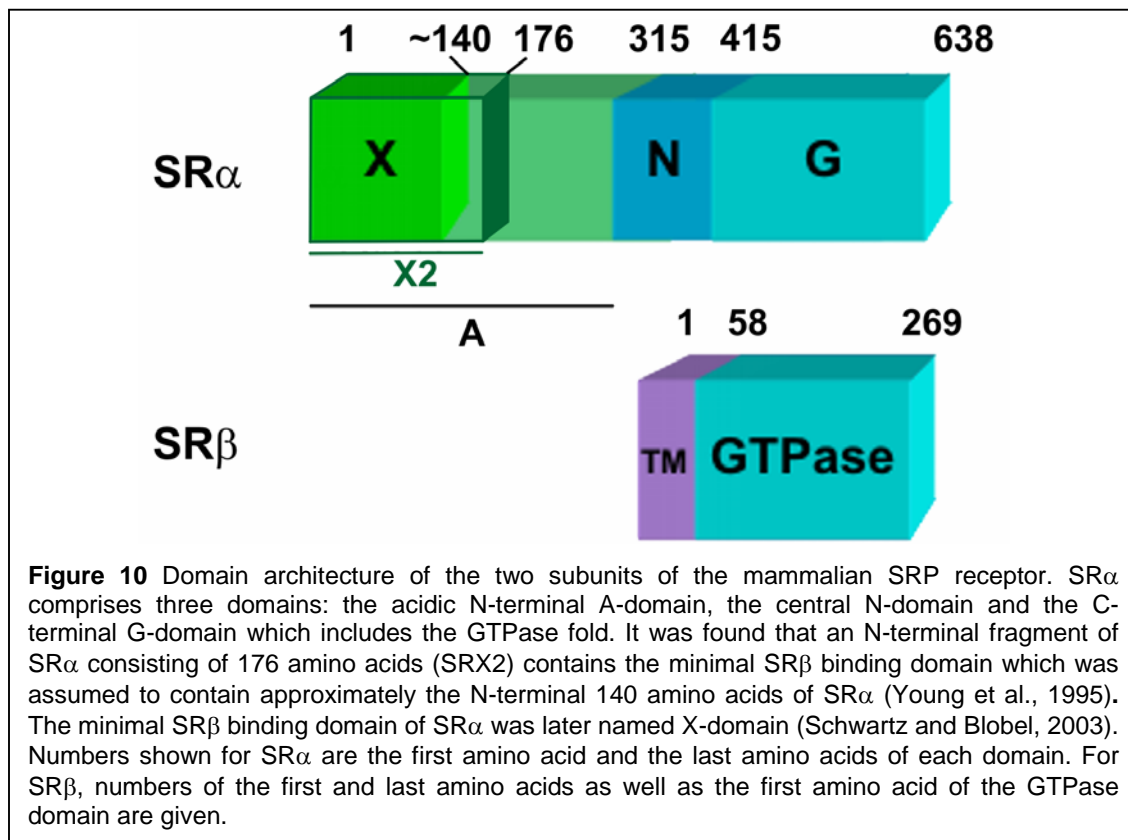
1.6.2 The Signal Recognition Particle Receptor

In eukaryotes, the signal recognition particle receptor is a heterodimer consisting of the two subunits SR α (70 kD) and SR β (30 kD) (Tajima et al., 1986).

SR α consists of the N-terminal A domain, the central N and the C-terminal G domain (Fig. 10). The GTPases SR α and SR β differ in their GTPase characteristics. SR β is more related to the 'classical' small GTPases. In contrast, SR α and SRP54 form the special subclass of SRP GTPases (see below). It was found that the N-terminal 176 amino acids of human SR α (SRX2) include the minimal domain required for SR β binding (Fig. 10) (Young et al., 1995). From proteinase K digestion of human SR α translated *in vitro* in rough reticulocyte lysate, it was estimated that the minimal SR β binding domain of SR α would comprise approximately 140 amino acids (Young et al., 1995). During this work, the minimal domain required for SR β binding was defined in yeast and termed SRX domain (Schwartz and Blobel, 2003).

SRX has been described as effector for SR β and only binds to the GTP-bound form of the GTPase (Legate et al., 2000). The SRX domain belongs to the SNARE-like superfamily including the N-terminal domains of non-syntaxin SNAREs, also known as longin domains (Filippini et al., 2001). Longin domains have been proposed to regulate a variety of membrane trafficking processes (Rossi et al., 2004). Members of this superfamily with known 3D structures include the SNAREs Sec22b (Gonzalez et al., 2001) and Ykt6 (Tochio et al., 2001), the component SEDL of the transport protein particle (TRAPP) (Jang et al., 2002), and the clathrin adaptor proteins AP- σ and AP-N μ (Collins et al., 2002; Heldwein et al., 2004).

SR β is a classical small Ras-GTPase most similar to Arf (ADP-ribosylation factor) and Sar1 (Secretion-associated and Ras-related 1) with an accordingly low K_D of ~30 nM for GTP (Bacher et al., 1999; Miller et al., 1995). Phylogenetically, SR β together with Arf and Sar1 separated from other small Ras-GTPases already in the earliest branching event indicating the functional importance of an ancestral SR β in eukaryotic evolution (Jekely, 2003). A special feature of SR β is its predicted membrane spanning helix, which is dispensable for SR function (Ogg et al., 1998). In comparison, proteins of the Arf and Sar1 family have an extra N-terminal helix that is preceded by an N-terminal hydrophobic patch in Sar1 (Huang et al., 2001) and becomes myristoylated in Arf (Chavrier and Goud, 1999). The GTPases are anchored in the GTP-bound state to their target membrane.



The functional homologues of the mammalian SR α subunit are in yeast SRP101p (Ogg et al., 1998) and in prokaryotes FtsY (Bernstein et al., 1989; Lührink et al., 1994; Miller et al., 1994). The protein homologous to SR β in yeast is named SRP102p (Ogg et al., 1998), in prokaryotes there is no such homologue (Lührink and Sinning, 2004). Accordingly, FtsY is N-terminally shorter when compared to SR α (Gill et al., 1986) and does consequently not contain a domain homologous to the SR β binding domain (Young et al., 1995). In prokaryotes, FtsY binds directly to the cytoplasmic membrane (Lührink et al., 1994) due to an affinity to phospholipids (de Leeuw et al., 2000; Millman et al., 2001). The lack of SR β in prokaryotic cells may be explained by the fact that SRP is not required to be targeted to a specific organelle such as the ER in eukaryotes. In prokaryotes, unspecific membrane affinity (Millman et al., 2001) and the ability to bind directly to the prokaryotic translocon (Angelini et al., 2005) allow FtsY to be functional in cotranslational translocation. SR β and the SRX domain of SR α can be regarded as molecular adaptations of the SRP system to the complex eukaryotic endomembrane system.

1.7 GTPases Regulate the SRP Cycle

In eukaryotic cells, three small GTPases are involved in the regulation of the SRP cycle: the SRP GTPases SRP54 and SR α , and the small Ras-like GTPase SR β . SR α and SR β form the SR.

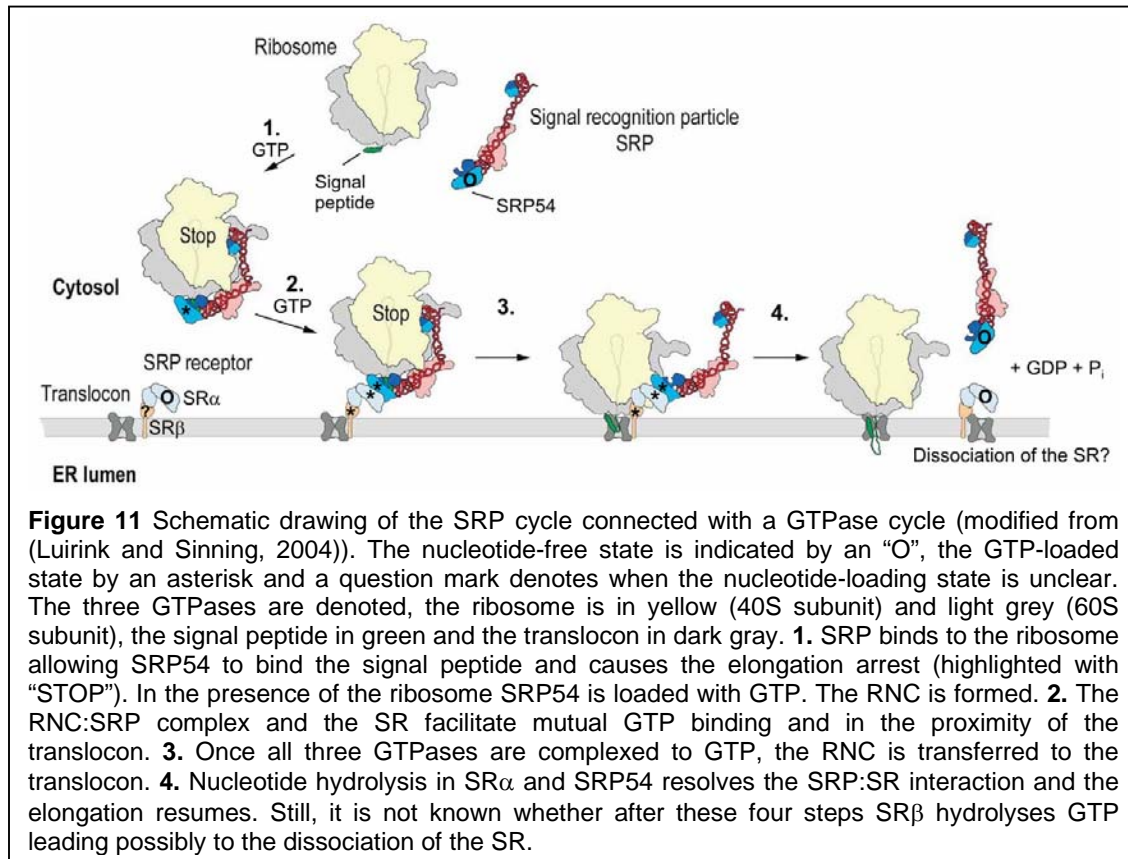
In the first step SRP binds to the ribosome. SRP54 scans the nascent chain emerging from the ribosomal exit tunnel for the signal peptide (Fig. 11). Once a nascent chain is bound to SRP54, the affinity of SRP54 for GTP is increased (Bacher et al., 1996). The RNC acts as a nucleotide loading factor for SRP54. GTP affinity for SRP54 is also increased by the SR and GTP hydrolysis in SRP54 is inhibited by signal peptide binding (Miller et al., 1993). The concomitant elongation arrest is mediated by the *Alu* domain of the SRP (Siegel and Walter, 1986).

In the second step the SRP:SR complex is formed. SRP54 is the SRP protein targeting the SRP:RNC complex to the ER membrane (Bacher et al., 1996) due to its interaction with the SR in a GTP dependent manner (Connolly and Gilmore, 1993). It was shown that the functional GTP binding site in SR α is crucial for protein translocation across the ER membrane (Rapiejko and Gilmore, 1992). Insights in the SRP:SR docking state were recently shown by the determination of the X-ray structures of the FtsY and Ffh NG domains from *Thermus aquaticus* (Egea et al., 2004; Focia et al., 2004) (Fig. 12) and *Sulfolobus solfataricus* (Sinning group, unpublished results). Due to the high degree of homology these structures can serve as general models of the SRP:SR interaction. The complexes were formed in presence of a non-hydrolysable GTP analogue. Two of these substrate molecules contribute to the interface in a uniquely twinned manner with each ribose contacting the γ -phosphate of the other substrate (Fig. 13). The SR:SRP54 complex is formed by cooperative binding of GTP. Dissociation requires mutual GTP hydrolysis (Rapiejko and Gilmore, 1997) following molecular mechanisms that are not yet understood.

SR β is suggested to co-ordinate the presence of the RNC:SRP:SR complex with the proximity of the translocon (Fulga et al., 2001) which is crucial for the third step in the cycle, the transfer of the signal peptide from SRP to the translocon.

SR β alone does not hydrolyse GTP (Legate and Andrews, 2003; Mandon et al., 2003). It is also not activated in complex with either SR α or SRX (Bacher et al., 1999). Like for other small Ras-GTPases, a GTPase-activating protein (GAP) and a

guanine nucleotide exchange factor (GEF) are necessary to drive the GTPase cycle (Bourne et al., 1990; Vetter and Wittinghofer, 2001).



RNCs interact with SR β in its GTP-bound state (Bacher et al., 1999). GTP binding to SR β is stimulated by the translocon and is suggested to be required to release the nascent chain from the SRP-SR complex (Fulga et al., 2001). The GAP function for trypsin-digested SR heterodimers that retain SR β and the N-terminal fragment of SR α (including SRX) has been attributed to the RNC complex (Bacher et al., 1999). In contrast, GAP function of the RNC for the isolated SR β could not be found (Legate and Andrews, 2003; Mandon et al., 2003).

In the yeast system, the GEF activity for SR β has been assigned to the two orthologues (Sbh1p, Sbh2p) of the Sec61 β subunit of the translocon (Helmers et al., 2003) and point mutations in the cytoplasmic loops of the yeast translocon severely affect the co-translational translocation pathway (Cheng et al., 2005). However, the molecular details for the initiation of GTP hydrolysis and the subsequent GDP release from SR β remain so far unclear.

All three GTPases involved in the SRP cycle have to be in the active GTP state to allow the transfer of the signal peptide (Fulga et al., 2001) (Fig. 11). Release of the signal peptide might enable the inhibited SRP54. SRP54 and SR act as mutual GAPs. GTP hydrolysis in both SRP GTPases leads to the dissociation of the SRP:SR complex (Connolly et al., 1991; Rapiejko and Gilmore, 1997) in the fourth step of the SRP cycle (Fig. 11). GDP can easily dissociate from SRP54 and SR α due to the low nucleotide affinity for SRP GTPases, and also relatively stable nucleotide-free forms of SR α and SRP54 can occur (Rapiejko and Gilmore, 1997). Finally, SRP is available for another round of targeting. For reviews see (Keenan et al., 2001; Lührink and Sinning, 2004; Wild et al., 2004).

It is not known whether GTP hydrolysis of SR β occurs in each SRP cycle.

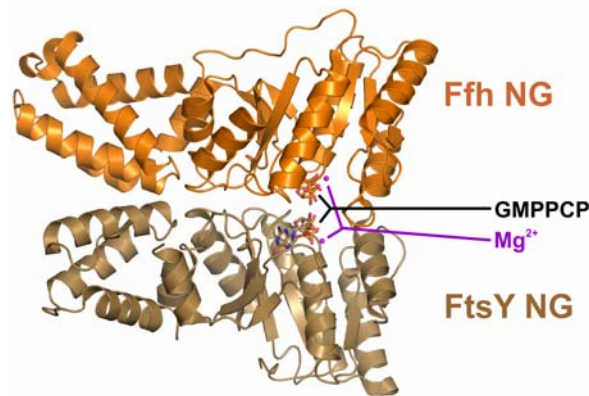


Figure 12 X-ray structure of the *Thermus aquaticus* FtsY Ffh NG NG complex (PDB accession code 1OKK). NG domains are in cartoon representation, the non-hydrolysable GTP analogue GMPPCP is in sticks, Mg²⁺ is depicted as magenta spheres.

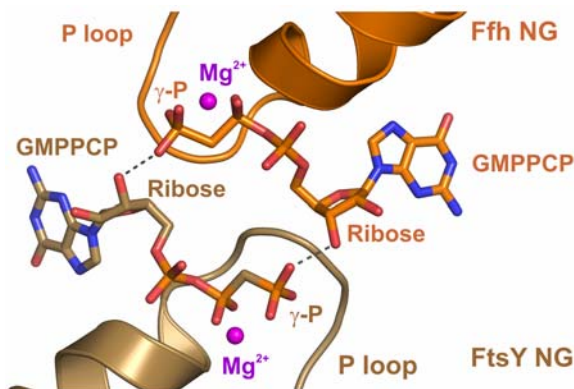


Figure 13 Close-up of the nucleotides in the FtsY Ffh NG NG complex. P loops (cartoon representation), Mg²⁺ (magenta spheres) and nucleotides (sticks). The ribose of each nucleotide is interacting with the γ -phosphate (γ -P) of the other substrate.

1.8 Aim of this Work

In the SRP cycle the roles of the two SRP GTPases SRP54 and SR α , and their respective homologues from other species, are rather well characterised. The intimate contact of the two NG domains allows the formation of the SRP:SR complex at the membrane. In eukaryotes, a third GTPase is present with SR β which is poorly understood. It was suggested that the translocon acts as a GEF for SR β and that the RNC might act as a GAP for SR β . Molecular details of the GTPase cycle of SR β were however not known. Therefore, this work focuses on the structural and functional analysis of SR β in the context of the SRP:SR complex.

In particular, these were the aims:

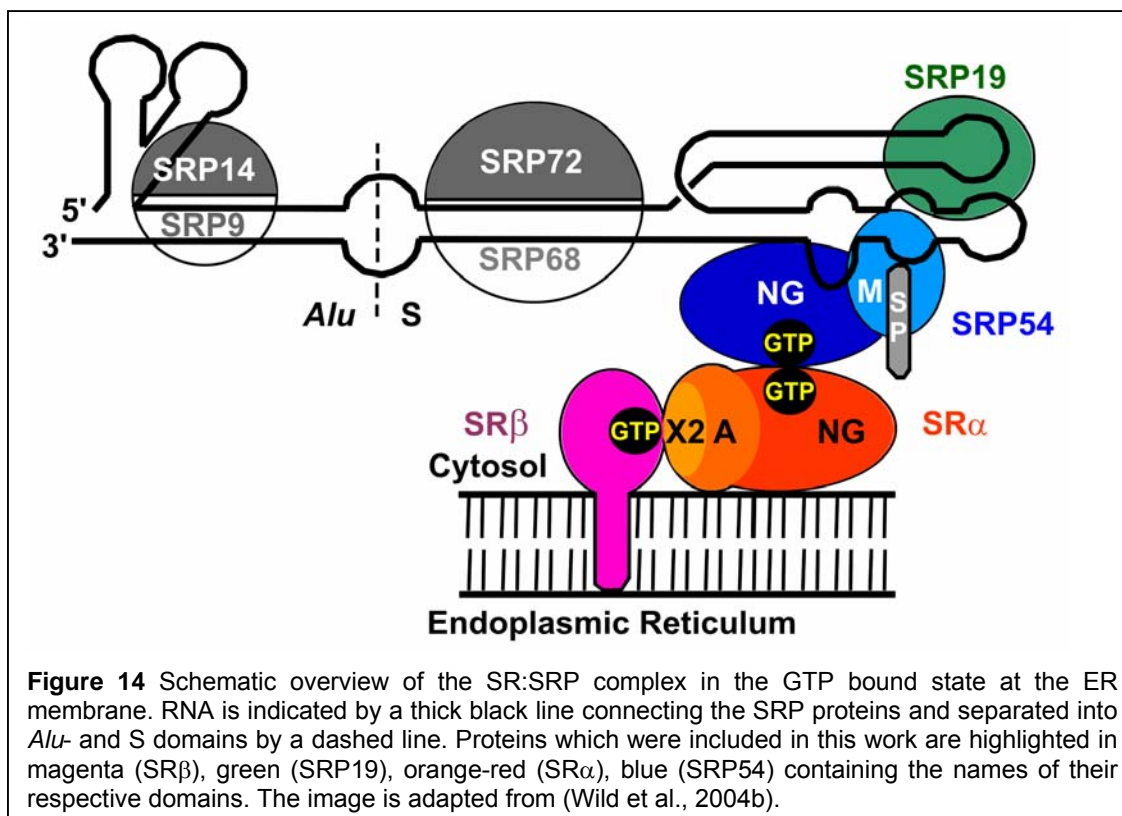
- Understanding the role of SR β in the SRP cycle by X-ray structure determination of relevant subcomplexes of SR α : β .
- Investigating the SRP:SR interaction by complex formation studies of a trimeric complex composed of SR α : β Δ TM and SRP54, and a pentameric complex consisting of SR α : β Δ TM, SRP54, SRP19 and RNA¹⁰⁴.
- Characterisation of the SR-translocon interactions.

2 Results

2.1 Expression and Purification of SR and SRP proteins

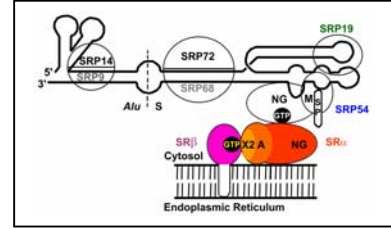
Proteins of the mammalian SRP system were cloned, expressed and purified in order to understand molecular mechanisms of the interaction of SRP with its receptor and the interaction of SR β with external regulators using mainly X-ray crystallography. Of particular interest were functionally relevant interfaces of SR β which anchors SR α to the ER membrane and was suggested to interact with the translocon. The second focus was the interface between SR α and SRP54 which allows the binding of the RNC:SRP complex to the SR. In order to examine the conformational arrangements of SRP when bound to its receptor, a complex of the SR and SRP54 was reconstituted (SR α^{His} : $\beta\Delta TM$:SRP54D^{His}) and SRP RNA and SRP19 were added to bind to the SRP54 subunit forming a pentameric complex (SR α^{His} : $\beta\Delta TM$:SRP54D^{His}:SRP19:RNA¹⁰⁴) from purified components.

The schematic overview from Figure 14 is introduced in order to highlight SRP proteins presented in this chapter in context with their binding partners. The scheme will be shown in the beginning of each subsection to highlight the proteins of interest.



2.1.1 SR α^{His} : $\beta\Delta$ TM

The mammalian SRP receptor is a heterodimeric complex consisting of the two GTPases SR α and SR β (Tajima et al., 1986). The SR lacking the transmembrane region (SR α : $\beta\Delta$ TM) complex has been shown to be functional *in vitro* (Abell et al., 2004; Fulga et al., 2001; Ogg et al., 1998).



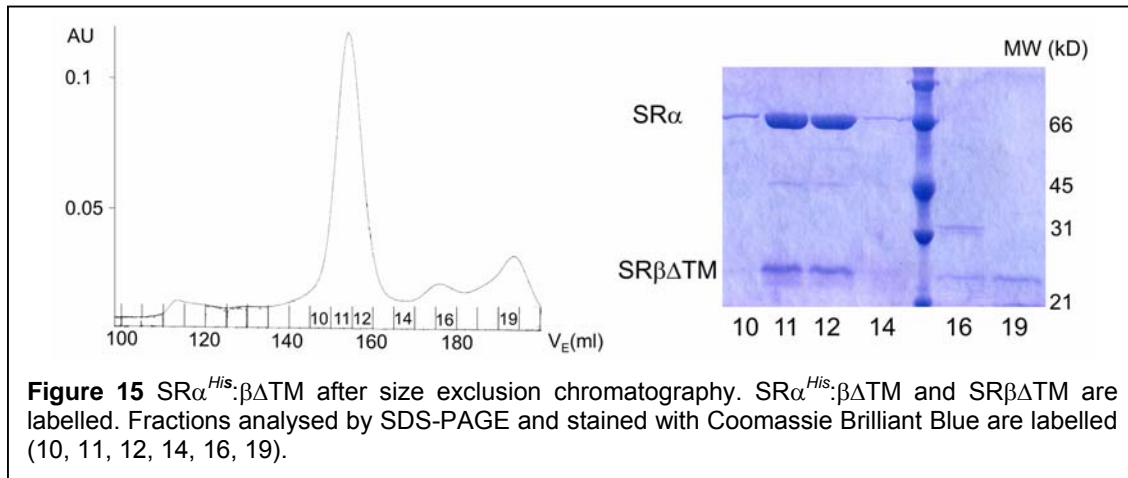
The SR subunits were co-expressed from a bicistronic plasmid generating a stable complex (SR α^{His} : $\beta\Delta$ TM) (Fulga, 2001). The preparation involves four purification steps and is based on (Fulga, 2001). Firstly, the N-terminal hexa-His tag of SR α in the SR α^{His} : $\beta\Delta$ TM complex was used for Ni²⁺-affinity purification.

Secondly, anion exchange chromatography is applied. Here, the pH is adjusted in a way that SR α^{His} : $\beta\Delta$ TM is positively charged and does not bind. The protein is therefore found in the flow-through. Minor contaminations and DNA are removed from the sample. Subsequently, in cation exchange chromatography the protein is bound to the resin, contaminations and minor amounts of SR α^{His} : $\beta\Delta$ TM are found in the flow-through.

Finally, the protein is purified via size-exclusion chromatography (Superdex 200 (26/60)) and appears as a single peak at elution volume (V_E) 155 ml with a calculated molecular mass of ~ 200 kD (Fig. 15). This molecular weight correlates to approximately the double molecular mass of SR α^{His} : $\beta\Delta$ TM and may be explained by an elongated shape caused by the polypeptide linking the SRX and NG domains since both subdomains do not show an elution volume correlating to a disproportionately high molecular weight (see below).

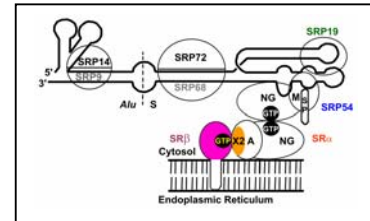
By sedimentation equilibrium centrifugation it has been shown before that SR α^{His} : $\beta\Delta$ TM appears as a 'monomer' (Fulga, 2001). Equilibrium centrifugation experiments performed by Karsten Rippe and Jacek Mazurkiewicz (Kirchhoff Institut für Physik, Heidelberg) supported this result but experiment could not be evaluated accurately because the protein aggregated partially during the equilibrium ultra-centrifugation run. Static light scattering experiments showed a molecular weight slightly elevated from the 'monomeric' complex, verifying its 'monomeric' state (not shown).

Results



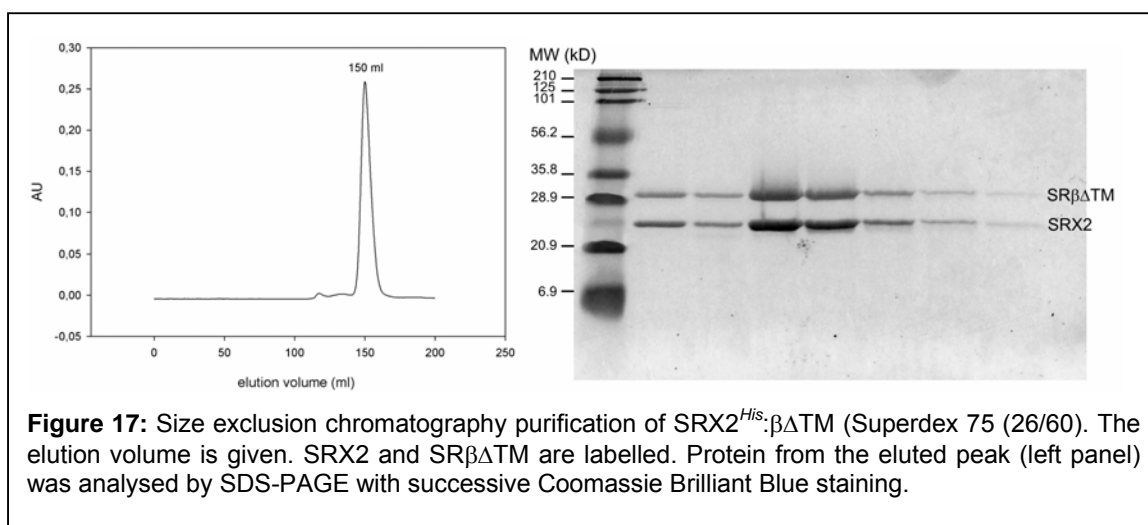
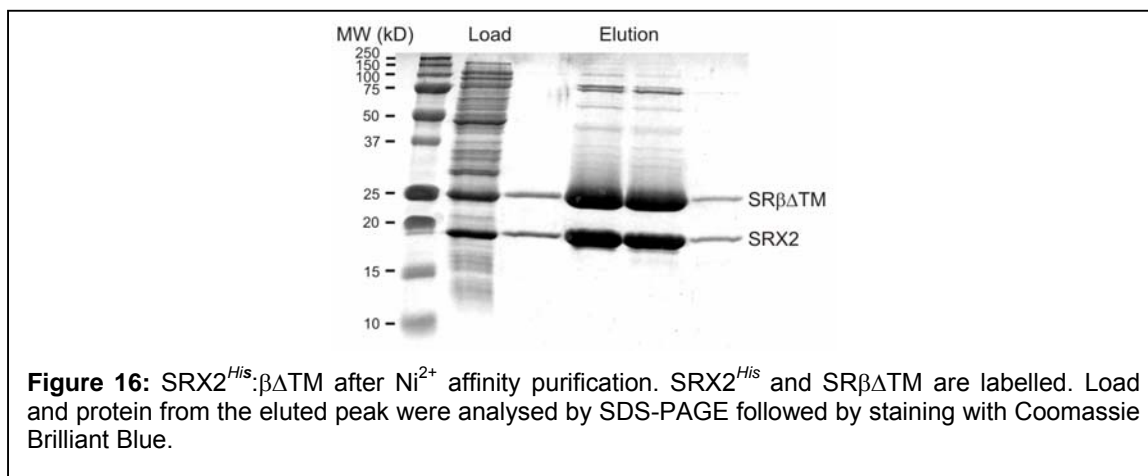
2.1.2 SRX2^{His}: $\beta\Delta TM$

The SRX2^{His}: $\beta\Delta TM$ construct contains SR $\beta\Delta TM$ and the N-terminal 176 amino acids of SR α including the minimal SR β -binding domain (Young et al., 1995) (SRX) with an N-terminal hexa-His tag.



The heterodimeric complex was expressed and purified based on the method used for SR α^{His} : $\beta\Delta TM$. Buffers were adjusted from previously published recipes (Fulga, 2001) in order to optimise the purification. The protein after Ni²⁺-affinity purification is shown in Fig. 16 and appears to be in a pure and 'monomeric' state after size exclusion chromatography (Fig. 17). SRX2^{His}: $\beta\Delta TM$ elutes at 146 ml from a Superdex 75 (26/60) column. The 'monomeric' state was also verified by analytical ultra-centrifugation experiments performed by Karsten Rippe and Jacek Mazurkiewicz (Kirchhoff Institut für Physik, Heidelberg (see below)). The protein showed a slight tendency to form dimers ($K_D = 270 \mu M$).

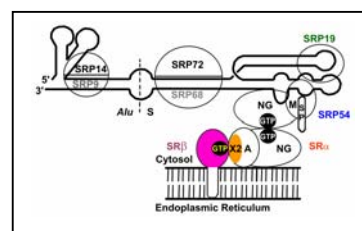
Results



2.1.3 Seleno-L-Methionine Substituted SRX2^{His}:βΔTM

Seleno-L-methionine substituted protein was expressed for crystallisation and the determination of phase information by a successive SAD experiment. Additional phase information was required in order to improve the model achieved from the Srax3-2 data set

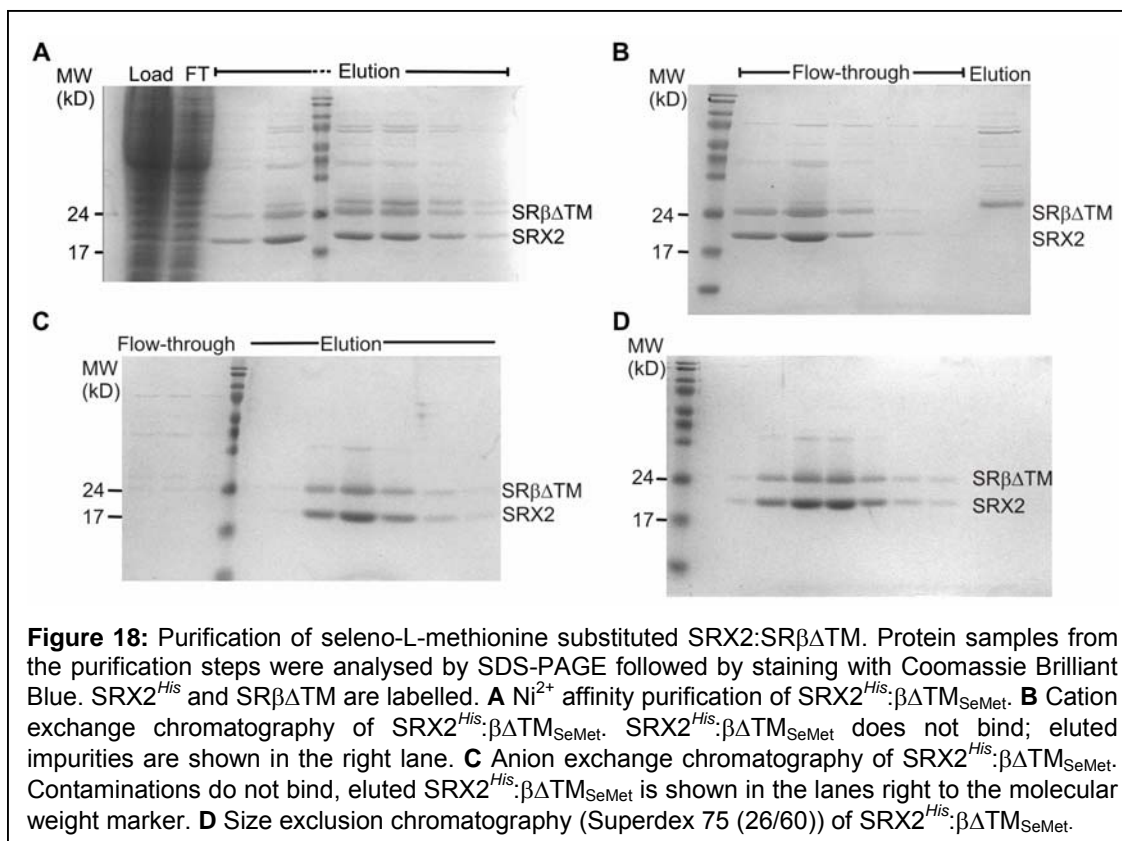
(see below). The protein expressed and purified as described here led to crystals subjected to a SAD experiment at beamline ID 14-4 (ESRF, Grenoble). Phase information obtained from this experiment was not included in the bootstrapping



Results

process for the final model due to the low phasing power of the seleno-L-methionine substituted crystals.

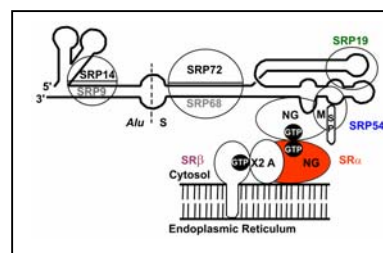
Expression of seleno-L-methionine substituted $\text{SRX2}^{\text{His}}:\beta\Delta\text{TM}$ was performed in methionine auxotroph cells and in a medium including all amino acids but not methionine which was replaced by seleno-L-methionine. Otherwise, conditions of expression and purification were kept as described for $\text{SRX2}^{\text{His}}:\beta\Delta\text{TM}$ (see above). The course of purification is illustrated in Fig. 18.



2.1.4 $\text{SR}\alpha\text{NG}^{\text{His}}$ ($\text{SR}\alpha\text{N}\Delta 314\text{-NHis}$)

In order to understand the function of the catalytic core of $\text{SR}\alpha$ its C-terminally located NG domain (residues 315 to 638) was cloned and expressed for crystallisation. It was assumed that the NG domain

would be a rigid protein suitable for crystallisation since homologues prokaryotic and archeal NG domains have been crystallised before (Egea et al., 2004; Focia et al.,



Results

2004; Freymann et al., 1997; Montoya et al., 1997; Montoya et al., 1999; Padmanabhan and Freymann, 2001; Ramirez et al., 2002).

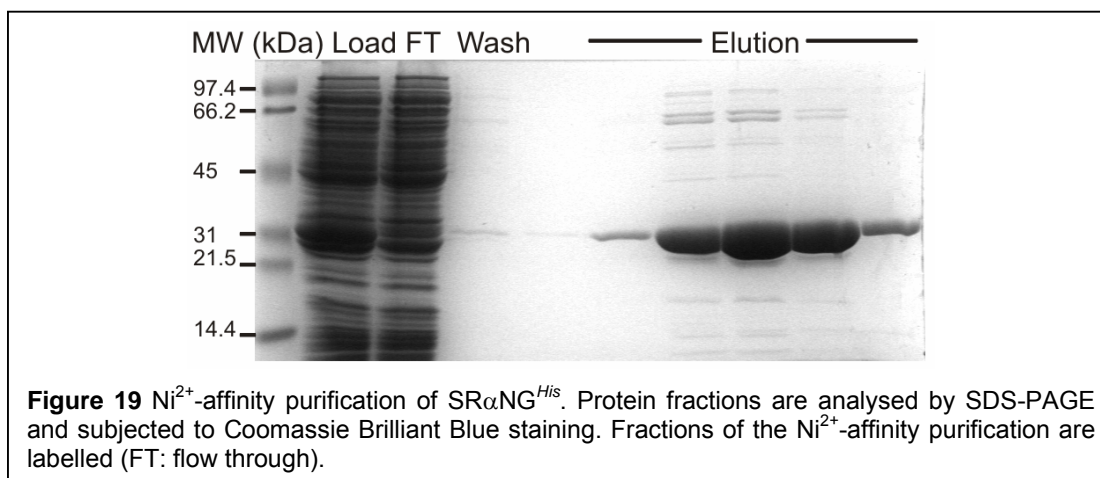
Cloning of SR α NG^{His} into pET16b resulted in a construct that could be easily expressed. Test-expressions are summarised in Table 4 and Fig. 19 shows the Ni²⁺-affinity tag purified protein. The purified protein easily precipitated. Protein precipitation could be prevented for more than 24 h by using protein concentrations below 2 mg/ml and including minimal 10% of glycerol into the buffer. The protein seemed to precipitate less at room temperature than at 4°C. Presumably, the conformation of SR α NG^{His} needs to be stabilised by a part of SR α not included in the construct.

N-terminal extension of SR α NG might stabilise the protein. Constructs which could be considered are the SR α degradation fragment described by Claudio Moser (SR α Δ 285) (Moser, 1998) or the SR α elastase fragment (Andrews et al., 1989; Young et al., 1995) which was also characterised by Claudio Moser (Moser, 1998). These constructs were not examined in this work.

Cells used for expression	Remarks
BL21 (DE3)	Expression works, gives not most but purest protein after Ni ²⁺ -affinity purification
Rosetta (DE3)	Weak expression
BL21 (DE3) pLysS	Weak expression
C43 (DE3)	Protein seems to degrade mainly to a 28.9 kD species
Rosetta (DE3) pLysS	Highest expression rate, more impurities after Ni ²⁺ -affinity purification compared to BL21 (DE3) expressed protein

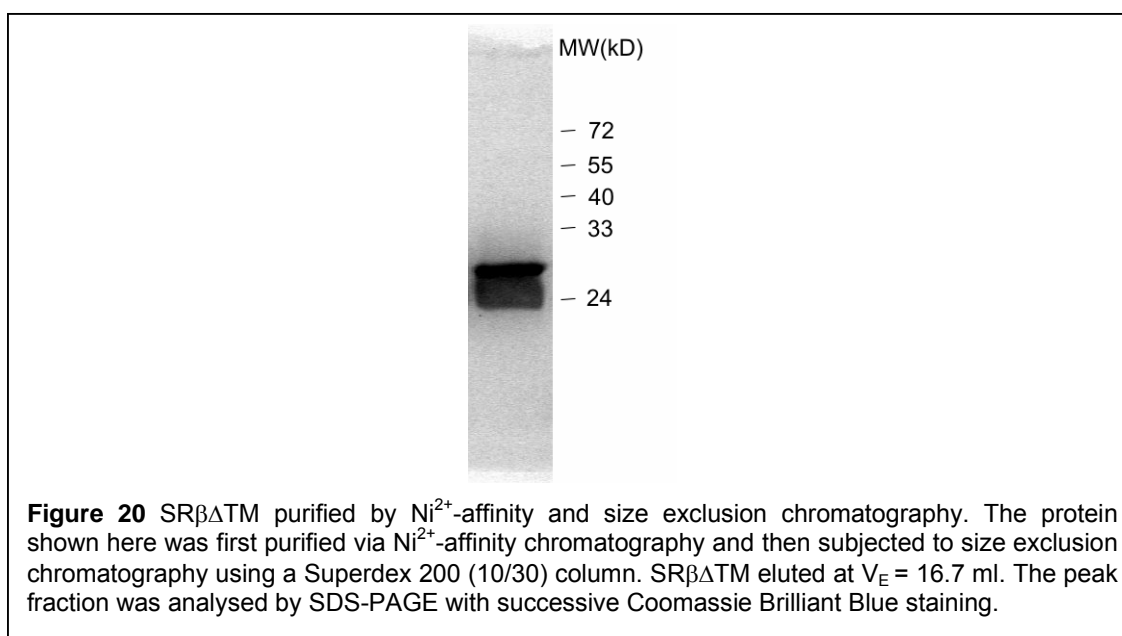
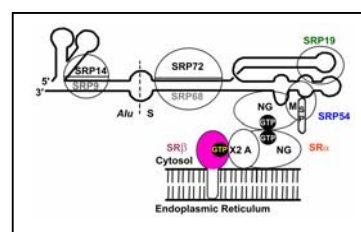
Table 4: Test-expression results of SR α NG^{His} expressed ON at 16°C, induced with 0.5 mM IPTG and purified by Ni²⁺-affinity chromatography.

Results



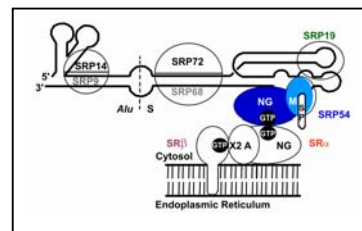
2.1.5 $\text{SR}\beta\Delta\text{TM}^{\text{His}}$

$\text{SR}\beta\Delta\text{TM}^{\text{His}}$ was expressed in order to analyse the interaction of the mammalian SR with cytosolic loops of the human translocon by an immobilised peptide library scan. Expression and purification were reproduced according the procedure described in (Fulga, 2001). Protein bound to the Ni^{2+} -saturated Fast Flow chelating resin was eluted in two steps (100 and 300mM imidazole). This led to two $\text{SR}\beta\Delta\text{TM}^{\text{His}}$ fractions, a nucleotide-free (300mM imidazole) and a mostly GTP containing fraction (100 mM imidazole) as observed before (Fulga, 2001). The nucleotide-free fraction is called here $\text{SR}\beta^{\text{His}}$ -apo. The purity of the protein after size exclusion chromatography is shown in Fig. 20.



2.1.6 SRP54^{His} (SRP54C^{term}Δ68-His)

SRP54 and its archeal and prokaryotic homologues represent the conserved core of the SRP including the catalytic NG domain and the C-terminal M-domain which binds signal sequences (High and Dobberstein, 1991; Zopf et al., 1990) and SRP RNA (Romisch et al., 1990). SRP54 interacts with the SR (Connolly and Gilmore, 1993) and a functional GTP binding site in SR α is crucial for protein translocation across the ER membrane (Rapiejko and Gilmore, 1992). SRP54 and SR α allow the GTP dependent formation of the docking complex including the RNC and the SR at the ER membrane.

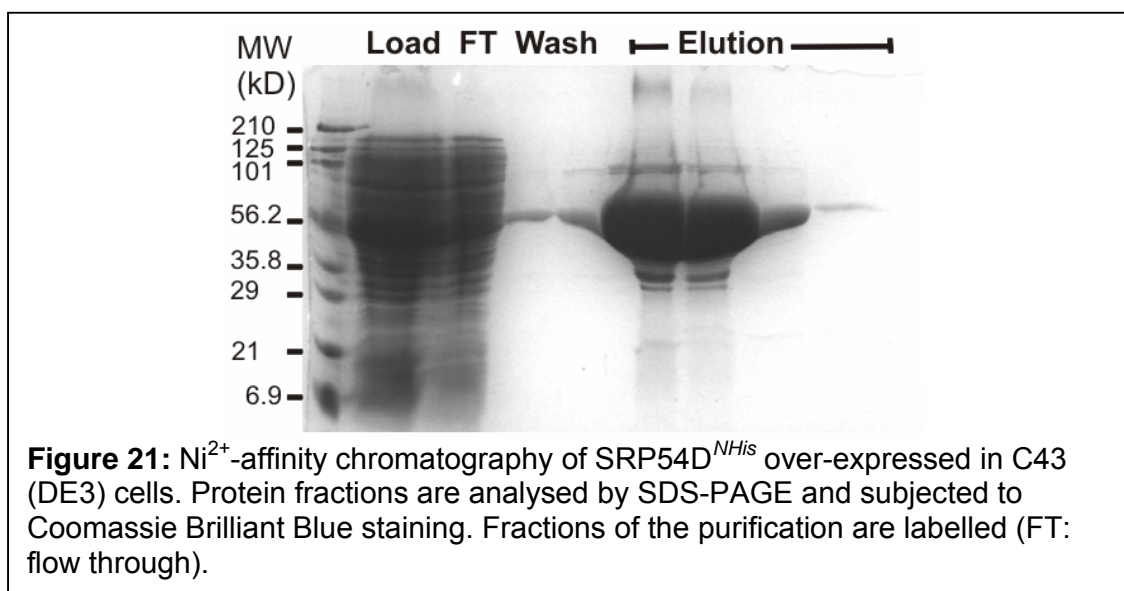


In order to understand the GTPase function of SRP54 alone or in complex with interacting proteins, SRP54 constructs with a hexa-His tag were cloned, expressed and purified containing the NG domain and 140 of the 208 residues of the C-terminal M-domain (SRP54D^{His}). SRP54D with a C-terminal hexa-His tag was named accordingly SRP54D^{CHis} and with a N-terminal hexa-His SRP54D^{NHis}. The C-terminus of the M-domain was defined according to the X-ray structure of the *E. coli* RNA:SRP54M domain complex and the respective sequence alignment of SRP54M domains from Doudna and co-workers (Batey et al., 2000). The C-terminal truncation was aimed to express a SRP54 construct with a rigid C-terminus suitable for crystallisation.

Cells used for expression	Remarks
BL21 (DE3) pLysS	Weak over-expression
Rosetta (DE3) pLysS	Over-expression level significantly higher than in BL21 (DE3), but weaker than in C43 (DE3)
C43 (DE3)	Best over-expression, used for all further expressions

Table 5 Results from SRP54 test expression experiments.

Results



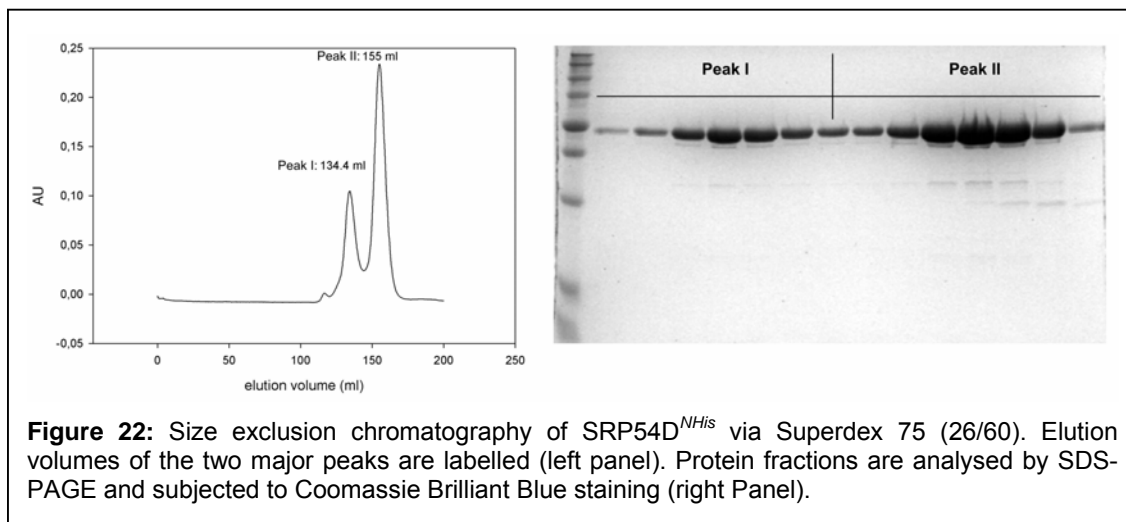
SRP54D^{His} was routinely expressed in C43 (DE3) cells (Table 5, Fig. 21). The protein was purified using Ni²⁺-affinity chromatography (Fig. 21). Size-exclusion chromatography using Superdex 75 (16/60) (Fig. 22) revealed that a part of the protein appeared as a dimer (V_E (dimer) = 134 ml) with a majority of the protein still in monomeric form (V_E = 155 ml).

SRP54D^{His} and SRP54NG^{His} (see below) expressed in *E. coli* showed a tendency to form homodimers. Both SRP54 constructs contained the SRP54NG domain. A homodimeric interface is likely formed similar to the one existing between the SRP54NG domain homologue (Ffh) from *Thermus aquaticus* and its respective SR NG domain homologue (FtsY) (Egea et al., 2004; Focia et al., 2004) and *Sulfolobus solfataricus* (Sinning group, unpublished results).

After successive complex reconstitution steps with SR $\alpha^{His}:\beta\Delta TM$ and SRP19^{His}:RNA¹⁰⁴, a 'monomeric' macromolecular complex could be obtained. In this complex, the SRP54NG surface used for homodimerisation is possibly occupied by the NG domain of SR α (Egea et al., 2004; Focia et al., 2004).

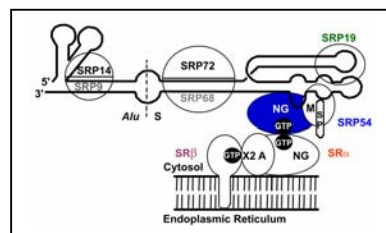
Homodimerisation of hexa-His tagged SRP54D could not be observed using protein expressed by Mark Brooks (EMBL Grenoble, Cusack group) in insect cells. Possibly, differences caused by the expression system are responsible for this behaviour.

Results



2.1.7 SRP54NG^{His} (SRP54C^{term}Δ208)

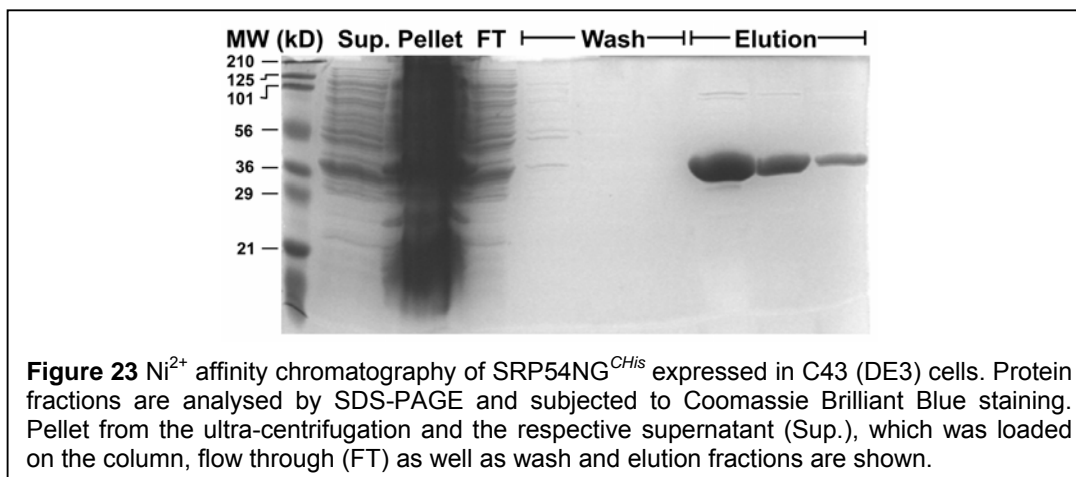
In order to examine structure and function of the human SRP54 GTPase, a construct of the human NG domain of SRP54 (SRP54NG) was cloned, expressed and purified. The expressed protein was named SRP54NG^{His} and over-expressed in C43 (DE3) cells (Table 6, Fig. 23).



Cells used for expression	Remarks
BL21 (DE3) Arg	Weak expression
Rosetta (DE3)	Weak expression
BL21 (DE3) pLysS	Expressed, but not as good yield as from C43 (DE3) or Rosetta (DE3) pLysS expression
C43 (DE3)	Nice expression, protein looks quite pure already after Ni ²⁺ -affinity purification
Rosetta (DE3) pLysS	Highest expression rate, little more impurities after Ni ²⁺ -affinity purification compared to C43 (DE3) expressed protein

Table 6: Results from SRP54NG^{His} test expression experiments.

Results



After Ni^{2+} -affinity chromatography, SRP54NG^{His} was subjected to size-exclusion chromatography and migrated as a symmetric peak ($V_E = 170$ ml on a Superdex 200 (26/60)), corresponding to the calculated molecular mass of a monomer, and a protein species with an elution volume of 136 ml, corresponding to the molecular mass of a dimer, when using a buffer with 5% glycerol and 350 mM NaCl (Fig. 24).

In high salt buffer lacking glycerol (600 mM NaCl), the monomer peak appears to be not homogeneous. A third protein species within the monomer peak can be seen ($V_E = 160$ ml). In order to examine whether the inhomogeneity in the monomeric protein peak might be caused by different nucleotide loading states, the SRP54NG^{His} was incubated ON at RT with 2 mM GDP or 1 mM EDTA supplemented buffer. The addition of GDP was intended to highlight the nucleotide loaded subfraction of the protein. In contrast, EDTA as a chelating agent for divalent cations removes Mg^{2+} from the GTP-binding site reducing concomitantly the nucleotide affinity of the GTPase. Therefore, EDTA was used often for nucleotide exchange experiments of small Ras-like GTPases such as SR β (Legate and Andrews, 2003) and Rab3A (Burststein and Macara, 1992).

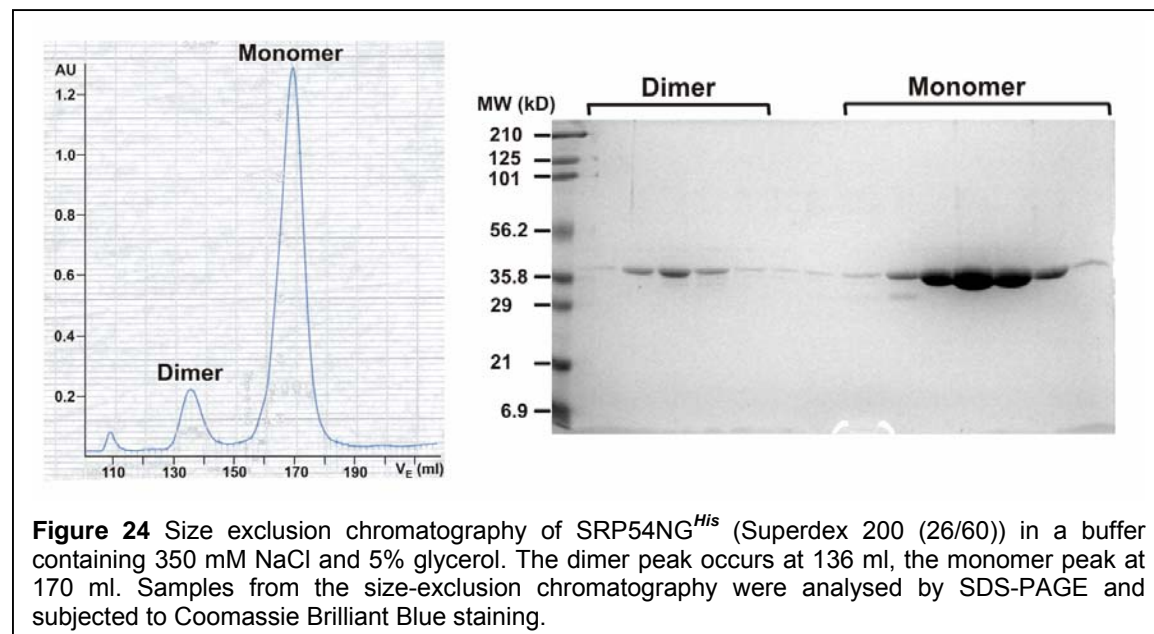
Both monomeric protein species ($V_E = 160$ ml and $V_E = 170$ ml) were present after the incubation of SRP54NG^{His} with GDP but the species at 170 ml was more prominent (Fig. 25). In contrast, in the presence of 1mM EDTA SRP54NG^{His}, most of the protein precipitated over night, implying that the removal of Mg^{2+} , and likely the bound nucleotide, from the active site led to a conformational destabilisation of SRP54NG^{His}. Analysis of the remaining soluble protein by size exclusion chromatography (Superdex 200 (26/60)) revealed the presence of only one protein

Results

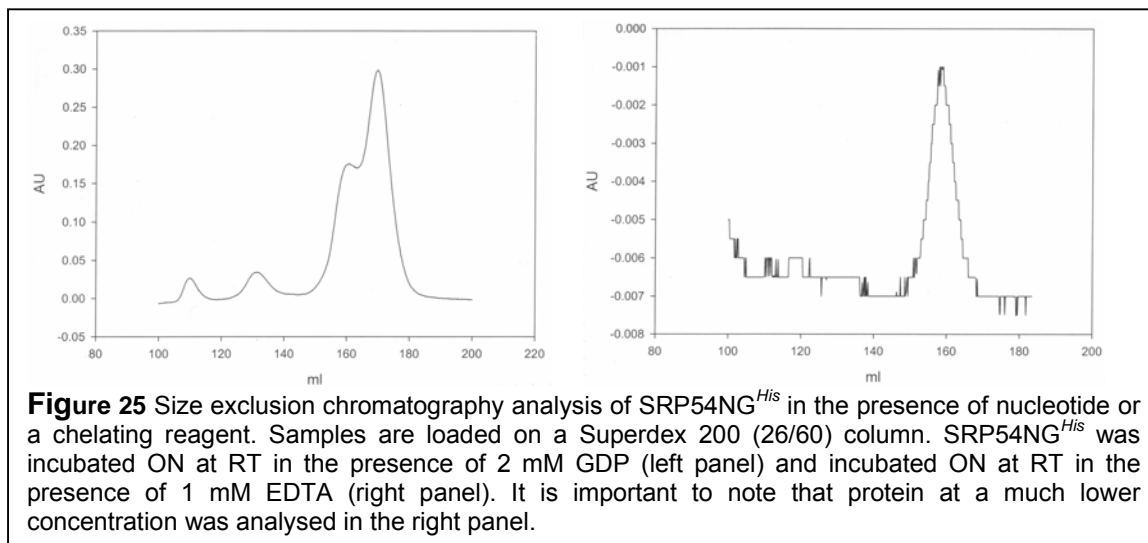
species which eluted at 160 ml, indicating that this might reflect SRP54NG^{His} in a nucleotide-free state.

The data suggest that the difference in nucleotide load is correlated to different protein conformations detected by size exclusion chromatography. This idea is supported by the fact that size exclusion chromatography separates proteins according to their Stokes radii which are dependent on the molecular weight and the shape of the protein. The observation of different nucleotide loading states is supported by measurements of the ratio of 260 nm / 280 nm absorptions. The coefficient increased over the inhomogeneous monomer peak from 0.65 to 0.98. This correlates to a six fold increase in nucleic acid contents from 0.5% to 3.0% (<http://www.bio.com/protocolstools/protocol.jhtml?id=p136>) (Layne, 1957). In summary, these results suggest that the apo- and nucleotide loaded forms of SRP54NG^{His} occur in different conformations that can be partially separated by size exclusion chromatography.

The precipitation of SRP54NG^{His} was unexpected since SRP GTPases are relatively stable in the nucleotide-free form (Moser et al., 1997; Rapiejko and Gilmore, 1997; te Kaat, 1999) supported by X-ray structures of SRP GTPases or their conserved NG domain core in the nucleotide-free state (Freyman et al., 1997; Montoya et al., 1997; Montoya et al., 2000; Ramirez et al., 2002; Rosendal et al., 2003). Future experiments have to elucidate these possibly species dependent differences in stability.



Results



2.2 Reconstitution of Different SR:SRP Complexes

In order to establish the basis for the structural characterisation of the SR in complex with the complete SRP S domain, *in vitro* reconstitution and crystallisation trials of SR:SRP S domain subcomplexes were carried out. *In vitro* reconstitution of SR:SRP complexes was set up as a tool for the functional analysis of each SR and SRP component in the assembly process.

In particular, the following complexes were reconstituted:

- (I) Trimeric complex of SR α (or the SR α (R524Q) mutant), SR $\beta\Delta$ TM and SRP54D (SR α^{His} : $\beta\Delta$ TM:SRP54D^{His} and SR α^{His} (R524Q): $\beta\Delta$ TM:SRP54D^{His} respectively).
- (II) Pentameric complex of SR α , SR $\beta\Delta$ TM, SRP54D, SRP19 and SRP RNA¹⁰⁴ (SR α^{His} : $\beta\Delta$ TM:SRP54D^{His}:SRP19^{His}:RNA¹⁰⁴).

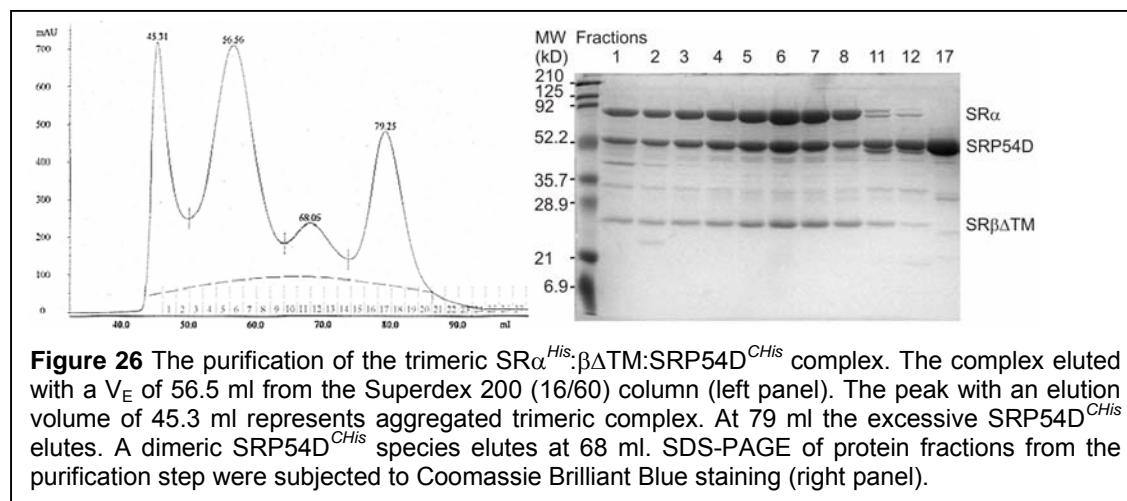
2.2.1 Reconstitution of Trimeric SR:SRP Complexes

The SR α^{His} : $\beta\Delta$ TM:SRP54D^{His} Complex

The trimeric SR α^{His} : $\beta\Delta$ TM:SRP54D^{His} complex was reconstituted with the three proteins in the stoichiometry 1:1:1. SRP54D^{His} was incubated with SR α^{His} : $\beta\Delta$ TM for one hour at 37°C in the presence of GMPPNP. The high incubation temperature was required for efficient reconstitution and made it possible to achieve the complex within a short time. A disadvantage of the high temperature was partial aggregation

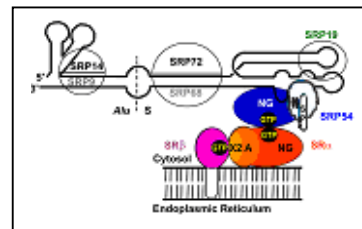
Results

of the protein. The $\text{SR}\alpha^{\text{His}}:\beta\Delta\text{TM}:\text{SRP54D}^{\text{His}}$ complex could be isolated from the reconstitution setup using size exclusion chromatography (Fig. 26).



Trimeric Complex Isolation by $\text{SRP54NG}^{\text{CHis}}$ pull-down

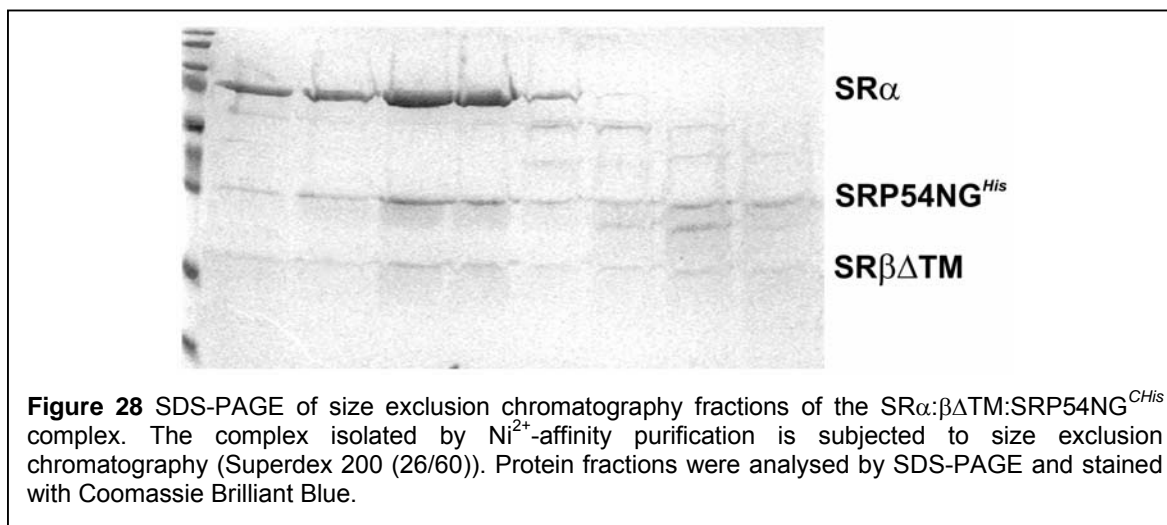
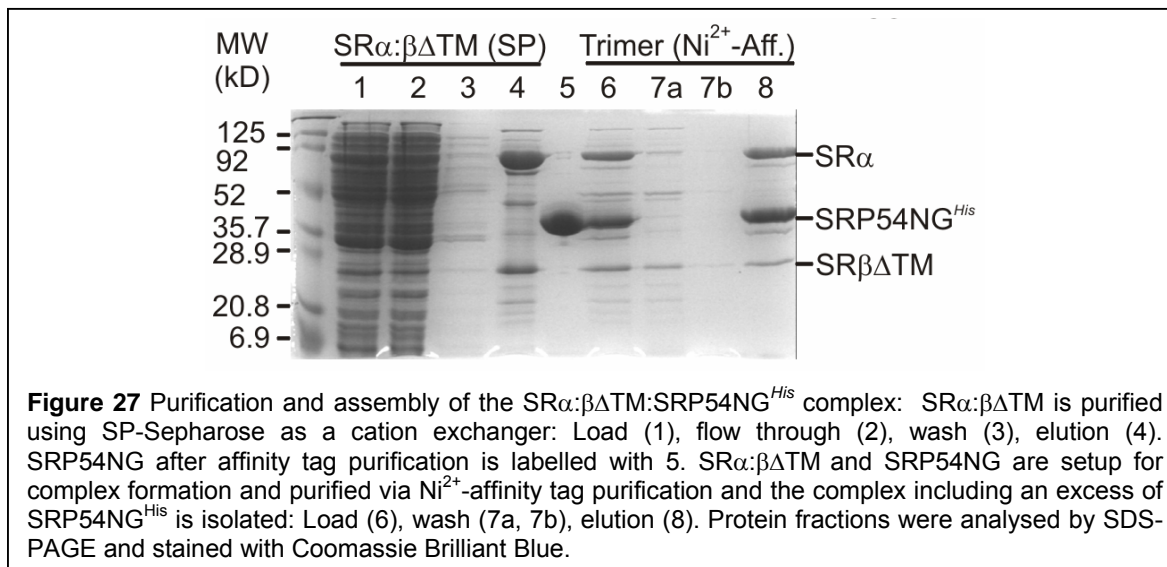
Purification of the $\text{SR}\alpha^{\text{His}}:\beta\Delta\text{TM}:\text{SRP54NG}^{\text{His}}$ complex using size exclusion chromatography includes the difficulty that $\text{SR}\alpha^{\text{His}}:\beta\Delta\text{TM}$ and the trimeric complex co-purify in the same fractions due to similar molecular weight (94.5 kD and 128 kD, respectively). This difficulty could be overcome by setting up a complex reconstitution reaction with SRP54NG and $\text{SR}\alpha:\beta\Delta\text{TM}$ where only SRP54NG included a tag ($\text{SRP54NG}^{\text{CHis}}$). $\text{SR}\alpha:\beta\Delta\text{TM}$ was pre-purified via cation exchange chromatography. After the complex reconstitution setup, the trimeric complex ($\text{SR}\alpha:\beta\Delta\text{TM}:\text{54NG}^{\text{CHis}}$) and unbound $\text{SRP54NG}^{\text{CHis}}$ were isolated by Ni^{2+} -affinity chromatography (Fig. 27). Free $\text{SR}\alpha:\beta\Delta\text{TM}$ could be found in the flow-through. An excess of $\text{SRP54NG}^{\text{CHis}}$ could easily be separated from the trimeric complex by size exclusion chromatography (Fig. 28) because of its significantly lower molecular mass of 33 kD compared to the 128 kD for $\text{SR}\alpha:\beta\Delta\text{TM}:\text{54NG}^{\text{CHis}}$.



Since the complex reconstitution step did not require 37°C, possibly the $\text{54NG}^{\text{CHis}}$ homodimer is less stable than the $\text{SRP54D}^{\text{His}}$ homodimer. This method overcomes the problem that $\text{SR}\alpha^{\text{His}}:\beta\Delta\text{TM}$ can not be separated by size exclusion chromatography from the $\text{SR}\alpha^{\text{His}}:\beta\Delta\text{TM}:\text{SRP54NG}^{\text{His}}$ complex. The same difficulty occurs in size-exclusion chromatography of a mixture of $\text{SR}\alpha^{\text{His}}:\beta\Delta\text{TM}$ and

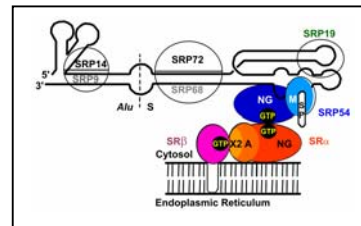
Results

$SR\alpha^{His}:\beta\Delta TM:SRP54D^{His}$ and could be solved by using $SR\alpha:\beta\Delta TM$ and $SRP54D^{His}$ in a similar approach.



The $SR\alpha^{His}(\underline{R524Q}):\beta\Delta TM:SRP54D^{His}$ Complex

When a non-hydrolysable nucleotide is used for complex formation, an inhomogeneous nucleotide load in $SR\beta$ might occur when only a partial population of $SR\beta$ exchanges GTP as shown for free $SR\beta\Delta TM$ (Legate and Andrews, 2003). The Arg524Gln mutation



was introduced into $SR\alpha$ in order to express SR with the capability to bind nucleotide like the wild type receptor but lacking the ability of hydrolysis (Rapiejko and Gilmore,

Results

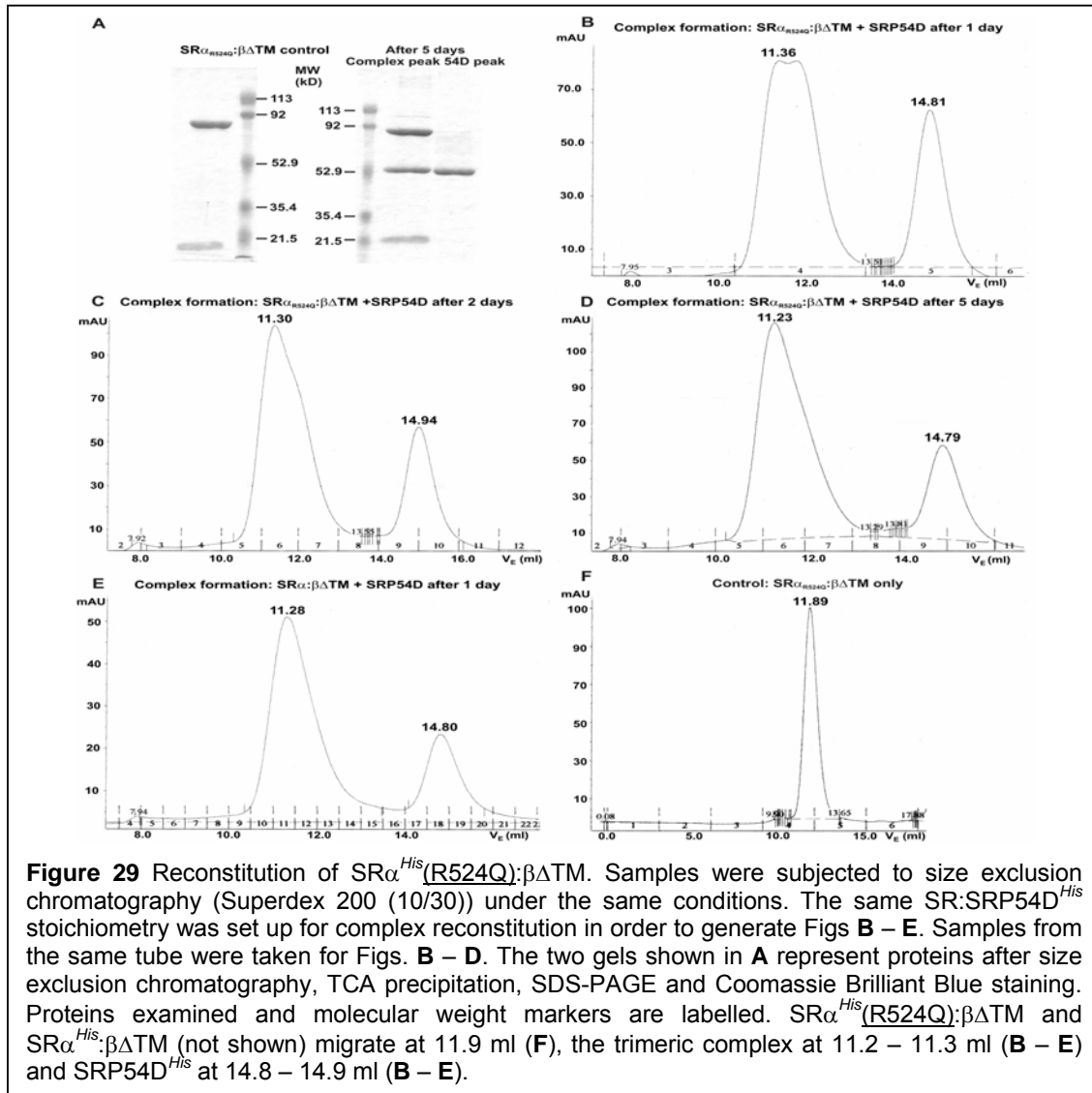
1992). The mutated SR α Arg524 is located C-terminally of the DTAG consensus motif in the switch II region (DTAGR). Complex reconstitution with the mutant could be performed in presence of GTP instead of a non-hydrolysable GTP analogue leading to a trimeric complex with a homogenous nucleotide load.

In these experiments, SRP54D^{His} protein expressed in insect cells was used which was kindly provided by Mark Brooks (EMBL Grenoble, Cusack group). Although SRP54D^{His} expressed in *E. coli* (in house) and in insect cells shared the same sequence, insect-cell expressed SRP54D^{His} did not require the high reconstitution temperature of 37°C. SR:SRP complexes (SR α ^{His}: β Δ TM:SRP54D^{His}, SR α ^{His}(R524Q): β Δ TM:SRP54D^{His}) using SRP54D^{His} expressed in insect-cells could also be reconstituted ON at 4°C. Due to the lower temperature the time required for efficient reconstitution was prolonged but protein aggregation was avoided. It is not clear why efficient reconstitution of trimeric SR:SRP complexes using SRP54D^{His} expressed in *E. coli* or insect cells behave differently, but the dimerisation observed for *E. coli* expressed SRP54D^{His} (see 2.1.6) might be the reason for the reduced affinity for SR α ^{His}: β Δ TM, which was overcome at 37°C. Possibly the SRP54D^{His} homodimer interface occupies the surface that is required for SR α ^{His}: β Δ TM binding.

Fig. 29 shows size exclusion chromatograms with SR α ^{His}: β Δ TM eluting at 11.9 ml, SRP54D^{His} at 14.8 ml and the peak representing the trimeric complex at 11.2 ml. Complex reconstitution, as obtained for the SR α ^{His}(R524Q): β Δ TM:SRP54D^{His} mutant complex after five days, occurs for the SR α ^{His}: β Δ TM:SRP54D^{His} wild-type complex already after one day. The SR α ^{His}(R524Q): β Δ TM:SRP54D^{His} complex is reconstituted with an approximately five-fold reduced complex formation rate compared to SR α ^{His}: β Δ TM:SRP54D^{His}.

From structural studies of the heterodimeric *Thermus aquaticus* NG domain complex from FtsY and Ffh (Egea et al., 2004; Focia et al., 2004) it can be observed, that the invariant and homologous residues Arg191 (Ffh_{T.aq.}), Arg195 (FtsY_{T.aq.}), in the respective G3 regions, point away from the active side and are therefore in both atomic models not involved in the interface (Egea et al., 2004; Focia et al., 2004). Arg191 (Ffh_{T.aq.}) is located close to Glu284 (FtsY_{T.aq.}), and Arg195 (FtsY_{T.aq.}) is found in proximity to Glu274 (Ffh_{T.aq.}) (see Figure 30).

Results



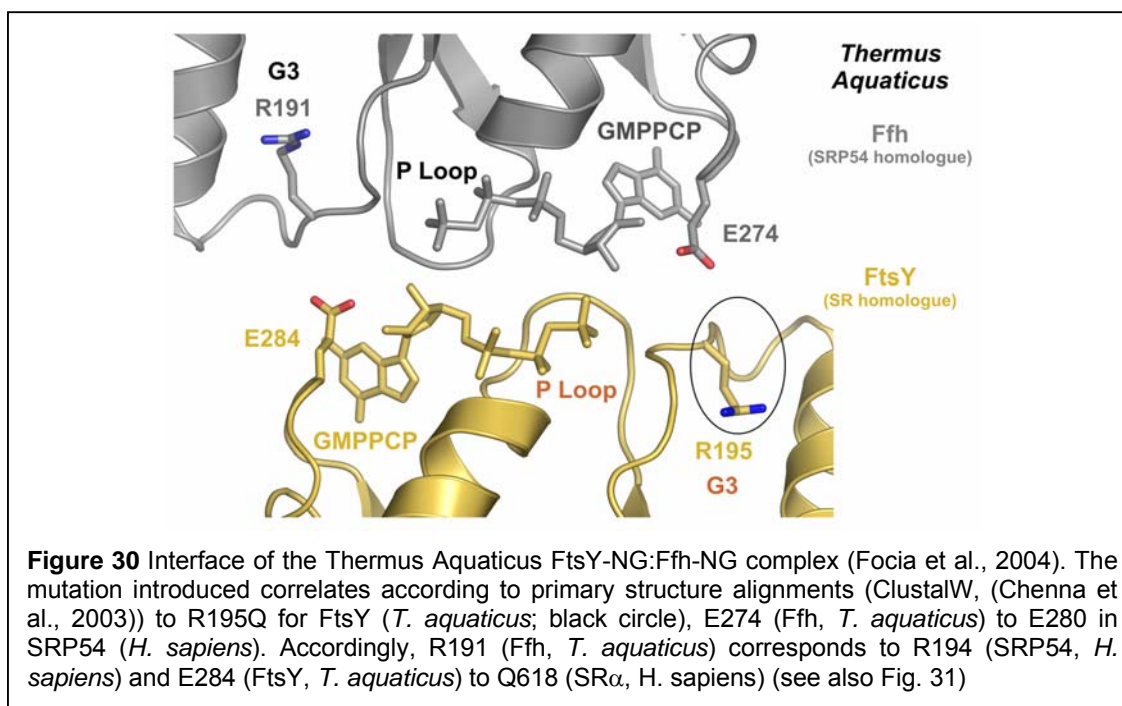
Therefore, it was assumed that by minor conformational changes the switch II region (G3) may be reoriented, suggesting the formation of a salt bridge meanwhile complex formation (Focia et al., 2004). According to primary sequence alignment (Chenna et al., 2003) Arg195 ($\text{FtsY}_{\text{T.Aq.}}$) correlates to Arg524 in human $\text{SR}\alpha$ and Glu274 ($\text{Ffh}_{\text{T.Aq.}}$) to Glu280 in human SRP54 (Figs. 30, 31). The second salt bridge is not conserved from *Thermus aquaticus* to *Homo sapiens* and *Sulfolobus Solfatarius* (Archae) because the negative charged residue corresponding to Glu284 ($\text{FtsY}_{\text{T.Aq.}}$) is in the other two species occupied by a Gln that would only allow the formation of a weaker polar contact.

Arg386 in *E. coli* FtsY is the residue homologous to Arg524 in human $\text{SR}\alpha$. The Arg386Ala mutant of *E. coli* FtsY does not inhibit formation of the $\text{SR}:\text{SRP}$

Results

complex in *E. coli* as observed from fluorescent spectroscopy experiments (Shan et al., 2004) but the Arg524Gln mutant of mammalian SR α slows down significantly reconstitution with SRP54D as shown here. The contradiction may be explained by species-dependent differences in SR:SRP complex formation which is reflected by the fact that not both in *E. coli* suggested salt bridges are conserved in *Homo sapiens* (Fig. 31). It is important to note that the formation of the SR:SRP complex, as shown in *E. coli* (Shan et al., 2004), is a complex process involving several different interactions.

It could be shown using size exclusion chromatography for complex reconstitution analysis that the trimeric complex reconstitution rate of SR α^{His} (R524Q): $\beta\Delta$ TM:SRP54D^{His} is approximately five-fold reduced compared to the wild-type complex. This implies that the suggested salt bridge could not be established during the reconstitution of the SRP:SR complex using SR α^{His} (R524Q): $\beta\Delta$ TM, in contrast to SR α^{His} : $\beta\Delta$ TM. A possible polar contact between Gln524 and Glu280 from SR α and SRP54D^{His}, respectively, could not stabilise the process of complex formation. The reduced binding strength between Gln524 (human SR α) and Glu280 (human SRP54) compared to a salt bridge may therefore be the reason for the lower affinity.



Results

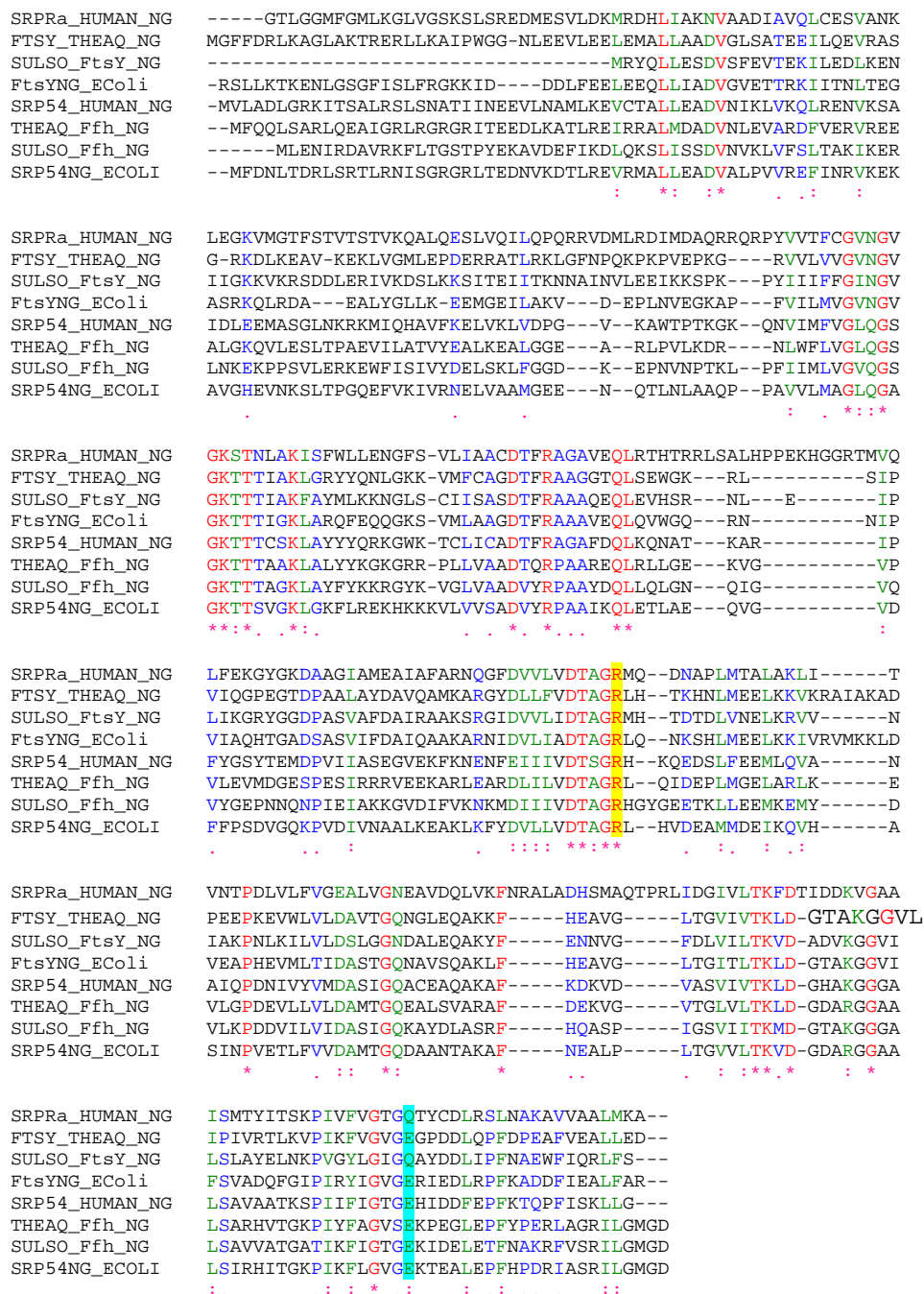


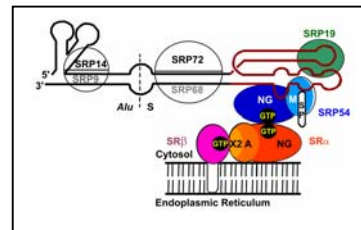
Figure 31 Primary sequence alignment of SR and SRP54 NG domain from *Homo sapiens* and FtsY and Ffh from *Thermus aquaticus* (Theaq) and *Sulfolobus solfataricus* (Sulso) according to ClustalW (Chenna et al., 2003). Hydrophobic residues are in red, polar residues green, positively charged pink and negatively charged blue. Conserved amino acids are labeled by an asterisk, similar ones by two spots and less similar ones by one spot. The conserved arginine is highlighted in yellow, the opposing residue in switch II (G3) is highlighted in cyan.

Results

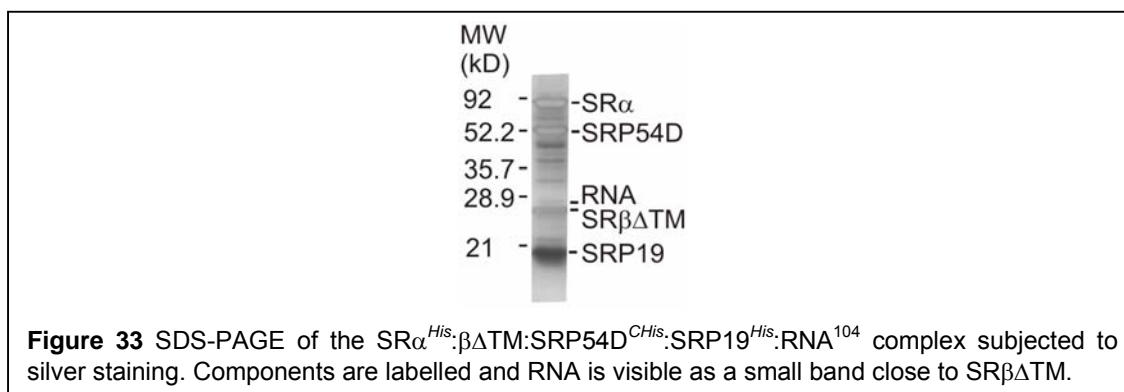
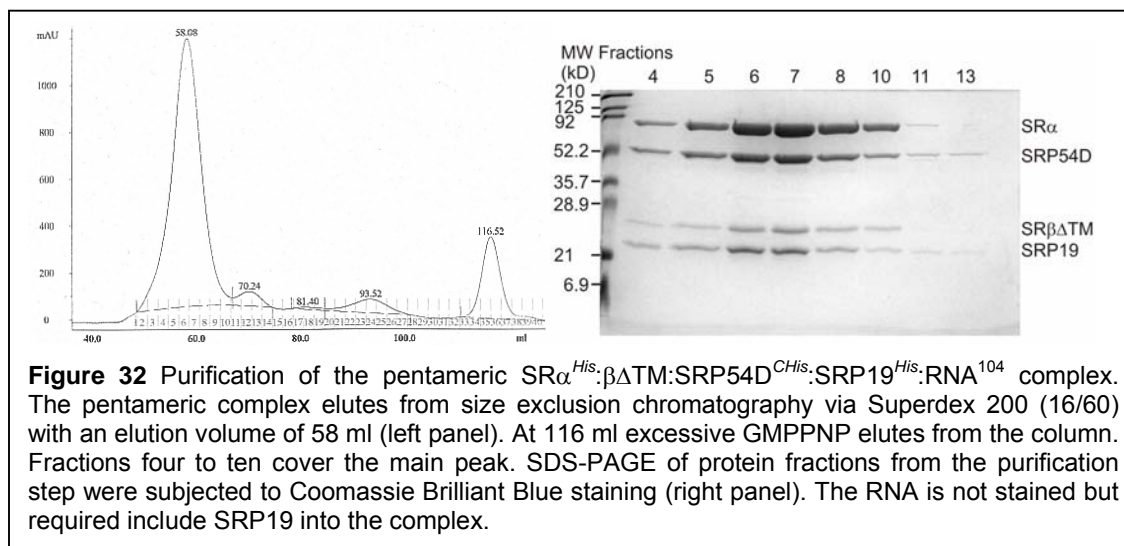
2.2.2 Pentameric Complex Reconstitution:



In order to form the pentameric complex, two sub-complexes ($\text{SR}\alpha^{\text{His}}:\beta\Delta\text{TM}:\text{SRP54D}^{\text{His}}$ and $\text{SRP19}:\text{RNA}^{104}$) were pre-formed. The heterotrimeric complex was subjected to size exclusion chromatography (Superdex 200 (26/60); see Fig. 26) and the heterodimer was purified via anion exchange chromatography by Klemens Wild (not shown). Both subcomplexes were mixed in a 1:1 ratio for the reconstitution of the pentameric complex which was purified using size exclusion chromatography (Superdex (26/60); Fig. 32). Size exclusion chromatography of the trimeric complex allowed removing excessive amounts of $\text{SRP54D}^{\text{His}}$ which later could compete with $\text{SR}\alpha^{\text{His}}:\beta\Delta\text{TM}$ for $\text{SRP19}^{\text{His}}:\text{RNA}^{104}$.



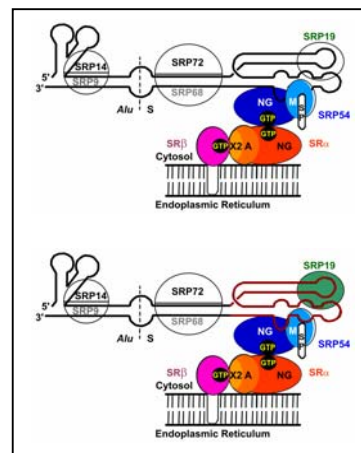
Once the $\text{SR}\alpha^{\text{His}}:\beta\Delta\text{TM}:\text{SRP54D}^{\text{His}}$ complex was formed, it readily associated with $\text{SRP19}^{\text{His}}:\text{RNA}^{104}$ to a pentameric complex at 4°C (Figs. 32, 33) which could be isolated by size exclusion chromatography.



2.2.3 Analysis of SR:SRP Complex

Reconstitution

Pull down experiments with Ffh, 4.5S SRP RNA and immobilised FtsY from *E. coli* suggested a stabilising function for 4,5S RNA in FtsY:Ffh complex formation (Miller et al., 1994). Further analysis by fluorescence spectroscopy showed that the association of *E. coli* Ffh to FtsY was increased by a factor of 200 to 400 in the presence 4.5S RNA compared to experiments without SRP RNA (Peluso et al., 2000; Peluso et al., 2001).



Therefore these experiments were performed to analyse the influence of SRP RNA and the RNA binding protein SRP19 on the formation of the SR:SRP complex in the mammalian system. Reconstitution of the pentameric ($\text{SR}\alpha^{\text{His}}:\beta\Delta\text{TM}:\text{SRP54D}^{\text{CHis}}:\text{SRP19}^{\text{His}}:\text{RNA}^{104}$) and the trimeric complex ($\text{SR}\alpha^{\text{His}}:\beta\Delta\text{TM}:\text{SRP54D}^{\text{CHis}}$) were compared by size exclusion chromatography. $\text{SRP54D}^{\text{His}}$ expressed in insect cells (Mark Brooks, EMBL Grenoble, former Cusack group member) was used for these studies.

Trimeric and pentameric complexes were setup in parallel from single purified components. SR α^{His} : $\beta\Delta TM$ was already pre-formed. Samples were examined after approximately 1, 4 and 7h and analysed by size exclusion chromatography (Superdex 200 (10/30)) for complex reconstitution (Figs. 34, 35).

In the time course shown in Fig. 34, the trimeric complex does not occur as an isolated peak because it could not be separated by size exclusion chromatography from $\text{SR}\alpha^{\text{His}}:\beta\Delta\text{TM}$. Nevertheless, trimeric complex reconstitution can be followed by the decrease of the peak representing free $\text{SRP54D}^{\text{His}}$ ($V_E = 14.9$ ml) relative to the peak correlated to a mixture of $\text{SR}\alpha:\beta\Delta\text{TM}$ and trimeric complex at 11.8 ml.

Pentameric complex reconstitution is easier to observe (Fig. 35) due to the presence of RNA¹⁰⁴. The largest peak observed after 1 h 20 min correlates to the trimeric SRP54D^{His}:SRP19^{His}:RNA¹⁰⁴ complex (V_E = 13.15 ml) which decreased by time until 10 h 30 min. During the time course of the experiment, the pentameric complex is formed (V_E = 11 ml) and the correlating peak exceeds the SRP54D^{His}:SRP19^{His}:RNA¹⁰⁴ peak after 10 h 30 min. These experiments show that the trimeric complex from SRP components (SRP54D^{CHis}:SRP19^{His}:RNA¹⁰⁴) is formed more rapidly than the SR:SRP complex, indicating that the affinity of

Results

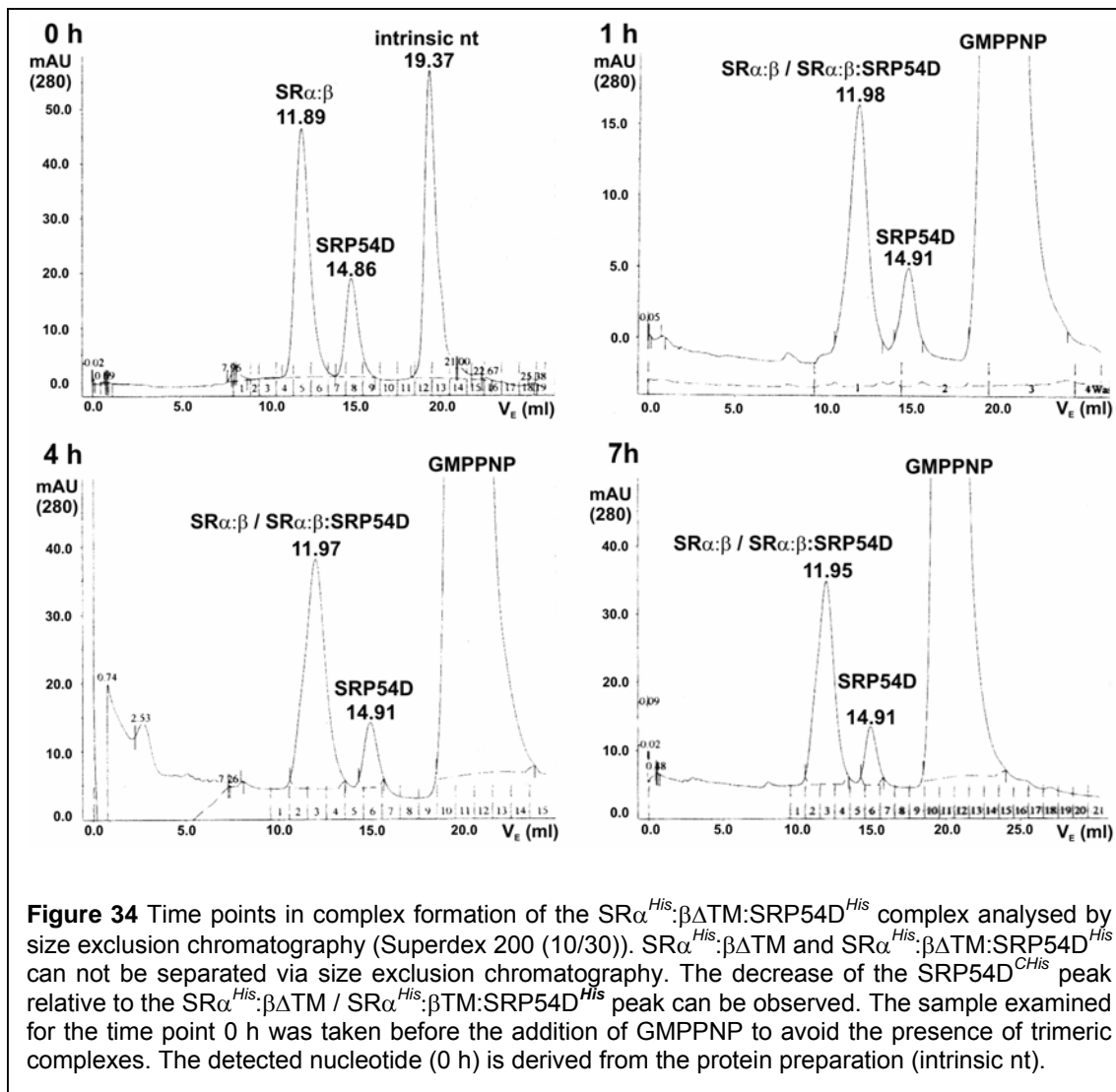
SRP54D^{His} is lower to SR α^{His} : $\beta\Delta$ TM than to SRP19^{His}:RNA¹⁰⁴. This is in agreement with observations from the optimisation of the complex reconstitution protocols. Here, the SR α^{His} : $\beta\Delta$ TM:SRP54D^{His} complex was assembled within 12 h at 4°C but SRP19:RNA¹⁰⁴ bound to the pre-formed SR α^{His} : $\beta\Delta$ TM:SRP54D^{His} complex within 1 h under the same conditions. This is reasonable considering the stability of the assembled SRP in contrast to the highly regulated SR:SRP interaction.

Between 1 h 20 min and 4 h 30 min, the pentameric complex reconstitution increases by 42% (peak at 11 ml; Fig. 35, Table 7) which is more compared to the 31% decrease of SRP54D^{His} (peak at 14.9 ml; Fig. 34, Table 7) between 1 h and 4 h in the trimeric SR α^{His} : $\beta\Delta$ TM:SRP54D^{His} complex reconstitution experiment. It is suggestive that the affinity of SRP54D^{His} to SR α^{His} : $\beta\Delta$ TM is enhanced with the formation of SRP54D^{His}:SRP19:RNA¹⁰⁴ complex. Between 4 h 30 min and 7h 30 min, the pentameric complex is still formed (+10%) but there is no measurable change for the trimeric complex assembly between 4 h and 7 h, indicating that the pentameric complex might be more stable.

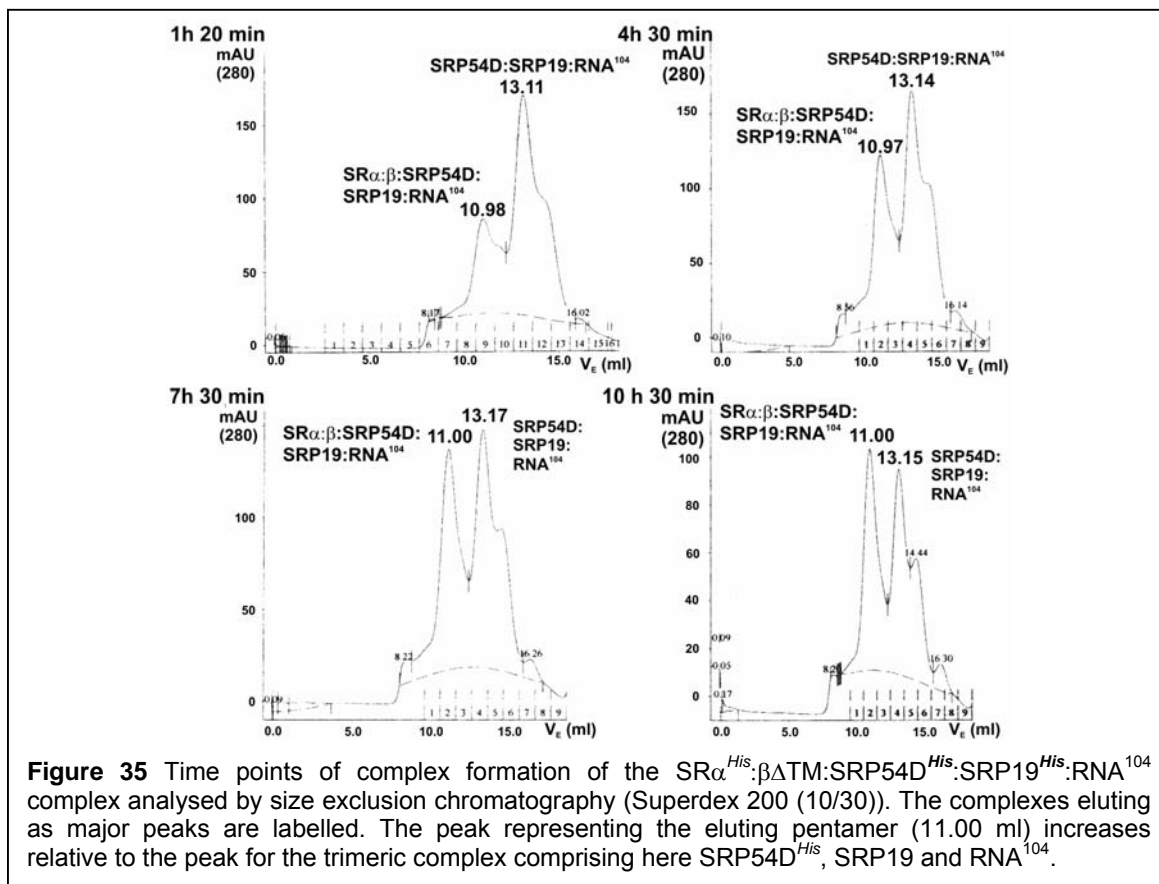
Comparing the pentameric and trimeric complex reconstitution experiments, analysis were not performed in exactly the same time frame since the setup of the pentameric SR α^{His} : $\beta\Delta$ TM:SRP54D^{His}:SRP19^{His}:RNA¹⁰⁴ complex was analysed 20 - 30 min after the corresponding sample of the trimeric SR α^{His} : $\beta\Delta$ TM:SRP54D^{His} complex. The numbers achieved for the pentameric complex were given from the Pharmacia Software UNICORNTM Version 4. They can not be considered to be precise since educts and products can not be separated by baseline. Values given here are only approximate numbers.

In summary, reconstitution of the SRP54D^{His}:SRP19^{His}:RNA¹⁰⁴ complex is formed more rapidly than the SR:SRP complexes and SRP19/RNA¹⁰⁴ seem to slightly facilitate the assembly of the SR:SRP complex. Additionally, the pentameric might be more stable than the trimeric complex since the reconstitution of the pentameric, but not the trimeric complex (SR α^{His} : $\beta\Delta$ TM:SRP54D^{His}), can be observed after 4 h.

Results



Results

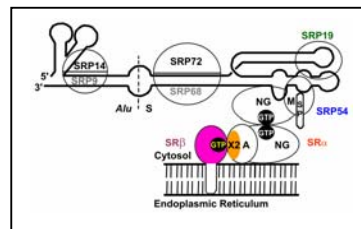


	Time	$\text{SR}\alpha^{\text{His}}:\beta\Delta\text{TM}:\text{SRP54D}^{\text{CHis}}$	$\text{SR}\alpha^{\text{His}}:\beta\Delta\text{TM}:\text{SRP54D}^{\text{CHis}}:\text{SRP19}^{\text{His}}:\text{RNA}^{104}$
Trimeric complex formed	1 – 4 h	+ ~31 %	
	4 – 7 h	Not measurable	
Pentameric complex formed	1h 20 min – 4 h 30 min		+ ~ 42 %
	4 h 30 min – 7 h 30 min		+ ~ 10 %

Table 7 Comparison of trimeric and pentameric complex reconstitution. Results were calculated from values obtained from the size exclusion chromatography runs from Figs. 34 and 35. The areas of the peaks were determined by the Pharmacia UNICORN software. The total areas of peaks in diagrams were normalised before comparison in order to keep the total amounts of proteins constant. Numbers for the pentameric complex reconstitution are approximate numbers since the peak resembling this complex can not be baseline separated from others. Pentameric complex reconstitution is measured via the increase of the pentameric complex peak, the reconstitution of the trimeric complex is measured via the decrease of the $\text{SRP54D}^{\text{His}}$ peak since $\text{SR}\alpha^{\text{His}}:\beta\Delta\text{TM}$ and the trimeric complex could not be separated by size exclusion chromatography.

2.3 Structure Determination of SRX^{His}: $\beta\Delta$ TM

SRX2^{His}: $\beta\Delta$ TM was set up for crystallisation but the structure determined showed only residues homologous to yeast SR $\beta\Delta$ TM and SRX not including the complete C-terminus of SRX2. A result of the structural analysis was the definition of the minimal SR β -binding domain of SR α (SRX) in mammals which was found to comprise the N-terminal 130 amino acids SRX2 (176 amino acids).



Initial phase information was achieved by molecular replacement from the data set Srax3-2. Model building and refinement led to a preliminary model with a high R-factor (R-factor = 38.0%, free R-factor = 47.3%). In order to improve the phase information two methods were carried out:

1. Crystallisation of L-selenomethionine substituted crystals for a SAD experiment. As a result crystals were obtained and the data set Peak 1_2 (SAD data set) could be collected. The phasing power was too low to include phase information into the refinement and model building process
2. Optimised Crystallisation trials in order to achieve higher diffracting crystals. Crystals were achieved diffracting to 2.45 Å (data set Sr2-1).

The space group was determined in the Srax3-2, SAD- and Sr2-1 data sets to be I222. The lattice parameters in all crystals were very similar. The final model (R-factor = 19.3%, free R-factor = 23.2%) was mainly build and refined from the Sr2-1 data set but also from phase information of the preliminary model.

The structure was determined by using the SR $\beta\Delta$ TM subunit of the *Saccharomyces cerevisiae* SRX: $\beta\Delta$ TM-GTP complex (Schwartz and Blobel, 2003) as a search model.

2.3.1 Crystallisation

SRX^{His}: $\beta\Delta$ TM crystallised as leaf-shaped crystals with the space group I222 in 100 mM sodium citrate pH 5.5, 2.0 M (NH₄)₂SO₄ and in the presence of 100 mM guanidinium chloride (Fig. 36). Hexagonal and leaf-shaped crystals with the same space group were also grown from seleno-L-methionine substituted protein (SRX^{His}: $\beta\Delta$ TM_{SeMet}, Fig. 36) in the same condition.

Results

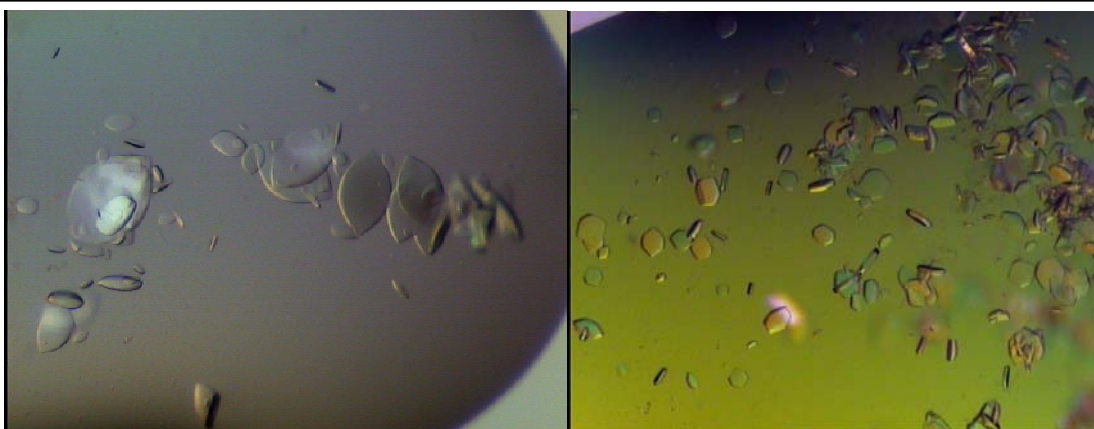


Figure 36 Crystallisation of SRX2^{His}: β ATM SRX^{His}: β ATM. Crystals diffracting to 2.45 Å (left image; giving the Sr2-1 data set) and crystals obtained from SRX2^{His}: β ATM_{SeMet} protein (right image).

2.3.2 Data Collection and Processing

The Srax3-2 data set

The Srax3-2 data set could be processed to 2.9 Å ($I/\sigma = 2.0$ and $R_{\text{sym}} = 0.50$). Reflections in the highest resolution shell (2.83 – 2.9 Å) were excluded due to weak signal ($I/\sigma = 1.5$) and high R_{sym} (0.64). Crystals belong to the space group I222 and one molecule was found per asymmetric unit. Data processing statistics are shown in Tables 8 and 9. From this data set the structure was solved and the first preliminary model was build. In Table 15 all relevant crystallographic data are summarised.

Shell limit	Lower Angstrom	Upper Angstrom	Average I	Average error	stat.	Norm. Chi**2	Linear R-fac	Square R-fac
	30.00	6.95	6118.7	245.0	80.2	1.002	0.041	0.060
	6.95	5.53	1776.3	98.2	42.5	1.000	0.052	0.051
	5.53	4.83	2189.0	122.1	59.5	1.000	0.053	0.056
	4.83	4.39	2515.6	127.8	53.7	1.000	0.052	0.055
	4.39	4.08	1870.4	100.4	51.5	1.000	0.059	0.069
	4.08	3.84	1129.6	82.7	47.7	1.000	0.075	0.071
	3.84	3.65	960.0	99.0	51.8	1.000	0.095	0.093
	3.65	3.49	723.5	76.4	48.5	1.000	0.111	0.095
	3.49	3.35	483.0	67.4	47.2	1.000	0.151	0.139
	3.35	3.24	377.1	64.4	47.8	1.000	0.195	0.174
	3.24	3.14	265.7	58.7	46.0	0.999	0.259	0.232
	3.14	3.05	202.5	63.1	49.7	1.000	0.364	0.335
	3.05	2.97	153.2	65.0	50.1	0.996	0.495	0.445
	2.97	2.90	119.4	59.8	48.1	1.000	0.568	0.504
	(2.90	2.83	92.7	60.7	49.0	0.997	0.778	0.640)
All reflections			1297.5	93.7	51.7	1.000	0.077	0.064

Table 8 Processing statistics of the Srax3-2 data set. Information is given about signal intensity (I , error) and reliability of the data (χ^2 , linear R-factor, square R-factor).

Results

Shell		I/Sigma in resolution shells:								
Lower limit	Upper limit	% of reflections with I / Sigma less than								
		0	1	2	3	5	10	20	>20	total
30.00	6.95	0.8	1.3	2.4	3.0	4.3	6.9	26.6	71.4	98.0
6.95	5.53	1.0	3.5	5.8	7.0	10.4	19.9	70.1	29.5	99.6
5.53	4.83	0.6	2.0	3.4	5.2	8.8	18.2	68.2	31.8	100.0
4.83	4.39	1.4	3.5	5.1	6.6	9.5	19.3	58.3	41.6	99.9
4.39	4.08	1.7	3.9	6.4	8.3	12.8	23.3	62.9	37.0	99.9
4.08	3.84	3.7	7.6	11.5	15.7	22.0	41.1	91.9	8.1	100.0
3.84	3.65	3.0	7.8	12.9	17.4	27.0	59.1	100.0	0.0	100.0
3.65	3.49	5.0	11.8	19.1	23.4	35.1	61.0	98.6	1.1	99.7
3.49	3.35	6.2	13.5	23.6	31.2	46.2	73.4	100.0	0.0	100.0
3.35	3.24	8.4	17.9	29.3	38.7	52.1	81.6	99.9	0.0	99.9
3.24	3.14	10.4	22.3	35.3	45.0	59.4	91.0	99.9	0.0	99.9
3.14	3.05	12.3	26.2	40.6	53.1	72.0	99.8	100.0	0.0	100.0
3.05	2.97	15.5	30.9	47.0	62.3	88.4	99.9	99.9	0.0	99.9
2.97	2.90	16.3	36.1	54.7	68.6	89.9	99.9	99.9	0.0	99.9
(2.90	2.83	20.6	40.7	61.3	79.9	98.0	100.0	100.0	0.0	100.0)
All hkl		7.0	15.0	23.6	30.6	41.8	58.9	84.5	15.2	99.8

Table 9 Completeness of the Srax3-2 data set. Overall completeness is 99.8%, and completeness in the highest processed resolution shell is 99.9%.

The SAD Data Set

The SAD data set (termed also Peak1_2) was collected in order to determine additional phase information to improve the model build from the Srax3-2 data set.

Seleno-L-methionine substituted SRX^{His}:SRβΔTM-GTP protein was crystallised and successively subjected to a Single Anomalous Dispersion (SAD) experiment at beamline ID 14-4 (ESRF, Grenoble). The fluorescent scan showed a prominent absorbance peak from K-Shell electrons of Selenium at 12659 eV (Fig. 37, Table 10). Methionine was successfully substituted by seleno-L-methionine but the crystals showed only low phasing power. Therefore, the data set (Table 11) was not included in the refinement of the final model.

The same day the SAD experiment was performed, also a higher resolution data set (Sr2-1) was collected. Refinement of the Sr2-1 data was successful to build an atomic model of high quality (see below).

In order to obtain a signal sufficient for structure determination, there should be at least about one anomalous scatterer per 80 amino acids. The protein crystallised contained 6 methionine residues, corresponding to one seleno-L-methionine per 67 residues. Due to disordered regions in the protein, only one methionine per 104 residues was observed in the final model. Therefore, the small number of ordered seleno-L-methionine residues might have been the reason for the weak phasing power.

Results

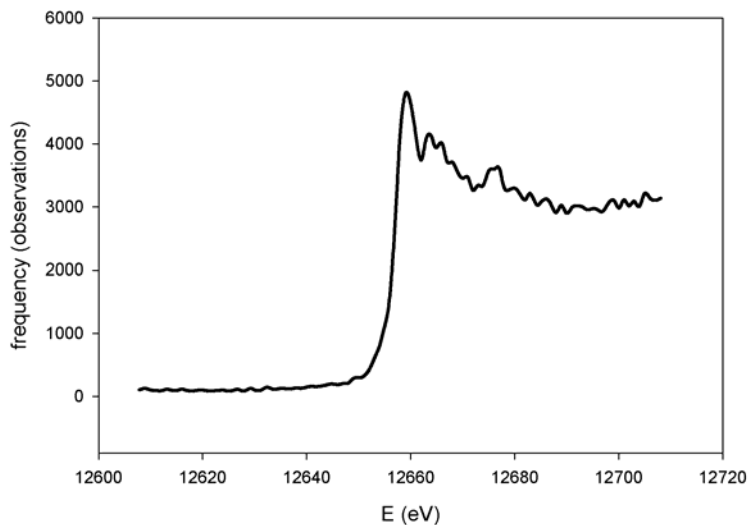


Figure 37 Fluorescent Scan of $\text{SRX}^{\text{His}}:\text{SR}\beta\Delta\text{TM}_{\text{SeMet}}$ crystals. Absorbance peak of K-shell electrons of Selenium occurs at 12660 eV.

```
Integration limits low/high : 1261.17 50632.18
First/last data points at   : 12607.80 12706.46
Energy scale increment      : 0.315
```

	E (eV)	f'	f''
F' minimum	12656.97	-9.8	2.8
F'' maximum	12659.49	-7.8	4.8

Table 10 Statistics of the Selenium K-shell electron peak from the fluorescent scan.

Data Collection	
Wavelength (Å)	0.933
Resolution range (Å)	50 – 3.5
Completeness (%)	94 (93)
R _{sym} (%)	16.6 (56.7)
<I/σ>	8 (2.5)
Space group	I222
Cell parameters	a = 67.9 Å, b = 120.0 Å, c = 118.1 Å
Total reflections	6650

Table 11 Crystallographic data from the SAD data set (Peak 1_2) of $\text{SRX}^{\text{His}}:\beta\Delta\text{TM}$ summarised. Values in parentheses are for the highest resolution shell.

Results

The Sr2-1 data set

The Sr2-1 data set was the best data set collected and processed between 2.45 and 50.0 Å. An overall completeness of 99.7% was achieved with 100% in the highest resolution shell (2.45 – 2.49 Å (Tables 11, 12). The space group was I222 with one molecule per asymmetric unit. The overall I/σ was 25.0 ($R_{\text{sym}} = 5.7\%$) and I/σ in the highest resolution shell 3.3 ($R_{\text{sym}} = 42.4\%$). In Table 16 all relevant crystallographic data are summarised.

Shell limit	Lower	Upper	Average					
	Angstrom	I	error	stat.	Chi**2	R-fac	Square	R-fac
50.00	6.65	12521.9	372.0	115.1	0.906	0.034	0.040	
6.65	5.28	5851.7	159.5	38.8	0.970	0.037	0.041	
5.28	4.61	8622.3	230.1	50.6	0.981	0.037	0.042	
4.61	4.19	8712.1	253.2	58.7	0.939	0.038	0.042	
4.19	3.89	6042.6	177.8	49.0	1.016	0.042	0.045	
3.89	3.66	4646.7	156.4	43.6	0.935	0.046	0.047	
3.66	3.48	3740.2	142.5	42.1	0.905	0.049	0.047	
3.48	3.32	2478.0	110.4	39.4	0.954	0.061	0.059	
3.32	3.20	2045.9	93.9	38.8	1.033	0.069	0.061	
3.20	3.09	1489.2	82.0	38.1	1.022	0.084	0.073	
3.09	2.99	1107.1	70.0	37.6	1.024	0.105	0.096	
2.99	2.90	913.5	72.3	37.8	0.983	0.122	0.107	
2.90	2.83	706.9	69.5	37.8	1.065	0.158	0.128	
2.83	2.76	613.4	71.1	38.7	1.022	0.180	0.142	
2.76	2.70	479.2	68.2	38.8	1.108	0.235	0.191	
2.70	2.64	401.5	69.0	39.1	1.055	0.277	0.221	
2.64	2.59	338.0	69.4	39.5	1.021	0.319	0.242	
2.59	2.54	279.9	68.3	40.1	1.020	0.391	0.318	
2.54	2.49	279.3	73.0	40.7	0.958	0.395	0.311	
2.49	2.45	243.6	74.4	42.3	0.940	0.424	0.335	
All reflections		3131.9	125.4	45.5	0.994	0.057	0.046	

Table 12 Processing Statistics of the Sr2-1 data set. Information is given about signal intensity (I, error) and reliability of the data (chi², linear R-factor, square R-factor).

Shell limit	Lower limit	Upper limit	Summary of observation redundancies: % of reflections with given No. of observations										
			0	1	2	3	4	5-6	7-8	9-12	13-19	>19	total
50.00	6.65	4.8	2.4	4.8	7.7	14.9	18.0	47.3	0.0	0.0	0.0	0.0	95.2
6.65	5.28	0.2	0.3	2.6	3.3	12.3	18.4	62.9	0.0	0.0	0.0	0.0	99.8
5.28	4.61	0.4	0.1	1.7	3.8	10.4	21.6	62.0	0.0	0.0	0.0	0.0	99.6
4.61	4.19	0.0	0.4	2.1	3.5	8.6	22.4	63.1	0.0	0.0	0.0	0.0	100.0
4.19	3.89	0.0	0.1	1.4	3.7	9.0	19.4	66.3	0.0	0.0	0.0	0.0	100.0
3.89	3.66	0.0	0.2	1.7	1.9	8.9	20.6	66.7	0.0	0.0	0.0	0.0	100.0
3.66	3.48	0.0	0.0	1.1	2.2	7.9	21.2	67.6	0.0	0.0	0.0	0.0	100.0
3.48	3.32	0.0	0.3	1.1	2.9	8.5	21.2	66.0	0.0	0.0	0.0	0.0	100.0
3.32	3.20	0.0	0.0	0.9	2.6	7.7	21.3	67.6	0.0	0.0	0.0	0.0	100.0
3.20	3.09	0.0	0.0	1.1	2.9	7.9	20.6	67.5	0.0	0.0	0.0	0.0	100.0
3.09	2.99	0.0	0.1	0.5	2.9	7.5	21.1	67.9	0.0	0.0	0.0	0.0	100.0
2.99	2.90	0.0	0.2	0.7	2.3	8.4	21.4	67.0	0.0	0.0	0.0	0.0	100.0
2.90	2.83	0.1	0.3	0.7	2.6	6.8	20.5	69.0	0.0	0.0	0.0	0.0	99.9
2.83	2.76	0.0	0.2	0.8	2.3	7.5	23.2	66.0	0.0	0.0	0.0	0.0	100.0
2.76	2.70	0.0	0.5	0.2	2.2	7.5	22.5	67.1	0.0	0.0	0.0	0.0	100.0
2.70	2.64	0.0	0.3	0.9	2.3	7.0	22.1	67.4	0.0	0.0	0.0	0.0	100.0
2.64	2.59	0.0	0.3	0.8	2.7	7.4	22.7	66.2	0.0	0.0	0.0	0.0	100.0
2.59	2.54	0.0	0.7	1.0	3.0	7.1	20.6	67.6	0.0	0.0	0.0	0.0	100.0
2.54	2.49	0.0	0.6	0.6	3.1	7.3	22.9	65.3	0.0	0.0	0.0	0.0	100.0
2.49	2.45	0.0	0.7	2.0	4.6	8.2	25.4	59.1	0.0	0.0	0.0	0.0	100.0
All hkl		0.3	0.4	1.4	3.1	8.6	21.3	64.9	0.0	0.0	0.0	0.0	99.7

Table 13 Completeness of the Sr2-1 data set in all resolution shells. Overall completeness is 99.7% and completeness in the highest resolution shell is 100.0%.

2.3.3 Structure Determination by Molecular Replacement

The structure was solved by molecular replacement (MR) using the yeast homologue of SR β Δ TM (PDB accession code 1NRJ) as a search model and the Srax3-2 data set. The model build from the MR solution was refined to a R-factor of 38.0% and a free R-factor 47.5%. Further improvement of the model was not possible due to high model bias and low resolution data. Here, the structure determination using the Srax3-2 data set is described.

In total, over 150 runs of the programs AMoRe (Navaza, 1994) and Molrep (Collaborative Computing Project, 1994) from the CCP4 suite (Collaborative Computing Project, 1994) were used for MR. Search models were generated from the yeast homologue of the heterodimeric SRX^{His}: β Δ TM-GTP complex (PDB accession code: 1NRJ). The sequence identities of SR β Δ TM and SRX2 to their yeast homologues are 26.5% and 15.7%, respectively. Therefore the yeast SRX^{His}: β Δ TM complex, SR β Δ TM and models with deleted loops were chosen as a search models. The possible solutions were evaluated according to the R-factor (expected to be < 50%), variations between correlation factors, the fitting of symmetry related molecules and importantly whether the R-factor decreased in the first refinement step.

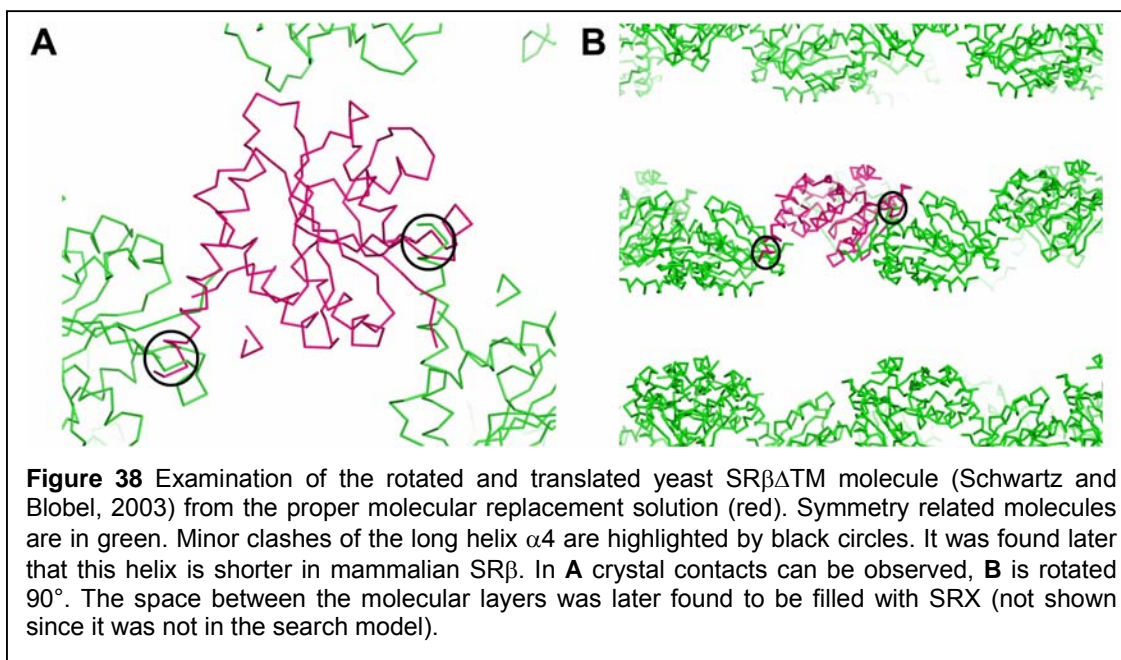
The proper solution was found by using the yeast homologue of SR β Δ TM (Schwartz and Blobel, 2003) as a search model. The molecular replacement result is shown in Table 14 and is characterised by an unusually high R-factor (58.5%) and a slightly higher correlation coefficient (Score) compared to the next best solution. This is likely due to the fact that yeast SR β Δ TM as search model covers only 54% of the total molecular mass of SRX2^{His}: β Δ TM-GTP.

After molecular replacement, symmetry related molecules of the rotated and translated model were inspected using O (Jones et al., 1991). Only minor clashes caused by the C-terminus of the long helix α 4 could be observed as shown in Figure 38 (illustrated by PyMOL (DeLano, 2002)). Later, it was determined that the clashing helix α 4 was shorter in SR β Δ TM than in yeast (see below) (Schwartz and Blobel, 2003).

Results

S_ RF TF	theta	phi	chi	tx	ty	tz	TFcnt	Rfac	Scor	
S__20__8	1	30.84	-155.65	115.00	0.212	0.491	0.182	4.23	0.585	0.245
S__30__10	2	30.26	-179.35	120.79	0.931	0.404	0.666	2.65	0.582	0.235
S__25__1	3	130.37	-173.01	122.87	0.205	0.942	0.369	1.65	0.592	0.231

Table 14 Proper solution of the phase determination by molecular replacement. The proper solution is labelled with “S__20__8”, the next best solutions are found below. The proper solution is characterised in this case by an R-factor (Rfac) of 0.585 and a slightly higher correlation coefficient expressed here as score value (Scor). The rotation angles (theta, phi, chi) and translation values (tx, ty, tz) of the solutions are given.



2.3.4 Refinement

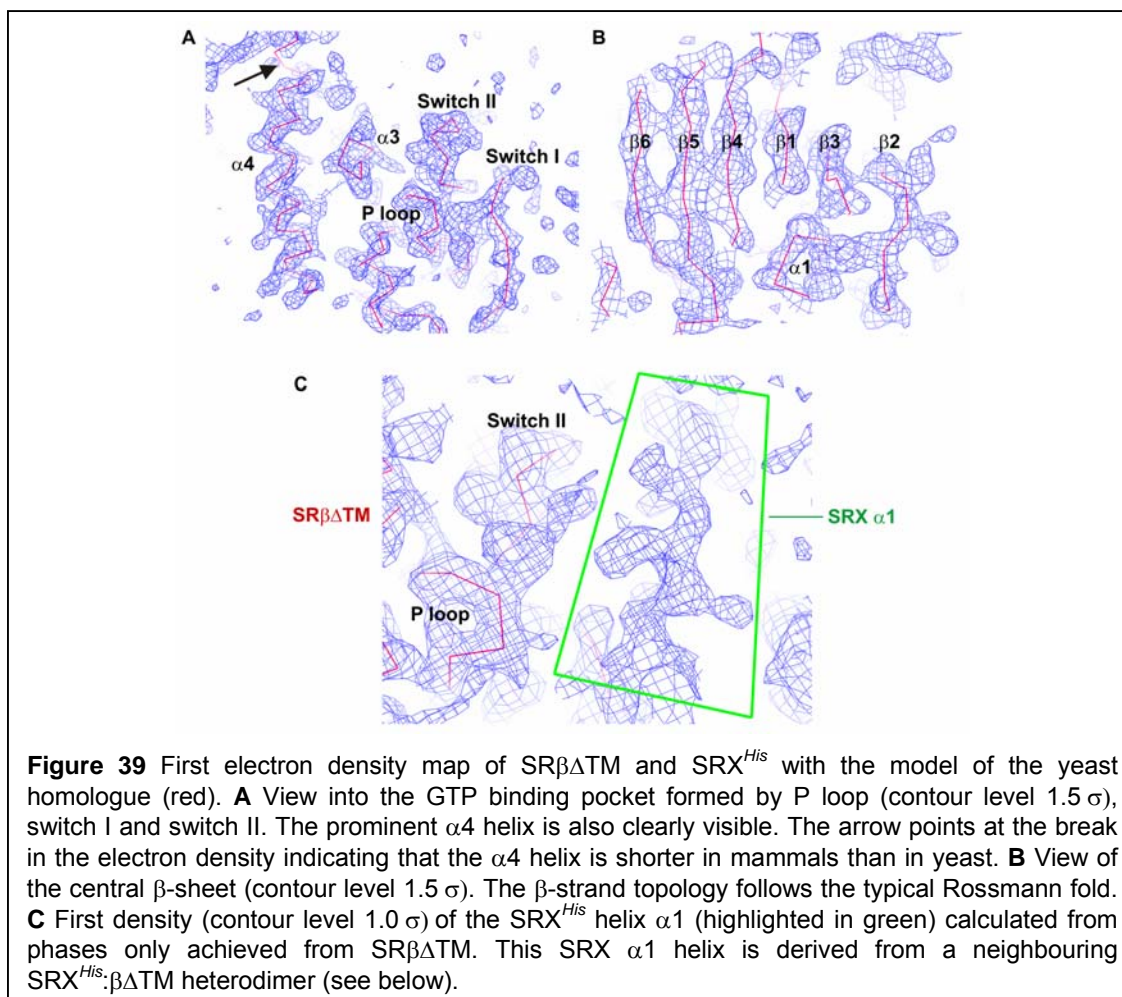
The molecular replacement model (yeast SRβΔTM, 1NRJ) was refined with the Srax3-2 data set at 2.9 Å using the CNS package (Otwinowski and Minor, 1997) to verify the solution and generate the first electron density map. The free R-factor decreased only slightly from 52.3% to 52.1% but the R-factor was reduced from 53.8% to 45.8% confirming the solution. The first electron density map included only phase information from the model of the yeast homologue of SRβΔTM (Schwartz and Blobel, 2003) and is shown for SRβΔTM in Fig. 39. Electron density from the SRX^{His} subunit was weakly visible. The SRX^{His} helix α_1 could be identified as shown in Figure 39.

The model could not be refined to a R-factor better than 38.0% (free R-factor 47.3%; Table 14). Therefore, two strategies were performed in order to build a better

Results

molecular model: 1. Trial for a higher resolution native data set; 2. expression, purification and crystallisation of seleno-L-methionine substituted protein and successive phase determination by a SAD experiment.

The SAD experiment was not successful but a higher resolution native data could be obtained (2.45 Å, Sr2-1 data set). In the data sets Srax3-2 and Sr2-1, the space group was identical (I222) and unit cell parameters were very similar. Rigid body refinement was used to fit the model obtained from the Srax3-2 data set to the Sr2-1 data. To improve the model, the auto-build function of Arp/wARP (Perrakis et al., 2001) was used to track the SRX^{His}:βΔTM-GTP main chain. The model was refined to a R-factor of 19.3% and a free R-factor of 23.2%. Detailed data collection and refinement statistics of the final model are shown in Table 16. The Improvement of the 2mFo-DFc electron density map from the first to the last refinement step is illustrated in Fig. 40.



Results

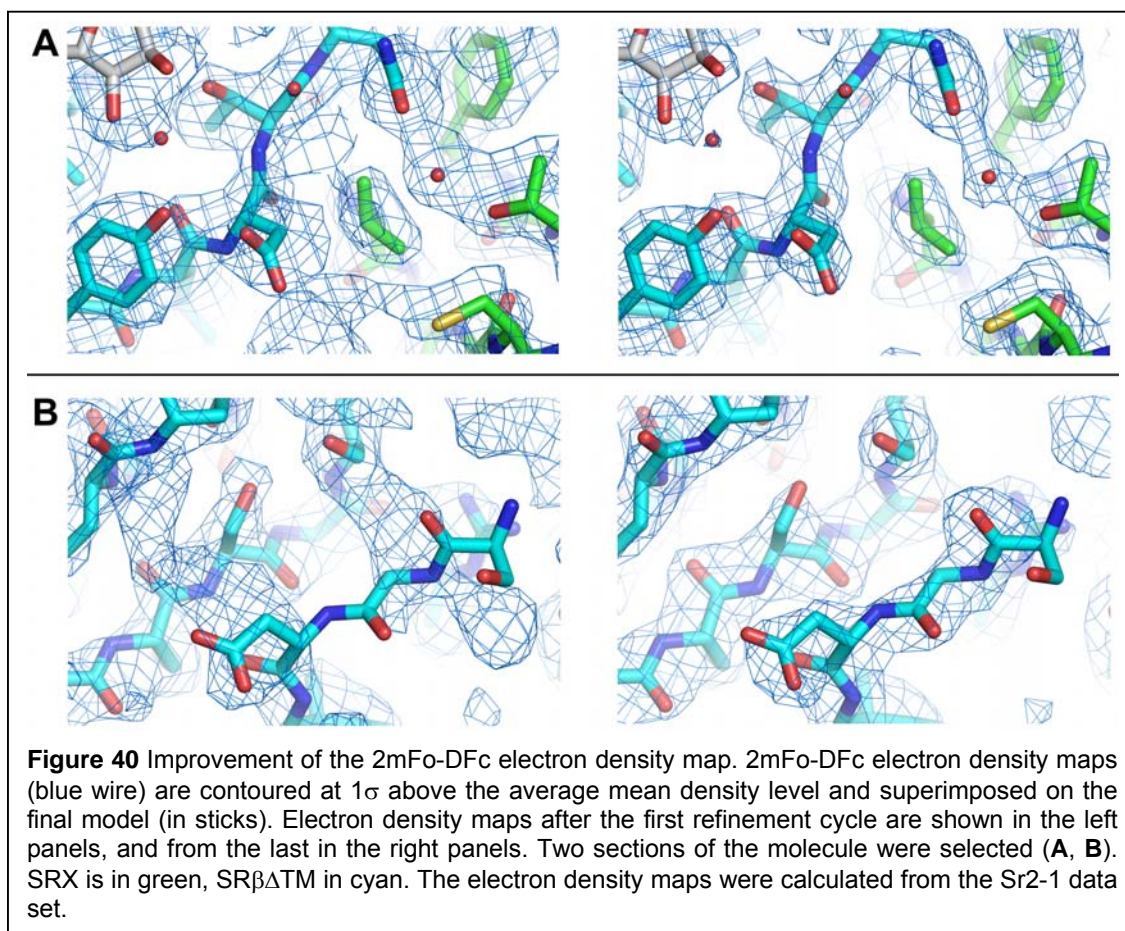
Data Collection	
Wavelength (Å)	0.933
Resolution range (Å)	50 – 2.8
Completeness (%)	99.8 (100.0, 99.9)
R _{sym} (%)	6.4 (64.0, 50.4)
<I/σ>	13.8 (1.5, 2)
Molecules per asymmetric unit	1
Refinement Statistics	
Space group	I222
Cell parameters	a = 68.3 Å, b = 118.9 Å, c = 120.6 Å
Resolution range (Å)	20 - 2.9
Total reflections	10097
Working set	9581
Test set	516
Number of refined atoms	
Protein	2344
GTP	32
Water molecules	0
Matthews coefficient (Å ³ /Da)	2.85
Solvent Content (%)	56.8
B-factor (Å ²)	64.7
R-factor (%) [§]	38.0
R _{free} (%) [§]	47.3
rmsd bond length (Å)	0.011
rmsd bond angle (°)	1.85
Estimated standard deviations (ESDs)	
From Luzzati plot (Å)	0.66
From SigmaA (Å)	0.71

Table 15 Crystallographic data from the Srax3-2 data set of SRX^{His}.βΔTM summarised. [†]: first values in parentheses are for the highest resolution shell: 2.90 – 2.83 Å, second values are for the second highest resolution shell: 2.97 – 2.90 Å. [§]: $R = \sum ||F_{obs}| - |F_{calc}|| / \sum |F_{obs}|$; R-factor and R_{free} were calculated from the working and test reflection sets, respectively. R_{free} was calculated with 5% of the data.

Results

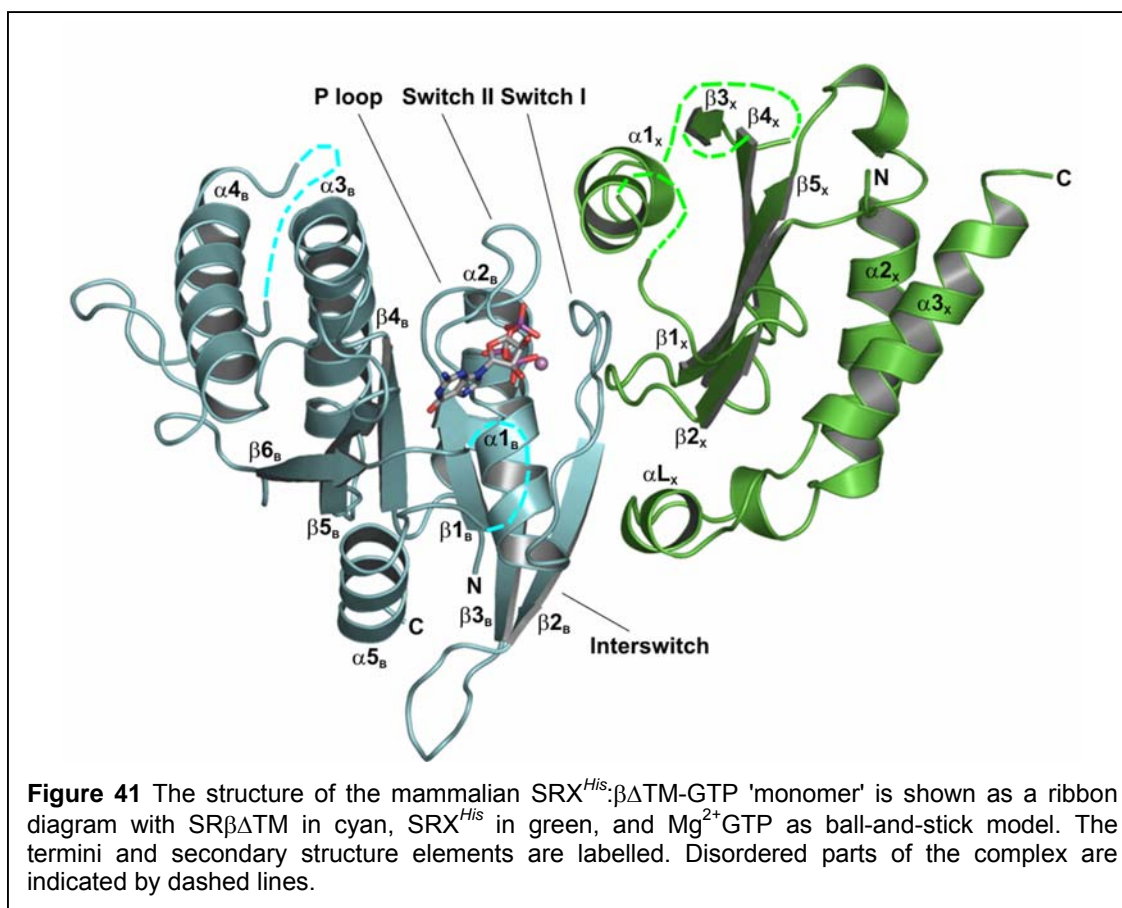
Data Collection	
Wavelength (Å)	0.979
Resolution range (Å)	50 – 2.45
Completeness (%)	99.7 (100.0)
R _{sym} (%)	5.7 (42.4)
<I/σ>	25.0 (3.3)
Molecules per asymmetric unit	1
Refinement Statistics	
Space group	I222
Cell parameters	a = 68.1 Å, b = 118.3 Å, c = 120.4 Å
Resolution range (Å)	20 - 2.45
Total reflections	18124
Working set	17202
Test set	922
Number of refined atoms	
Protein	2500
Mg ²⁺ GTP	35
Water molecules	104
Matthews coefficient (Å ³ /Da)	2.70
Solvent Content (%)	54.5
B-factor (Å ²)	56.4
R-factor (%) [§]	19.3
R _{free} (%) [§]	23.2
rmsd bond length (Å)	0.011
rmsd bond angle (°)	1.50
Estimated standard deviations (ESDs)	
From Luzzati plot (Å)	0.27
From SigmaA (Å)	0.30
Ramachandran plot (%)	
Most favoured region	90.9
Additionally allowed region	8.8
Generously allowed region	0.4
Disallowed region	0.0

Table 16 Crystallographic data from the best data set (Sr2-1) for the SRX^{His}:βΔTM-GTP model summarised. *: values in parentheses are for the highest resolution shell: 2.49 – 2.45 Å. §: R = $\sum ||F_{obs}| - |F_{calc}|| / \sum_h |F_{obs}|$; R-factor and R_{free} were calculated from the working and test reflection sets, respectively. R_{free} was calculated with 5% of the data.



2.4 The Structure of SRX^{His}: $\beta\Delta$ TM-GTP

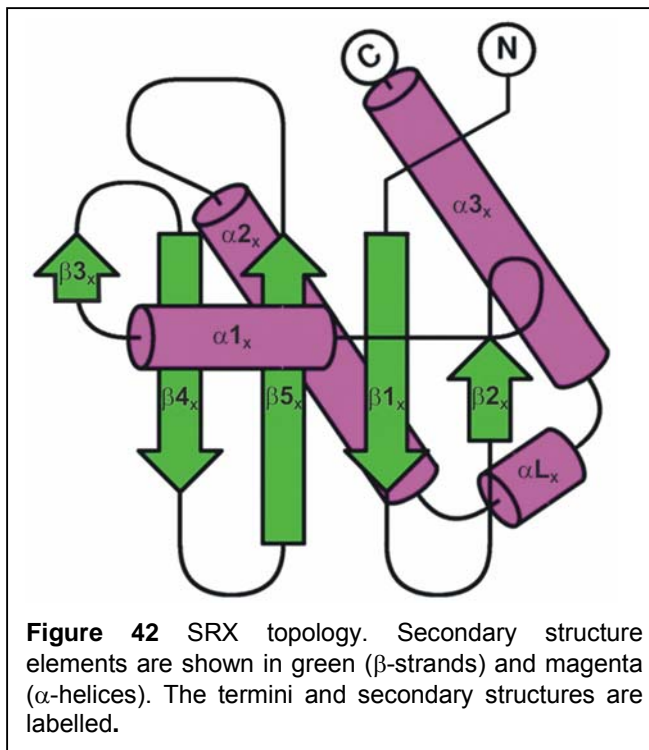
2.4.1 Overall Structure



In this section the final model of SRX^{His}: $\beta\Delta$ TM-GTP is presented. To distinguish between SR $\beta\Delta$ TM and SRX the subscript letters B and X are used, respectively. The overall structure of the refined SRX^{His}: $\beta\Delta$ TM-GTP model is depicted in Fig. 41. SR β is a typical small GTPase and features a classical Rossmann fold with a central six-stranded ($\beta 1_B$ - $\beta 6_B$) mixed β -sheet packed in between five helices. In the SRX^{His}: $\beta\Delta$ TM-GTP complex SR β is in a state not competent for GTP hydrolysis as the catalytic histidine residue (His119_B) points away from the active site (see below).

The SRX domain (Figs. 41 and 42) belongs to the mixed α/β class proteins sharing topology ($\beta\beta\alpha\beta\beta\alpha\alpha$) and fold of the SNARE-like protein superfamily (<http://scop.mrc-lmb.cam.ac.uk/scop/>) including the N-terminal domains of non-syntaxin SNAREs (longin domains).

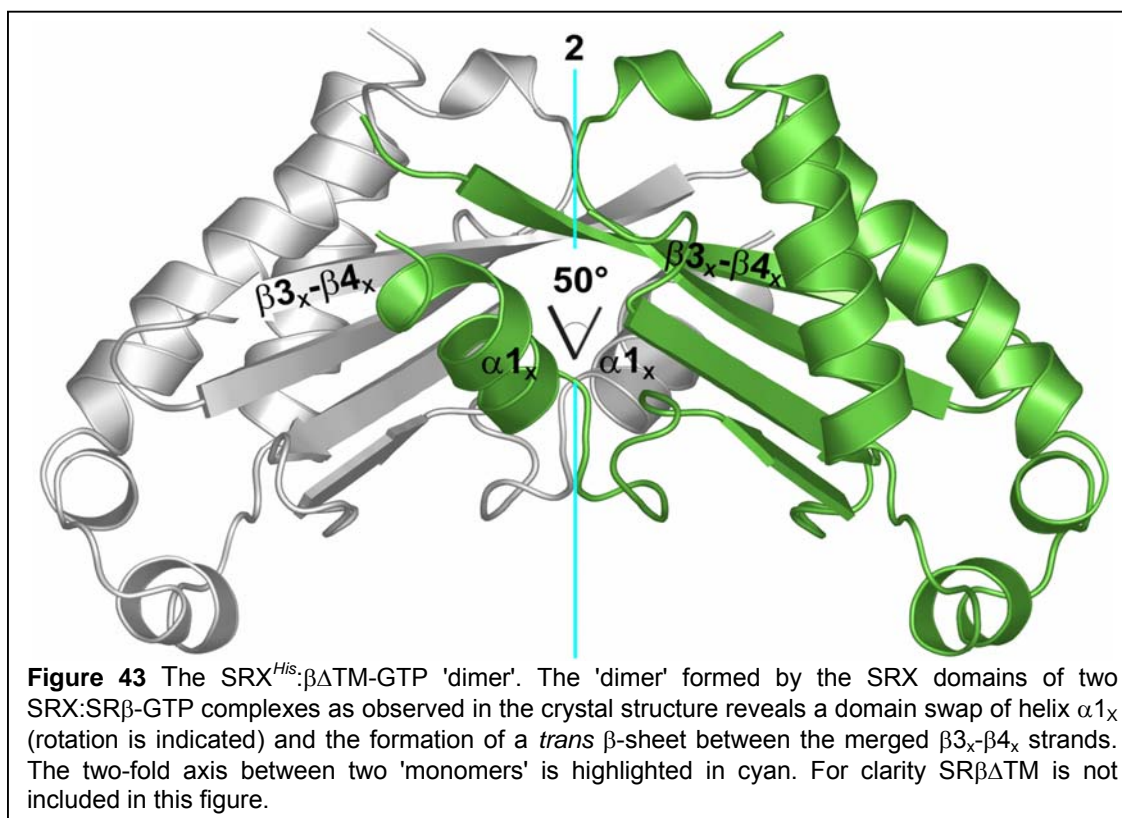
The fold is defined by a three-layer architecture with a central five-stranded antiparallel β -sheet packed against helix $\alpha 1_x$ on the concave side of the β -sheet and two C-terminal anti-parallel helices $\alpha 2_x$ and $\alpha 3_x$ on the other side (secondary structure numbering is according to the SCOP nomenclature which is different to the nomenclature used for the yeast structure). At the N-terminus the two anti-parallel β -strands $\beta 1_x$ - $\beta 2_x$ are connected by a conserved β -hairpin. Helix $\alpha 1_x$ locates almost perpendicular to the β -strands on the concave



side and connects the peripheral β -strands of the β -sheet ($\beta 2_x$ and $\beta 3_x$). The helix flanking loop regions are not conserved and only partially visible in the structure. Strands $\beta 3_x$, $\beta 4_x$ and $\beta 5_x$ are connected by short β -hairpin structures. The central strand $\beta 5_x$ is followed by the long helix $\alpha 2_x$, the $\alpha 2_x$ - $\alpha 3_x$ loop in the plane of the β -sheet, and the C-terminal helix $\alpha 3_x$ running anti-parallel to helix $\alpha 2_x$. Helix $\alpha 2_x$ is kinked and wraps around the convex side of the β -sheet like a clamp and helix αL_x is inserted in the $\alpha 2_x$ - $\alpha 3_x$ loop.

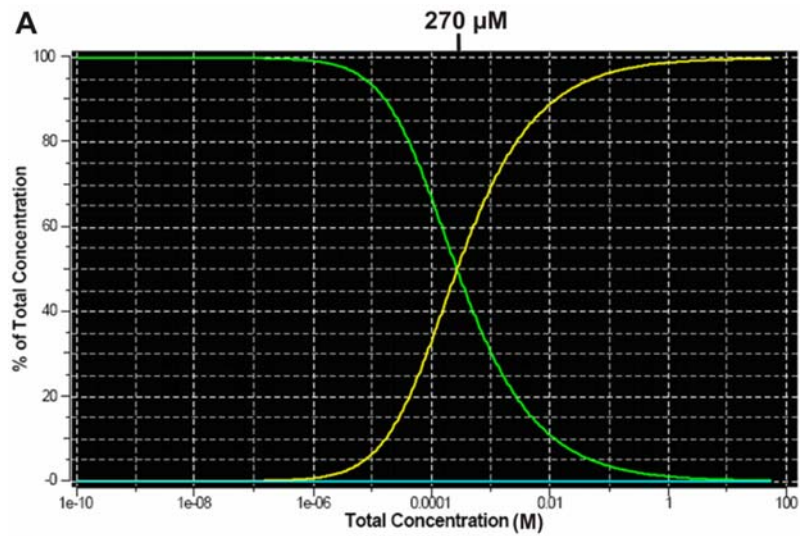
2.4.2 The $\text{SRX}^{\text{His}}:\beta\Delta\text{TM-GTP}$ Homodimer

The mammalian $\text{SRX}^{\text{His}}:\beta\Delta\text{TM-GTP}$ complex forms a 'dimer' in the crystal due to an interaction of the SRX domains, which is stabilised by a domain swap of helix $\alpha 1_x$ ($\sim 50^\circ$ rotation around helical N-terminus) and the formation of a continuous *trans* β -sheet (Fig. 43). Here, strands $\beta 3_x$ - $\beta 4_x$ of one 'monomer' merge and align anti-parallel across the 'dimer' interface. Dimerisation leads to an additional buried interface of approximately 1000 \AA^2 between the two $\text{SRX}^{\text{His}}:\beta\Delta\text{TM-GTP}$ 'monomers'.



In order to analyse the oligomerisation state of mammalian SRX^{His}:βΔTM-GTP in solution, analytical ultra centrifugation was performed by Karsten Rippe and Jacek Mazurkiewicz (Kirchhoff Institut für Physik, Heidelberg) and a K_D of 270 μ M for the 'dimer' was determined (see Fig. 43). The SRX^{His}:βΔTM-GTP complex showed a tendency for aggregation. Therefore, the K_D of the SRX^{His}:βΔTM-GTP complex could not be determined. and the physiological relevance for the dimerisation of SRX^{His}:βΔTM-GTP is not yet clear. Comparison with the yeast structure ('monomer', see below) showed that the domain-swapped helix α1_x of the second SRX molecule of the mammalian receptor superposes with its corresponding position in the yeast 'monomer' (see Discussion, section 3.1.3). Therefore, a 'monomeric' mammalian receptor complex is used for further analysis.

Results



B

Fitted Model: Monomer-Dimer Equilibrium
Parameters for this model:
Molecular Weight for component 1: 4.577e+04 dalton (fitted)
Partial Specific Volume for component 1 (at 20°C): 7.405e-01 ccm/g (fixed)
Association (Dissociation) Constant 1: 3.705e+03 (2.699e-04) (fitted)
Global Fitting Statistics:
Variance: 8.0245e-06
Standard Deviation: 2.8328e-03
Number of floated Parameters: 20
Number of Datasets: 9
Number of Datapoints: 1899
Number of Degrees of Freedom: 1879
Number of Runs: 355 (36.484 %, corrected)
Expected Number of Runs: 487 (corrected)
Run Variance: 2.429e+02 (corrected)

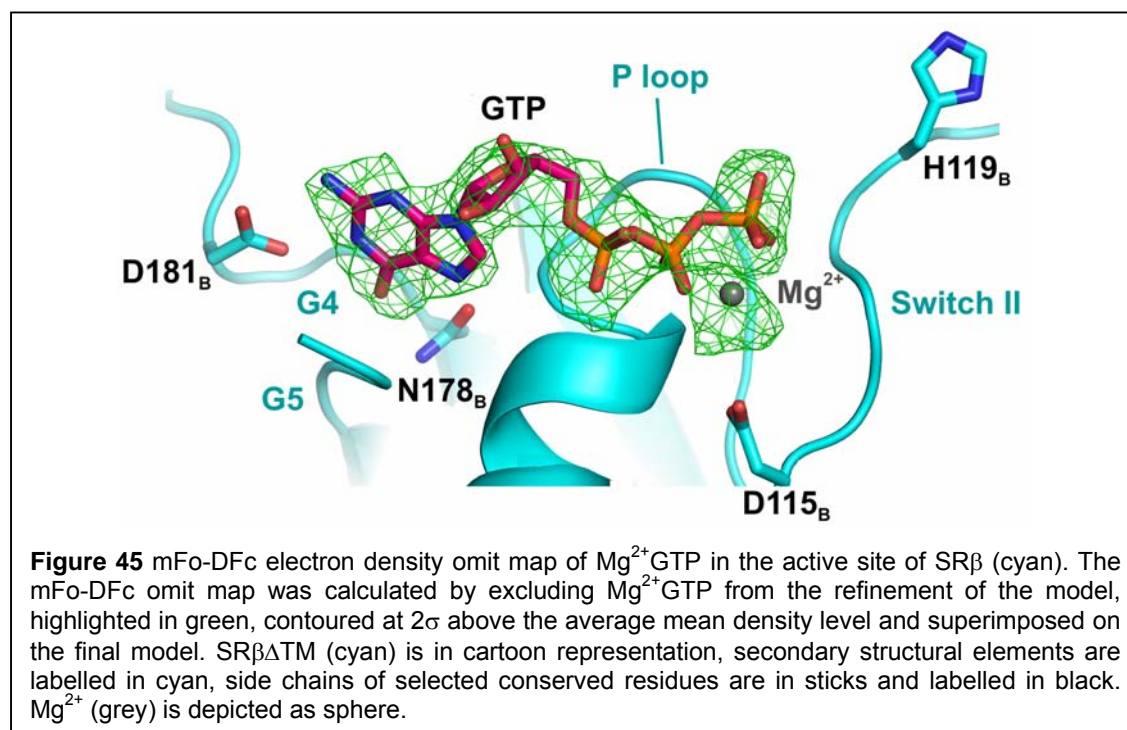
Figure 44 Analytical equilibrium ultracentrifugation of SRX^{His}: $\beta\Delta$ TM-GTP. (A) Percentage of 'monomer' (green) and 'dimer' (yellow) vs. protein concentration. The K_D is 270 μ M in a 'monomer'-dimer equilibrium. (B) Statistics of the data obtained from the experiment.

2.4.3 The GTP-binding pocket

Within the family of small Ras-like GTPases, SR $\beta\Delta$ TM is a rare case because it contains GTP in its native active site as shown by an electron density map of Mg²⁺GTP at a contour level of 2 σ (mFo-DFc Mg²⁺GTP omit map, Fig. 45). Normally GDP or a non-hydrolysable GTP analogue is crystallised in complex with the native small Ras-like GTPase.

In Fig. 45 interactions between GTP, important water molecules and residues of the nucleotide binding pocket are shown in detail. Asp72_B, Ser73_B, G74_B, Lys75_B and Thr76_B from the P loop (G1) establish polar main chain contacts to the β -phosphate of the GTP. Side chain contacts from the P loop to GTP involve the Lys75_B forming salt bridges to the β - and γ -phosphate of GTP and the Thr76_B hydroxyl group binding Mg²⁺.

From the switch I region (G2) Thr90_B binds with the side chain hydroxyl group the α -phosphate. Ser93_B coordinates with the main chain carbonyl group the Mg²⁺, with the main chain amide nitrogen the γ -phosphate. Ser93_B forms a hydrogen bond with its side chain hydroxyl group to a water molecule (H₂O_{cat}) that is suggested to be polarised by the catalytic residue from the switch II region (His119_B; homologous to Gln51 in Ras) for GTP hydrolysis.

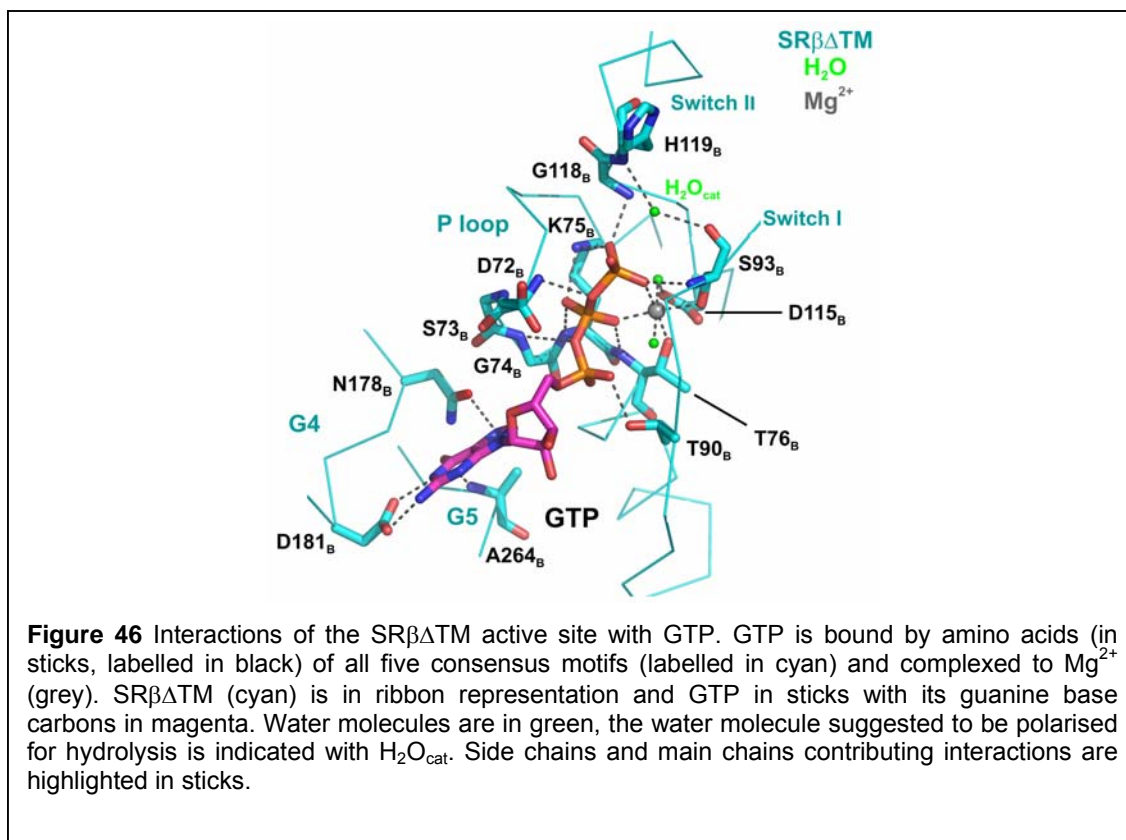


Results

In the switch II region, the main chain amide groups of His119_B and the neighbouring Gly118_B interact with the H₂O_{cat} and the γ -phosphate, respectively. Asp115_B forms with its carbonyl group a hydrogen bond to one of the two water molecules belonging to the coordination sphere of the Mg²⁺.

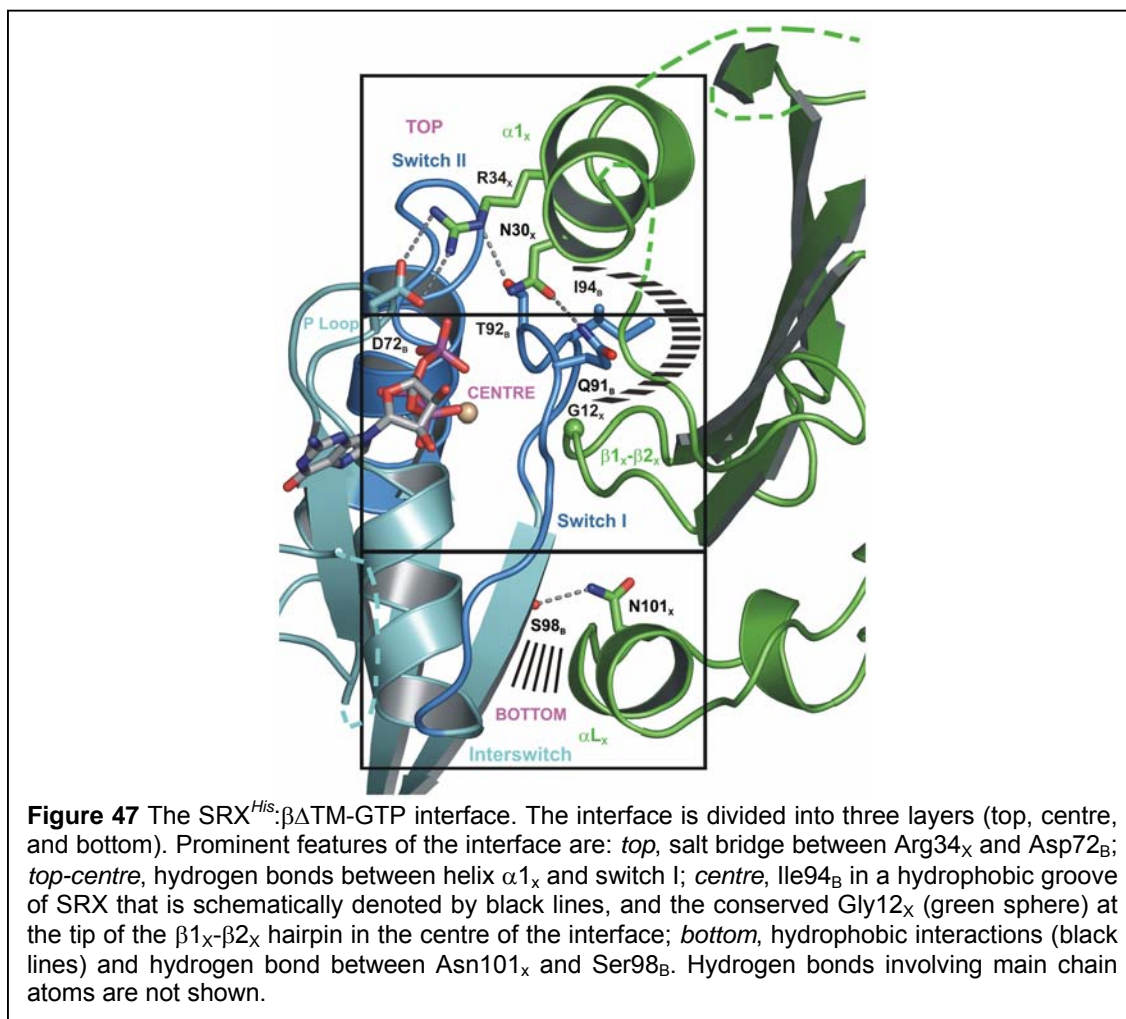
The octahedral coordination sphere of Mg²⁺ consists of two water molecules, the main chain carbonyl group of the Ser93_B, the Thr76_B side chain hydroxyl group and the β - and γ -phosphate groups of the GTP.

The P loop, switch I and switch II regions bind to the three phosphate groups. In contrast, the G4- and G5 regions interact with the guanine base. The G4 region is known to be important for substrate selectivity. An Asp181_BAsn mutation in the G4 region alters the nucleotide binding to favour XTP over GTP (Legate et al., 2000). The guanine base establishes two polar contacts to the carboxyl group of Asp181_B and one to the side chain amide group of Asn178_B. The GTP-binding pocket is completed by the G5 region ('closing loop') from where only one main chain interaction of the Ala264_B amide nitrogen with the guanine base can be observed.



2.4.4 The SRX^{His}: $\beta\Delta$ TM-GTP interface

The SRX^{His}: $\beta\Delta$ TM-GTP interface involves the predominant effector-binding region of Ras-like GTPases (Corbett and Alber, 2001) (Fig. 46). The buried surface between SR $\beta\Delta$ TM-GTP and SRX^{His} is 1850 Å², which is similar to the yeast structure and other GTPase-effector complexes (Schwartz and Blobel, 2003). SR $\beta\Delta$ TM contributes to the interface with its G1 element (P loop, GLCDSGKT), switch I, interswitch, and switch II regions. The complete switch I region snugly binds into a hydrophobic groove of SRX^{His} and spans the whole interface. This groove is situated between the amphipathic helix $\alpha 1_X$ and the hydrophobic concave surface of the SRX^{His} β -sheet. Although the protein interface forms a continuous surface, three regions of SRX organised in three layers contribute to the interface (Fig. 47, 48): (i) helix $\alpha 1_X$, (ii) the β -hairpin between strands $\beta 1_X$ and $\beta 2_X$ and (iii) the $\alpha 2_X$ - $\alpha 3_X$ loop including the short helix αL_X .



Results

In the top layer, the amphipathic helix $\alpha 1_X$ binds the switch I and II regions and the P loop of SR β . The side chain of the conserved Asn30_X forms hydrogen bonds to the side chain Gln91_B (not conserved) and the main chain of Thr92_B in switch I. One helical turn further, Arg34_X forms a salt bridge to Asp72_B in the P loop bridging the active site and forming a hydrogen bond to the side chain of Thr92_B. Three residues of helix $\alpha 1_X$ (Ile33_X, Leu37_X, and Leu38_X) are part of a hydrophobic pocket which accommodates Ile94_B and the aliphatic part of Gln91_B in the centre of the interface. Leu38_X forms an additional hydrophobic interaction with Leu122_B of switch II.

In the central layer, SRX^{His} exclusively interacts with the switch I region of SR $\beta\Delta$ TM. The central hydrophobic pocket is completed by Val14_X and the aliphatic part of Lys10_X. The conserved β -hairpin between $\beta 1_X$ and $\beta 2_X$ contributes a number of hydrophilic interactions which are surrounded by a hydrophobic rim. All hydrophilic interactions are established by main chain atoms of the β -hairpin, which contains a conserved glycine (Gly12_X) at the tip. The carbonyl oxygen of Lys10_X forms a hydrogen bond to the amide nitrogen of Ile94_B. The carbonyl oxygen of Gly11_X approaches the Mg²⁺ binding site in SR β and forms a hydrogen bond with the side chain of Ser93_B which is essential for Mg²⁺ coordination. Residues Gly12_X to Val14_X form a short stretch of an anti-parallel *trans* β -sheet with residues Gln91_B to Asp89_B of switch I.

In the third layer, SRX^{His} binds to the switch I and interswitch regions of SR $\beta\Delta$ TM. Interactions are formed by the $\alpha 2_X$ - $\alpha 3_X$ loop including the short helix αL_X . Three hydrophobic side chains (Ala103_X, Leu104_X and Leu107_X) from helix αL_X interact with residues Phe79_B, Val80_B, Leu83_B and the hydrophobic methyl group of Thr84_B from switch I as well as with Ala99_B and Ile100_B from the interswitch region. Hydrophilic interactions are established by main chain atoms of Ala103_X and Leu107_X, which hydrogen bond to the main chain of Ser98_B and the guanidinium group of Arg88_B, respectively. The layer is completed by the interaction of the side chains of Asn101_X and Ser98_B.

Results

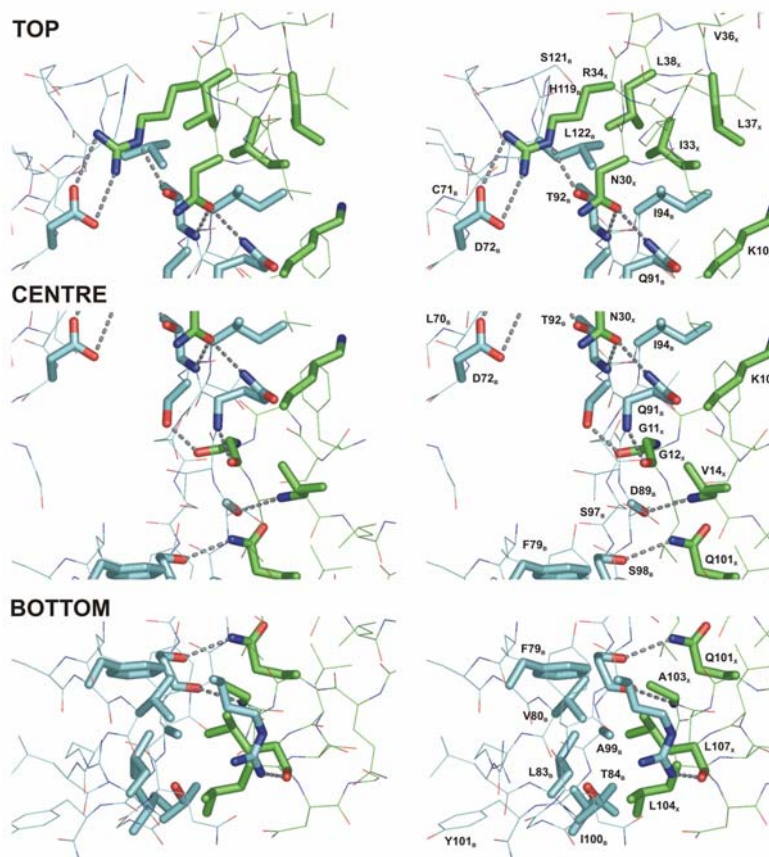


Figure 48 Detailed stereo views of the SRX^{His}:βΔTM-GTP interface. Detailed stereo views of the SRX:SRβ-GTP interface. SRβΔTM is shown in cyan and SRX^{His} in green. Residues discussed in the text are highlighted in sticks. Polar interactions are represented by dashed lines. The three layers (top, centre and bottom, see also Fig. 3) are separated in the figure. The top layer includes interactions to helix α1_X. The centre involves the interactions of the SRβ switch I region with the β1_X-β2_X loop. The bottom layer completes the interface by αL_X binding to the switch I and interswitch regions of SRβΔTM.

2.5 Characterisation of Interactions with SR and Components of the SRP Cycle

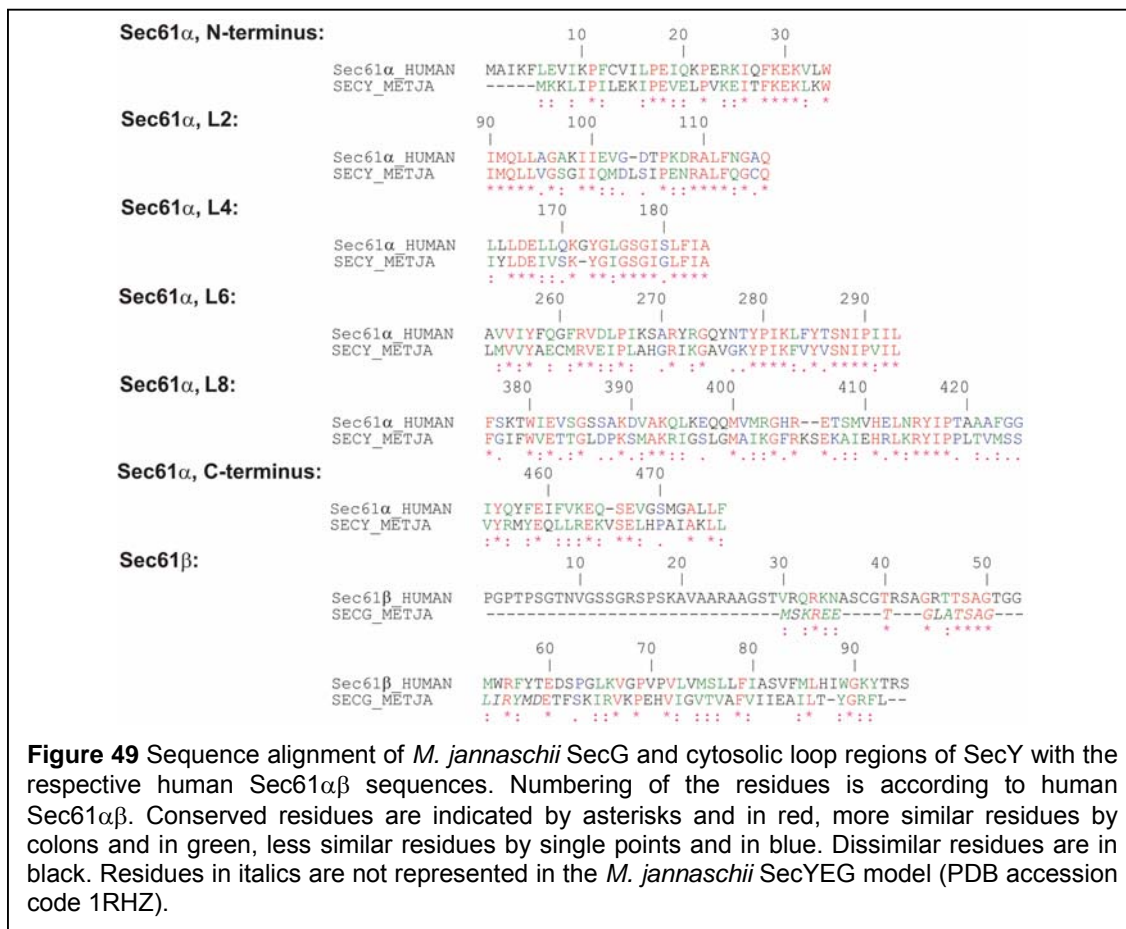
2.5.1 SR β Δ TM Translocon Interaction

In previous experiments Sec61 β has been proposed as a GEF for SR β (Helmers et al., 2003) and the cytosolic loops L6 and L8 of Sec61 α were shown to be important for different steps in protein translocation (Cheng et al., 2005). Therefore, the aim was to analyse the interaction of SR β and SR with the Sec61 complex in more detail. An immobilised peptide library representing the cytosolic loops of Sec61 α and Sec61 β was created. Due to the high sequence conservation within the translocon family, the cytosolic loops of human Sec61 could be defined from the structure of the *M. jannaschii* homolog (Cheng et al., 2005; Van den Berg et al., 2004).

Human Sec61 $\alpha\beta$ and *M. jannaschii* YG sequences were aligned with ClustalW (Thompson et al., 1994) and cytosolic loop regions were defined from the *M. jannaschii* SecYEG structure (Cheng et al., 2005; Van den Berg et al., 2004). The immobilised peptide library covered the sequences as shown in Fig. 49 including the N-terminus of human Sec61 α (amino acids 2-34), loop 2 (amino acids 90-116), loop 4 163-184), loop 6 (253-193), loop 8 (375-425), the C-terminus (454-476) and full length Sec61 β .

The peptide library contained the hydrophobic transmembrane anchor of Sec61 β as a control for unspecific hydrophobic interactions. No signal was obtained with these peptides. In addition, when SR β -apo had gone through a freezing and thawing cycle it did not give any signals (as in Fig. 50B), whereas fresh protein (Fig. 50A) gave reproducible signals indicating that the native protein conformation or stable protein is essential for the interaction.

Results

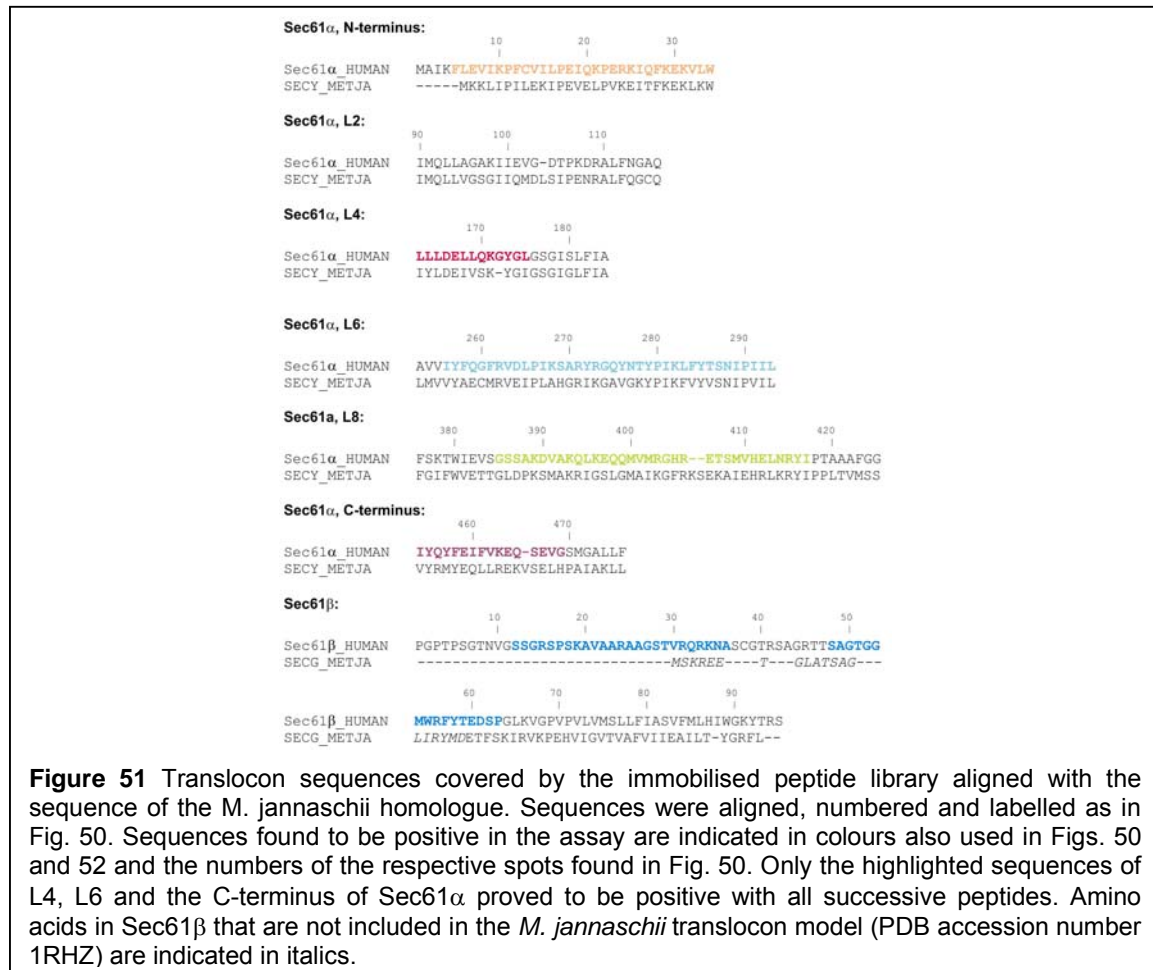
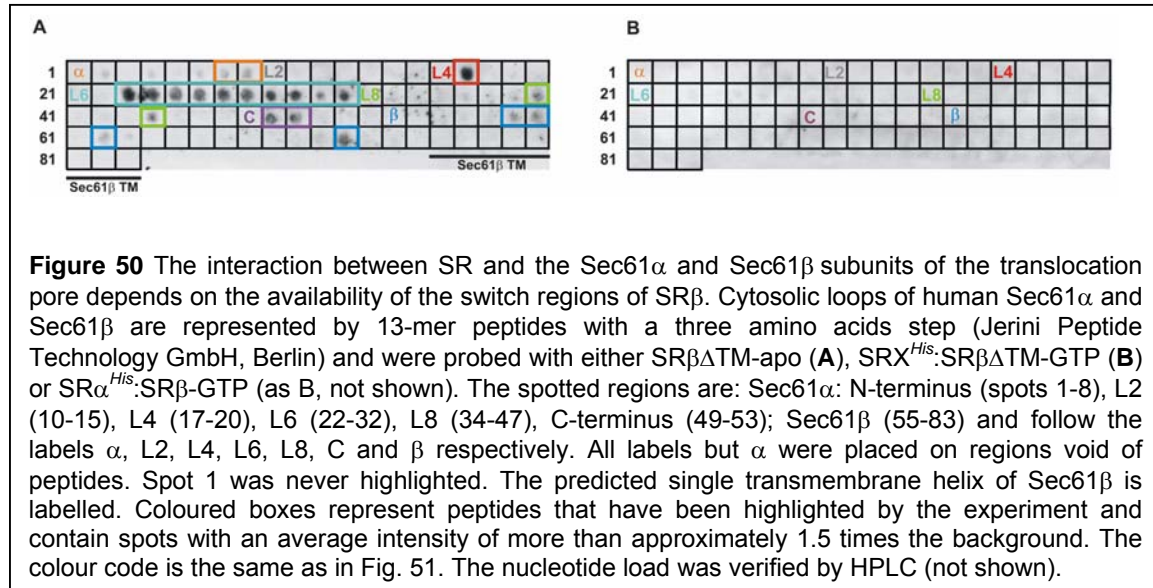


The library was probed with SRβΔTM-apo or SRβΔTM-GTP in complex with either SRX^{His} or SRα^{His}. Strikingly, heterodimeric SR did not show any interaction while several cytosolic loops of Sec61α and the N-terminus of Sec61β were recognised by SRβΔTM-apo (Fig. 50). This indicates that the SRβΔTM surface required for Sec61αβ binding is the same as observed in the SRX^{His}:SRβΔTM-GTP structure (see 2.4.4).

In order to test nucleotide specific binding of SRβΔTM to cytosolic Sec61αβ loops, cytosolic loops of Sec61αβ have to be tested with SRβΔTM in the apo-form and homogeneously loaded SRβΔTM-GDP and SRβΔTM-GTP species. Only SRβΔTM-apo could be obtained homogeneously from the SRβΔTM preparation. Due to the insufficient reloading of SRβΔTM-apo with either GDP or GTP homogeneous SRβΔTM-GDP or SRβΔTM-GTP could not be obtained. Therefore, the nucleotide dependent binding of SRβΔTM to Sec61αβ could not be tested. Nevertheless, peptides from cytosolic Sec61αβ loops were highlighted by the apo form of SRβΔTM, but not by SRβΔTM in complex with GTP and either SRX^{His} or SRα^{His} (Fig. 50).

Results

Since GEFs facilitate the release of GDP from GTPases and stabilise the apo form, these observations are in agreement with Sec61 $\alpha\beta$ acting as GEF for SR $\beta\Delta$ TM.



Results

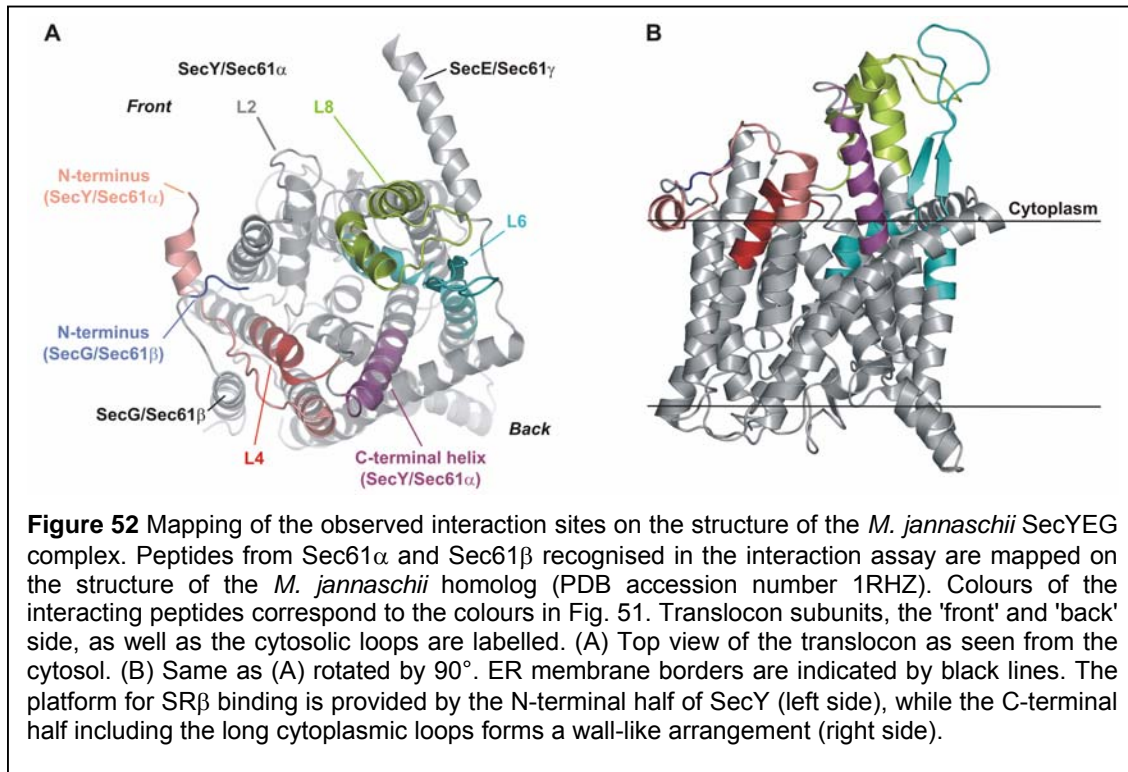
Above the interaction of SR $\beta\Delta$ TM-apo with cytosolic Sec61 $\alpha\beta$ loops was analysed focussing SR $\beta\Delta$ TM-apo. Here, the cytosolic loops of Sec61 $\alpha\beta$ are described.

The strongest signals were obtained for SR $\beta\Delta$ TM-apo and the 'back' side of the translocon (Figs. 50 and 52). L6 consists of a β -hairpin structure protruding from the translocon channel and peptides representing almost the complete loop give strong signals (spot numbers 23-32). The C-terminal helix of Sec61 α is highlighted by a pair of spots with high intensity (spot numbers 49 and 50). The end of helix 4 and the N-terminus of loop L4 also give a strong signal.

Weaker but still significant signals are observed for peptides close to the 'front' side of the translocon including the binding site of the signal peptide (Fig. 52) (Van den Berg et al., 2004). SR $\beta\Delta$ TM-apo interacts with the N-terminus of Sec61 α (spot numbers 2, 4, 6-8) and with loop L8 (spot numbers 37, 39, 40, 44). Importantly, loop L2 which is close to the channel opening did not give any signals.

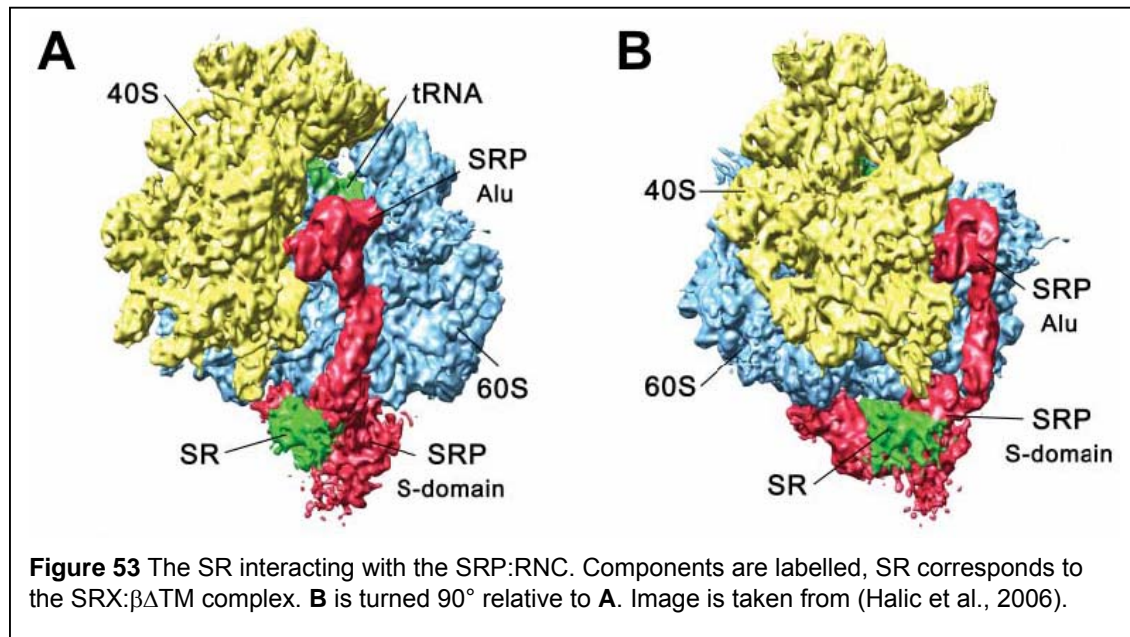
For the small translocon subunit Sec61 β , the N-terminus gives weak signals (Fig. 50; spot numbers 59, 60, 62, 63) and two spots of different intensity are observed closer to the predicted TM (Figs. 50 and 52; spots 71, 72). The N-terminus of human Sec61 β is 36 residues longer than in the homologous *M. jannaschii* SecG (Kinch et al., 2002); Fig. 51). Secondary structure predictions of the N-termini do not show a clear preference for secondary structure (Ouali and King, 2000) and in the crystal structure the first 20 residues of SecG are disordered (Van den Berg et al., 2004). Therefore, a structural interpretation of this interaction site is not possible (see discussion). The signal close to the TM is part of a Sec61 β motif that is conserved in archaeal and eukaryotic SR β homologues (Kinch et al., 2002). It is predicted to include a small β -strand between Trp56 and Thr60 (Ouali and King, 2000), but in the crystal structure this region is part of a loop that folds on top of the Sec61 α platform and points towards the translocation pore (Fig. 52).

In summary, SR $\beta\Delta$ TM-apo is likely to bind to cytosolic loops of the translocon with a surface that is at least partially occupied by SR α or SRX as observed in the SRX: $\beta\Delta$ TM structure. The data suggest that SR $\beta\Delta$ TM-apo binds on top of the translocation channel. The intensities of the signals obtained with peptides from the 'back' side of the translocon suggest stronger interactions than with the 'front' side. Sec61 β peptides highlighted by SR $\beta\Delta$ TM-apo involve a binding motif that is conserved in archeal and eukaryotic SR β homologues.



2.5.2 SR-SRP:RNC Interaction

Another important interaction partner of the SR is the SRP:RNC complex. Binding of the SR to the SRP:RNC leads to the formation of the docking complex and represents a crucial step in cotranslational targeting. During the course of this study, the SRP:RNC complex was determined at 12 Å by cryo-EM (Halic et al., 2004) and the structural rearrangements upon complex formation were analysed in detail (Wild et al., 2004a). As a logical next step, cryo-EM analysis of the complete mammalian docking complex was an important goal. In collaboration with Beckmann and co-workers, the SR $\alpha^{His}:\beta\Delta TM$ complex was employed in the reconstitution of the mammalian docking complex. Cryo-EM analysis led to the determination of this complex at 8 Å (Halic et al., 2006) shown in Fig. 53. SR $\alpha^{His}:\beta\Delta TM$ was only partially ordered. Determination of the SRX $^{His}:$ SR $\beta\Delta TM$ X-ray structure presented in this thesis allowed to fit the mammalian SRX $^{His}:\beta\Delta TM$ model into the cryo-EM electron density.



3 DISCUSSION

The eukaryotic signal recognition particle (SRP) and its receptor (SR) play a central role in co-translational targeting of secretory and membrane proteins to the endoplasmic reticulum (Keenan et al., 2001; Egea, 2005 #1078). SR is known to bind SRP in presence of GTP (Rapiejko and Gilmore, 1992). The SR is a heterodimeric complex assembled by the two GTPases $SR\alpha$ and $SR\beta$ (Tajima et al., 1986), whereas $SR\beta$ anchors $SR\alpha$ to the ER membrane (Miller et al., 1995). *In vitro* the eukaryotic SR lacking its transmembrane anchor is fully functional (Abell et al., 2004; Fulga et al., 2001; Ogg et al., 1998). $SR\alpha$ is tethered by its N-terminal part to $SR\beta$ (Young et al., 1995). The binding of nucleotide to $SR\beta$ is required for complex formation with $SR\alpha$ (Legate et al., 2000; Ogg et al., 1998).

Here, three important topics are discussed:

- 1.) The structure of the N-terminal domain of $SR\alpha$ in complex with a soluble form of $SR\beta$ ($SRX^{His}:\beta\Delta TM$) as prototype for the interaction of small GTPases with longin domains.
- 2.) $SR\beta\Delta TM$ binds in its nucleotide-free form to the translocon with the surface known from the $SRX^{His}:\beta\Delta TM$ X-ray structure.
- 3.) Cryo-EM structure of the mammalian docking complex carried out in collaboration with Beckmann and co-workers.

3.1 The Structure of the Mammalian SRP Receptor: SRX^{His}: $\beta\Delta$ TM

SR β reveals highest similarity to the GTP-bound structures of Sar1 in complex with Sec23/Sec24 (Bi et al., 2002) (rmsd: 1.30 Å over 143 C α -positions) and Arf1 (Shiba et al., 2003) (rmsd of 1.50 Å over 150 C α -positions) reflecting their evolutionary neighbourhood (Jekely, 2003). Besides the N-terminal membrane anchoring regions, the most striking structural difference between SR β and Arf or Sar1 is an insertion between helix α_{4B} and strand β_{6B} (37 residues compared to Sar1). Helix α_{4B} is extended by two turns and protrudes from the protein core as described earlier (Schwartz and Blobel, 2003). The insertion is partially disordered and no particular function has been attributed to it so far.

The SRX domain (see Figs. 41, 42) belongs to the mixed α/β class proteins sharing topology ($\beta\beta\alpha\beta\beta\alpha\alpha$) and fold of the SNARE-like protein superfamily (<http://scop.mrc-lmb.cam.ac.uk/scop>) including the N-terminal domains of non-syntaxin SNAREs (longin domains). Helix α_{1X} flanking loop regions are not conserved and only partially visible in the structure. The buried surface between SR β -GTP and SRX is 1850 Å², which is similar to the yeast structure and other GTPase-effector complexes (Schwartz and Blobel, 2003).

3.1.1 The SRX^{His}: $\beta\Delta$ TM-GTP 'Dimer'

The mammalian SRX^{His}:SR $\beta\Delta$ TM-GTP complex forms a crystallographic 'dimer' due to an interaction of the SRX domains involving a domain swap of helix α_{1X} and the formation of a continuous *trans* β -sheet (see Fig. 43). Considering that α_{1X} satisfies the hydrophobic core in the 'monomeric' and 'dimeric' state, this buried surface can not be taken into account to reflect the stability of the 'dimer'. Therefore, dimerisation leads to an additional buried interface of approximately 1000 Å² between the two SRX^{His}:SR $\beta\Delta$ TM-GTP 'monomers'. This reflects a complex that is much more labile than SRX associated to SR $\beta\Delta$ TM. In fact, in solution a K_D of 270 μ M was determined for the 'dimer' (Jacek Mazurkiewicz and Karsten Rippe from the Kirchhoff Institut für Physik, Heidelberg). The low K_D is also reflected by the fact that crystals took usually four weeks to grow and that the 'dimer' was not observed meanwhile size exclusion chromatography of the protein. This can be explained by the dilution of the protein over the column, reducing the amount of 'dimer' below the level of detection.

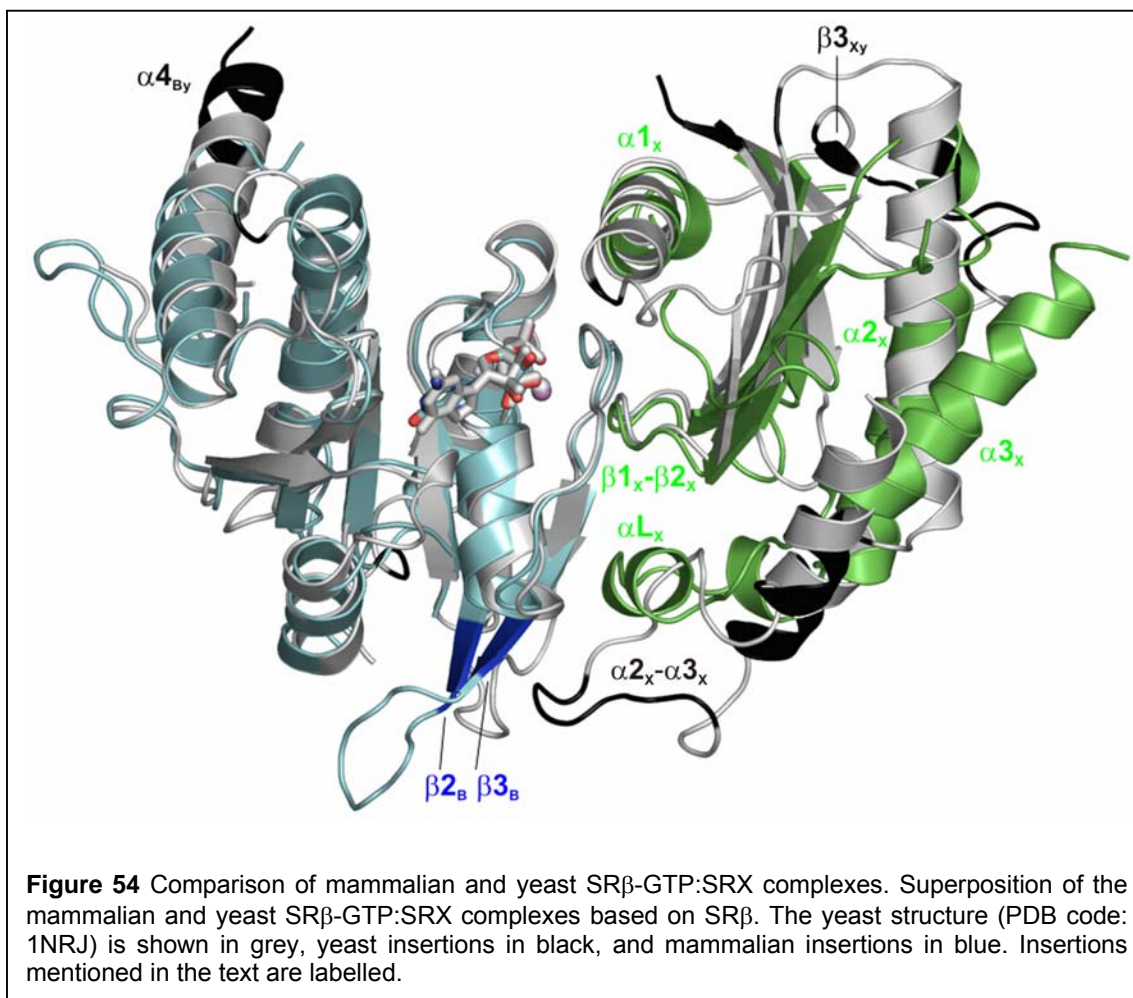
We cannot directly conclude from this result in solution to the state of the complete SR complex at the membrane since full length SR $\alpha\beta$ is anchored to the membrane *in vivo*. It is considerable that the membrane anchored receptor occurs in locally elevated concentrations increasing the likelihood of homodimerisation. The 'dimer' has not been reported before. Therefore, the physiological relevance for the dimerisation of SRX^{His}:SR $\beta\Delta$ TM-GTP is not clear. The 'dimer' might be as well enforced by crystal packing. It is not clear whether the crystal symmetry favours the domain swap of the flexibly linked helix α_1 (see below) due to steric hindrance or, more likely, the dimer selects this crystal symmetry. The simultaneous formation of the *trans* β -sheet stabilises oligomerisation by main chain hydrogen bonding.

Still, a potential homodimeric form is unlikely existing when the SR is complexed to SRP54 because of sterical hindrances. Therefore, one could think of the homodimeric state as a stabilisation of the SR, especially SR α with its floppy linker region between X domain and NG domain, in its inactive state when it is not complexed to SRP54. The low affinity between two SRs could be useful *in vivo* in order to allow a fast release of the monomeric form on demand.

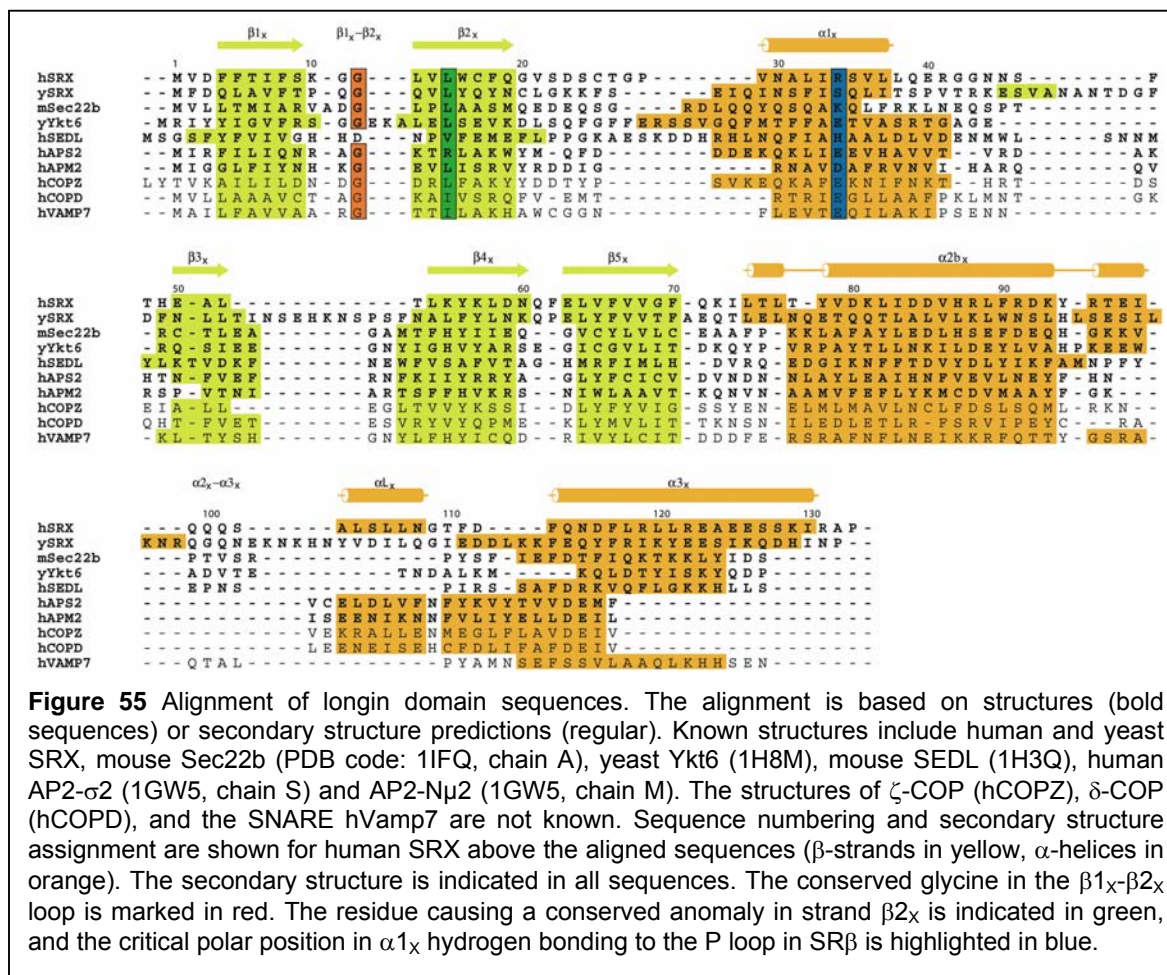
Interestingly, the comparison with the yeast structure ('monomer', see below) showed that the domain-swapped helix α_{1X} of the second SRX molecule of the mammalian receptor superimposes with its corresponding position in the yeast 'monomer'. Therefore, a 'monomeric' mammalian receptor complex was used for analysis.

3.1.2 Comparison with SRX:SR $\beta\Delta$ TM-GTP from Yeast

The structures of mammalian and yeast SR $\beta\Delta$ TM-GTP (Schwartz and Blobel, 2003) are conserved (rmsd of 1.16 Å over 158 C α -positions, yeast is distinguished in the following by a 'y' subscript). Differences include the lengths of the β -strands β_{2B} and β_{3B} that are almost twice as long in mammals and helix α_{4B} that is two turns shorter (Fig. 54).

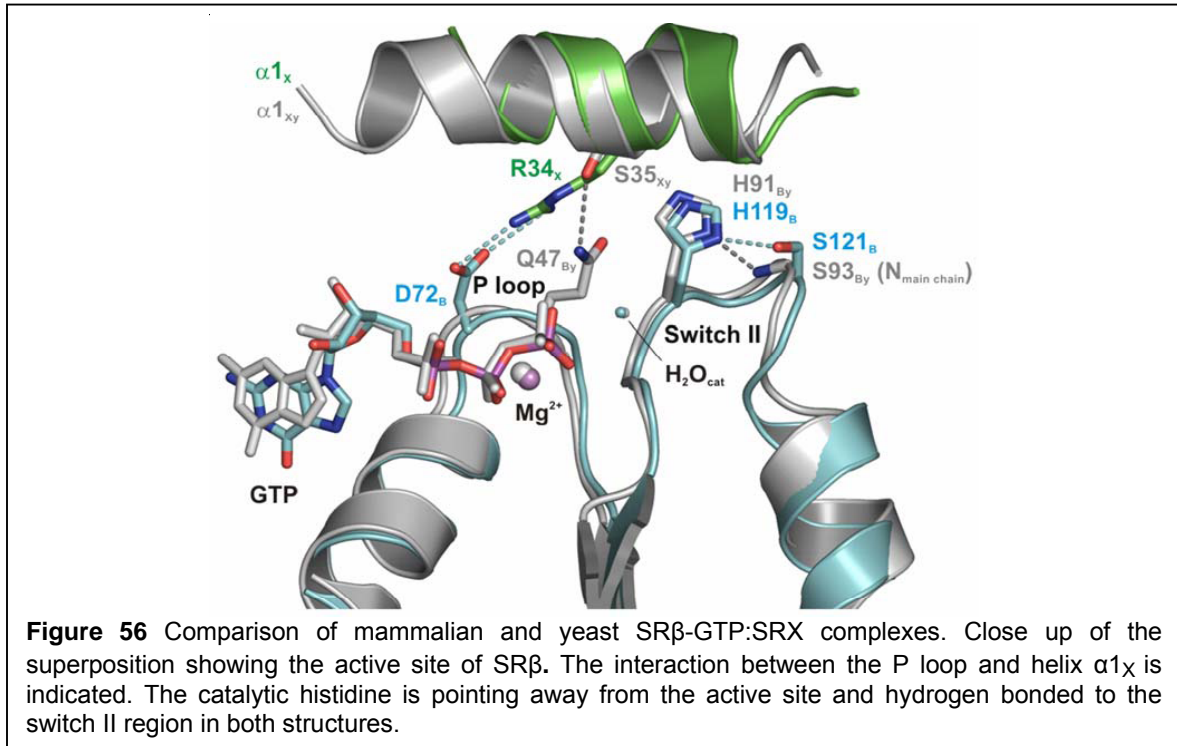


In contrast, there are significant differences in SRX (rmsd of 1.81 Å over 75 C α -positions) (Fig. 54). In the yeast structure there is no helix swap leading to a SRX^{His}:SRβΔTM-GTP 'dimer'. Instead, the central β -sheet of SRX_y is extended by one strand (β_{3xy}) between helix α_{1xy} and strand β_{4xy} (β_{4xy} corresponds to strand β_{3x} in our structure), which apparently stabilises the position of helix α_{1x} and thereby prevents 'dimer' formation. While helix α_{1x} and the β_{1x} - β_{2x} hairpin in the interface superimpose very well, the central β -sheet and the connected helices α_{2x} and α_{3x} do not. Differences increase with distance from the SRX^{His}:SRβΔTM interface.



Yeast SRX shows two major insertions (Figs. 54, 55). A 20 residue insertion elongates the central β-sheet by introducing the sixth β-strand (β3_{xy}: Glu46_{xy} to Ala49_{xy}) and a loop touching helix α2_{xy} on the convex side of the β-sheet. A 15 residue insertion changes the conformation of the loop between helices α2_x and α3_x and the herein inserted helix αL_x is not present. The C-terminal helices (α4_{xy} and α3_x) do not align which might be due to a truncation of this helix in the yeast structure. With its insertions, yeast SRX is unusual compared to other SRX domains. The observed structural differences between mammalian and yeast SRX are reflected by the low degree of conservation on the sequence level (14.2% identity, Fig. 55). Low sequence conservation is a general feature of the SRX family (Schwartz and Blobel, 2003). One functionally important exception is the conserved Gly12_x in the β1_x-β2_x hairpin (Figs. 54, 55). It facilitates the β-hairpin turn and a bulky side chain would sterically interfere with binding of SRβ. Position and amphipathic

character of the important helix $\alpha 1_x$ are conserved. Asn30_x is conserved between human and yeast and interacts with SR β by hydrogen bonding to the switch I region.



A polar residue one turn further appears to occupy a crucial position within helix $\alpha 1_x$. Arg34_x forms a salt bridge with Asp72_B in the P loop and thereby influences the position of the catalytic histidine (His119_B) with respect to the active site of SR β (Fig. 56). Although this salt bridge is not conserved, a polar interaction is observed in the yeast structure between Ser35_{xy} and Gln47_{By} within the P loop, suggesting a similar role.

3.1.3 SRX as Effector for SR β

SRX occupies large parts of a typical GAP binding site (Corbett and Alber, 2001) as it interacts with the P loop and the switch regions of SR β -GTP resulting in the stabilisation of switch II. However, in the SRX:SR β Δ TM-GTP complex the catalytic histidine (His119_B) in switch II of SR β (Gln61 in Ras, Gln71 in Arf) is in a 'resting' position pointing away from the active site (Fig. 56), the characteristic arginine finger of a GAP (Scheffzek et al., 1998) is not present, and the complex is stable when bound to GTP. Therefore, the SRX:SR β Δ TM-GTP complex is not a GTPase:GAP complex and for the stimulation of GTP hydrolysis an additional binding partner is needed. The RNC has been shown to stimulate GTP hydrolysis of SRX:SR β Δ TM-

GTP (Bacher et al., 1999). However, the RNC does not act as GAP for SR β Δ TM-GTP alone (Legate and Andrews, 2003). Therefore, the SRX domain can be assigned as co-GAP for SR β which fulfils one part of the GAP function by stabilising switch II. Examples for a split GAP function have been reported before. The GAP for the α -subunit of a heterotrimeric G protein ($G_{i\alpha 1}$) also stabilises the switch regions, but the arginine finger is supplied *in cis* by an additional domain of the GTPase (Tesmer et al., 1997). A unique feature of the Arf1:ArfGAP1 structure is the exclusive stabilisation of the switch II region (Goldberg, 1999). The switch I region is recognised by the heptameric coat protein complex (COPI) (Zhao et al., 1999), which is found to stimulate GTP hydrolysis (Goldberg, 1999). Most likely an arginine finger is needed to trigger GTP hydrolysis in Arf1 (Goldberg, 1999), which might be the case as well in SR β .

The co-GAP function can be explained by a comparison of SRX:SR β -GTP with the structure of the Ras-GDP-AlF₃:RasGAP transition-state complex (Scheffzek et al., 1997). When SR β is superimposed on Ras, the loop of RasGAP containing the arginine finger (Arg789_{RasGAP}) fits between SR β and SRX (Fig. 57). The only sterical clash concerns the arginine finger itself, which would interfere with the salt bridge between Arg34_X and Asp72_B. In addition, the Ras-GDP-AlF₃:RasGAP complex contains a second arginine (Arg903_{RasGAP}) in close proximity to Arg34_X (Fig. 57). Arg903_{RasGAP} forms a salt bridge to Glu63_{Ras} in the switch II region of Ras thereby stabilising the switch II region. In SRX:SR β -GTP the catalytic residue His119_B is hydrogen bonded to the corresponding residue of Glu63_{Ras} (Ser121_B) (Fig. 57B).

The comparison of SRX:SR β -GTP with the Ras-GDP-AlF₃:RasGAP complex suggests that upon the insertion of an arginine finger into the GTP binding pocket the salt bridge between Arg34_X and Asp72_B can be disrupted. The liberated Arg34_X may then swing from the P loop towards Ser121_B in switch II forming a hydrogen bond (Fig. 57C). His119_B would therefore be released, the catalytic water can be positioned and hydrolysis occurs. Mutants in which the salt bridge is disrupted (Asp72_BGly and an Arg34_XAla) still form the SRX:SR β -GTP complex (data not shown) indicating that the missing GAP is essential to stimulate GTP hydrolysis. The large conformational changes that are typically observed in the effector region upon GTP hydrolysis are expected to disrupt the SRX:SR β interface and lead to the dissociation of the SR complex (Schwartz and Blobel, 2003).



3.1.4 Longin Domains

SRX belongs to the superfamily of SNARE-like proteins with the longin domain fold (Filippini et al., 2001). Sequence homology within the superfamily is low (Fig. 55), but the structural homology is high (Fig. 59) as illustrated by the comparison of SRX with SEDL (Jang et al., 2002), with the SNAREs Sec22b (Gonzalez et al., 2001) and Ykt6 (Tochio et al., 2001), and the μ 2 (N-terminal domain) and σ 2 adaptins (Collins et al., 2002).

In order to determine conserved elements within the longin domain fold we prepared a structure based sequence alignment of structurally known longin domains and of important longin domain candidates (ζ -COPI, N δ -COPI, VAMP7; Fig. 55). Among longin domains with known structures, SRX_y reveals specific insertions like

strand $\beta 3_x$ whereas the mammalian structure is closer to other members of the superfamily. Longin domains share the $\beta\beta\alpha\beta\beta\alpha$ topology as described for SRX (Fig. 55). The glycine residue (Gly12_x in SRX) in the $\beta 1$ - $\beta 2$ hairpin is highly conserved (Fig. 55), and the hairpin adopts a similar conformation in all longin domain structures. Only in SEDL this glycine is exchanged for an aspartate and the change is compensated by adjustments in the adjacent β -strands. Ykt6 comprises a unique insertion of three residues. Helix $\alpha 1$ is an essential component of the longin domains (see below). The amphipathicity of helix $\alpha 1$ is highly conserved, while there is no conservation on the sequence level and the length ranges from three (SRX) to six turns (Ykt6). The orientation of helix $\alpha 1$ with respect to the central β -sheet varies in the different longin domains (Fig. 59). Flexibility is reflected by elevated temperature factors in the loops connecting helix $\alpha 1$ to the β -sheet (not shown) and in the SRX structure the flexibility is responsible for 'dimer' formation by the swap of helix $\alpha 1_x$.

A conserved β -sheet anomaly (down-up-up-down) is the insertion of a bulky hydrophobic residue (Leu15_x in SRX, Fig. 5) within strand $\beta 2$. It seems to be important for stabilising the protein core and indicates an evolutionary relationship between the longin domains. The C-terminal helix $\alpha 3$ differs in length and orientation between the individual structures and superimposes best for Sec22b, SEDL and SRX. Helix $\alpha 3$ is truncated in the longin domains of the AP2-complex ($N\mu 2$, $\sigma 2$), which according to secondary structure predictions is also the case in other AP complexes and the COPI-complex ($N\delta$ -, ζ -COPI) (Fig. 55). Here, the longin domain fold is extended by a β -hairpin structure followed by another helix forming a fourth layer in the back of the longin domain fold (not shown). The length and the conformation of the loop regions vary significantly (Fig. 59).

3.1.5 GTPase: Longin Domain Complexes at Endomembranes

The localisation of longin domains at the endomembrane system correlates with the presence of small membrane-associated GTPases like the Arf and Sar1 proteins which are the closest relatives of SR β . The structural conservation and the co-localisation strongly suggest that other GTPase:longin domain interactions may exist. Two hydrophobic patches flanking helix α 1 were noticed previously in longin domain structures and were proposed as protein-protein interaction surfaces (Gonzalez et al., 2001; Jang et al., 2002; Tochio et al., 2001). Interestingly, these patches are conserved in structurally determined longin domains (Fig. 59). In the SRX^{His}:SR β Δ TM complex, SR β binds to this interaction surface. SR β Δ TM intercalates its switch I region between helix α 1x and the SRX β -sheet, one of the helix flanking hydrophobic patches is extended and forms a hydrophobic groove (Figs. 59, 60). In free longin domain structures the hydrophobic groove is absent (Fig. 59). The opening of the groove can be envisaged by rolling the conserved amphipathic helix α 1 onto the second hydrophobic surface patch on the other side of the helix. The flexibility of helix α 1 is therefore a prerequisite for the interaction of longin domains with their respective GTPase.

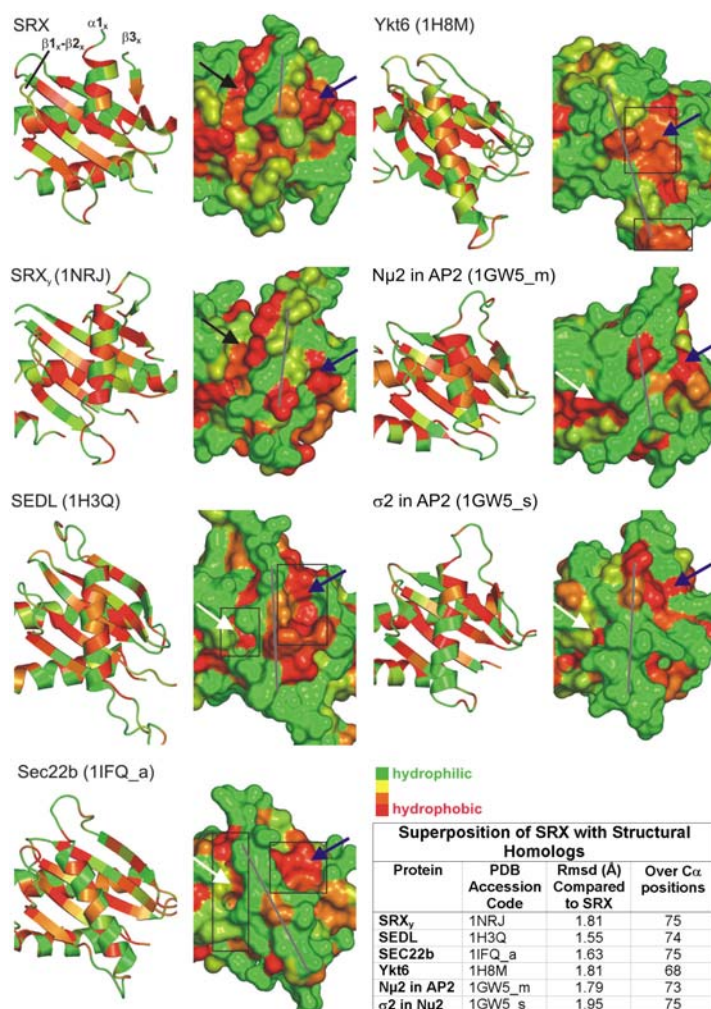
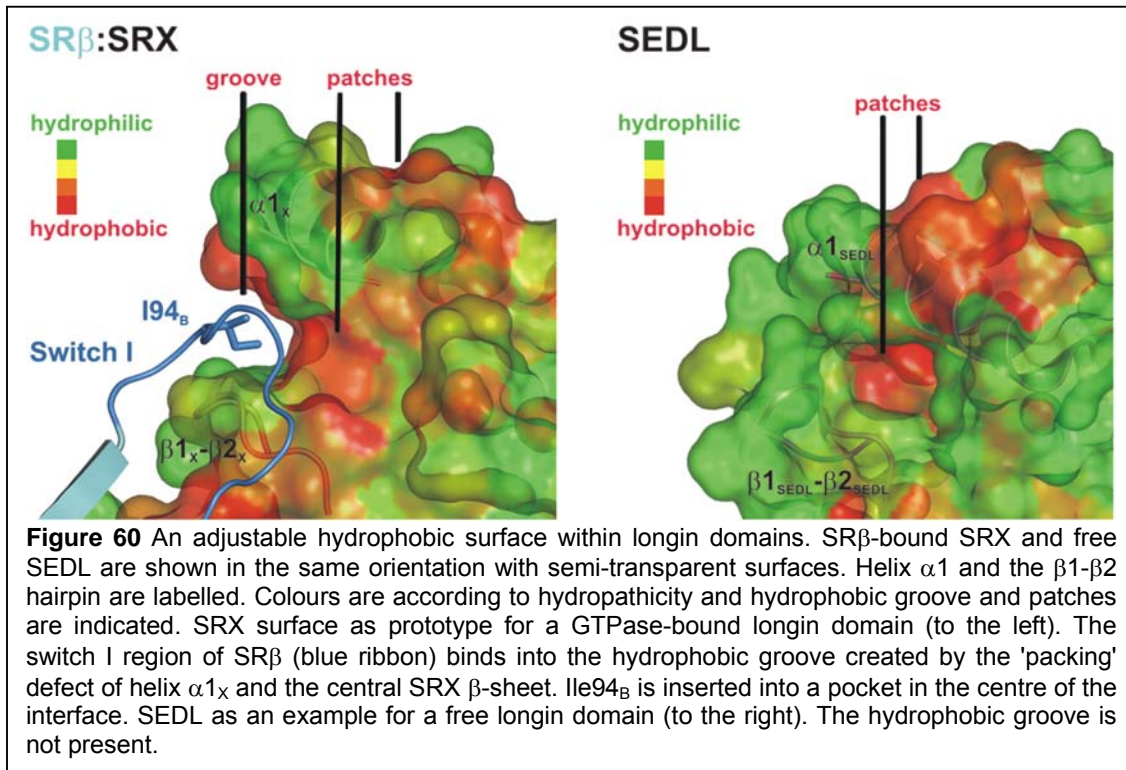


Figure 59 Comparison of longin domains and flexibility of helix $\alpha 1$. Longin domain structures are depicted in ribbon and surface representations (PDB codes are given). SRX is oriented to show the surface interacting with SR β . All structures are oriented accordingly. The structures of longin domains other than SRX have been determined as monomers or in context of the AP-2 'trunc' (N μ 2 and σ 2). Colour code corresponds to hydrophobicity (Kyte and Doolittle, 1982). The different orientations of helix $\alpha 1$ are indicated by a grey line. The hydrophobic grooves in SRX and SRX $_{\gamma}$ are marked by black arrows. Hydrophobic patches are shown by blue and white arrows, respectively. Previously described hydrophobic patches are boxed (SEDL (Jang et al., 2002); Sec22b (Gonzalez et al., 2001); Ykt6 (Tochio et al., 2001)). The rmsd values of all longin domains in respect to SRX are given.



While the conservation of the hydrophobic patches suggests a similar mode of GTPase:longin domain interaction, the low degree of conservation reflects the special adaptations of the individual systems. For example, in all known longin domains the equivalent position of Arg34_x within helix $\alpha 1_x$ (Figs. 47, 48 and 56) seems to be occupied by a charged or polar residue (Fig. 58). In the respective GTPases the same is true for the residue at the position equivalent or adjacent to Asp72_B in the P loop. Therefore, a polar contact between helix $\alpha 1$ and the P loop might be present in all GTPase:longin domain interactions. As discussed for the co-GAP function of SRX (see above), the residues corresponding to Arg34_x could also participate in the stabilisation of the switch II regions of the respective GTPases. The mammalian SRX^{His}:SRβΔTM complex can thus be regarded as a structural prototype for a GTPase:longin domain interaction. Although there is no direct experimental proof, to our knowledge this idea does not contradict any previous data.

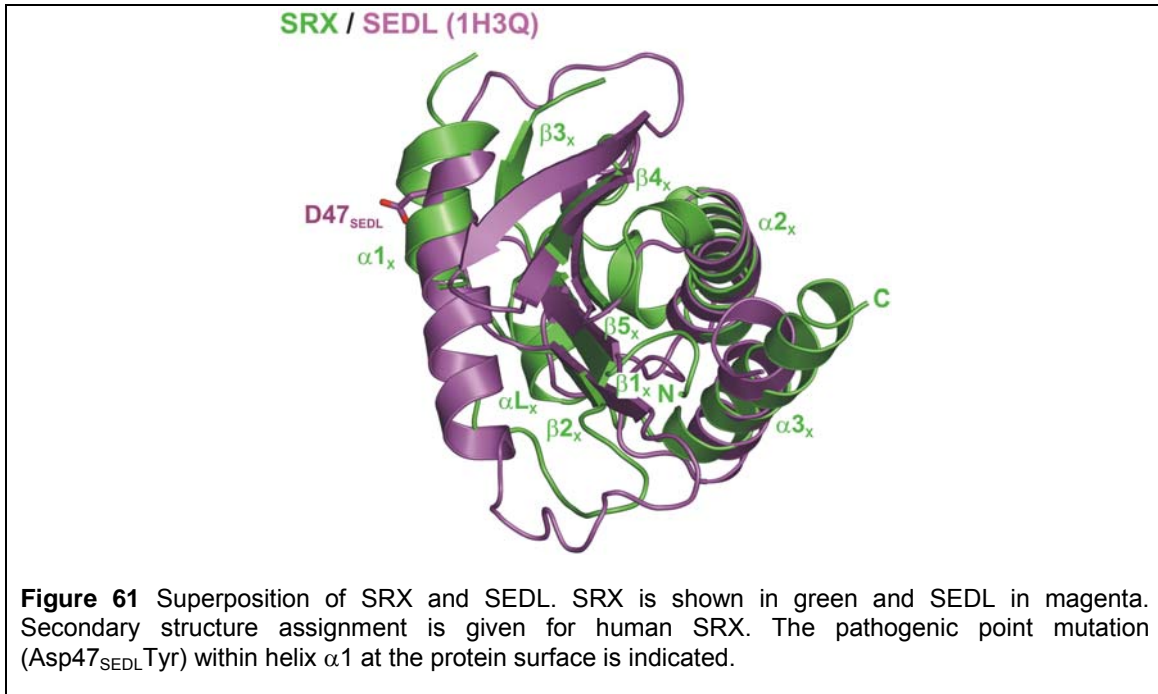
Structures of longin domains other than SRX have been determined as monomers (Sec22b, Ykt6, SEDL) or in context of the AP adaptor 'trunc' complex. All clathrin adaptor complexes (AP-1,-2,-3,-4) and COPI share a tetrameric 'trunc' organisation that consists of two large, a medium and a small subunit (McMahon and Mills, 2004). COPI- and AP-complexes contain two copies of longin domains (Nδ- and ζ-COPI, and AP-Nμ and -σ, respectively). In the structure of the AP-2 complex

(Collins et al., 2002), the two longin domains form the core of the 'trunc' with the respective $\alpha 1$ helices being in close proximity. Therefore, a tandem GTPase:longin domain interaction might be an important feature in all these complexes.

3.1.3 A molecular Explanation for a Genetic Disease

The GTPase:longin domain concept offers a structural explanation for the occurrence of spondyloepiphyseal dysplasia tarda (SED), an X-linked skeletal disorder characterised by a short trunk (MacKenzie et al., 1996). Point mutations in the human SEDL protein seem to be involved in a defect in cartilage transport from the ER to the Golgi apparatus (Sacher, 2003). The yeast homologue of SEDL (Trs20p) has been shown to be part of the highly conserved transport protein particle I (TRAPP I) that is required to tether ER-derived vesicles to the Golgi (Sacher et al., 1998) and consists of ten subunits (Wang et al., 2000).

When the structure of SEDL is superimposed with SRX in the $\text{SRX}^{\text{His}}:\text{SR}\beta\Delta\text{TM}$ complex (Fig. 61), the pathogenic Asp47Tyr mutation in human SEDL would be located on the protein surface within helix $\alpha 1_X$ in close proximity to the catalytic residue His119_B and the interacting Ser121_B of SR β (see Fig. 56). There is no structure of the corresponding SEDL:GTPase complex, however Ypt1p has been shown as the TRAPP interacting GTPase (Jones et al., 2000; Sacher et al., 2001; Wang et al., 2000) and according to our model Gln67 and Arg69 in Ypt1p could form a favourable interaction with Asp47_{SEDL}. Thus, the mutation most likely disturbs the GTPase regulation by interfering with the positioning of the catalytic residue.



3.2 Analysis of Interactions with SR and Components of the SRP Cycle

3.2.1 SR $\beta\Delta$ TM Binds in its Nucleotide-free Form to the Translocon

Data obtained from this work suggest interactions between a binding surface of SR $\beta\Delta$ TM-apo which binds to SRX in the SRX^{His}:SR $\beta\Delta$ TM complex. Additionally, there is indication that SR $\beta\Delta$ TM-apo interacts with defined regions of both Sec61 α and Sec61 β .

The Sec61 β homolog in yeast (Sbh) has been previously proposed to act as GEF for SR β (Helmers et al., 2003). Since GEFs facilitate the release of GDP from GTPases and stabilise the empty form, it seems likely that SR $\beta\Delta$ TM-GDP interacts with the translocon similar to the apo-form. These data localise the GTPase-effector interaction to cytosolic loop regions in Sec61 α and β . For the yeast translocation pore sequence alignments show a homology of the Sec61 β and the Sec7 protein family (Helmers et al., 2003; Jackson and Casanova, 2000; Mossessova et al., 1998). Sec7 acts as GEF for Arf proteins and the structure of the Sec7/Arf complex shows the relevant interactions (Mossessova et al., 2003; Renault et al., 2003). However, the homology between Sec61 β and Sec7 is very low, important residues are missing in

Sec61 β , and the secondary structure is not conserved. The Sec7 domain consists of 200 residues, whereas the cytosolic domain of Sec61 β is much shorter (66 residues for human SR β) and shows only low conservation (Kinch et al., 2002). Since structural information is missing, it is still possible that the signals obtained here for Sec61 β correspond to an interaction surface like in the Arf/Sec7 complex (Helmerts et al., 2003).

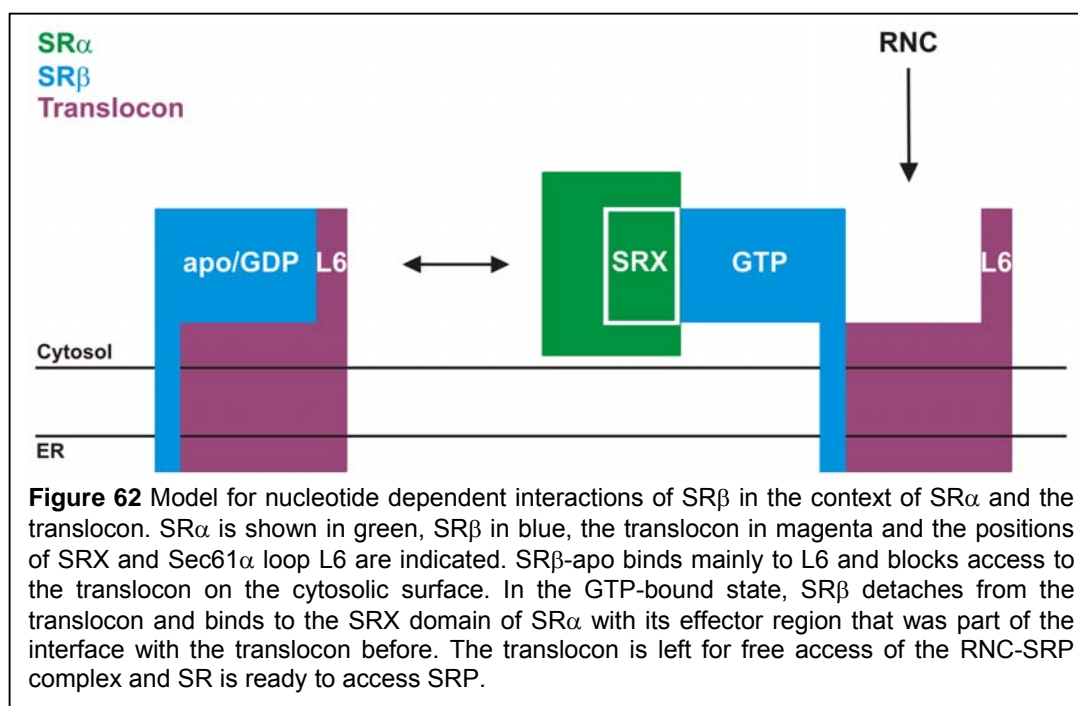
So far, a precise role of the Sec61 α subunit for SR β binding has not been described. Recent studies showed that L6 was not involved in ribosome binding, and the binding partner of L6 was not identified. However, L6 seems to be important in co-translational translocation, and an interaction of L6 with the SR was recently proposed based on pulse labelled protein translocation experiments in yeast (Cheng et al., 2005). Our data suggest that almost the complete loop L6 is an important component of the interaction with SR β -apo and SR β -GDP. Since in addition to loop L6 a number of cytosolic loop regions also contribute to SR β binding, Sec61 α might act as a binding platform for SR β .

The structure of Sec61 α shows a pseudo-two-fold symmetry which divides it in two halves comprising TMs 1-5 and TMs 6-10 (Fig. 52) (Van den Berg et al., 2004). Cytoplasmic loops of the C-terminal half (L6, L8, and C-terminus) of Sec61 α protrude significantly into the cytosol (Fig. 52). Since almost the complete cytoplasmic surface is involved in SR β binding, the following model for the SR β -Sec61 α complex is proposed: The β -hairpin structure of L6 forms a β -sheet *in trans* with SR β as it is known to occur in the interaction between other Ras-like GTPases and their effectors (Corbett and Alber, 2001). Taking the Arf-Sec7 complex as a model (Mossessova et al., 2003; Renault et al., 2003), the L6 β -hairpin could even insert between the so-called interswitch region and the central β -sheet of SR β (not shown). This interaction would still leave room for Sec61 β to bind to the adjacent switch I and II regions of the GTPase as observed in the Arf-Sec7 crystal structure and thereby to act as a GEF. If Sec61 α contributes to the GEF function remains to be seen.

Taking into account the structural information on Sec61 and the small size of the small GTPase SR β the contribution of all regions of Sec61 that interact with SR β according to our data suggests that SR β binds on top of the translocation channel (Fig. 52). The N-terminal half of Sec61 α with its short loop regions might form a binding platform, whereas the C-terminal half including loop L6 acts as a docking

station (Figs. 52 and 62). Although the intensity of the signals obtained with peptides from the 'back' side of the translocon suggests stronger interactions than the 'front' side, detailed binding experiments with isolated peptides have to be performed to confirm the preferred binding site. The most prominent signal in the assay (spot number 17) includes significant parts of helix $\alpha 4$. As the following peptide (shifted by three residues towards the L4 loop) does not give a signal, helix integrity might play a role for stable SR β docking.

Since the strong signals obtained with SR β -apo are completely lost when the SRX^{His}:SR β Δ TM or SR α ^{His}:SR β Δ TM complexes are used, the surface of SR β Δ TM-GTP binding to SRX, as known from the structure of the SRX^{His}:SR β Δ TM-GTP complex, must at least partially overlap with the surface of SR β Δ TM-apo generating signals in this assay. Since a GEF would facilitate GDP release from a GTPase and stabilise the apo form, this data supports previous data indicating a GEF function of the translocon (Helmers et al., 2003). A nucleotide-dependent model of the translocon SR β interaction can be envisaged as follows: While SR β -apo is likely to block the translocation pore, in its GTP bound form it might swing aside to bind SR α leaving the translocon accessible for an incoming RNC-SRP complex (Fig. 62).

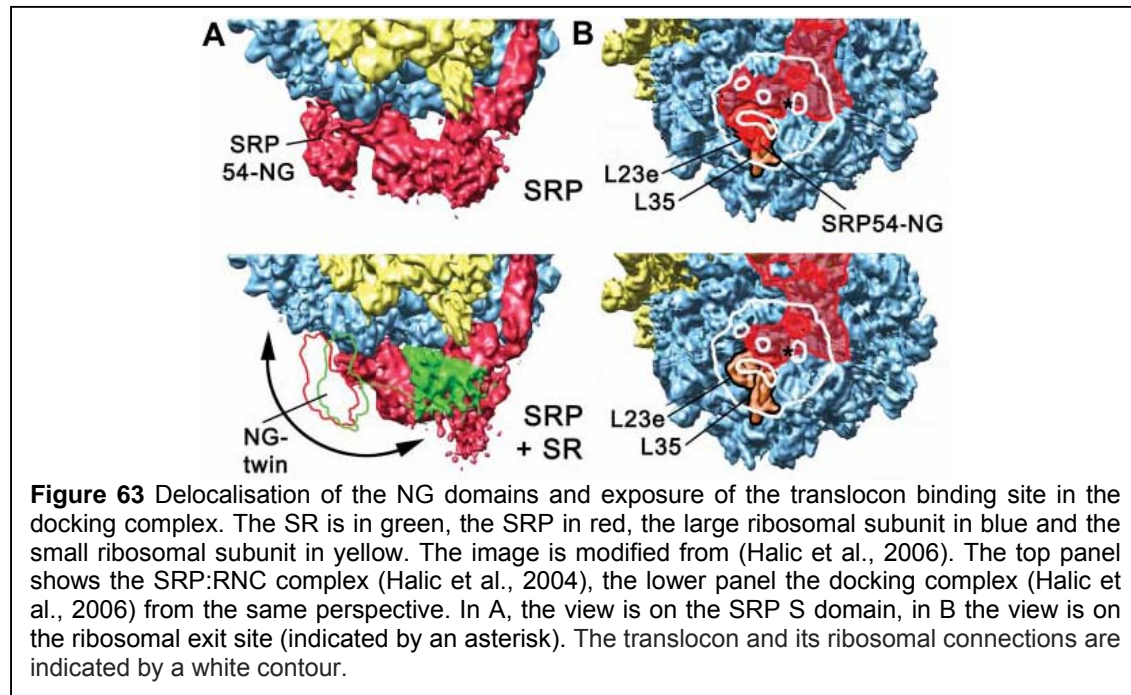


This model is consistent with GTP binding to SR β being necessary for efficient protein translocation (Fulga et al., 2001). It is not known, whether GTP hydrolysis in SR β occurs in each SRP cycle and which would likely lead to the dissociation of SR. The location of the transmembrane helix of SR β with respect to the transmembrane helices of the translocon is not known. With the extensive contacts between the SR β GTPase and the cytosolic loops of the translocon it seems possible that the TM of SR β attaches to the translocon within the membrane. Interestingly, the bacterial Sec61 β homolog SecE comprises two TMs and cryo-EM data (Breyton et al., 2002) place them side-by-side on the SecY surface. Bacteria do not code for SR β , which makes it tempting to speculate that the TM of SR β might have replaced the extra TM of the SecE protein and could therefore be located in direct neighbourhood of the Sec61 β TM.

The translocation pore is known to form oligomers in the membrane, but despite a high resolution crystal structure (Van den Berg et al., 2004) the architecture in the membrane is still under debate (Beckmann et al., 1997; Beckmann et al., 2001; Breyton et al., 2002; Manting et al., 2000; Menetret et al., 2000; Mitra et al., 2005; Mori et al., 2003). One model suggests a back-to-back associated dimer of SecY complexes derived from a 2D-crystal structure (Breyton et al., 2002) while another one suggests a front-to-front arrangement derived from cryo electron microscopy (Mitra et al., 2005). A third model prefers a tetrameric arrangement (Manting et al., 2000). A back-to-back arrangement could merge with a tetrameric assembly into an assembly of two dimers side-by-side (Van den Berg et al., 2004). Crosslink data support an oligomeric SecY complex assembly but neither go along with a front-to-front nor back-to-back orientation of the monomers (Veenendaal et al., 2001). The implications of translocon oligomerisation for the co-translational targeting process are not clear (Dobberstein and Sinning, 2004; Mitra et al., 2005; Van den Berg et al., 2004). In principle, one SR β subunit could bind stoichiometrically to a single translocon complex. From cryo-EM data (Beckmann et al., 2001; Mitra et al., 2005) it is evident that only one translating ribosome can be bound to an oligomeric translocon, and therefore only one SR β would be necessary to support SRP dependent targeting. However, several SRP receptors bound to a translocon oligomer could be advantageous for efficient co-translational targeting as it has been suggested for the recruitment of enzymes required for modification of the synthesised protein (Dobberstein and Sinning, 2004).

Taken together, this data support the idea of an interaction of SR β with the translocon depending on the nucleotide load of SR β . It is suggestive that the surface of SR $\beta\Delta$ TM participating in the SRX^{His}:SR $\beta\Delta$ TM complex at least partially overlaps with the surface of SR $\beta\Delta$ TM-apo highlighting to the cytosolic translocon loops. SR $\beta\Delta$ TM binds in its nucleotide-free form, but not when in complex with GTP and either SRX or SR α , to the translocon, supporting data that the translocon acts as a GEF for SR β . SR $\beta\Delta$ TM-apo binds to the Sec61 α and Sec61 β subunits. The observed signals are best explained by a model in which Sec61 α functions as a binding platform for SR β with an important contribution by the cytosolic loop L6. Therefore, Sec61 α might contribute to the GEF function which was previously attributed to Sec61 β .

3.2.2 Analysis of the SR Interacting with the SRP:RNC Complex



Comparing the structures of the SRP:RNC complex and the docking complex, it is interesting to note, that the SRP54NG and the SR α NG domains can not be localised (Fig. 63A), implying a high flexibility of these domains upon docking complex formation. It is interesting to note that in previous cross-linking studies (Pool et al., 2002) SRP54 could be cross-linked to two ribosomal proteins. However, in the presence of SR one of these cross-links was lost. While a more detailed

interpretation of this observation was not possible before, the cryo-EM data put it now on a structural basis. With the observed delocalisation of the NG domains, an important part of the ribosomal translocon binding site is exposed (Beckmann et al., 2001)

So far, it is not clear whether a monomeric or oligomeric translocon arrangement binds to the SRP:RNC complex. The oligomerisation state of the translocon or the translocon:ribosome complex has been analysed before by different techniques. A homodimeric covalently linked SecYEG complex was shown to form a functional translocon by complementation assays (Duong, 2003). Homodimers are also proposed from analysis of two-dimensional crystals (Breyton et al., 2002). Fluorescence resonance energy transfer (FRET) experiments suggest that two or more SecYE complexes associate in the lipid bilayer (Mori et al., 2003). Functional assays, negative stain EM data and mass measurements with the scanning transmission microscope point towards a tetrameric translocon assembly (Manting et al., 2000). Also, EM data of detergent treated yeast and mammalian translocons reveal homotrimeric to homotetrameric translocon complexes (Hanein et al., 1996). Cryo-EM data showed before that a translocating ribosome can bind either to a homotrimeric translocon (Beckmann et al., 2001) or an unusual homodimeric assembly (Mitra et al., 2005). Although the latter one seems questionable, it is still under debate.

The relatively small spatial rearrangements occurring upon docking complex formation (Fig. 63) (Halic et al., 2006) suggest now that a monomeric translocon could bind to the docking complex. This would be in agreement with the X-ray structure of a monomeric SecYEG complex suggesting that a single translocon forms a functional translocation unit (Van den Berg et al., 2004). This proposal is supported by immunoprecipitation experiments showing that no co-immunoprecipitation was found between translocation complexes assembled from HA-tagged and wild-type SecE (Yahr and Wickner, 2000).

In summary, the cryo-EM docking complex structure (Halic et al., 2006) highlights the flexibility of the NG:NG complex which leads to the exposure of an important translocon binding site at the ribosome. Whether the translocon binds as a monomer or as an oligomer remains to be shown.

4 Outlook

The data presented here emphasises the importance of the interaction between longin domains and small GTPases at the endomembrane system of eukaryotic cells. As a next step the interaction between Ypt1p and SEDL could be further examined *in vitro* and *in vivo* in order to explain one of the mutations in SEDL leading to the disease SEDT. Another interesting result is the suggestion of a functional interaction between Arf1 and ζ -COPI or $N\delta$ -COPI. Binding studies should give further insights in the assembly of COPI vesicles.

SR β binds in its nucleotide-free and likely GDP state to the translocon. This is in agreement with the translocon acting as a GEF for SR β . Peptides that were highlighted in the binding assay by SR β Δ TM-apo could be used in isothermal calorimetry or fluorescence spectroscopy experiments. This would allow to further narrow down and determine crucial SR β translocon interactions.

The reconstitution of a part of the mammalian SRP S domain was the basis for further structural characterisation. Crystallisation experiments have to be continued for SRP and the SRP:SR complexes. Mutants of SRP and SR proteins will characterise the kinetics of complex formation of the SRP:SR complex. SRP68 and SRP72 are poorly characterised. Reconstitution experiments of the complete S domain with the SR could analyse the functional role of SRP68 and SRP72 in more detail.

In collaboration it was shown that binding of the SR to the SRP:RNC complex leads to the exposure of an important translocon binding site on the ribosome. Cryo-EM analysis of the SRP:RNC:SR complex with translocon proteins will answer the question whether a monomeric or an oligomeric translocon contacts the ribosome.

5 MATERIALS AND METHODS

5.1 *CHEMICALS, ENZYMES AND CLONING KITS*

Chemicals were bought from Sigma-Aldrich Chemie GmbH (Germany) and Merck (Germany). Columns and resins for protein purification were obtained from Pharmacia, Sweden. Restriction enzymes and buffers were obtained from NEB (New England Biolabs, USA). Nucleotides and nucleotide analogues were bought from Sigma-Aldrich Chemie GmbH (Germany). Protease inhibitor tablets Complete were EDTA free and purchased from Boehringer (Germany). Blotting membranes were purchased from Schleicher and Schuell (Germany). Immobilised peptide libraries were synthesised on a PepSPOT membrane from Jerini, Germany. Crystallisation kits from the following companies were used: Emerald BioSystems (USA), Hampton Research (USA).

Standard Mini-, Midi- and Maxi-Prep Kits from Qiagen (Germany) were used to prepare DNA according to the manual. Kits for the purification of DNA (QIAquick PCR purification kit and QIAquick Gel Extraction Kit) were obtained from Qiagen (Germany) and used according to manufacturer's instructions. The following cell lines were used for plasmid preparation and cloning purposes: XL1-Blue (Stratagene, USA), DH5 α (Invitrogen, USA) and NovaBlue (Novagen, USA). In general, either Pfu-Polymerase (Stratagene) or HighFidelity DNA Polymerase (Merck, Germany) was used for PCR. For site-directed mutagenesis the Stratagene QuickChange site-directed mutagenesis kit was used according to manufacturer's instruction. Primers were purchased from MWG Biotech AG (Germany). All constructs were verified by sequencing. Constructs were sequenced by MWG Biotech AG (Germany).

Remark

If not stated differently all experiments involving proteins were performed at 4°C.

5.2 Cloning, Expression and Purification of SR- and SRP Proteins

5.2.1 SR α^{His} : $\beta\Delta TM$

Expression was performed in *E. coli* BL21 (DE3) Arg cells that are based on BL21 (DE3) cells (Novagen, USA) and contain λ lysogen under the lacUV5 promotor and tRNA genes for two rare codons in *E.coli* (AGG/AGA). Cells were grown at 37°C in 3 – 6 l LB medium up to a density of 0.3 – 0.4, then temperature was reduced to 18°C. Cells were induced with 0.5mM IPTG at an optical density of 0.6 – 0.8, grown ON and harvested by centrifugation at 5300 g for 30 min. Cells were washed in 1 x PBS at 4°C and transferred to 50 ml Falcon tubes. Cells were flash frozen in liquid nitrogen and stored at -80°C. For protein preparation, cells from 3 l cell pellet were resuspended in 50 ml lysis buffer (L $\alpha\beta$).

The cells were lysed using a sonicator followed by emulsiflex disruption. The cell debris was removed by centrifugation at 120000 g for 1 hour and the supernatant was filtered through a 0.22 μ m sterile low protein binding filter (Millipore, USA). Subsequently, the protein was bound to Chelating Sepharose Fast Flow resin loaded with Ni²⁺ and washed with resuspension buffer lacking Triton X-100 (A_{Ni}($\alpha\beta$)) until baseline was reached. The protein was eluted usually in a single step at 300mM imidazole (B_{Ni}($\alpha\beta$)). Successively, two ion exchange purification steps were performed. The protein was prepared by dialysis ON into the ion exchange buffer (Q($\alpha\beta$)).

The protein solution was then applied on a column with Q-Sepharose Fast Flow resin equilibrated in the ion exchange buffer. The flow-through was collected since the positively charged complex (theoretical pI: 9.25) does not bind to a strong anion exchanger. In the next step the protein was purified via a strong cation exchanger (SP-Sepharose Fast Flow resin) equilibrated with the buffer A_{SP}($\alpha\beta$). The protein was washed with this buffer until baseline was reached and eluted with the buffer B_{SP}($\alpha\beta$). Last purification step was size exclusion chromatography via a Superdex 200 (26/60) column in the buffer GF($\alpha\beta$). The bicistronic SR α^{His} : $\beta\Delta TM$ construct includes human full length SR α with an N-terminal His-tag and mouse SR β lacking the predicted transmembrane spanning anchor in a pet16b vector (N-terminus $\Delta 57$; (Fulga et al., 2001)). For cloning details see (Fulga et al., 2001). The expression and purification protocol has been modified from (Fulga et al., 2001).

5.2.2 Cloning of $SR\alpha:\beta\Delta TM$

The bicistronic insert for this construct was excised from the $SR\alpha^{His}:\beta\Delta TM$ construct (Fig. 64) and ligated into pET21d vector. Both were restricted with NcoI and BamHI for two hours at 37°C in NEB restriction buffer 2. Both digestions were separated via agarose gel electrophoresis (1 % gel). The $SR\alpha:\beta\Delta TM$ insert and the pET21d were purified via QIAquick Gel Extraction Kit and ligated via NEB Quick Ligation Kit according to manufacturers' instructions.

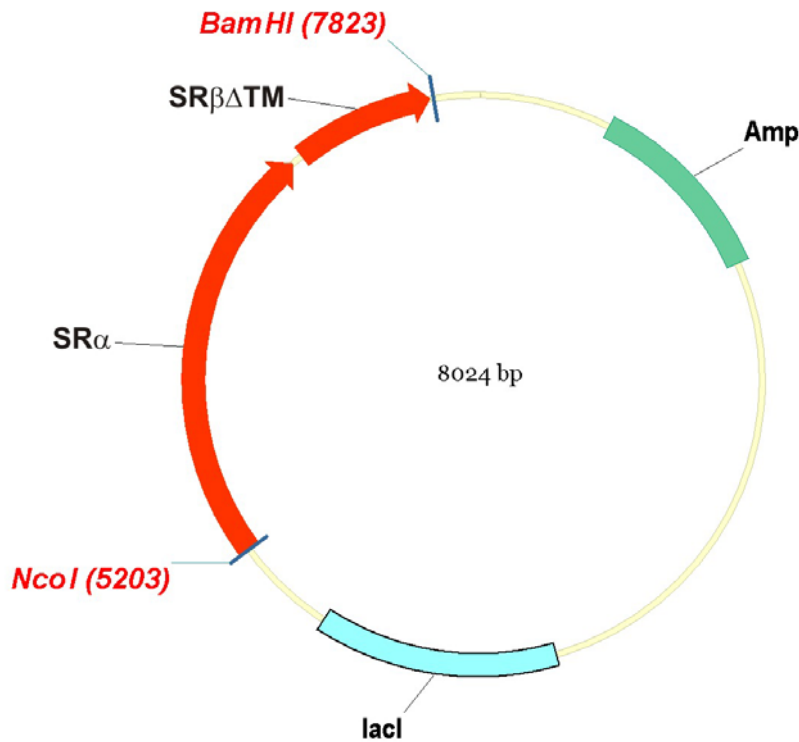


Figure 64 Map of $SR\alpha:\beta\Delta TM$ cloned in vector pET21d. The map was generated using the program Vector NTI.

5.2.3 $SRX2^{His}:\beta\Delta TM$

$SRX2^{His}:\beta\Delta TM$ was over-expressed and cells were harvested as described for $SR\alpha^{His}:\beta\Delta TM$. Pellets from 3 l expressed cell culture were disrupted in 50 ml lysis buffer (L(X2 β)). In the first purification step (affinity purification) the same buffer without protease inhibitor (A_{Ni}(X2 β)) was used to equilibrate the Fast Flow Chelating resin loaded with Nickel. Buffer (B_{Ni}(X2 β)) corresponds to buffer A_{Ni}(X2 β) but included 500 mM imidazole. The protein was eluted via a gradient from 10 to 500mM imidazole. The eluted protein was collected and dialysed over night against buffer

Q(X2 β). Fast Flow Q-resin from Pharmacia was also equilibrated in buffer Q(X2 β), and the flow-through was collected. SP Fast Flow resin equilibrated with A_{SP}(X2 β)-buffer was used next. The protein was eluted via a salt gradient from 150 to 1000 mM NaCl (B_{SP}(X2 β)). Before the last purification step the protein was dialysed against the buffer used for size exclusion chromatography column GF(X2 β). The bicistronic pSRX2^{His}: $\beta\Delta$ TM construct includes the N-terminal 176 amino acids of human SR α with an N-terminal His-tag and mouse SR β lacking the predicted transmembrane spanning anchor in a pet16b vector (Fulga et al., 2001). For cloning details see also (Fulga et al., 2001).

5.2.4 Seleno-L-Methionine Substituted Expression and Purification of SRX2^{His}: $\beta\Delta$ TM_{SeMet}

In order to perform a seleno-L-methionine (SeMet) substituted expression an expression cell strain had to be chosen that is methionine auxotroph (B834 (DE3)). Additionally, it is very important to degas the buffers in order to prevent oxidation of SeMet ($4 \text{ R-SeH} + \text{O}_2 \rightarrow 2 \text{ R-Se-Se-R} + 2 \text{ H}_2\text{O}$). This protocol is based on a protocol available on the homepage of Venki Ramakrishnan (<http://alf1.mrc-lmb.cam.ac.uk/~ramak/madms/segrowth.html>). For the cell growth, the medium GM(SeMet) is used.

Pre-cultures were grown on plates, using 1/3 plate per litre of growth medium. SRX2^{His}: $\beta\Delta$ TM was induced at OD 0.6 with 400 μ l 1 M IPTG and expressed ON at 18°C. The preparation was performed as described above for SRX2^{His}: $\beta\Delta$ TM. Buffers were slightly changed. The names of the respective buffers are also termed L, A_{Ni}, B_{Ni}, Q, A_{SP}, B_{SP} and GF, but with the index 'SeMet'. The buffer GF(SeMet) was also used for crystallisation experiments.

5.2.5 SRX2^{His}: $\beta\Delta$ TM / SR α ^{His}: $\beta\Delta$ TM mutants

All mutations but SR α R524Q are based on our SRX^{His}: $\beta\Delta$ TM-GTP structure. The mutation R524Q was introduced in order to prevent GTP hydrolysis in SR α (Rapiejko and Gilmore, 1992). The mutations α R34A, β D72G and β H119A were introduced in

Materials and Methods

the bicistronic plasmids of SRX2^{His}: $\beta\Delta$ TM and SR α ^{His}: $\beta\Delta$ TM. Table 17 shows names, locations and probable features of the mutations.

Site-directed mutagenesis was performed according to the manufacturer's instructions in order to generate the outlined mutations.

Mutation	Location	Feature
SR α R524Q	SR α , G-3 (switch II)	Should prevent GTP hydrolysis, but keep nucleotide binding of the wild-type.
SR α R34A	Helix α 1 in SR α /SRX, interface to P loop of SR β	Disrupts the interface from the side of SR α /SRX and eliminates a possible further function of R34
SR β D72G	P loop of SR β , interface to helix α 1 from SR α /SRX	Disrupts the interface from the side of SR β
SR β H119A	Catalytic residue in the switch II region of SR β	Should completely rule out GTP-hydrolysis. Similar mutation (Q71L) has also been used for Arf1 to prevent GTP hydrolysis (Shiba et al., 2003)

Table 17 SR α /SRX2 mutants. Location and probable features of the mutant proteins.

5.2.6 SR α NG^{His} (SR α N Δ 314-N^{term}His)

Cloning of SR α NG^{His}

The NG-domain of human SR α was cloned into a pET16b vector. The vector is derived from the SR α ^{His}: $\beta\Delta$ TM construct. The construct contains an N-terminal His-tag and starts with MSHHHHHHSM N-terminally in front of the NG-domain that begins with GTLGG. Cleavage Sites are NcoI (N-terminally, located at the second methionine) and BamHI (C-terminally) (Fig. 65).

Template: SR α ^{His}: $\beta\Delta$ TM, primer: SR α NG-Forward, SR α NG-Reverse

PCR: 1 min 95°C -> 25 cycles (30s 95°C, 30s 45°C, 50s 72°C) -> 5 min 72°C -> 4°C

The PCR product was purified via QIAquick PCR purification kit. Successively, the sample was digested by NcoI and BamHI restriction endonucleases for 2 h at 37°C in NEB restriction buffer 2. The restricted DNA was separated via agarose gel

electrophoresis on a 1 % agarose gel and the anticipated insert of 983 bp was excised. The gel was removed via QIAquick Gel Extraction Kit. The insert was cloned into the vector of the $SR\alpha^{His}:\beta\Delta TM$ construct, which was digested the same way as $SR\alpha NG^{His}$. To separate it from and $SR\alpha:\beta\Delta TM$, the digested vector was run on a 1 % TAE gel. The cleaved vector was excised and purified via QIAquick Gel Extraction Kit. Finally, cleaved insert and vector were set up for ligation using New England Biolabs' Quick Ligation Kit according to manufacturer's instructions.

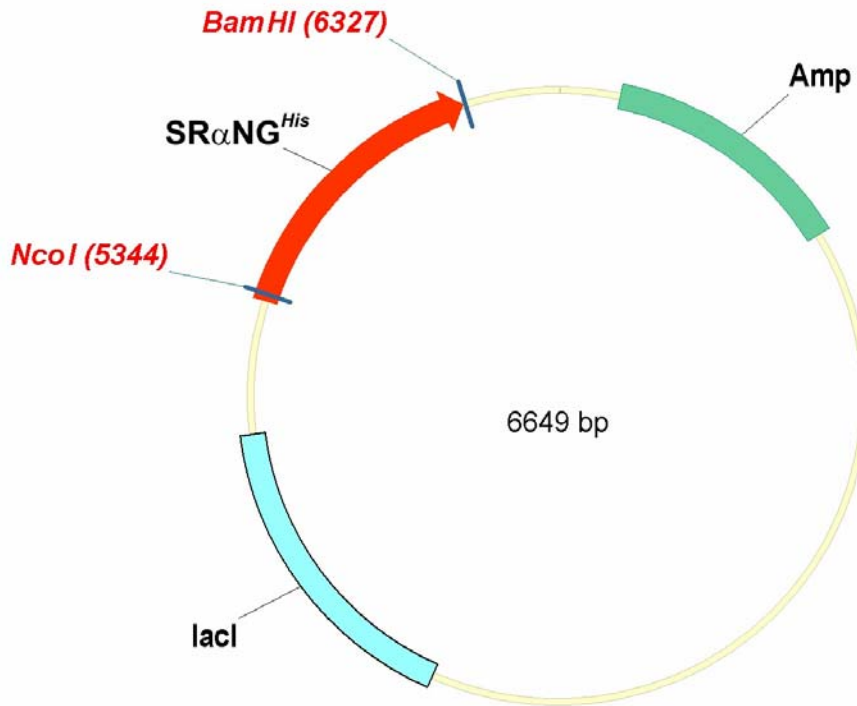


Figure 65 Map of $SR\alpha NG^{His}$ cloned in vector pET16b. The map was generated using the program Vector NTI.

Preparation of $SR\alpha NG^{His}$

Test expression

The construct was test-expressed in Rosetta (DE3), C43 (DE3), BL21 (DE3), Rosetta (DE3) pLysS and BL21 (DE3). Cells were grown until OD 0.6 at 37°C and induced with 0.5 mM IPTG over night at 16°C. Cells were lysed in the buffer $L(\alpha NG)$, lysed via Emusiflex (3 passes at 10000-15000 psi) in a volume of 50 ml buffer $A_{Ni}(\alpha NG)$ (see below) and loaded on dripping columns filled with 1 ml Pharmacia Fast Chelating resin saturated with Ni^{2+} .

Columns were washed with buffer $A_{Ni}(\alpha NG)$ until the protein concentration was minimal and visibly not changing anymore (detected via Bradford Reagent) and eluted in a step using buffer $B_{Ni}(\alpha NG)$.

Standard preparation

Two litres of BL21 (DE3) cell culture were grown as described in the test-expression above and lysed in 50 ml buffer L(α NG). Cells were sonicated (6 min, power 6, 70 % duty cycle) and further disrupted via Emusiflex (3 passes at 10000 – 15000 psi).

Centrifugation was performed according to the description of SR α^{His} : $\beta\Delta$ TM. For affinity purification protein was applied on a column filled with Fast Chelating Flow resin that was saturated with Ni²⁺. The column was washed with buffer A_{Ni}(α NG) until baseline was reached and eluted via gradient from 10 – 500 mM imidazole using buffer A_{Ni}(α NG) and B_{Ni}(α NG).

5.2.7 SR $\beta\Delta$ TM

Here, the construct was used, in which SR β lacking the N-terminal 57 amino acids was cloned into a pHAT2 vector. The protein was expressed in BL21 (DE3) Arg cells, purified via affinity purification (Fast Flow Chelating Sepharose resin saturated with Ni²⁺) and analysed via size exclusion chromatography (Superdex 75 (10/30)). The protein was eluted from the affinity chromatography column in two steps. A 100 mM step led to SR $\beta\Delta$ TM with a nucleotide-free and GTP-loaded SR β , meanwhile a 300 mM step eluted only the nucleotide-free form as observed from HPLC analysis (Fulga et al., 2001). The nucleotide-free form of SR $\beta\Delta$ TM is much more sensitive to aggregation and precipitation than the nucleotide loaded SR $\beta\Delta$ TM and could be stabilised at 1 mg / ml in a buffer containing 50 mM Tris pH 8, 500 mM NaCl, 10 mM MgCl₂, 100 mM imidazole and 20 % glycerol. For further information of cloning and purification see (Fulga et al., 2001).

5.2.8 SRP54D (SRP54C^{term} Δ 68)

SRP54D is a construct derived from canine SRP54 DNA. Canine SRP54 is on the DNA level not equal to human but on the protein level both sequences are identical. The C-terminus of the construct refers to the length of the *E. coli* SRP54 M-domain, which is visible in the crystal structure of the Ffh:RNA complex published by Jennifer Doudna in 2000 (Batey et al., 2000) and is therefore called SRP54D. The constructs

Materials and Methods

with N-terminal and C-terminal His-tags are called SRP54D^{NHis} SRP54D^{CHis}, respectively. In cases where a method is applicable to SRP54D^{NHis} or SRP54D^{CHis}, the term SRP54D^{His} is used.

Cloning of SRP54D^{NHis} and SRP54D^{CHis}

The length of the insert coding for SRP54D is 1340 bp, which corresponds to a molecular weight of 49.25 kD. The insert was cloned between the NcoI and XhoI restriction sites into pET24d (Fig. 66). For SRP54D^{NHis} the forward primer contained a hexa-histidine tag (MGHHHHHH), for SRP54D^{CHis} the reverse primer contained the hexa-histidine tag and stop codon. The C-terminal amino acids of SRP54D are KKMGG-436. Amino acid one is counted from the methionine coding the SRP54 sequence not including the tag. As a template, the full length SRP54 gene in a viral vector was used, kindly provided by Mark Brooks (laboratory of Stephen Cusack, EMBL Grenoble, France).

Template: Full length SRP54 in viral vector, Primers: SRP54DN-Forward, SRP54DN-Reverse or SRP54DC-forward, SRP54DC-Reverse, respectively.

PCR: 1 min 95°C -> 25 cycles (30s 95°C, 30s 50°C, 60s 72°C) -> 5 min 72°C -> 4°C

SRP54D^{NHis} and SRP54D^{CHis} were cloned according to the description below. The PCR product was ligated into the TOPO vector (SRP54D-TOPO) using the TOPO cloning kit (Invitrogen, Germany) according to manufacturer's instructions. SRP54D^{His}-TOPO and pet24d vector were cleaved for 2 h at 37°C with NcoI and XhoI in NEB restriction buffer 2. Both restriction setups were applied on a 1 % TAE gel and the bands of the cleaved pet24d vector (5213 bp) and the SRP54D^{His} insert (1340 bp) were excised. The gel was removed via QIAquick Gel Extraction Kit. Finally, cleaved insert and vector were set up for ligation using New England Biolabs' Quick Ligation Kit according to manufacturer's instructions.

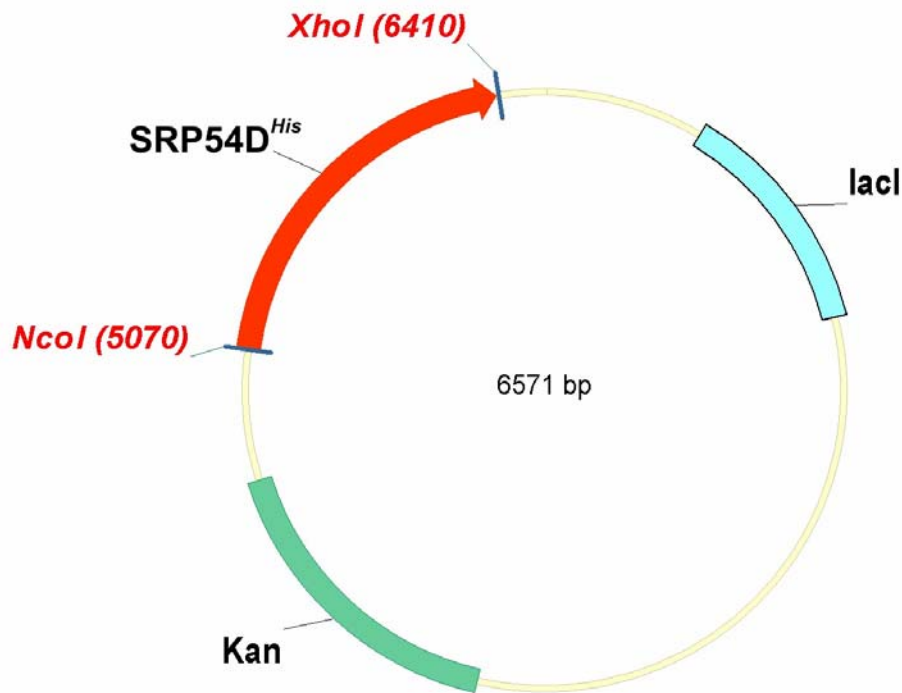


Figure 66 Map of SRP54D^{His} cloned in vector pET24d. The map was generated using the program Vector NTI.

Preparation of SRP54D^{His}

Test expression

This construct was test-expressed in BL21 (DE3) pLysS, C43 (DE3), BL21 (DE3), Rosetta (DE3) pLysS. Cells were grown until OD 0.6 at 37°C and induced with 0.5 mM IPTG over night at 18°C. Cells were harvested as described for SR α^{His} : $\beta\Delta TM$, lysed via Emusiflex (3 passes at 10000-15000 psi) in a volume of 50 ml buffer L(54Dt). Successively, the lysed cells were loaded on dripping columns filled with 1 ml Fast Chelating resin saturated with Ni²⁺.

The protein was washed on the column with buffer A_{Ni}(54Dt) until the protein concentration was minimal and visibly not changing anymore (detected via Bradford Reagent) and eluted in a step using buffer B_{Ni}(54Dt).

Complete preparation

Two litres of C43 (DE3) cell culture were grown as described as in the test-expression above and lysed in 50 ml buffer L(54D) (see below) supplemented with one tablet of protease inhibitor. Cells were disrupted via Emusiflex (3 passes at 10000-15000 psi). Protein harvested as described for SR α^{His} : $\beta\Delta TM$, washed with buffer A_{Ni}(54D) until baseline was reached and eluted in a step using buffer B_{Ni}(54D).

For cation exchange chromatography the sample was dialysed against buffer A_{SP}(54D) ON. The protein was then loaded on a column filled with SP-Sepharose Fast Flow resin equilibrated with buffer A_{SP}(54D). The column was washed with buffer A_{SP} until baseline and eluted in a step with buffer B_{SP}(54D). The protein was successively dialysed against the size exclusion chromatography buffer (GF(54D)), concentrated and loaded on the gel filtration column (Superdex 75 (26/60)).

5.2.9 SRP54NG (SRP54C^{term}Δ208)

The SRP54NG construct comprises the NG-domain of SRP54, lacking the C-terminal M-domain. The protein is truncated C-terminally in the linker between NG- and M-domain after LG from the sequence LGMGD. The amino acid sequence of the protein ends with SKLLG-296. It contains 940 bp with a corresponding mass of the translated protein of 33.47 kD. The constructs with N-terminal and C-terminal His-tags are named SRP54NG^{NHis} SRP54NG^{CHis}, respectively. In cases where a method is applicable to SRP54NG^{NHis} or SRP54NG^{CHis}, the term SRP54NG^{His} is used.

Cloning of SRP54NG^{NHis}

The construct (Fig. 67) is derived from the SRP54D^{NHis} construct (see above) by inserting a stop codon via site-directed mutagenesis between Gly296 and Met297. Site-directed mutagenesis was performed according to manufacturers' instructions.

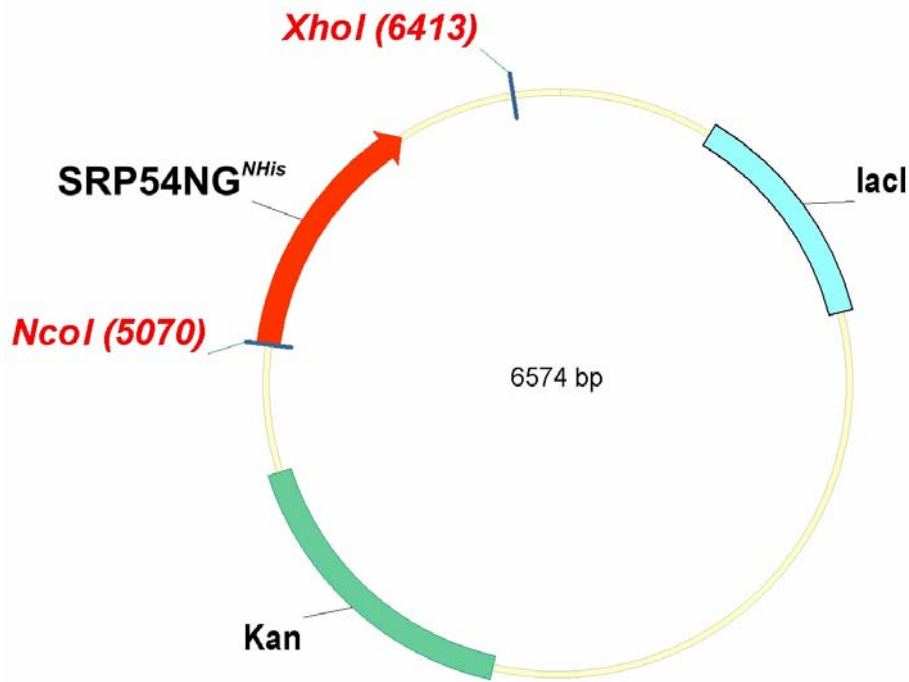


Figure 67 Map of SRP54NG^{NHIS} cloned in vector pET24d. The map was generated using the program Vector NTI.

Test Expression of SRP54NG^{NHIS}

Test-expressions were performed for 3h at 30°C and ON at 16°C. The plasmid was tested with BL21 (DE3) Arg, Rosetta (DE3), C43 (DE3), BL21 (DE3) pLysS and Rosetta (DE3) pLysS cells. Rosetta (DE3) pLysS cells over-expressed SRP54NG^{NHIS} in highest amounts followed by C43 (DE3).

Preparation of SRP54NG^{His}

Rosetta (DE3) pLysS cells were grown until OD 0.6 and induced with 0.5mM IPTG at 16°C ON. Cells were disrupted using an Emulsiflex and ultra-centrifuged for 45 min @ 40000 rpm 120000 g in order to separate the lysate from the cell debris. The protein was loaded on Fast Chelating Resin saturated with Ni²⁺ equilibrated with buffer L(54NG). The protein was washed with buffer A_{Ni}(54NG) until baseline and eluted in a step with 18 % B_{Ni}(54NG) (115 mM imidazole). In order to deplete DNA from the sample a Q-column can be used. The sample was dialysed ON against buffer Q(54NG) (see below) and purified next day via anion exchange chromatography (Q-Sepharose Fast Flow resin). The protein was in the flow-through but the DNA was bound to the resin due to a higher negative charge. Finally, the protein was dialysed against GF buffer (GF(54NG)) and purified using size exclusion chromatography via a Superdex 75 (26/60) column.

Cloning of SRP54NG^{CHis}

The SRP54NG^{CHis} construct (Fig. 68) correlates to SRP54NG^{NHis} but differs in the position of the hexa-histidine tag which is located C-terminally. The protein sequence ends with SKLLG(296)HHHHHH. SRP54D^{CHis} was used as template for the SRP54NG^{CHis} PCR, primers were SPR54NGC-Forward and SRP54NGC-Reverse. PCR: 1 min 95°C -> 30 cycles (30s 95°C, 30s 45°C, 75s 72°C) -> 7 min 72°C -> 4°C

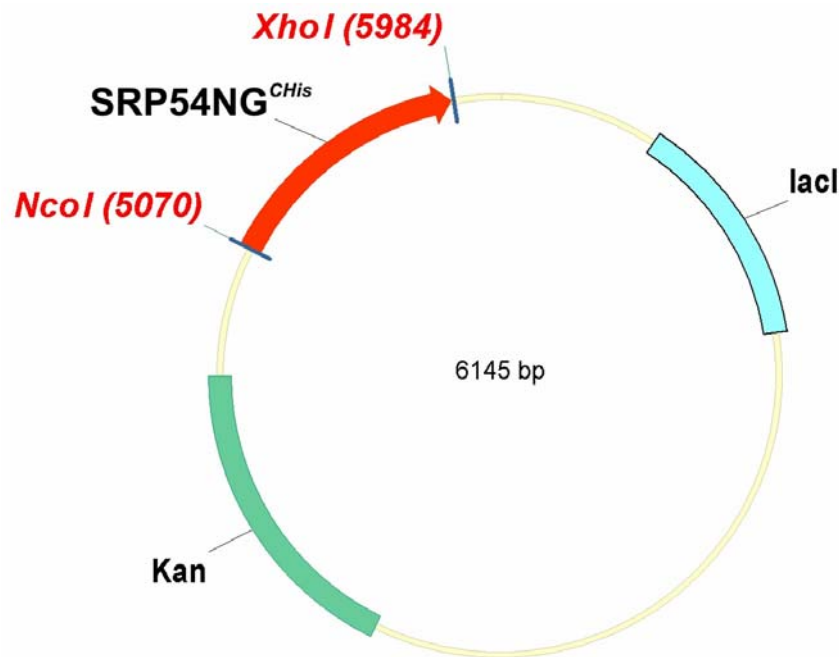


Figure 68 Map of SRP54NG^{CHis} cloned into pET24d.

5.3 Complex Formation Studies

5.3.1 Trimeric Complex: SRα^{His}:βΔTM:SRP54D^{His}

Proteins were over-expressed and purified as described in sections 5.2.1 and 5.2.8. The proteins were dialysed ON into the complex formation buffer (CF(T.)) and SRP54D^{His} was added to SRα^{His}:βΔTM with SRP54D^{His} in excess in presence of 2 mM GMPPNP. Depending on the amount of SRP54D^{His} available, the SRα^{His}:βΔTM:SRP54D^{His} ratios varied from 1:1.25 to 1:2. Final concentrations of SRα^{His}:βΔTM varied between 23 and 30 μM. The complex was formed within 1 h at

37°C. An addition of glycerol (10% final concentration) to the sample before warmed up to 37°C did not affect the ability of complex formation but decreased aggregation.

The trimeric complex is purified via size exclusion chromatography (Superdex 200 (26/60)) using the complex formation buffer without GMPPNP and glycerol (GF(T)). Fractions containing the complex were stabilised immediately by the addition of GMPPNP (0.1 mM). Fractions were analysed via polyacrylamide gel electrophoresis and further staining with Coomassie Brilliant Blue. Since SR α : $\beta\Delta$ TM could not be separated from the trimeric complex, only fractions were pooled for successive pentameric complex formation or crystallisation that contained stoichiometric amounts of SR α^{His} : $\beta\Delta$ TM and SRP54D^{His}. The stoichiometry was examined by eye according to the Coomassie Brilliant Blue staining intensity of the respective bands.

5.3.2 Pentameric Complex Formation:

SR α^{His} : $\beta\Delta$ TM:SRP54D^{His}:SRP19:RNA¹⁰⁴

In parallel to the formation of the trimeric complex the complex of SRP19 and RNA is formed. SRP19 and RNA¹⁰⁴ and the SRP19:RNA¹⁰⁴ complex have been kindly provided by Klemens Wild. In principle, the dimeric complex was assembled by pre-treating the RNA¹⁰⁴ with urea, heating it up to 70°C briefly and snap-cooling on ice. SRP19 was added in excess and in a 20-fold larger volume in order to dilute the urea. The mixture was incubated for 30 min on ice in order to allow the complex to be formed and subsequently concentrated. The complex was isolated via anion exchange chromatography.

Dimeric (SRP19:RNA¹⁰⁴) and trimeric (SR α^{His} : $\beta\Delta$ TM:SRP54D^{His}) complex were mixed in equimolar concentrations (0.7 μ M) and GMPPNP was added to a concentration of 0.1 mM. This setup was incubated on ice for one hour and concentrated for the final purification step via size exclusion chromatography (Superdex 200 (26/60)) using buffer GF(P).

The fractions were analysed on a 12 % polyacrylamide gel, stained with Coomassie Brilliant Blue and eventually by silver staining with SilverXpress silver stain kit (Invitrogen, Germany) according to manufacturers' instructions. In contrast to Coomassie Brilliant Blue dyeing, silver-staining allows to stain RNA which can be recognised due to its orange colour. Fractions containing the complex were

immediately stabilised by the addition of GMPPNP (to 0.1 mM) and concentrated. Finally, at protein concentrations of 4 mg/ml or higher GMPPNP was added (up to 2 mM) and the protein was set up for crystallisation. The complex was also crystallised in 96-well plates using the sitting drop method performed by a crystallisation robot (Cartesian) at Aventis, Frankfurt (Germany) and EMBL (Heidelberg).

5.3.3 Trimeric Complex Formation Pull-Down: $\text{SR}\alpha:\beta\Delta\text{TM}:\text{SRP54NG}^{\text{CHis}}$

Purification of the trimeric complex includes a methodical difficulty in the last purification step (size exclusion chromatography): Free $\text{SR}\alpha:\beta\Delta\text{TM}$ (92 kD) can not be separated from the whole complex (125 kD) because both molecular weights are too similar. This is also true for the $\text{SR}\alpha:\beta\Delta\text{TM}:\text{SRP54D}^{\text{His}}$ complex purification. Here, one approach was examined that took advantage of the fact that just $\text{SRP54NG}^{\text{His}}$ was tagged with a hexa-his tag. A pull-out experiment via Ni^{2+} -affinity chromatography would allow unbound $\text{SR}\alpha:\beta\Delta\text{TM}$ to flow through meanwhile the complex and free $\text{SRP54NG}^{\text{CHis}}$ would bind to the Fast Flow Chelating resin. Non-complexed $\text{SRP54NG}^{\text{His}}$ could be easily separated from the approximately 4-fold larger complex via size-exclusion chromatography (Superdex 200).

$\text{SR}\alpha:\beta\Delta\text{TM}$ was expressed as pointed out before for $\text{SR}\alpha:\beta\Delta\text{TM}$. In order to pre-purify $\text{SR}\alpha:\beta\Delta\text{TM}$ anion exchange chromatography was applied directly after lysis using buffer L($\alpha\beta 2$). Fast Flow SP-Sepharose was equilibrated with buffer $\text{SP}_A(\alpha\beta 2)$ (see below), the loaded protein was washed until baseline and eluted with buffer $\text{SP}_B(\alpha\beta 2)$ (see below). $\text{SRP54NG}^{\text{CHis}}$ was purified as described above. Both components were diluted into the complex formation buffer (CF2). A 3-fold molar excess of $\text{SRP54NG}^{\text{CHis}}$ was incubated with $\text{SR}\alpha:\beta\Delta\text{TM}$ in presence of 2 mM GMPPNP ON on ice.

Successively, Fast Flow Chelating resin saturated with Ni^{2+} was equilibrated with buffer $\text{A}_{\text{Ni}}(\text{T2})$, the resin with loaded protein was washed until baseline and eluted over a gradient from 15 to 500 mM imidazole using buffers $\text{A}_{\text{Ni}}(\text{T2})$ and $\text{B}_{\text{Ni}}(\text{T2})$.

Finally, the complex was purified via size exclusion chromatography (Superdex 200 (26/60)) in buffer GF(T2).

5.3.4 Analysis of SR:SRP Complex Formation

These studies have been performed using SRP19^{His}:RNA¹⁰⁴ complex kindly provided by Klemens Wild and SRP54D kindly provided by Mark Brooks (EMBL Grenoble, Stephen Cusack group). Mark Brooks expressed the protein in insect cells and used a heparin resin procedure for purification. This experiment examines the difference in complex formation rate comparing the trimeric SR α : β Δ TM:SRP54D^{His} and the pentameric SR α ^{His}: β Δ TM:SRP54D^{His}:SRP19^{His}:RNA¹⁰⁴ complexes.

250 μ l of SR α ^{His}: β Δ TM at 8 mg/ml (21 nmol) in buffer SR in were added to 750 μ l SRP54D^{His} at 1.4 mg/ml (21.7 nmol) in buffer B54. Before GMPPNP was added a sample (250 μ l) was taken resembling the starting point. Then GMPPNP was added to a final concentration of 2 mM. In parallel a second setup was prepared like this one but SRP19^{His}:RNA¹⁰⁴ was added stoichiometrically (21 nmol) in a volume of 200 μ l (5.2 mg/ml in the buffer B19RNA). Both setups were stored on ice. After the addition of GMPPNP samples were taken from the trimeric complex formation setup after one, four and seven hours and from the pentameric complex formation setup after 1 h 20 min, 4 h 30 min, 7 h 30 min and 10 h 30 min. All samples were run immediately on a Superdex 200 (10/30) column equilibrated with buffer GF(5).

5.4 Crystallisation and Structure Determination of SR α X2^{His}: β Δ TM

5.4.1 Crystallisation of SR α X2^{His}: β Δ TM

All crystallisation experiments were performed using the hanging drop method in a 24-well plate. First crystals of SR α X2^{His}: β Δ TM appeared after 3 months at 20°C using 100 μ l of 2 M ammonium sulphate as precipitant buffered by 0.1 M sodium citrate at pH 5.5 in the reservoir (WIZARD sparse matrix screen, Emerald Biosciences, USA). One μ l of protein solution at 14 mg/ml in the buffer Cryst was mixed with one μ l of the reservoir. The initial successful condition was 2 M (NH₄)₂SO₄, 0.1 M sodium citrate pH 5.5 (buffer Res1).

After trying different grid screens altering buffers, pH-values, salt concentrations, protein concentrations, and additives, the finally best diffracting crystals were obtained using the same method as the one used for the initial condition supplemented with 100 mM guanidinium hydrochloride (buffer Res2) mixed

with a protein solution at 12 mg/ml. In general, crystals appeared after four to six weeks, rarely earlier.

5.4.2 Freezing and Mounting

As a cryo-buffer (BCryo), 20% glycerol was added to 2M (NH₄)₂SO₄, 0.1 M sodium citrate pH 5.5 and 100 mM guanidinium hydrochloride was used. The cryo-protectant is used in order to prevent the formation of ice crystals. 20% glycerol was added as cryoprotectant to the freezing buffer. Crystals were transferred with a loop (CryoLoops, Hampton Research, USA) to a drop containing the buffer Cryo. Successively, the crystals were flash frozen in liquid nitrogen and then either stored in liquid nitrogen or mounted immediately in the cryo-stream of the X-ray source.

5.4.3 Data Collection

Crystals were exposed X-rays at beamline ID 14.4 at European Synchrotron Radiation Facility (ESRF), Grenoble (France) with the parameters from Table 18. First, a single exposure (test) allowed the determination of the space group. The image could be examined using the software MOSFLM (Leslie, 1992) in order to determine the oscillation start. The data were indexed, scaled and merged using the HKL program package (Otwinowski and Minor, 1997).

X-ray wavelength (Å)	0.979
Detector-dependent theoretical max. resolution (Å)	2.50
Frame number to start	1
Oscillation start (°)	70
Oscillation range (°)	1
Overlap between frames	-
Exposure time per frame (s)	0.9
Number of passes per frame	3
Number of frames to collect	180

Table 18 Parameters of the data collection for the final data set (Sr 2.1) for the SRX^{His}:βΔTM-GTP X-ray structure .

5.4.4 Structure Determination and Model Refinement

The structure was determined by molecular replacement using the program AMoRe implemented in the CCP4 program suite (Collaborative Computing Project, 1994)

and the SR β Δ TM-subunit of the yeast homolog (PDB accession code 1NRJ, (Schwartz and Blobel, 2003)). The model for refinement was created with the auto-build function of Arp/wArp (Perrakis et al., 1999) implemented in the CCP4 program suite (Collaborative Computing Project, 1994) run in warpNtrace-mode. The model was refined with the program CNS (Brunger et al., 1998) using the input files generate.inp and refine.inp. In this way simulated annealing, energy minimization, B-factor refinement, and map calculation were combined. GTP and Mg²⁺ were added to the model. For CNS refinement GTP and Mg²⁺ topology and parameter files were obtained from the Hetero-compound Information Centre - Uppsala (HIC-Up; (Kleywegt and Jones, 1998)). Cycles of model building and refinement ('bootstrapping') were performed in order to generate the final model. Water molecules were added using CNS with the file water_pick.inp as a template (Brunger et al., 1998) and were manually checked for correctness. The model building was performed with the program O (Jones et al., 1991). The model was analysed for correctness of various parameters with the help of the programs PROCHECK (Morris et al., 1992) and WHATCHECK (Hooft et al., 1996).

5.4.5 Determination of the Selenium K-shell absorbance peak

Data of the performed Single Anomalous Dispersion (SAD) experiment were neither included in structure determination of SRX^{His}: β Δ TM nor refinement of its model because the refinement process went on very well after molecular replacement and ArpWarp (Perrakis et al., 1999) autobuilding in the warpNtrace mode. Still, the absorbance of Selenium K-shell electrons was measured at beamline ID 14.4 at ESRF (Grenoble, France) in a Fluorescent Scan experiment. Hereby, the X-ray energy is varied in the range of the absorption of Selenium K-shell electrons leading typically to an absorbance edge of 12632 eV for a wavelength of 0.9797 Å.

5.5 Immobilised Peptide Library Scan

5.5.1 Probing the SR β :Sec61p interaction by an immobilised peptide library

This technique was applied in order to find out whether mammalian SR α^{His} : $\beta\Delta$ TM, SR α X2 His : $\beta\Delta$ TM or SR $\beta\Delta$ TM interact with cytosolic loops of the human translocon. Therefore, the sequences of the translocons from *Homo sapiens* and *Methanococcus jannaschii* were aligned with ClustalW (Chenna et al., 2003) and cytosolic loop regions were deduced from the *M. jannaschii* SecYEG structure. The sequence chosen for each cytosolic loop included one helix turn of transmembrane helix sequence. A 13-mer peptide library was synthesised with a three amino acids step (Jerini Peptide Technology GmbH, Berlin). Each spot carried approximately 5 nmol peptide covalently bound via the C-terminus to a cellulose PEG-membrane. The predicted Sec61 β transmembrane helix was included as an internal control to detect unspecific hydrophobic interaction. The immobilized peptide library covered the following sequences:

N-terminus of human Sec61 α (spots 1-8): 2-

AIKFLEVIKPFVCVILPEIQKPERKIQFKEKVLW-34

Loop 2 (TM2-TM3, spots 10-15): 90-IMQLLAGAKIIEVGDTDPKDRALFNGAQ-116

Loop 4 (TM4-TM5, spots 17-20): 163-LLLDELLQKGYGLGSGISLFIA-184

Loop 6 (TM6-TM7, spots 22-32): 253-

AVVIYFQGFRVDLPIKSARYRGQYNTYPIKLFYTSNIPIL-293

Loop 8 (TM8-TM9, spots 34-47): 375-

FSKTWIEVSGSSAKDVAKQLKEQQMVMRGHRETSMVHELNRYIPTAAAFGG-425

C-terminus (spots 49-53): 454-IYQYFEIFVKEQSEVGSMGALLF-476

Sec61 β (full length, spots 55-83):

MPGPTPSGTNVGSSGRSPSKAVAARAAGSTVRQRKNASCGTRSAGRTTSAGTGG
MWRFYTEDSPGLKVGPPVPLVMSLLFIASVFMLHIWGKYTRS

Membranes were prepared according to Jerini PepSPOT manual and blocked in blocking buffer (buffer BLK) for 1h.

SR $\beta\Delta$ TM-apo, SRX His : $\beta\Delta$ TM-GTP and SR α^{His} : $\beta\Delta$ TM-GTP were probed over night at 4°C at 400nM in the same buffer. Due to the high affinity of SR $\beta\Delta$ TM for GTP and incomplete reloading of SR $\beta\Delta$ TM-apo with GDP (not shown), populations of

homogenously loaded SR $\beta\Delta$ TM-GTP and SR $\beta\Delta$ TM-GDP could not be included in this assay. The membrane was washed briefly with blocking buffer lacking BSA and blotted at 2 mA/cm² membrane for 30 min in blotting buffer BLT onto 0.2 μ m PVDF membranes (Schleicher & Schuell, Immobilon) with the spots facing the cathode.

After blocking for one hour with PMT (see below), proteins were decorated with an anti-pentahis/mouse antibody (Qiagen) diluted in PMT for one hour at RT, followed by an anti-mouse horseradish peroxidase-coupled secondary antibody for one hour at RT and ECL detection. PepSPOT membranes were regenerated according to Jerini Regeneration Protocol I.

5.5.2 Probing the SR β ribosome interaction by an immobilised peptide library

The sequences of the subunits L23a and L35 of the human ribosome were mapped on an immobilised peptide library in 13mers with a step size of three synthesised by Jerini Peptide Technology GmbH, Berlin. These studies were performed as described above with the only difference that the protein concentrations were reduced to 100 nM in order to reduce unspecific interactions with the membrane.

5.6 HPLC analysis

The nucleotide load of SR α^{His} : $\beta\Delta$ TM, SRX2: $\beta\Delta$ TM and SR $\beta\Delta$ TM was verified by HPLC on Waters Delta 600 Multisolvant Delivery System equipped with a 2487 dual lambda absorbance detector and a Vydac protein & peptide C18 column. Measurements were performed at 280 nm. A phosphate buffer with tetra-*n*-butylammonium bromide (TBAB) (buffer HP) was used (see below) for analysis and an isocratic flow of 1.8 ml/min. TBAB binds due to its positive charge the more to the negatively charged nucleotides the higher they are charged. In this way the highest charged nucleotides are neutralised most, resulting in an increased affinity to the hydrophobic C18 column. Therefore for example, GTP is expected to elute after GDP.

20 μ l of 70 μ M nucleotide solutions were used in order to calibrate the system and 20 μ l of 100 to 150 μ M protein solutions were used for the protein experiments. The experiments were analysed with the program MASSLYNX.

5.7 Programs used for Figures in the Text

All three-dimensional pictures of molecules were created with PyMol (DeLano, 2002). Superpositions of molecules were performed using either PyMol or O (Jones et al., 1991). Figures have been edited using COREL Photopaint®. The image of the Ewald sphere construction was created with the help of the program XRayView (Open_Software_Foundation, 1991).

5.8 Crystallographic Background

In order to resolve an object, the wavelength of the light used for the examination of the object can roughly not be larger than the size of the object. Carbon-carbon bonds have a length of about 1.5 Å (1.5×10^{-10} m or 0.15 nm). Therefore electromagnetic waves (X-rays) are required for structural analysis of biological material. Since X-rays are three dimensional electromagnetic waves, they can be described by the common features of waves and photons. The exact knowledge of the X-ray waves that generated the diffraction from a crystal is essential for the determination of the 3D structure of the molecule in the crystal.

5.8.1 Crystal Systems and Bravais Lattices

Crystals are organised by lattices which are Bravais lattices. They are setup by a set of points generated by discrete translation operations. The crystal is composed of molecules that are repeated at every lattice point. When viewed from any of the lattice points, the crystal looks the same. The basic building brick of a crystal is the unit cell which is repeated to form the crystal. The axes of the unit cell are noted as a, b, c, its angles are α , β , γ . The symmetry of the unit cell is described by its space group which is expressed in a term including information about the lattice centring and symmetry operations that can be applied on the unit cell without changing its appearance (e.g. I222, where I describe the lattice centring explained below and the numbers describe symmetry operations). There are 230 space groups of which 65 are possible for chiral objects such as proteins and 14 Bravais lattices organised in seven crystal systems (Table 19). The smallest unit required for the reconstruction of

the crystal is the asymmetric unit which excludes the presence of any further crystallographic symmetry operations.

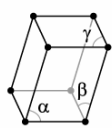
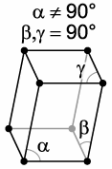
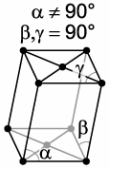
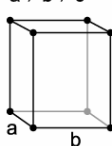
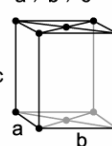
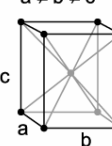
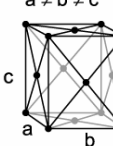

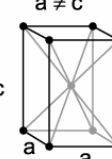
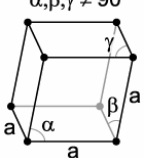
Different lattice centring:

P: Primitive; lattice points in the corners of the unit cell.

I: Body centred; lattice points in the corners and an additional lattice point in the centre of the unit cell.

F: Face centred; lattice points in the corners and an additional lattice point in the centre of each of the faces of the unit cell.

A, B, C: Centring on single faces; lattice points in the corners and an additional lattice point at one of the faces of the unit cell.

Crystal System	Bravais Lattices
triclinic	$\alpha, \beta, \gamma \neq 90^\circ$  P
monoclinic	$\alpha \neq 90^\circ, \beta, \gamma = 90^\circ$  $\alpha \neq 90^\circ, \beta, \gamma = 90^\circ$  P C
orthorhombic	$a \neq b \neq c$  $a \neq b \neq c$  $a \neq b \neq c$  $a \neq b \neq c$  P C I F
tetragonal	$a \neq c$  $a \neq c$  P I
rhombohedral (trigonal)	$\alpha, \beta, \gamma \neq 90^\circ$ 

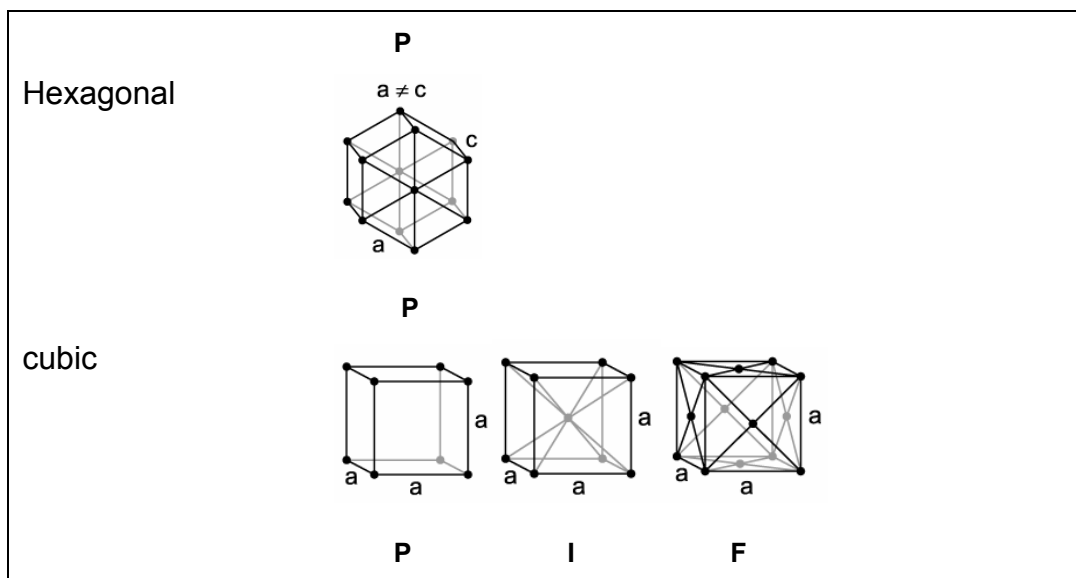


Table 19 The seven crystal systems and 14 relevant Bravais lattices. Bravais lattices are sorted according to the crystal system they belong to. P, I and F describes the molecule centring in the unit cell where P means primitive, I body centred and F face centred (see above). Images are taken from <http://en.wikipedia.org/>.

5.8.2 Bragg's Law

Crystals can be thought of molecules organised in planes with certain lattice spacing (d). The condition at which ordered molecules amplify the signal of scattered waves with a wavelength λ is described by Bragg's law.

$$BC/d = \sin \theta \quad (\text{see Fig. 69})$$

$$\Rightarrow BC = d \sin \theta \quad // \quad 2BC = n \lambda \quad (\text{the distance } 2BC \text{ must be an integer multiple of } \lambda)$$

$$\Rightarrow \underline{n \lambda = 2d \sin \theta} \quad (\text{Bragg's law})$$

When two rays hit a crystal lattice (Fig. 69) in phase and the first is diffracted by one molecule and the second by another molecule in a neighbouring plane, then the second beam travels an additional distance between the planes ($2BC$) which is dependent on the lattice spacing d . When $2BC$ equals an integer multiple of the wavelength λ , then the second beam can amplify the first one.

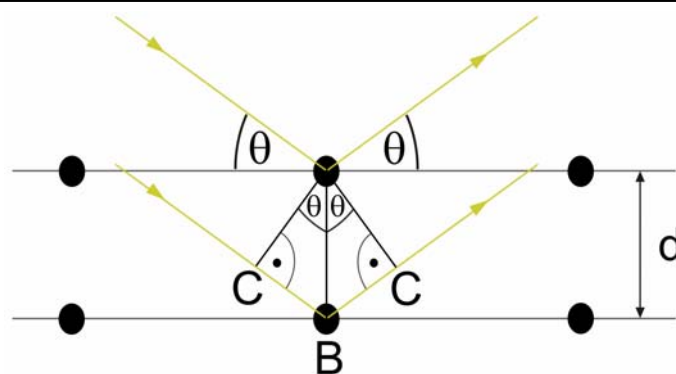
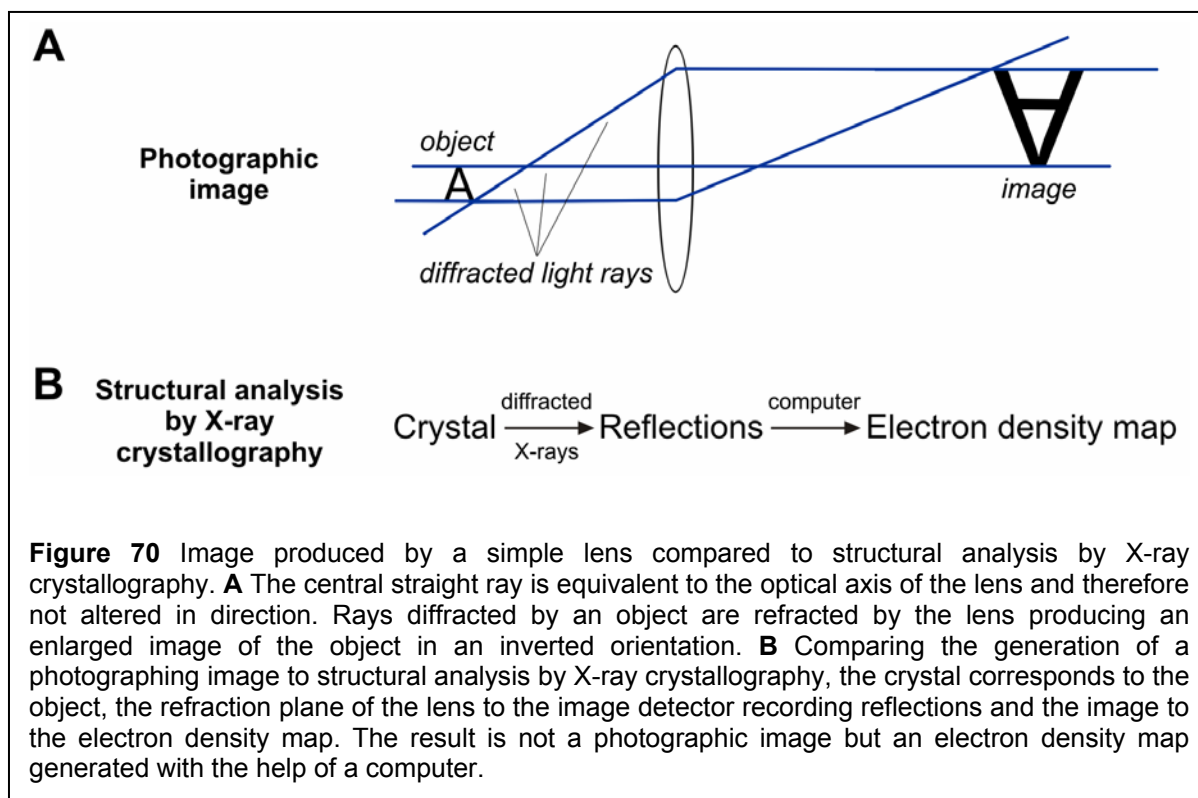


Figure 69 Requirement for an amplified diffracted ray. The upper incident beam is in phase with the lower beam and hits a molecule (black circle) with the angle θ relative to the lattice plane. The lower beam must travel the extra distance $2BC$. When $2BC$ is an integer multiple of the wavelength λ then the lower beam can amplify the upper beam. d is the lattice spacing.

5.8.3 Data Collection and Reciprocal Lattice

For a crystallographic experiment a crystal positioned on a goniometer ('mounted') is exposed to an X-ray beam and diffracted X-rays are recorded. Usually prior to a crystallographic experiment, crystals are frozen in liquid nitrogen (100 K) and meanwhile the experiment exposed to a stream of gaseous nitrogen in order to reduce radiation damage, thermal vibrations and conformational disorder. Diffracted X-rays are recorded using an image plate detector or Charge-Coupled Device (CCD). All electrons of the crystallised molecules contribute to the signals that are recorded. For structure determination, a three dimensional reconstruction of the recorded signal is used. The result of the experiment is the representation of the electron distribution ('electron density map') for the crystallised molecule.

Diffracted X-rays generate reflections on the image plate detector which can be compared to light in the plane of a lens leading to images produced by visible light (400 – 700 nm) (Fig. 70).

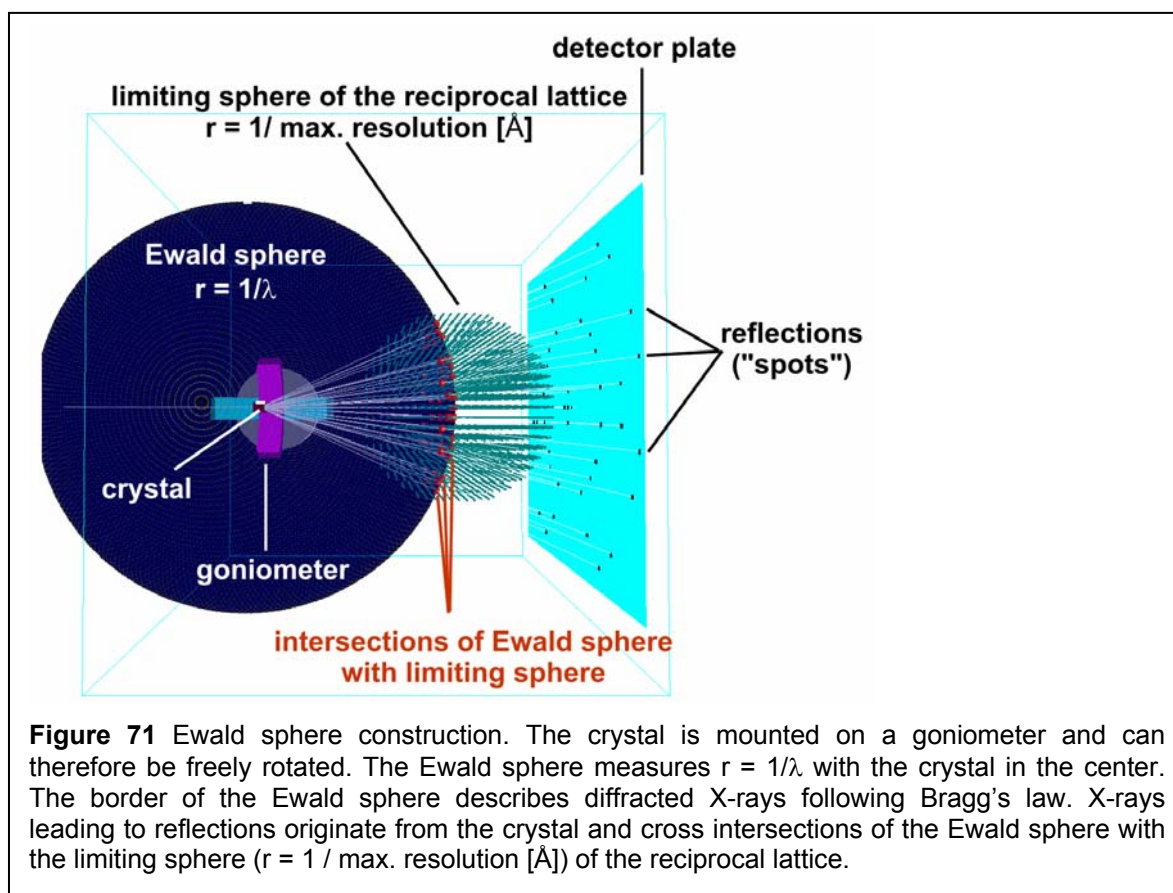


The lattice of the examined crystal (the 'object', see Fig 70) leads to diffracted X-rays forming a virtual lattice with inverted lattice spacing which is therefore called reciprocal lattice. The axes of the unit cell in real space are a , b , c and the corresponding axes of the unit cell in the inverted lattice in reciprocal space are a^* , b^* , c^* . Coordinates in real space are defined as xyz values, the corresponding coordinates in reciprocal space are noted as hkl values (Miller indices).

In order to employ a graphical representation of Bragg's law, the Ewald construction can be used. X-rays diffracted from the crystal, passing through points of the reciprocal lattice in a distance of $1/\lambda$ can be recorded as reflections (Fig. 71). The sphere with the radius $1/\lambda$ around the crystal is deduced from Bragg's law and called according to the German physicist Peter Ewald (Ewald sphere). The borders of the reciprocal lattice are described by the 'limiting sphere' that is originating in the centre of the reciprocal lattice with a radius of the inverse of the maximal resolution ($r = 1/D_{\max.}[\text{\AA}]$). Therefore, a crystal leading to high resolution data creates a larger limiting sphere and more reflections than a crystal generating lower resolution data.

The aim of data collection is to record every unique reflection at least once. One image of the diffraction pattern of the crystal is sufficient to estimate the space group. In order to generate data for the three dimensional representation of the electron density, more images are required which are taken from different angles.

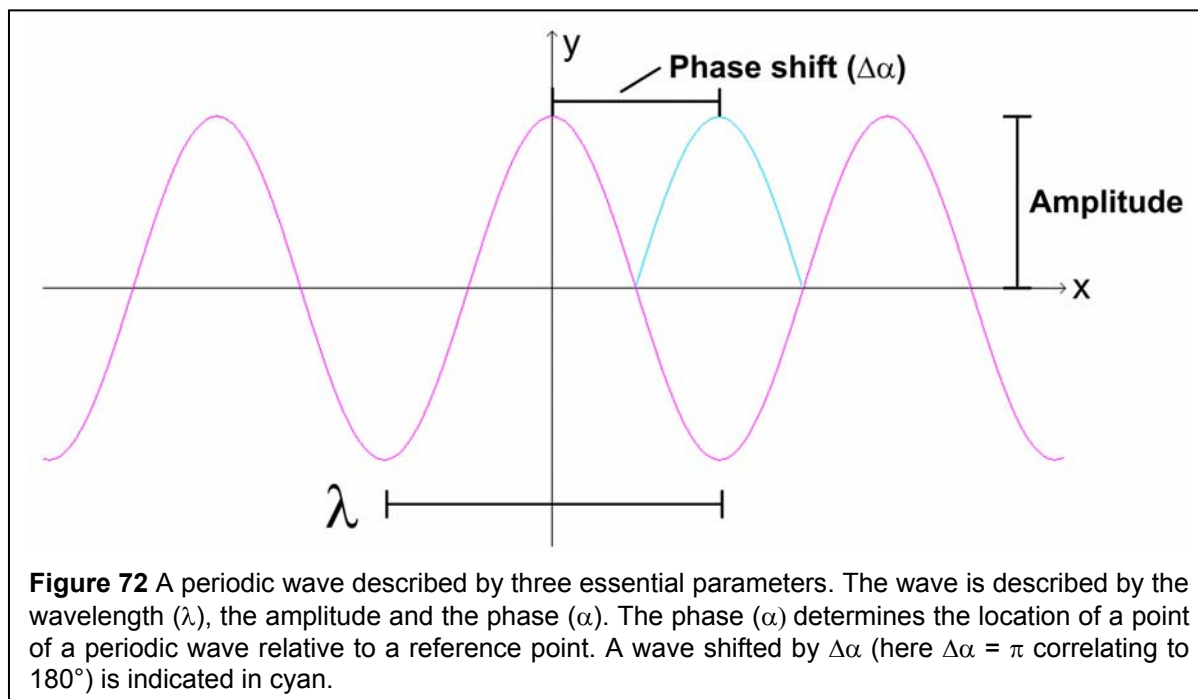
The crystal is rotated on the goniometer and for example after every turn of a degree, a diffraction pattern is recorded. In this way the (reciprocal) crystal lattice is examined. Due to symmetry in the diffraction pattern (Friedel symmetry: $hkl = -h -k -l$) images covering 180° of a native crystal are enough to generate a complete data set. An additional symmetry of the space group can reduce the oscillation range for a complete data set (e.g. 60° rotation for a trigonal space group due to 3-fold symmetry). In general, the amount of data collected depends on the symmetry of the space group and its position relative to the X-ray beam.



5.8.4 The Phase Problem and Electron Density Calculation

Every wave has three basic parameters: Wavelength (λ or frequency (f) which is $1/\lambda$), amplitude (A) and phase (α) (Fig. 72). In order to determine an electron density map, the waves that generate the reflections must be defined. The amplitude is proportional to the square root of the reflection intensity ($(I_{hkl})^{1/2}$); the wave length is equal to the one from the X-ray source. The phase (α) plays a major role in the process of structure determination because it is the parameter that is not directly

measurable from the data collection experiment but requires further expertise. This circumstance is known as the “phase problem”.



The X-ray generating a reflection is a complex three dimensional wave. The French mathematician Jean Baptiste Joseph Fourier described 1822 that any periodic function can be described by a series of terms of simpler periodic functions (Fourier series). The resulting function is a Fourier transform. The X-ray leading to a reflection can therefore be described as a Fourier transform of the ordered molecules in the crystal with the crucial variable of the phase.

Every recorded X-ray can be considered as the reflection of an infinitesimal small volume element of the dissected molecule and is fully described by a structure factor equation, often only called structure factor (F_{hkl}). For a complete data set, all structure factors recorded can be interpreted as contour map of the electron density ($\rho_{x,y,z}$) for the examined molecule. $\rho_{x,y,z}$ can be calculated by the following Fourier transform of the structure factors:

$$\rho(x, y, z) = \frac{1}{V} \sum_h \sum_k \sum_l |F_{hkl}| e^{i\alpha(hkl)} e^{-2\pi i(hx + ky + lz)}$$

ρ : value of the electron density at xyz

F: structure factor at the reflection at hkl

α : phase of the reflection at hkl

5.8.5 Molecular Replacement

Molecular replacement is a method to generate phases in order to determine a structure. Structurally determined proteins that are supposed to have a similar fold as the undetermined protein are used as search models and applied on the experimental data. Basically, the search model is rotated and translated in order to fit the experimental data. Disadvantage of the method is phase bias from the probe model.

Since the fold of the protein of interest is not determined, functionally homologous proteins with a similar size can be used as probe models. A protein with a sequence identity of 50% or more is most likely a good search model since, at this high sequence identity level, examined and probe protein should be structurally very similar. Molecular replacement is usually performed with data between 3.5 and 10 Å resolutions because higher resolutions include conformational information that is very specific for the probe model and lower resolution data contains information that is too much dependent on the packing of the molecule.

For the understanding of the evaluation of the rotation function it is important to define the Patterson map. Patterson maps are achieved by Fourier synthesis of the squared amplitudes ($F \cdot F^*$) resulting in a phase angle of 0.0 and centre of symmetry. The Patterson coordinate system is noted as uvw . Importantly, phases are not considered in Patterson maps. A Patterson map contains vectors between atoms in the unit cell without specification of the absolute positions of the atoms. For molecular replacement the Patterson map of the search model is placed at the origin of a virtual unit cell with primitive centring (P_1) and rotated for a maximum correlation with the Patterson map of the desired protein.

Successively, a translation search is performed. The search model is placed on a grid and the position is altered. During the search, the structure factor amplitudes of the search model are compared to the amplitudes of the protein of interest until the so called reliability factor (R-factor) is minimal. R-factors in molecular replacement can be high (exceed 0.6) but still represent a proper solution. This depends importantly also on how complete the search model is compared to the protein of interest. Searching a heterodimer with a monomer might result an R-factor of above 0.5 but still indicate the solution. The R-factor is defined in the following formula:

$$R = \frac{\sum \|F_{obs} - F_{calc}\|}{\sum |F_{obs}|}$$

R: R-Factor

F_{obs} : observed structure factor

F_{calc} : calculated structure factor

Another, more robust method to observe the success of the translation search is the calculation of a correlation function because scaling errors are avoided. The higher the correlation coefficient the better is the result. A relatively large difference between the highest and second best correlation coefficient might indicate that the top score is the solution.

Molecular replacement represents today a very powerful method because of an enormous pool of structural information and sufficiently fast computers to execute large numbers of rotation and translation operations within a very short time. The major disadvantage of molecular replacement is the bias from the phase information of the search model.

5.8.6 Anomalous Dispersion

Single anomalous dispersion (SAD) and multiple anomalous dispersion (MAD) are methods used to obtain phases relying on the crystallisation of proteins including anomalous scatterers in their structure. For SAD a single and for MAD a multiple wavelength approach is used.

For anomalous scattering the symmetry given by Friedel's law (reflections with identical intensities at hkl and $-h-k-l$ and $\alpha_{hkl} = -\alpha_{-h-k-l}$) is broken down (Fig. 73). The two reflections at hkl and $-h-k-l$ are called Friedel pair. Anomalous scatterers generate Friedel pairs that are not equivalent in amplitude and inverse in phase due to the fact that electrons from these atoms interact in a resonant manner with the incident X-ray used for the experiment. The resonant interaction occurs around a certain wavelength as a sharp peak (absorption peak) characteristic for the anomalous scatterer but also dependent on its chemical environment.

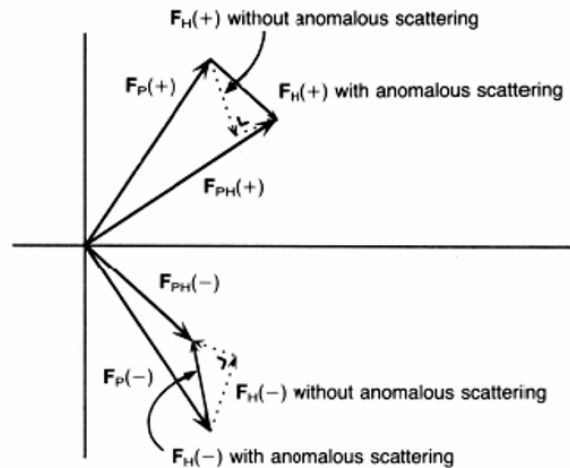


Figure 73 Breakdown of Friedel's law. Structure factors are shown as vectors with the length representing the amplitude and the angle the phase. $F_P(+)$ and $F_P(-)$ indicate structure factors following Friedel's law, $F_{PH}(+)$ and $F_{PH}(-)$ those where Friedel's law is broken down (anomalous scatterer). $F_H(+)$ and $F_H(-)$ indicate difference vectors. The anomalous scatterer generates Friedel pairs with different amplitude and the phases $\alpha(F_{PH}(+)) \neq -\alpha(F_{PH}(-))$. Image taken from (Drenth, 1994).

In general, SAD or MAD phase determination depends on an accessible absorption peak from K-, L- or M-shell electrons. In models for X-ray scattering in matter, excitations are thought to occur localised on single electrons ('independent particle approximations'). A commonly used anomalous scatterer is Selenium, where a K-shell electron is promoted. Selenium can be introduced into proteins by seleno-L-methionine substituting methionine during over-expression. In order to estimate whether anomalous dispersion gives rise to a signal sufficient for structure determination, there should be at least about one anomalous scatterer per 80 amino acids.

Normal scattering of X-ray photons is elastic scattering; no energy is transferred to the atom. When the energy of X-rays is close to the absorption edge of an (anomalous scattering) atom the following scattering effects occur:

1. Partial normal scattering.
2. Absorption leading to fluorescence. The photon is absorbed by an electron and emitted with lower energy (lower wavelength) and altered phase.
3. The X-ray photon hits a K-, L- or M-shell electron, no energy is absorbed but the electron is emitted with altered phase (strong coupling to absorbance edge energy).
4. Retardation of the photon causing the phase shift generates an imaginary (negative) component to the absorption term in the atomic form factor calculation.

Atomic form factors ($f(\theta, \lambda)$) consider the normal scattering ($f_0(\theta)$), the dispersive ($f'(\lambda)$) and the imaginary ($if''(\lambda)$) contribution to the scattering in order to predict diffraction, scattering and attenuation processes of light through matter.

$$f(\theta, \lambda) = f_0(\theta) + f'(\lambda) + if''(\lambda)$$

$f(\theta, \lambda)$: atomic scattering factor | θ : Bragg angle, λ : wave length

$f_0(\theta)$: normal scattering term

$f'(\lambda)$: dispersive term, matches the change in the real part of the scattering

$f''(\lambda)$: absorption term (negative since it describes an energy absorption),
equals the change in the imaginary part of the scattering

f' and f'' are determined in a fluorescence scan. The dispersive term is 90° advanced in phase compared to the normal term also stating the breakdown of Friedel's law (Fig. 74).

The experimental wavelength giving the largest signal is close to the wavelength of largest absorption ('absorption edge'; $f''(\lambda) = \text{maximal}$) where the dispersive term ($f'(\lambda)$) has its maximum reflecting the largest amplitude difference of the two structure factors of the Friedel pair. In total, for a MAD experiment three wavelengths are measured: one at the absorption edge ('inflection') for the largest dispersive difference of the Friedel pair, one to optimise anomalous differences ('peak' or 'white line'), and one at a wavelength remote from the absorption (Fig. 74).

The phase information of the anomalous scatterer is extracted from the difference of the anomalous reflections of the Friedel pair. Consequently, a substructure including only the anomalous scatterers can be calculated which gives the first phases for the electron density map of the protein containing the anomalous scatterer. If the anomalous scatterer is present due to substitution (e.g. for selenomethionine crystals), phases for the native data set can be achieved by molecular replacement using the structure of the non-native protein as a search model for the native data set.

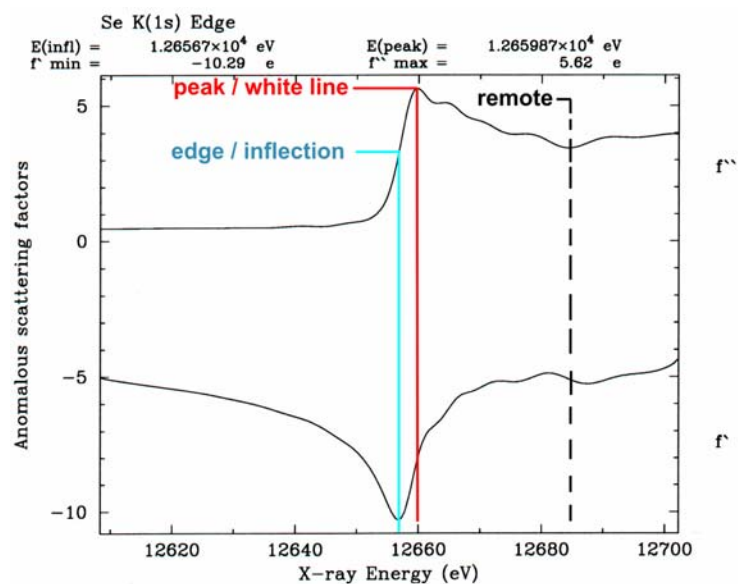


Figure 74 Selenium fluorescence scan of the *A. fulgidus* hjc enzyme performed for a SAD experiment. Anomalous scattering factors are plotted versus X-ray energy. The energies of the absorption edge (inflection) and peak (white band) are noted and highlighted in cyan and red, respectively. A possible remote X-ray energy is highlighted as dashed black line. The image is modified from (Biertümpfel, 2005).

5.8.7 Isomorphous Replacement

Other methods using anomalous scatterers are called isomorphous replacement. Here, interpretation of the anomalous signal is possible but not required. The goal of an isomorphous replacement experiment is to alter the structure factor of a native protein of interest, without modifying crystal form or unit cell dimensions, upon addition of an intensively scattering atom (such as Pd, Ag, Gd, Pt, Au, Hg, Pb or U). After successful soaking, information about the structure factor of the native protein (F_P) can be achieved by the knowledge of the structure factors of the derivatised protein (F_{PH}) and the derivative itself (F_H):

$$F_P = F_{PH} - F_H$$

The heavy atom is added to the crystallisation buffer and incorporated into the mature crystal ('soaking'). Since the scattering intensity per atom is correlated to the square of the number of electrons per atom, only one heavy atom per 20 kD of protein can generate a signal sufficient for the determination of F_{PH} and F_H . The small number of heavy atoms required for the generation of a measurable signal allows to easily deconvoluting a Patterson map in order to determine a substructure for the hetero atoms.

In single isomorphous replacement (SIR) one type of heavy atom derivative is applied to determine F_{PH} and F_H , in multiple isomorphous replacement (MIR) more heavy atom derivatives are included. In contrast to MIR, phase determination using SIR is not sufficient to determine a *de novo* structure without further phase information.

The dispersive effects in isomorphous replacement are the same as for anomalous dispersion. For additional phase information, the anomalous signal of one or more heavy atoms can be analysed giving rise to SIRAS (single isomorphous replacement with anomalous scattering) or MIRAS (multiple isomorphous replacement with anomalous scattering).

The important difference between isomorphous replacement and SAD/MAD is that for isomorphous replacement the introduced hetero atom is not part of the protein and might also alter or destroy the crystal package. SAD and MAD have the advantage to be 'automatically' isomorphous since the anomalous scatterer is part of the protein.

5.8.8 Data Processing

Data processing prepares the collected data for the refinement which leads to the generation of the electron density map. For data processing, first the space group is determined from a single image recorded and different parameters of data collection are adjusted such as distance from crystal to X-ray source. Then reflections are indexed ('indexing') on all images recorded in order to determine unique reflections and outliers are filtered out. Successively, the data is scaled which means that identical intensities are assigned to reflections with the same index. Then reflections with common indices are put together ('merging'). This step generates the redundancy of the data set. The accuracy of the processed data can be evaluated by a value called R_{sym} which compares the variance of symmetry-related reflections. Overall R_{sym} values below 0.05 can be considered to be good and values up to 0.10 are probably useable. In comparison, processed random data might give an overall R_{sym} value of up to 0.35.

5.8.9 Refinement and Evaluation of the Model

With the information of the wavelength, the structure factor amplitudes from data processing and the preliminary phase information (e.g. from molecular replacement),

the first electron density map can be calculated. Meanwhile the refinement process the model is improved to better fit the experimental data. Iterative steps of calculation and model building ('bootstrapping') lead to enhanced phases and therefore a better electron density map.

The first density map calculated is called F_o because it was generated with a Fourier transform from only the observed structure factor amplitudes. When the figure of merit (FOM) is taken into account, describing the quality of the map, the map is termed mF_o map. An electron density map reflecting the structure factor amplitudes expected from the current model is called F_c map ('Fourier calculated'). Considering the average coordinate error of the model (Luzzati, 1952), the map is named DF_c map (see below).

In the first refinement cycle, a model from a molecular replacement solution can be evaluated via the R-factor (see below) which states the difference between the calculated and observed structure factor amplitudes. An R-factor of 0.45 – 0.50 indicates that the correlation is not random.

The model can be evaluated according to different parameters:

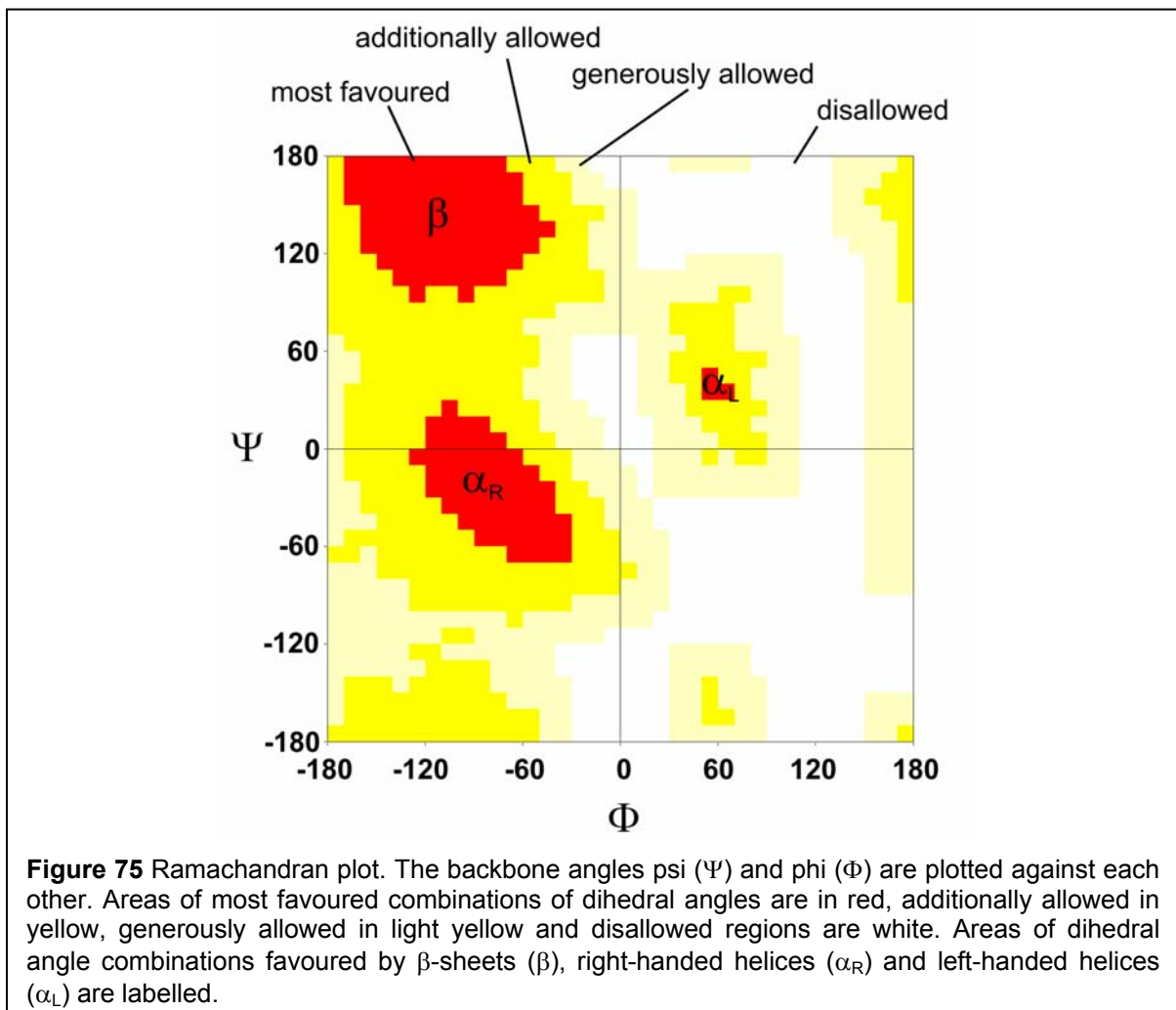
R-factor / Free R-factor

For a correct solution the R-factor drops during the bootstrapping process. It reflects how well the current model reflects the entire data set. The model can also bias the successively calculated electron density. Therefore, a randomly chosen small part of the reflections (about 5%) is excluded from the refinement process ('test set') and gives rise to the free R-factor (R_{free}), stating how well the model corresponds to the test set. Since reflections of the test set are not used for refining the model, the R_{free} value is higher than the R-factor and less biased from the model. During bootstrapping a dropping R_{free} value indicates a true improvement on the model.

Ramachandran Plot

The Ramachandran Plot allows evaluating the correctness of the main chain stereochemistry of the model. Here, the psi (Ψ) angle is plotted against the phi (Φ) angle (Fig. 75). Both main chain angles are also known as dihedral angles. Regions are indicated where a phi-psi combination is most favoured, additionally allowed, generously allowed and disallowed. In secondary structural elements, the ranges of

dihedral angles are restrained. Therefore, dihedral angles assigned to amino acids in secondary structural elements can be easily verified by the Ramachandran plot.



Coordinate Error

The model can be validated by determining the average coordinate error of the model by Luzzati (Kleywegt et al., 1994; Kleywegt and Brunger, 1996; Luzzati, 1952) and SigmaA (Read, 1986) analysis. The Luzzati coordinate error is determined by plotting the crystallographic R-factor versus resolution (Luzzati plot) assuming a Gaussian error distribution. The program SIGMAA (Read, 1986) combines calculated with previously determined phase information using phase probability profiles. Phase information calculated from a model structure or the combination of phase probabilities, from experimental phases with those from one or model structures, allows the calculation of weighted Fourier coefficients. The program calculates iteratively the SigmaA value as defined by (Srinivasan, 1966). For each reflection, the

figure of merit m , describing the quality of the map, and the estimate of the error in the partial structure from coordinate errors D (Luzzati, 1952) are determined. Consequently, SigmaA weighted electron density maps are termed e.g. $mFo - DFc$ when a SigmaA weighted $Fo - Fc$ electron density map is calculated. In this work the program CNS (Brunger et al., 1998) was used to generate SigmaA weighted electron density maps for model building refinement.

Other Evaluation Parameters

For the evaluation of the model it is important to confirm that the interatom distances are proper. In general, interatom distances should be at least the radii of their Van der Waals radii minus 0.4 Å. Bond lengths and angles should be within a range as stated by Engh and Huber (Engh and Huber, 1991). Important non-covalent bonds are hydrogen bonds which can vary in length between 1.6 and 2.4 Å with the O-H bond vector pointing directly at the acceptor ion pair.

Torsion angles can be compared to torsion angles of well refined structures in the protein data bank and scored by the program WHATCHECK (Hooft et al., 1996). WHATCHECK (Hooft et al., 1996) can also compare rotamers of side chains to a database of proper rotamer conformations. Unusual conformations are reported accordingly. It is further important to inspect the planarity of rings in side chains where e.g. aromatic rings (in Phe, Tyr, Trp) are flat. Additionally, water molecules integrated into the atomic model should be bound to the protein.

5.9 List of Buffers

5.9.1 SR α^{His} : $\beta\Delta TM$

Name	Buffer
L($\alpha\beta$)	50 mM Tris-HCl pH 8.0, 500 mM NaCl, 5mM MgCl ₂ , 10 mM imidazole, 0.1%, Triton X-100, 0.02% MTG and one tablet of protease inhibitor
A_{Ni}($\alpha\beta$)	50 mM Tris-HCl pH 8.0, 500 mM NaCl, 5mM MgCl ₂ , 10 mM imidazole, 0.1%, 0.02% MTG
B_{Ni}($\alpha\beta$)	50 mM Tris-HCl pH 8.0, 500 mM NaCl, 5 mM MgCl ₂ , 300 mM imidazole, 0.1%, 0.02% MTG
Q($\alpha\beta$)	20 mM Tris-HCl pH 7, 200 mM NaCl, 5 mM MgCl ₂ , 0.02% MTG
A_{SP}($\alpha\beta$)	20 mM Tris-HCl pH 7, 200 mM NaCl, 5 mM MgCl ₂ , 0.02% MTG
B_{SP}($\alpha\beta$)	20 mM Tris-HCl pH 7, 350 mM NaCl, 5 mM MgCl ₂ , 0.02% MTG
GF($\alpha\beta$)	10 – 50 mM Tris pH 8, 500 mM NaCl, 5 mM MgCl ₂ and 0.02 % MTG

5.9.2 SRX2 His : $\beta\Delta TM$

Name	Buffer
L(X2β)	50mM Tris pH 8.0, 500 mM NaCl, 5 mM MgCl ₂ , 10 mM imidazole, 0.01% MTG, supplemented with one tablet of protease inhibitor
A_{Ni}(X2β)	50mM Tris pH 8.0, 500 mM NaCl, 5 mM MgCl ₂ , 10 mM imidazole, 0.01% MTG
B_{Ni}(X2β)	50mM Tris pH 8.0, 500 mM NaCl, 5 mM MgCl ₂ , 500 mM imidazole, 0.01% MTG
Q(X2β)	20mM HEPES pH=7, 150 mM NaCl, 5 mM MgCl ₂ , 0.02 % MTG
A_{SP}(X2β)	20mM HEPES pH=7, 150 mM NaCl, 5 mM MgCl ₂ , 0.02 % MTG
B_{SP}(X2β)	20mM HEPES pH=7, 1 M NaCl, 5 mM MgCl ₂ , 0.02 % MTG
GF(X2β)	10 mM Tris pH 8, 150 mM NaCl, 5 mM MgCl ₂ , 0.02% MTG

5.9.3 SRX2^{His}: β Δ TM_{SeMet}**GM(SeMet):**

Added per litre of medium	Name	Contents
2 ml	MgSO ₄	1 M MgSO ₄ *
65 ml	M9 (20X)	0.375 mM NH ₄ Cl, 2.265 M KH ₂ PO ₄ , 2.1 M Na ₂ HPO ₄ x2H ₂ O *
10 ml	Amino acid mix I	All amino acids but Met, Tyr, Trp, Phe at 4 mg/ml **
10 ml	Amino acid mix II	Tyr, Trp, Phe at 4 mg/ml, stirred slowly ON at RT, not all dissolves **
20ml	Glucose	20 % Glucose *
1 ml	Vitamin mix	Niacinamide, pyridoxine monochloride, thiamine at 1mg/ml **
1 ml	Riboflavin	1 mg / ml Riboflavin in 0.1 % acetic acid, stirred 6 h at RT, not all dissolves **
40 mg	Selenomethionine	Added directly

*: autoclaved, **: filtered sterile

Name	Buffer
L(SeMet)	50 mM Tris pH 7.4 (measured at 4°C), 500 mM NaCl, 30 mM imidazole, 10 mM MgCl ₂ , 0.02% MTG , supplemented with one tablet of protease inhibitor
A_{Ni}(SeMet)	50 mM Tris pH 7.4 (measured at 4°C), 500 mM NaCl, 30 mM imidazole, 10 mM MgCl ₂ , 0.02 % MTG
B_{Ni}(SeMet)	50 mM Tris pH 7.4 (measured at 4°C), 500 mM NaCl, 500 mM imidazole, 10 mM MgCl ₂ , 0.02% MTG
Q(SeMet)	20 mM HEPES pH7, 150 mM NaCl, 5 mM MgCl ₂ , 1 mM DTT
A_{SP}(SeMet)	20 mM HEPES pH 7, 150 mM NaCl, 5 mM MgCl ₂ , 1 mM DTT
B_{SP}(SeMet)	20 mM HEPES pH 7, 1 M NaCl, 5 mM MgCl ₂ , 1 mM DTT
GF(SeMet)	10 mM Tris pH 8.0, 150mM NaCl, 5 mM MgCl ₂ , 1 mM DTT

5.9.4 SR α NG^{His}

Name	Buffer
L(αNG)	50 mM Tris-HCl pH 8.0, 500 mM NaCl, 5mM MgCl ₂ , 10 mM imidazole, 0.1%, Triton X-100, 0.02% MTG and one tablet of protease inhibitor
A_{Ni}(αNG)	50 mM BisTris pH 7, 300 mM NaCl, 10 mM imidazole, 5 mM MgCl ₂ , 0.02% MTG
B_{Ni}(αNG)	50 mM BisTris pH 7, 300 mM NaCl, 500 mM imidazole, 5 mM MgCl ₂ , 0.02% MTG

5.9.5 SRP54D^{His}**Test expression**

Name	Buffer
L(54Dt)	50 mM Tris pH 8, 500 mM NaCl, 5 mM MgCl ₂ , 0.02% MTG and one tablet of protease inhibitor
A_{Ni}(54Dt)	50 mM Tris pH 8, 500 mM NaCl, 5 mM MgCl ₂ , 0.02 % MTG
B_{Ni}(54Dt)	50 mM Tris pH 8, 500 mM NaCl, 5 mM MgCl ₂ , 0.02 % MTG

Standard Preparation

Name	Buffer
L(54D)	50 mM Tris pH 7.3, 500 mM NaCl, 5 mM MgCl ₂ , 0.02% MTG, supplemented with one tablet of protease inhibitor
A_{Ni}(54D)	50 mM Tris pH 7.3, 500 mM NaCl, 5 mM MgCl ₂ , 0.02% MTG
B_{Ni}(54D)	50 mM Tris pH 7.3, 500 mM NaCl, 5 mM MgCl ₂ , 0.02% MTG
A_{SP}(54D)	50 mM BisTris pH 6, 120 mM NaCl, 5 mM MgCl ₂ , 0.02% MTG
B_{SP}(54D)	50 mM BisTris pH 6, 500 mM NaCl, 5 mM MgCl ₂ , 0.02% MTG
GF(54D)	10 mM Tris pH 8, 250 mM NaCl, 5 mM MgCl ₂ , 0.02% MTG

5.9.6 SRP54NG^{His}

Materials and Methods

Name	Buffer
L(54NG)	50 mM BisTris pH 7, 150 mM NaCl, 5 mM MgCl ₂ , 30 mM imidazole, 0.02% MTG, supplemented with one tablet of protease inhibitor
A_{Ni}(54NG)	50 mM BisTris pH 7, 150 mM NaCl, 5 mM MgCl ₂ , 30 mM imidazole, 0.02% MTG
B_{Ni}(54NG)	50 mM BisTris pH 7, 150 mM NaCl, 5 mM MgCl ₂ , 500 mM imidazole, 0.02% MTG
Q(54NG)	25 mM BisTris pH 6, 150 mM NaCl, 5 mM MgCl ₂ , 0.02% MTG
GF(54NG)	20 mM Tris pH 7.5, 350 mM NaCl, 2 mM MgCl ₂ , 0.02% MTG

5.9.7 Trimeric Complex: SR α^{His} : $\beta\Delta$ TM:SRP54D^{His}

Name	Buffer
CF(T)	20 mM Tris/HCl pH 8, 10% glycerol, 250 mM NaCl, 5 mM MgCl ₂ , 0.02% MTG, 2mM GMPPNP
GF(T)	20 mM Tris/HCl pH 8, 250 mM NaCl, 5 mM MgCl ₂ , 0.02% MTG

5.9.8 Pentameric Complex Formation:



Name	Buffer
GF(P)	20 mM Tris pH 8, 250 mM NaCl, 10 mM KCl, 10 mM MgCl ₂ , 0.02% MTG

5.9.9 Trimeric Complex Formation Pull-Down: SR α : $\beta\Delta$ TM:SRP54NG^{CHis}

Name	Buffer
L($\alpha\beta$2)	50 mM BisTris pH 7, 150 mM NaCl, 5 mM MgCl ₂ , 0.01% Triton X-100, 0.02 % MTG, supplemented with one tablet of protease inhibitor
A_{SP}($\alpha\beta$2)	50 mM BisTris pH 7, 150 mM NaCl, 5 mM MgCl ₂ , 0.02% MTG
B_{SP}($\alpha\beta$2)	50 mM BisTris pH 7, 350 mM NaCl, 5 mM MgCl ₂ , 0.02% MTG
CF2	25 mM BisTris pH 7, 150 mM NaCl, 5 mM MgCl ₂ , 15 mM imidazole,

	0.02% MTG, 2 mM GMPPNP
A_{Ni}(T2)	50 mM BisTris pH 7, 150 mM NaCl, 15 mM imidazole, 0.02% MTG
B_{Ni}(T2)	50 mM BisTris pH 7, 150 mM NaCl, 500 mM imidazole, 0.02 % MTG
GF(T2)	10 mM BisTris pH 7, 150 mM NaCl, 5 mM MgCl ₂ , 0.02 % MTG

5.9.10 Analysis of SR:SRP Complex Formation

Name	Buffer
SR	10 mM Tris pH 8, 250 mM NaCl, 10 mM MgCl ₂ , 0.02 % MTG
B54	50 mM HEPES pH 7.5, 200 mM NaCl, 10 % glycerol, 5 mM MgCl ₂
B19RNA	20 mM Tris pH 8, 400 mM NaCl, 10 mM KCl, 10 mM MgCl ₂
GF(5)	10 mM Tris pH 8, 250 mM NaCl, 10 mM MgCl ₂ , 0.02 % MTG

5.9.11 Immobilised Peptide Library Scan

Name	Buffer
BLK	50 mM HEPES pH 7.5, 150 mM KOAc, 5mM MgCl ₂ , 0.2 % BSA
BLT	30 mM Tris, 20 % methanol
PMT	PBS, 0.5 % milkpowder, 0.05 % Tween-20

5.9.12 Buffer for HPLC analysis

Name	Buffer
HP	50mM K ₂ H/KH ₂ PO ₄ pH 6.3, 10 mM TBAB, 6 % acetonirile

5.9.13 Crystallisation and Structure Determination of SR α X2^{His}: β Δ TM

Name	Buffer
Cryst	10 mM Tris pH 8, 150 mM NaCl, 5 mM MgCl ₂ , 1 mM DTT
Res1	2 M (NH ₄) ₂ SO ₄ , 0.1 M sodium citrate pH 5.5
Res2	2 M (NH ₄ SO ₄) ₂ , 0.1 M sodium citrate pH 5.5, 100 mM guanidinium

	hydrochloride
BCryo	2 M (NH ₄) ₂ SO ₄ , 0.1 M sodium citrate pH 5.5, 100 mM guanidinium hydrochloride, 20% glycerol

5.10 List of Primers

5.10.1 SRX2^{His}:βΔTM / SRα^{His}:βΔTM mutants

Mutation	Sequence (5'-3')
SRα R524Q	Forward (-Fo): ggtggacacggcaggg CAG atgcaagacaatgcccc Reverse (-Re): ggggcattgtcttgcat CTG gcctgccgtgtccacc
SRα R34A	Forward (_f): cccgttaacgcgttgatt GCT tccgtgctgctgcagg Reverse (_r): cctgcagcagcacgga AGC aatcaacgcgttaacggg
SRα D72G	Forward (_f): ctcttcgttggtctctgt GGA tctgggaaaacgttgctg Reverse (_r):cagcaacgttttcccaga TCC acagagaccaacgaagag
SRβ H119A	Forward (_f): gatcgacctccccggg GCT gagagcttgaggtttcagc Reverse (_r): gctgaaacctcaagctctc AGC ccccggggagggtcgatc

Sequences coding for mutated amino acids are highlighted in capital and bold letters.

5.10.2 SRαNG^{His}

Name	Sequence (5'-3')
SRαNG-Forward	CATCACTCCATGGGAACACTGGGTGGCATG
SRαNG-Reverse	AGTGTGGGATCCTCATTAAGCCTTCATGAGGGCAGCCAC

5.10.3 SRP54D^{His}

Name	Sequence (5'-3')
SRP54DN-Forward	GTCAGTACCATGGGACACCACCACCACCACATGGTACTAGCAG ACCTTGGAAGAAAAATAACATCAGC

Materials and Methods

SRP54DN-Reverse	GGGTGACCTCGAGTCATTAACCTCCCATCTTTTTTACCATCTG
SRP54DC-Forward	GTCAGTACCATGGTACTAGCAGACCTTGGAAGAAAAATAACATCA GC
SRP54DN-Reverse	GGGTGACCTCGAGTTATCAGTGGTGGTGGTGGTGGTGACCTCCCAT CTTTTTTACCATCTGTGCAAATTTGG

5.10.4 SRP54NG^{His}

Name	Sequence (5'-3')
SRP54NGN-Forward	cagcaagcttcttgggt TGA atgggtgacatcgaag
SRP54NGN-Reverse	cttcgatgtcacccat TCA accaagaagcttgctg
SRP54NGC-Forward	GTCAGTACCATGGTACTAGCAGACCTTGGAAGAAAAATAACATCAAGC
SRP54NGC-Reverse	TACTCGCCTCGAGTTACTAATGGTGATGGTGATGGTGACCAAGAAGCTTGC TGATAAAAGGCTGTGTTTTGAAAGG

Bold and capital letters indicate the inserted stop codon.

Bibliography

- Abell, B.M., Pool, M.R., Schlenker, O., Sinning, I. and High, S. (2004) Signal recognition particle mediates post-translational targeting in eukaryotes. *Embo J*, **23**, 2755-2764.
- Alberts, B., Johnson, R.A., Lewis, J., Raff, M., Roberts, K. and Walter, P. (2002) *Molecular Biology of the Cell*. Garland Scienc, New York.
- Andersen, E.S., Rosenblad, M.A., Larsen, N., Westergaard, J.C., Burks, J., Wower, I.K., Wower, J., Gorodkin, J., Samuelsson, T. and Zwieb, C. (2006) The tmRDB and SRPDB resources. *Nucleic Acids Res*, **34**, D163-168.
- Andrews, D.W., Lauffer, L., Walter, P. and Lingappa, V.R. (1989) Evidence for a two-step mechanism involved in assembly of functional signal recognition particle receptor. *J Cell Biol*, **108**, 797-810.
- Angelini, S., Deitermann, S. and Koch, H.G. (2005) FtsY, the bacterial signal-recognition particle receptor, interacts functionally and physically with the SecYEG translocon. *EMBO Rep*, **6**, 476-481.
- Bacher, G., Lutcke, H., Jungnickel, B., Rapoport, T.A. and Dobberstein, B. (1996) Regulation by the ribosome of the GTPase of the signal-recognition particle during protein targeting. *Nature*, **381**, 248-251.
- Bacher, G., Pool, M. and Dobberstein, B. (1999) The ribosome regulates the GTPase of the beta-subunit of the signal recognition particle receptor. *J. Cell. Biol.*, **146**, 723-730.
- Batey, R.T., Rambo, R.P., Lucast, L., Rha, B. and Doudna, J.A. (2000) Crystal structure of the ribonucleoprotein core of the signal recognition particle. *Science*, **287**, 1232-1239.
- Beckmann, R., Bubeck, D., Grassucci, R., Penczek, P., Verschoor, A., Blobel, G. and Frank, J. (1997) Alignment of conduits for the nascent polypeptide chain in the ribosome-Sec61 complex. *Science*, **278**, 2123-2126.
- Beckmann, R., Spahn, C.M., Eswar, N., Helters, J., Penczek, P.A., Sali, A., Frank, J. and Blobel, G. (2001) Architecture of the protein-conducting channel associated with the translating 80S ribosome. *Cell*, **107**, 361-372.
- Bernstein, H.D., Poritz, M.A., Strub, K., Hoben, P.J., Brenner, S. and Walter, P. (1989) Model for signal sequence recognition from amino-acid sequence of 54K subunit of signal recognition particle. *Nature*, **340**, 482-486.
- Bi, X., Corpina, R.A. and Goldberg, J. (2002) Structure of the Sec23/24-Sar1 pre-budding complex of the COPII vesicle coat. *Nature*, **419**, 271-277.
- Biertümpfel, C. (2005) Crystallization and structural studies on T4 endonuclease VII-substrate complexes and the Holliday junction-cutting enzyme from *Archaeoglobus fulgidus*. *Combined Faculties of the Natural Sciences and for Mathematics*. Ruperto-Carola University of Heidelberg, Germany, Heidelberg.
- Bourne, H.R., Sanders, D.A. and McCormick, F. (1990) The GTPase superfamily: a conserved switch for diverse cell functions. *Nature*, **348**, 125-132.
- Bourne, H.R., Sanders, D.A. and McCormick, F. (1991) The GTPase superfamily: conserved structure and molecular mechanism. *Nature*, **349**, 117-127.
- Breyton, C., Haase, W., Rapoport, T.A., Kuhlbrandt, W. and Collinson, I. (2002) Three-dimensional structure of the bacterial protein-translocation complex SecYEG. *Nature*, **418**, 662-665.

Bibliography

- Brown, J.D., Hann, B.C., Medzihradszky, K.F., Niwa, M., Burlingame, A.L. and Walter, P. (1994) Subunits of the *Saccharomyces cerevisiae* signal recognition particle required for its functional expression. *Embo J*, **13**, 4390-4400.
- Brunger, A.T., Adams, P.D., Clore, G.M., DeLano, W.L., Gros, P., Grosse-Kunstleve, R.W., Jiang, J.S., Kuszewski, J., Nilges, M., Pannu, N.S., Read, R.J., Rice, L.M., Simonson, T. and Warren, G.L. (1998) Crystallography & NMR system: A new software suite for macromolecular structure determination. *Acta Crystallogr D Biol Crystallogr*, **54** (Pt 5), 905-921.
- Burstein, E.S. and Macara, I.G. (1992) Interactions of the ras-like protein p25rab3A with Mg²⁺ and guanine nucleotides. *Biochem J*, **282** (Pt 2), 387-392.
- Chang, D.Y., Hsu, K. and Maraia, R.J. (1996) Monomeric scAlu and nascent dimeric Alu RNAs induced by adenovirus are assembled into SRP9/14-containing RNPs in HeLa cells. *Nucleic Acids Res*, **24**, 4165-4170.
- Chavrier, P. and Goud, B. (1999) The role of ARF and Rab GTPases in membrane transport. *Curr Opin Cell Biol*, **11**, 466-475.
- Cheng, Z., Jiang, Y., Mandon, E.C. and Gilmore, R. (2005) Identification of cytoplasmic residues of Sec61p involved in ribosome binding and cotranslational translocation. *J Cell Biol*, **168**, 67-77.
- Chenna, R., Sugawara, H., Koike, T., Lopez, R., Gibson, T.J., Higgins, D.G. and Thompson, J.D. (2003) Multiple sequence alignment with the Clustal series of programs. *Nucleic Acids Res*, **31**, 3497-3500.
- Clemons, W.M., Jr., Gowda, K., Black, S.D., Zwieb, C. and Ramakrishnan, V. (1999) Crystal structure of the conserved subdomain of human protein SRP54M at 2.1 Å resolution: evidence for the mechanism of signal peptide binding. *J. Mol. Biol.*, **292**, 697-705.
- Collaborative Computing Project, N. (1994) The CCP4 Suite: Programs for Protein Crystallography. *Acta Crystallogr. D*, **50**, 760-763.
- Collins, B.M., McCoy, A.J., Kent, H.M., Evans, P.R. and Owen, D.J. (2002) Molecular architecture and functional model of the endocytic AP2 complex. *Cell*, **109**, 523-535.
- Connolly, T. and Gilmore, R. (1993) GTP hydrolysis by complexes of the signal recognition particle and the signal recognition particle receptor. *J Cell Biol*, **123**, 799-807.
- Connolly, T., Rapiejko, P.J. and Gilmore, R. (1991) Requirement of GTP hydrolysis for dissociation of the signal recognition particle from its receptor. *Science*, **252**, 1171-1173.
- Corbett, K.D. and Alber, T. (2001) The many faces of Ras: recognition of small GTP-binding proteins. *Trends Biochem Sci*, **26**, 710-716.
- Corsi, A.K. and Schekman, R. (1996) Mechanism of polypeptide translocation into the endoplasmic reticulum. *J Biol Chem*, **271**, 30299-30302.
- de Leeuw, E., te Kaat, K., Moser, C., Menestrina, G., Demel, R., de Kruijff, B., Oudega, B., Luirink, J. and Sinning, I. (2000) Anionic phospholipids are involved in membrane association of FtsY and stimulate its GTPase activity. *Embo J*, **19**, 531-541.
- DeLano, W.L. (2002) The PyMOL Molecular Graphics System. DeLano Scientific, San Carlos, CA, USA.
- Dobberstein, B. and Sinning, I. (2004) Structural biology. Surprising news from the PCC. *Science*, **303**, 320-322.
- Drenth, J. (1994) *Principles of Protein X-ray Crystallography*. Springer, Berlin.
- Duong, F. (2003) Binding, activation and dissociation of the dimeric SecA ATPase at the dimeric SecYEG translocase. *Embo J*, **22**, 4375-4384.

Bibliography

- Egea, P.F., Shan, S.O., Napetschnig, J., Savage, D.F., Walter, P. and Stroud, R.M. (2004) Substrate twinning activates the signal recognition particle and its receptor. *Nature*, **427**, 215-221.
- Engh, R.A. and Huber, R. (1991) Accurate bond and angle parameters for X-ray protein structure refinement. *Acta Cryst.*, **A47**, 392-400.
- Filippini, F., Rossi, V., Galli, T., Budillon, A., D'Urso, M. and D'Esposito, M. (2001) Longins: a new evolutionary conserved VAMP family sharing a novel SNARE domain. *Trends Biochem Sci*, **26**, 407-409.
- Focia, P.J., Shepotinovskaya, I.V., Seidler, J.A. and Freymann, D.M. (2004) Heterodimeric GTPase core of the SRP targeting complex. *Science*, **303**, 373-377.
- Freymann, D.M., Keenan, R.J., Stroud, R.M. and Walter, P. (1997) Structure of the conserved GTPase domain of the signal recognition particle. *Nature*, **385**, 361-364.
- Fulga, T.A. (2001) Functional Characterization of the Mammalian SRP Receptor. *EMBL*. University of Heidelberg, Heidelberg, pp. 1-122.
- Fulga, T.A., Sinning, I., Dobberstein, B. and Pool, M.R. (2001) SRbeta coordinates signal sequence release from SRP with ribosome binding to the translocon. *Embo J.*, **20**, 2338-2347.
- Gill, D.R., Hatfull, G.F. and Salmond, G.P. (1986) A new cell division operon in *Escherichia coli*. *Mol Gen Genet*, **205**, 134-145.
- Goldberg, J. (1999) Structural and functional analysis of the ARF1-ARFGAP complex reveals a role for coatamer in GTP hydrolysis. *Cell*, **96**, 893-902.
- Gonzalez, L.C., Jr., Weis, W.I. and Scheller, R.H. (2001) A novel snare N-terminal domain revealed by the crystal structure of Sec22b. *J Biol Chem*, **276**, 24203-24211.
- Groves, M.R., Mant, A., Kuhn, A., Koch, J., Dubel, S., Robinson, C. and Sinning, I. (2001) Functional characterization of recombinant chloroplast signal recognition particle. *J. Biol. Chem.*, **276**, 27778-27786.
- Gundelfinger, E.D., Krause, E., Melli, M. and Dobberstein, B. (1983) The organization of the 7SL RNA in the signal recognition particle. *Nucleic Acids Res.*, **11**, 7363-7374.
- Halic, M., Becker, T., Pool, M.R., Spahn, C.M., Grassucci, R.A., Frank, J. and Beckmann, R. (2004) Structure of the signal recognition particle interacting with the elongation-arrested ribosome. *Nature*, **427**, 808-814.
- Halic, M. and Beckmann, R. (2005) The signal recognition particle and its interactions during protein targeting. *Curr Opin Struct Biol*, **15**, 116-125.
- Halic, M., Gartmann, M., Schlenker, O., Mielke, T., Pool, M.R., Sinning, I. and Beckmann, R. (2006) Signal recognition particle receptor exposes the ribosomal translocon binding site. *Science*, **312**, 745-747.
- Hanein, D., Matlack, K.E., Jungnickel, B., Plath, K., Kalies, K.U., Miller, K.R., Rapoport, T.A. and Akey, C.W. (1996) Oligomeric rings of the Sec61p complex induced by ligands required for protein translocation. *Cell*, **87**, 721-732.
- Heldwein, E.E., Macia, E., Wang, J., Yin, H.L., Kirchhausen, T. and Harrison, S.C. (2004) Crystal structure of the clathrin adaptor protein 1 core. *Proc Natl Acad Sci U S A*, **101**, 14108-14113.
- Helmers, J., Schmidt, D., Glavy, J.S., Blobel, G. and Schwartz, T. (2003) The beta-subunit of the protein-conducting channel of the endoplasmic reticulum functions as the guanine nucleotide exchange factor for the beta-subunit of the signal recognition particle receptor. *J Biol Chem*, **278**, 23686-23690.

Bibliography

- High, S. and Dobberstein, B. (1991) The signal sequence interacts with the methionine-rich domain of the 54-kD protein of signal recognition particle. *J Cell Biol*, **113**, 229-233.
- Hooft, R.W., Vriend, G., Sander, C. and Abola, E.E. (1996) Errors in protein structures. *Nature*, **381**, 272.
- Huang, M., Weissman, J.T., Beraud-Dufour, S., Luan, P., Wang, C., Chen, W., Aridor, M., Wilson, I.A. and Balch, W.E. (2001) Crystal structure of Sar1-GDP at 1.7 Å resolution and the role of the NH2 terminus in ER export. *J Cell Biol*, **155**, 937-948.
- Jackson, C.L. and Casanova, J.E. (2000) Turning on ARF: the Sec7 family of guanine-nucleotide-exchange factors. *Trends Cell Biol*, **10**, 60-67.
- Jagath, J.R., Rodnina, M.V., Lentzen, G. and Wintermeyer, W. (1998) Interaction of guanine nucleotides with the signal recognition particle from Escherichia coli. *Biochemistry*, **37**, 15408-15413.
- Jang, S.B., Kim, Y.G., Cho, Y.S., Suh, P.G., Kim, K.H. and Oh, B.H. (2002) Crystal structure of SEDL and its implications for a genetic disease spondyloepiphyseal dysplasia tarda. *J Biol Chem*, **277**, 49863-49869.
- Jekely, G. (2003) Small GTPases and the evolution of the eukaryotic cell. *Bioessays*, **25**, 1129-1138.
- Jones, S., Newman, C., Liu, F. and Segev, N. (2000) The TRAPP complex is a nucleotide exchanger for Ypt1 and Ypt31/32. *Mol Biol Cell*, **11**, 4403-4411.
- Jones, T.A., Zou, J.Y., Cowan, S.W. and Kjeldgaard. (1991a) Improved methods for building protein models in electron density maps and the location of errors in these models. *Acta Crystallogr A*, **47** (Pt 2), 110-119.
- Jones, T.A., Zou, J.Y., Cowan, S.W. and Kjeldgaard, M. (1991b) Improved methods for building protein models in electron density maps and the location of errors in these models. *Acta Crystallogr. A*, **47**, 110-119.
- Keenan, R.J., Freymann, D.M., Stroud, R.M. and Walter, P. (2001) The signal recognition particle. *Annu. Rev. Biochem.*, **70**, 755-775.
- Keenan, R.J., Freymann, D.M., Walter, P. and Stroud, R.M. (1998) Crystal structure of the signal sequence binding subunit of the signal recognition particle. *Cell*, **94**, 181-191.
- Kinch, L.N., Saier, M.H., Jr. and Grishin, N.V. (2002) Sec61beta--a component of the archaeal protein secretory system. *Trends Biochem Sci*, **27**, 170-171.
- Kleywegt, G.J., Bergfors, T., Senn, H., Le Motte, P., Gsell, B., Shudo, K. and Jones, T.A. (1994) Crystal structures of cellular retinoic acid binding proteins I and II in complex with all-trans-retinoic acid and a synthetic retinoid. *Structure*, **2**, 1241-1258.
- Kleywegt, G.J. and Brunger, A.T. (1996) Checking your imagination: applications of the free R value. *Structure*, **4**, 897-904.
- Kleywegt, G.J. and Jones, T.A. (1998) Databases in protein crystallography. *Acta Crystallogr D Biol Crystallogr*, **54**, 1119-1131.
- Krengel, U. (1991) STRUKTUR UND GUANOSINTRIPHOSPHAT-HYDROLYSEMECHANISMUS DES C-TERMINAL VERKUEERTEN MENSCHLICHEN KREBSPROTEINS P21-H-RAS. *Max-Planck-Institut fur medizinische Forschung Abteilung Biophysik*. University of Heidelberg, Heidelberg.
- Kuglstatter, A., Oubridge, C. and Nagai, K. (2002) Induced structural changes of 7SL RNA during the assembly of human signal recognition particle. *Nat. Struct. Biol.*, **9**, 740-744.

Bibliography

- Kyte, J. and Doolittle, R.F. (1982) A simple method for displaying the hydropathic character of a protein. *J Mol Biol*, **157**, 105-132.
- Layne, E. (1957) Spectrophotometric and turbidometric methods for measuring proteins. *Meth Enzymol*, **3**, 447
- Legate, K.R. and Andrews, D.W. (2003) The beta-subunit of the signal recognition particle receptor is a novel GTP-binding protein without intrinsic GTPase activity. *J Biol Chem*, **278**, 27712-27720.
- Legate, K.R., Falcone, D. and Andrews, D.W. (2000) Nucleotide-dependent binding of the GTPase domain of the signal recognition particle receptor beta-subunit to the alpha-subunit. *J Biol Chem*, **275**, 27439-27446.
- Leslie, A.G.W. (1992) Recent changes to the MOSFLM package for processing film and image plate data. *Joint CCP4 + ESF-EAMCB Newsletter on Protein Crystallography*, **26**.
- Luirink, J. and Sinning, I. (2004) SRP-mediated protein targeting: structure and function revisited. *Biochim Biophys Acta*, **1694**, 17-35.
- Luirink, J., ten Hagen-Jongman, C.M., van der Weijden, C.C., Oudega, B., High, S., Dobberstein, B. and Kusters, R. (1994) An alternative protein targeting pathway in Escherichia coli: studies on the role of FtsY. *Embo J*, **13**, 2289-2296.
- Lutcke, H., High, S., Romisch, K., Ashford, A.J. and Dobberstein, B. (1992) The methionine-rich domain of the 54 kDa subunit of signal recognition particle is sufficient for the interaction with signal sequences. *Embo J*, **11**, 1543-1551.
- Luzzati, V. (1952) Traitement statistique des erreurs dans la détermination des structures cristallines. *Acta Cryst.*, **5**, 802-810.
- MacKenzie, J.J., Fitzpatrick, J., Babyn, P., Ferrero, G.B., Ballabio, A., Billingsley, G., Bulman, D.E., Strasberg, P., Ray, P.N. and Costa, T. (1996) X linked spondyloepiphyseal dysplasia: a clinical, radiological, and molecular study of a large kindred. *J Med Genet*, **33**, 823-828.
- Mandon, E.C., Jiang, Y. and Gilmore, R. (2003) Dual recognition of the ribosome and the signal recognition particle by the SRP receptor during protein targeting to the endoplasmic reticulum. *J Cell Biol*, **162**, 575-585.
- Manting, E.H., van Der Does, C., Remigy, H., Engel, A. and Driessen, A.J. (2000) SecYEG assembles into a tetramer to form the active protein translocation channel. *Embo J*, **19**, 852-861.
- Matlack, K.E., Mothes, W. and Rapoport, T.A. (1998) Protein translocation: tunnel vision. *Cell*, **92**, 381-390.
- McMahon, H.T. and Mills, I.G. (2004) COP and clathrin-coated vesicle budding: different pathways, common approaches. *Curr Opin Cell Biol*, **16**, 379-391.
- Menetret, J.F., Neuhaus, A., Morgan, D.G., Plath, K., Radermacher, M., Rapoport, T.A. and Akey, C.W. (2000) The structure of ribosome-channel complexes engaged in protein translocation. *Mol Cell*, **6**, 1219-1232.
- Miller, J.D., Bernstein, H.D. and Walter, P. (1994) Interaction of E. coli Ffh/4.5S ribonucleoprotein and FtsY mimics that of mammalian signal recognition particle and its receptor. *Nature*, **367**, 657-659.
- Miller, J.D., Tajima, S., Lauffer, L. and Walter, P. (1995) The beta subunit of the signal recognition particle receptor is a transmembrane GTPase that anchors the alpha subunit, a peripheral membrane GTPase, to the endoplasmic reticulum membrane. *J Cell Biol*, **128**, 273-282.
- Miller, J.D., Wilhelm, H., Gierasch, L., Gilmore, R. and Walter, P. (1993) GTP binding and hydrolysis by the signal recognition particle during initiation of protein translocation. *Nature*, **366**, 351-354.

Bibliography

- Millman, J.S., Qi, H.Y., Vulcu, F., Bernstein, H.D. and Andrews, D.W. (2001) FtsY binds to the Escherichia coli inner membrane via interactions with phosphatidylethanolamine and membrane proteins. *J Biol Chem*, **276**, 25982-25989.
- Mitra, K., Schaffitzel, C., Shaikh, T., Tama, F., Jenni, S., Brooks, C.L., 3rd, Ban, N. and Frank, J. (2005) Structure of the E. coli protein-conducting channel bound to a translating ribosome. *Nature*, **438**, 318-324.
- Montoya, G., Svensson, C., Lührink, J. and Sinning, I. (1997) Crystal structure of the NG domain from the signal-recognition particle receptor FtsY. *Nature*, **385**, 365-368.
- Montoya, G., te Kaat, K., Moll, R., Schafer, G. and Sinning, I. (1999) Crystallization and preliminary x-ray diffraction studies on the conserved GTPase domain of the signal recognition particle from *Acidianus ambivalens*. *Acta Crystallogr. D*, **55**, 1949-1951.
- Montoya, G., te Kaat, K., Moll, R., Schafer, G. and Sinning, I. (2000) The crystal structure of the conserved GTPase of SRP54 from the archaeon *Acidianus ambivalens* and its comparison with related structures suggests a model for the SRP-SRP receptor complex. *Structure*, **8**, 515-525.
- Mori, H., Tsukazaki, T., Masui, R., Kuramitsu, S., Yokoyama, S., Johnson, A.E., Kimura, Y., Akiyama, Y. and Ito, K. (2003) Fluorescence resonance energy transfer analysis of protein translocase. SecYE from *Thermus thermophilus* HB8 forms a constitutive oligomer in membranes. *J Biol Chem*, **278**, 14257-14264.
- Morris, A.L., MacArthur, M.W., Hutchinson, E.G. and Thornton, J.M. (1992) Stereochemical quality of protein structure coordinates. *Proteins*, **12**, 345-364.
- Moser, C. (1998) Functional studies on the receptor of the signal recognition particle. *EMBL*. University of Heidelberg, Heidelberg.
- Moser, C., Mol, O., Goody, R.S. and Sinning, I. (1997) The signal recognition particle receptor of Escherichia coli (FtsY) has a nucleotide exchange factor built into the GTPase domain. *Proc. Natl. Acad. Sci. U S A*, **94**, 11339-11344.
- Mossessova, E., Corpina, R.A. and Goldberg, J. (2003) Crystal structure of ARF1*Sec7 complexed with Brefeldin A and its implications for the guanine nucleotide exchange mechanism. *Mol Cell*, **12**, 1403-1411.
- Mossessova, E., Gulbis, J.M. and Goldberg, J. (1998) Structure of the guanine nucleotide exchange factor Sec7 domain of human arno and analysis of the interaction with ARF GTPase. *Cell*, **92**, 415-423.
- Navaza, J. (1994) AMoRe: an automated package for molecular replacement. *Acta Crystallogr. A*, **50**, 157-163.
- Ogg, S.C., Barz, W.P. and Walter, P. (1998) A functional GTPase domain, but not its transmembrane domain, is required for function of the SRP receptor beta-subunit. *J Cell Biol*, **142**, 341-354.
- Open_Software_Foundation. (1991) XRayView. *OSF/Motif Programmer's Reference*, Prentice Hall, New Jersey.
- Otwinowski, Z. and Minor, W. (1997) *Methods in Enzymology*. Academic Press, San Diego.
- Ouali, M. and King, R.D. (2000) Cascaded multiple classifiers for secondary structure prediction. *Protein Sci*, **9**, 1162-1176.
- Padmanabhan, S. and Freymann, D.M. (2001) The conformation of bound GMPPNP suggests a mechanism for gating the active site of the SRP GTPase. *Structure*, **9**, 859-867.

Bibliography

- Peluso, P., Herschlag, D., Nock, S., Freymann, D.M., Johnson, A.E. and Walter, P. (2000) Role of 4.5S RNA in assembly of the bacterial signal recognition particle with its receptor. *Science*, **288**, 1640-1643.
- Peluso, P., Shan, S.O., Nock, S., Herschlag, D. and Walter, P. (2001) Role of SRP RNA in the GTPase cycles of Ffh and FtsY. *Biochemistry*, **40**, 15224-15233.
- Perrakis, A., Harkiolaki, M., Wilson, K.S. and Lamzin, V.S. (2001) ARP/wARP and molecular replacement. *Acta Crystallogr D Biol Crystallogr*, **57**, 1445-1450.
- Perrakis, A., Morris, R. and Lamzin, V.S. (1999) Automated protein model building combined with iterative structure refinement. *Nat Struct Biol*, **6**, 458-463.
- Pool, M.R., Stumm, J., Fulga, T.A., Sinning, I. and Dobberstein, B. (2002) Distinct modes of signal recognition particle interaction with the ribosome. *Science*, **297**, 1345-1348.
- Ramirez, U.D., Minasov, G., Focia, P.J., Stroud, R.M., Walter, P., Kuhn, P. and Freymann, D.M. (2002) Structural basis for mobility in the 1.1 Å crystal structure of the NG domain of *Thermus aquaticus* Ffh. *J. Mol. Biol.*, **320**, 783-799.
- Rapiejko, P.J. and Gilmore, R. (1992) Protein translocation across the ER requires a functional GTP binding site in the alpha subunit of the signal recognition particle receptor. *J Cell Biol*, **117**, 493-503.
- Rapiejko, P.J. and Gilmore, R. (1997) Empty site forms of the SRP54 and SR alpha GTPases mediate targeting of ribosome-nascent chain complexes to the endoplasmic reticulum. *Cell*, **89**, 703-713.
- Rapoport, T.A., Jungnickel, B. and Kutay, U. (1996) Protein transport across the eukaryotic endoplasmic reticulum and bacterial inner membranes. *Annu Rev Biochem*, **65**, 271-303.
- Read, R.J. (1986) Improved Fourier coefficients for maps using phases from partial structures with errors. *Acta Cryst.*, **A42**, 140-149.
- Renault, L., Guibert, B. and Cherfils, J. (2003) Structural snapshots of the mechanism and inhibition of a guanine nucleotide exchange factor. *Nature*, **426**, 525-530.
- Romisch, K., Webb, J., Lingelbach, K., Gausepohl, H. and Dobberstein, B. (1990) The 54-kD protein of signal recognition particle contains a methionine-rich RNA binding domain. *J. Cell Biol.*, **111**, 1793-1802.
- Rosendal, K.R., Wild, K., Montoya, G. and Sinning, I. (2003) Crystal structure of the complete core of archaeal signal recognition particle and implications for interdomain communication. *Proc Natl Acad Sci U S A*, **100**, 14701-14706.
- Rossi, V., Banfield, D.K., Vacca, M., Dietrich, L.E., Ungermann, C., D'Esposito, M., Galli, T. and Filippini, F. (2004) Longins and their longin domains: regulated SNAREs and multifunctional SNARE regulators. *Trends Biochem Sci*, **29**, 682-688.
- Rossmann, M.G., Moras, D. and Olsen, K.W. (1974) Chemical and biological evolution of nucleotide-binding protein. *Nature*, **250**, 194-199.
- Sacher, M. (2003) Membrane traffic fuses with cartilage development. *FEBS Lett*, **550**, 1-4.
- Sacher, M., Barrowman, J., Wang, W., Horecka, J., Zhang, Y., Pypaert, M. and Ferro-Novick, S. (2001) TRAPP I implicated in the specificity of tethering in ER-to-Golgi transport. *Mol Cell*, **7**, 433-442.
- Sacher, M., Jiang, Y., Barrowman, J., Scarpa, A., Burston, J., Zhang, L., Schieltz, D., Yates, J.R., 3rd, Abeliovich, H. and Ferro-Novick, S. (1998) TRAPP, a highly conserved novel complex on the cis-Golgi that mediates vesicle docking and fusion. *Embo J*, **17**, 2494-2503.

Bibliography

- Scheffzek, K., Ahmadian, M.R., Kabsch, W., Wiesmuller, L., Lautwein, A., Schmitz, F. and Wittinghofer, A. (1997) The Ras-RasGAP complex: structural basis for GTPase activation and its loss in oncogenic Ras mutants. *Science*, **277**, 333-338.
- Scheffzek, K., Ahmadian, M.R. and Wittinghofer, A. (1998) GTPase-activating proteins: helping hands to complement an active site. *Trends Biochem Sci*, **23**, 257-262.
- Schunemann, D. (2004) Structure and function of the chloroplast signal recognition particle. *Curr Genet*, **44**, 295-304
- Schwartz, T. and Blobel, G. (2003) Structural basis for the function of the Beta subunit of the eukaryotic signal recognition particle receptor. *Cell*, **112**, 793-803.
- Shan, S.O., Stroud, R.M. and Walter, P. (2004) Mechanism of association and reciprocal activation of two GTPases. *PLoS Biol*, **2**, 320.
- Shiba, T., Kawasaki, M., Takatsu, H., Nogi, T., Matsugaki, N., Igarashi, N., Suzuki, M., Kato, R., Nakayama, K. and Wakatsuki, S. (2003) Molecular mechanism of membrane recruitment of GGA by ARF in lysosomal protein transport. *Nat Struct Biol*, **10**, 386-393.
- Siegel, V. and Walter, P. (1985) Elongation arrest is not a prerequisite for secretory protein translocation across the microsomal membrane. *J Cell Biol*, **100**, 1913-1921.
- Siegel, V. and Walter, P. (1986) Removal of the Alu structural domain from signal recognition particle leaves its protein translocation activity intact. *Nature*, **320**, 81-84.
- Sprang, S.R. (1997) G protein mechanisms: insights from structural analysis. *Annu Rev Biochem*, **66**, 639-678.
- Srinivasan, R. (1966) Weighting functions for use in the early stage of structure analysis when a part of the structure is known. *Acta Cryst.*, **20**, 143-144.
- Strub, K., Moss, J. and Walter, P. (1991) Binding sites of the 9- and 14-kilodalton heterodimeric protein subunit of the signal recognition particle (SRP) are contained exclusively in the Alu domain of SRP RNA and contain a sequence motif that is conserved in evolution. *Mol Cell Biol*, **11**, 3949-3959.
- Tajima, S., Lauffer, L., Rath, V.L. and Walter, P. (1986) The signal recognition particle receptor is a complex that contains two distinct polypeptide chains. *J Cell Biol*, **103**, 1167-1178.
- te Kaat, K. (1999) SRP GTPases: Structural analysis and GTP hydrolysis mechanism. *EMBL Heidelberg*. University of Heidelberg, Heidelberg
- Tesmer, J.J., Berman, D.M., Gilman, A.G. and Sprang, S.R. (1997) Structure of RGS4 bound to AIF4-activated Gi alpha1: stabilization of the transition state for GTP hydrolysis. *Cell*, **89**, 251-261.
- Thompson, J.D., Higgins, D.G. and Gibson, T.J. (1994) Improved sensitivity of profile searches through the use of sequence weights and gap excision. *Comput Appl Biosci*, **10**, 19-29.
- Tochio, H., Tsui, M.M., Banfield, D.K. and Zhang, M. (2001) An autoinhibitory mechanism for nonsyntaxin SNARE proteins revealed by the structure of Ykt6p. *Science*, **293**, 698-702.
- Van den Berg, B., Clemons, W.M., Jr., Collinson, I., Modis, Y., Hartmann, E., Harrison, S.C. and Rapoport, T.A. (2004) X-ray structure of a protein-conducting channel. *Nature*, **427**, 36-44.
- Van Nues, R.W. and Brown, J.D. (2004) Saccharomyces SRP RNA secondary structures: a conserved S-domain and extended Alu-domain. *Rna*, **10**, 75-89.

Bibliography

- Veenendaal, A.K., van der Does, C. and Driessen, A.J. (2001) Mapping the sites of interaction between SecY and SecE by cysteine scanning mutagenesis. *J Biol Chem*, **276**, 32559-32566.
- Vetter, I.R. and Wittinghofer, A. (2001) The guanine nucleotide-binding switch in three dimensions. *Science*, **294**, 1299-1304.
- Voet, D. and Voet, J.G. (1995) *Biochemistry*. John Wiley & Sons, Inc., New York.
- Walter, P. and Blobel, G. (1981) Translocation of proteins across the endoplasmic reticulum III. Signal recognition protein (SRP) causes signal sequence-dependent and site-specific arrest of chain elongation that is released by microsomal membranes. *J Cell Biol*, **91**, 557-561.
- Wang, W., Sacher, M. and Ferro-Novick, S. (2000) TRAPP stimulates guanine nucleotide exchange on Ypt1p. *J Cell Biol*, **151**, 289-296.
- Weiner, A.M. (1980) An abundant cytoplasmic 7S RNA is complementary to the dominant interspersed middle repetitive DNA sequence family in the human genome. *Cell*, **22**, 209-218.
- Wickner, W. and Leonard, M.R. (1996) Escherichia coli preprotein translocase. *J Biol Chem*, **271**, 29514-29516.
- Wild, K., Halic, M., Sinning, I. and Beckmann, R. (2004a) SRP meets the ribosome. *Nat Struct Mol Biol*, **11**, 1049-1053.
- Wild, K., Rosendal, K.R. and Sinning, I. (2004b) A structural step into the SRP cycle. *Mol Microbiol*, **53**, 357-363.
- Yahr, T.L. and Wickner, W.T. (2000) Evaluating the oligomeric state of SecYEG in preprotein translocase. *Embo J*, **19**, 4393-4401.
- Young, J.C., Ursini, J., Legate, K.R., Miller, J.D., Walter, P. and Andrews, D.W. (1995) An amino-terminal domain containing hydrophobic and hydrophilic sequences binds the signal recognition particle receptor alpha subunit to the beta subunit on the endoplasmic reticulum membrane. *J Biol Chem*, **270**, 15650-15657.
- Zanen, G., Antelmann, H., Westers, H., Hecker, M., van Dijl, J.M. and Quax, W.J. (2004) FlhF, the third signal recognition particle-GTPase of Bacillus subtilis, is dispensable for protein secretion. *J Bacteriol*, **186**, 5956-5960.
- Zhao, L., Helms, J.B., Brunner, J. and Wieland, F.T. (1999) GTP-dependent binding of ADP-ribosylation factor to coatamer in close proximity to the binding site for dilysine retrieval motifs and p23. *J Biol Chem*, **274**, 14198-14203.
- Zopf, D., Bernstein, H.D., Johnson, A.E. and Walter, P. (1990) The methionine-rich domain of the 54 kd protein subunit of the signal recognition particle contains an RNA binding site and can be crosslinked to a signal sequence. *Embo J*, **9**, 4511-4517.
- Zwieb, C. and Eichler, J. (2002) Getting on target: the archaeal signal recognition particle. *Archaea*, **1**, 27-34.